Alaska Department of Transportation & Public Facilities
Alaska University Transportation Center

Creep Behavior of Shallow Anchors in Ice-rich Silt

Prepared By:

Xiong Zhang, Ph.D., P.E.

Liangbiao Chen, Graduate Student

Chuang Lin, Graduate Student

Dept. of Civil and Environmental Engineering

University of Alaska Fairbanks

Robert McHattie

GZR Engineering

July 2013

Prepared By:

Alaska University Transportation Center
Duckering Building Room 245
P.O. Box 755900
Fairbanks, AK 99775-5900

INE #: INE/AUTC 13.16

Alaska Department of Transportation
Research, Development, and Technology Transfer
2301 Peger Road

DOT # T2-08-20

CREEP BEHAVIOR OF SHALLOW ANCHORS IN ICE-RICH SILT

Final Project Report

by

Chuang Lin

Research Assistant

Department of Civil and Environmental Engineering

Liangbiao Chen

Research Assistant

Department of Civil and Environmental Engineering

Xiong Zhang

Associate Professor

Department of Civil and Environmental Engineering

Robert Mchattie

Consultant GZR Engineering

Performed in Cooperation with

Alaska Department of Transportation & Public Facilities

and

Alaska University Transportation Center

July 2013

University of Alaska Fairbanks

Fairbanks, AK 99775-5900

Notice

This document is disseminated under the sponsorship of the U.S. Department of Transportation in the interest of information exchange. The U.S. Government assumes no liability for the use of the information contained in this document. The U.S. Government does not endorse products or manufacturers. Trademarks or manufacturers' names appear in this report only because they are considered essential to the objective of the document.

Quality Assurance Statement

The Federal Highway Administration (FHWA) provides high-quality information to serve Government, industry, and the public in a manner that promotes public understanding. Standards and policies are used to ensure and maximize the quality, objectivity, utility, and integrity of its information. FHWA periodically reviews quality issues and adjusts its programs and processes to ensure continuous quality improvement.

Author's Disclaimer

Opinions and conclusions expressed or implied in the report are those of the authors. They are not necessarily those of the Alaska DOT&PF or funding agencies.

REPORT DOCUMENTATION PAGE

Form approved OMB No.

Public reporting for this collection of information is estimated to average 1 hour per response, including the time for reviewing instructions, searching existing data sources, gathering and maintaining the data needed, and completing and reviewing the collection of information. Send comments regarding this burden estimate or any other aspect of this collection of information, including suggestion for reducing this burden to Washington Headquarters Services, Directorate for Information Operations and Reports, 1215 Jefferson Davis Highway, Suite 1204, Arlington, VA 22202-4302, and to the Office of Management and Budget, Paperwork Reduction Project (0704-1833), Washington, DC 20503

1. AGENCY USE ONLY (LEAVE BLANK)	2. REPORT DATE	3. REPORT TYPE AND DATES COVERED
DOT&PF Number: T2-08-20	July 2013	Final Report

4. TITLE AND SUBTITLE	5. FUNDING NUMBERS
Creep Behavior of Shallow Anchors in Ice-rich Silt	UAF: G3238, UTC-33842 AK DOT&PF T2-08-20
6. AUTHOR(S) Xiong Zhang, Ph.D., P.E. Liangbiao Chen, Graduate Student Chuang Lin, Graduate Student Robert McHattie, PE	
7. PERFORMING ORGANIZATION NAME(S) AND ADDRESS(ES) Alaska University Transportation Center University of Alaska Fairbanks Duckering Building Room 245 P.O. Box 755900 Fairbanks, AK 99775-5900	8. PERFORMING ORGANIZATION REPORT NUMBER INE/AUTC 13.16
9. SPONSORING/MONITORING AGENCY NAME(S) AND ADDRESS(ES) State of Alaska, Alaska Dept. of Transportation and Public Facilities Research and Technology Transfer 2301 Peger Rd Fairbanks, AK 99709-5399	10. SPONSORING/MONITORING AGENCY REPORT NUMBER T2-08-20

11. SUPPLENMENTARY NOTES

Performed in cooperation with the Alaska Department of Transportation and Public Facilities

12a. DISTRIBUTION / AVAILABILITY STATEMENT	12b. DISTRIBUTION CODE
No restrictions	

13. ABSTRACT (Maximum 200 words)

Grouted anchors have become a common technique in the application of earth retention systems, slope stability problems and tie-down structures in unfrozen soils due to its cost and time efficiency. However, within much of Alaska area, permafrost is a common type of soil and might contain large amount of visible ice. The highly time and temperature dependent properties of ice-rich soil make it a challenge for the application of anchors in permafrost area. This project evaluates the effect of water content and temperature on the creep behavior of shallow anchors in cold room lab. Also, field test was conducted to determine effectiveness of three types of grouting materials, including Bentonite clay, Microsil Anchor Grout and special cement formula. The temperature along the anchor was monitored to evaluate the degradation of the surrounding frozen soil. Research results may applicable in the design of shallow anchors in ice-rich permafrost at various ice content and temperature range. Also, the load distribution and the pullout test results could give a general guidance for the shallow anchor design in permafrost area.

14- KEYWORDS : Creep Tests (Gbgf),Frozen soils (Rbesfh),Cement grouts (Rbmndfc)	15. NUMBER OF PAGES 115
	16. PRICE CODE N/A

17. SECURITY CLASSIFICATION OF REPORT	18. SECURITY CLASSIFICATION OF THIS PAGE	19. SECURITY CLASSIFICATION OF ABSTRACT	20. LIMITATION OF ABSTRACT
Unclassified	Unclassified	Unclassified	N/A

NSN 7540-01-280-5500

STANDARD FORM 298 (Rev. 2-98)
Prescribed by ANSI Std. 239-18 298-1

SI* (MODERN METRIC) CONVERSION FACTORS

APPROXIMATE CONVERSIONS TO SI UNITS

Symbol	When You Know	Multiply By	To Find	Symbol
		LENGTH		
in	inches	25.4	millimeters	mm
ft	feet	0.305	meters	m
yd	yards	0.914	meters	m
mi	miles	1.61	kilometers	km
		AREA		
in^2	square inches	645.2	square millimeters	mm^2
ft^2	square feet	0.093	square meters	m^2
yd^2	square yard	0.836	square meters	m^2
ac	acres	0.405	hectares	ha
mi^2	square miles	2.59	square kilometers	km^2
		VOLUME		
fl oz	fluid ounces	29.57	milliliters	mL
gal	gallons	3.785	liters	L
ft^3	cubic feet	0.028	cubic meters	m^3
yd^3	cubic yards	0.765	cubic meters NOTE: volumes greater than 1000 L shall be	m^3
		MASS		
oz	ounces	28.35	grams	g
lb	pounds	0.454	kilograms	kg
T	short tons (2000 lb)	0.907	megagrams (or "metric ton")	Mg (or "t")
		TEMPERATURE (exact degrees)		
°F	Fahrenheit	5 (F-32)/9 or (F-32)/1.8	Celsius	°C
		ILLUMINATION		
fc	foot-candles	10.76	lux	lx
fl	foot-Lamberts	3.426	$candela/m^2$	cd/m^2
		FORCE and PRESSURE or STRESS		
lbf	poundforce	4.45	newtons	N
lbf/in^2	poundforce per square inch	6.89	kilopascals	kPa

APPROXIMATE CONVERSIONS FROM SI UNITS

Symbol	When You Know	Multiply By	To Find	Symbol
		LENGTH		
mm	millimeters	0.039	inches	in
m	meters	3.28	feet	ft
m	meters	1.09	yards	yd
km	kilometers	0.621	miles	mi
		AREA		
mm^2	square millimeters	0.0016	square inches	in^2
m^2	square meters	10.764	square feet	ft^2
m^2	square meters	1.195	square yards	yd^2
ha	hectares	2.47	acres	ac
km^2	square kilometers	0.386	square miles	mi^2
		VOLUME		
mL	milliliters	0.034	fluid ounces	fl oz
L	liters	0.264	gallons	gal
m^3	cubic meters	35.314	cubic feet	ft^3
m^3	cubic meters	1.307	cubic yards	yd^3
		MASS		
g	grams	0.035	ounces	oz
kg	kilograms	2.202	pounds	lb
Mg (or "t")	megagrams (or "metric ton")	1.103	short tons (2000 lb)	T
		TEMPERATURE (exact degrees)		
°C	Celsius	1.8C+32	Fahrenheit	°F
		ILLUMINATION		
lx	lux	0.0929	foot-candles	fc
cd/m^2	$candela/m^2$	0.2919	foot-Lamberts	fl
		FORCE and PRESSURE or STRESS		
N	newtons	0.225	poundforce	lbf
kPa	kilopascals	0.145	poundforce per square inc h	lbf/in^2

*SI is the symbol for the International System of Units. Appropriate rounding should be made to comply with Section 4 of ASTM E380.Revised March 2003)

TABLE OF CONTENTS

LIST OF FIGURES

LIST OF TABLES

Chapter 1 Introduction

1.1 General

Grouted anchors have been in use for over 40 years and have become a common technique in the application of earth retention, slope stability and tie-down structure due to its cost and time efficiency. They have been successfully used in unfrozen soils in the design and installation of different types of structures including highway application, slope stabilization and foundation excavation projects. The theory for the application of grouted anchors in unfrozen soil is relatively completed and can be seen in a series of publications (Adams and Hayes 1967; Bhatnagar 1969; Hanna and Carr 1971; Adam and Klym1972). Yet, when it comes to permafrost, especially in ice-rich permafrost, the creep behavior of ice-rich soil under constant loading becomes one of the major concerns in the design of grouted anchors. In order to provide a better and more accurate method to predict the long-term loading capacity and allowable settlement of grouted anchors in areas like Alaska, which has a harsh climate condition, the creep behavior of grouted anchors needs to be evaluated.

1.2 Problem Statement

In cold regions, ice-rich permafrost is a common soil type. In order to further explore the applicability of shallow anchor in discontinuous permafrost area like much of Alaska, the creep behavior of grouted anchors needs to be comprehensively studied. The temperature and water content will have a large impact on the creep behavior of ice-rich frozen soil. As the temperature increases, the unfrozen water content will increase, which will result in a large difference in the creep behavior of ice-rich soil. Moreover, the creep behavior of ice-rich soil at the temperature range near melting point still not clearly explored. The soil with higher water content will exhibit larger creep rates compared with ice-poor frozen soil at same stress level. Moreover, steady state creep dominates the total displacement of ice-rich soil for long term run. In contrast, primary creep

dominates the total displacement of ice-poor soil. All of those unsolved problems make it necessary and urgent to study the creep behavior of grouted anchors in ice-rich soils.

1.3 Objective

The major objectives of this study are:

1. Exploration of the creep behavior of grouted anchor at different temperatures;
2. Evaluating the effects of soil moisture content on the creep behavior of grouted anchor in ice-rich soils;
3. Analyzing the process of load redistribution along the anchor;
4. Comparison of the effect of grouting temperature and creep behavior of three different backfill materials.

1.4 Research Methodology

In order to achieve the objectives, the following major tasks were conducted:

1. Literature review

Chapter 2 provides a comprehensive overview of research progress, past and present, regarding grouted anchors and creep behavior, especially in permafrost areas. The review provided essential background information on creep theory, anchor design, test methods, and practical experience necessary to plan and conduct work on this research project.

2. Laboratory Tests

Chapter 3 provides details concerning a series of laboratory tests conducted at the University of Alaska, Fairbanks (UAF) on anchors in frozen soils. The purpose of these tests was to determine temperature and moisture effects on the creep behavior of ice-rich soil, using one type of backfill material, under highly controlled conditions. The type of soil used exclusively for this testing was a remolded Fairbanks Silt. In total, 19 anchors were tested in a laboratory cold room, with soil moisture contents ranging from 50% to 120 % and temperature varying from 30.2ºF (-1ºC) to 28.4 ºF (-2ºC). These were the first soil anchor tests completed as part of this research effort. Data obtained from these tests were analyzed prior to the field tests indicated below.

3. Field Tests

Chapter 4 discusses field testing of 13 steel bar anchors and 4 duckbill anchors. These anchors were installed into in situ ice-rich permafrost soils at a site near Fox, Alaska. Details of the drilling, anchor installation, and the loading system setup procedure are discussed in this chapter. Three load levels were performed on each anchor with a time period of 3 days for each level. Four anchors were selected for long-term testing, i.e., for a period of 1 month.

4. Test Results and Data Analysis

Chapter 5 presents test results and data analyses. The effects of hydration heat on the surrounding soil were first evaluated. Then, the load redistribution process of anchors with different types of backfill materials is demonstrated. Finally, the strain rates at different load level are presented.

5. Project Summary and Recommendation

Chapter 6 gives a summary of the test results and conclusions based on Tasks 1 through 4. Recommendations are offered regarding the use of shallow anchors in ice-rich permafrost.

Chapter 2 Literature Review

In this chapter, background information on grouted anchors and the creep behavior of grouted anchors in ice-poor and ice-rich soils are introduced.

2.1 Background on Grouted Anchors

Grouted anchors consist of three basic parts: anchorage, unbonded length and bonded length. Anchorage transmits the pre-stressed force to support structures like soldier beams or wire mesh retainment components. The components of anchorage include anchor nut which is used to lock the stress, bearing or wedge plate and tendon. In general, there are two different types of tendons: bar tendons and strand tendons.

In general, grouted anchors can be classified into 4 types:

1. Straight Shaft Gravity-Grouted Ground Anchor. This type of anchor is commonly used in rock and very stiff to hard cohesive soil. The resistance is provided by the shear stress at the grout-soil or rock interface.
2. Straight Shaft Pressure-Grouted Ground Anchor. This type of anchor is most compatible with coarse granular soil, cohesionless fine-grained soil and fracture-weakened rock. Grout cement is injected into the annulus between the tendon and soil or rock surface with pressure greater than 51psi (about 0.35 MPa). The grout bulb can provide a higher shear resistance due to the increased confining pressure caused by injected pressure grout and the increased contact surface of grout bulb.
3. Post-grouted Ground Anchor. Multiple grout injection was used to enlarge the grout body. The time interval between adjacent grout bulbs is one or two days. The high pressure grout extends into the interconnected fissures of soil or rock to effectively enlarge the contact area of the grout body, and thereby provide higher resistance strength.
4. Underreamed Anchor. This type of anchor contains the boreholes drilled by gravity displacement method and could be used in firm to hard cohesive soil. The bell-like grout bulb serves as a plate which can provide extra end bearing or pull-out resistance.

Compared with a conventional earth retention system, a grouted anchor system has several benefits. The construction workspace and time required for installing a grouted anchor is relatively

small. A grouted anchor provides a comparatively large amount of resistance strength considering the amount of material used in the anchor itself. Moreover, temporary support is not required in many anchor-type systems, thus providing a cost savings over most other systems.

A common application of grouted anchors in a highway project is the use of anchored walls to stabilize excavations and slopes. Another application for grouted anchors is in slope and landslide stabilization. Grouted anchors combined with horizontal beams or concrete blocks are often used to prevent the slopes from failing. The resistance strength generated at the grout and soil interface is transformed to the horizontal beam or concrete block.

2.2 Creep Theory

The creep behavior of soil plays a significant role in the grouted anchor design process. This section focuses on the creep behavior of grouted anchors in permafrost areas. The creep theory of unfrozen soil is only briefly introduced in this paper. In order to provide a systematic overview of the development of creep theory in frozen soils, the general creep behavior of soil is presented first. Then the deformation behavior of ice and ice-rich soils is illustrated. Finally, a summation of the development of creep theory of frozen soil is given.

1. General Creep Behavior

The creep behavior of grouted anchors under constant load at constant temperature is shown in Figure 2.1. Both laboratory and field test results have indicated behavior, such as indicated by this creep curve, for grouted anchors and piles. The creep curve shown in the figure was used to develop the constitutive equation for grouted anchors in frozen soil. Hult (1966) established a method to approximate the creep curve by using a straight line rather than the actual creep curve. Creep is a critical consideration for the practical design of anchors in order to determine the ultimate stress and allowable displacement (Johnston and Ladanyi, 1972; Biggar and Kong, 2001).

Figure 2.1 plots the creep curvature for grouted anchors under constant load (displacement vs. time). In general, three distinguishing periods can be identified from the figure:

1. Primary stage: Displacement increases with time, but the displacement rate decreases gradually with time.
2. Secondary stage: This stage can also be called steady-state stage. In this period of time, the displacement rate remains a constant.

3. Tertiary stage: Displacement rate increases rapidly with time. The onset of the tertiary stage is always considered to be the beginning of failure.

In general, creep curves plotted for each anchor or pile under different load levels and loading rates, soil types and temperatures show distinct primary, secondary and tertiary creep stages. However, at higher loads anchors exhibit a short secondary stage, and the tertiary stage will not appear for very low loads (Johnston and Ladanyi, 1972). The onset of the tertiary stage is considered as the beginning of slip between the grout and soil. Consequently, answering the question of when and at what load the tertiary stage occurs is very important in order to determine the acceptable application and load capacity for a particular anchor.

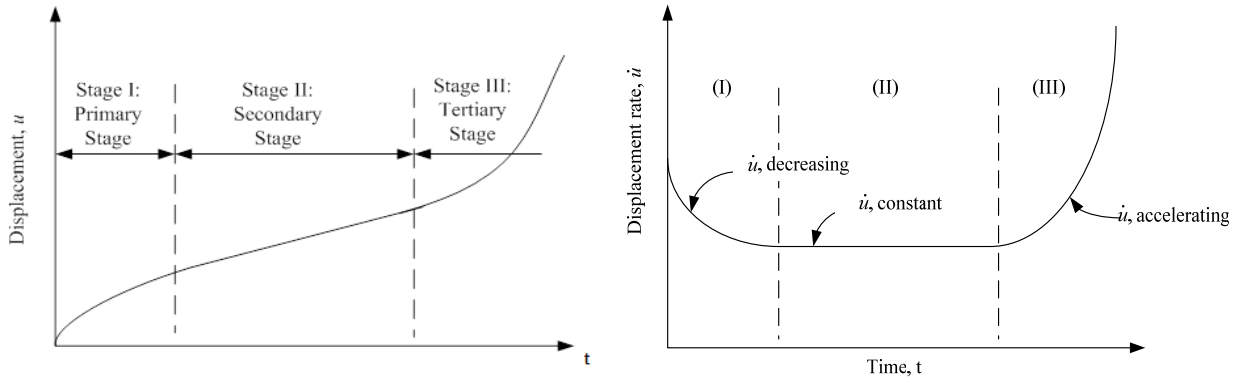

(a) (b)

Figure 2.1 Basic Creep Behavior of Grouted Anchor (After Vialov et al., 1969; Biggar and Kong, 2001)

2.Creep Behavior of Ice

Glen (1952, 1955) was one of the first researchers to conduct comprehensive creep tests to study polycrystalline ice. Test results indicated that under low stress, the ice went through an instantaneous strain at the moment load was applied, and continued to deform at a decreased rate until a steady creep rate was obtained. When under high load level, the stationary or secondary creep stage was replaced by a reaccelerating state until the ice finally failed at the ultimate load. Since ice behaved similar to metals, which are also crystalline materials, a simple power law was proposed by Glen to describe the creep behavior of ice in equation [2.1]:

$$\dot{\varepsilon} = A\sigma^{n} \qquad [2.1]$$

Where $\dot{\varepsilon}$: axial strain rate; σ: axial stress; A: parameter dependent on temperature and ice type; n: experimentally derived exponent.

However, the tests performed by Glen were under relatively high stress levels which did not fit the actual geotechnical engineering problems. For tests using lower stress states at temperatures near the melting point, the exponent n is higher. Butkovich and Landauer (1959, 1960) observed the viscous behavior of ice near the melting point at low stress levels. Several types of ice were used in the test, such as commercial ice, artificial single crystal ice and Greenland glacier ice. The test results indicated that some variations occurred in the creep law parameters for the various ice types. Also, the general format of the flow law under different stress states was similar. Mellor and Testa (1969a) further explored the influence of the viscosity property of ice on the secondary creep rate at a low stress level, and tested with a temperature under -2°C. Temperature and stress dependent secondary creep behavior was observed during the test. They developed a constitutive relationship which extended predictions of secondary creep through a broader range of stress.

Barnes et al. (1971) assumed the creep behavior of polycrystalline ice consisted of three parts: elastic strain, transient strain and steady-state creep strain. Therefore they proposed equation [2.2] to describe the total strain:

$$\varepsilon = \varepsilon_0 + \beta t^{\frac{1}{3}} + \dot{\varepsilon} t \qquad [2.2]$$

Where ε: total strain; ε_0: instantaneous elastic strain; β: constant for transient creep; $\dot{\varepsilon}$: steady-state creep rate; t: time

This equation enabled the secondary creep rate to be defined for a wide range of temperature and stress by extracting the steady-state strain rate from the short-term, low stress tests.

Meier (1960) analyzed the effect of self-weight on ice body deformation. By analyzing both vertical and transverse velocity of Saskatchewan Glacier, a creep law was provided to demonstrate the constitutive relationship as follows:

$$\dot{\varepsilon} = B\sigma + A\sigma^n \qquad [2.3]$$

Where A and B: constant given the same temperature and ice type; σ and n: axial stress and experimentally derived exponent.

Meier tried to use two flow mechanisms to demonstrate the departure of his test results from Glen's under low stress situations. He suggested that the deformation of polycrystalline ice was controlled

by two flows simultaneously: Newtonian viscous flow which represents the slide along the grain boundaries and steady-state flow associated with intracrystalline glide. However, his explanation of the test results encountered great difficulty due to the scatter evident in the field test data. Several researchers (Budd, 1969; Paterson and Savage, 1963) also performed tests with the temperature near the melting point and under low stress, which were subjected to interpretation difficulties as well. Yet, Shreve and Sharp's (1970) test results indicated a good match with Glen's simple flow law. Moreover, Raymond (1973) used three-dimensional velocity distribution to interpret the field data of glacier ice and validated the method of using a simple power law under low stress conditions.

Thomas's (1973a) equation for describing the creep behavior of floating ice shelves was in good agreement with Barnes' et al (1971) laboratory test results under higher stress state. He reduced some of the difficulties in interpreting the deformation of glacier ice by assuming well-defined upper and lower surfaces that remained uniform over a relatively long distance. The good agreement of results from field and laboratory tests enabled a better understanding of the flow law of ice under low stresses.

3. Creep behavior of Frozen Soils

Vialov (1959) was one of the first researchers who systematically studied the strength and stability of frozen soils. Experimental research was done at the Igarskii Permafrost Scientific Research Station from 1950 to 1953. He pointed out that one of the most important characteristics of frozen soil was the time and temperature dependent constitutive relationship. Frozen soil contained both the solid and liquid phase of water. Plus, he also noticed that the behavior of frozen soil was significantly affected by rheological deformation when the temperature was close to the melting point. The soil exhibited a highly plastic-viscous property which meant the strength of that frozen soil would decrease rapidly under the influence of load. Equation [2.4] was provided by Vialov to demonstrate the allowable stress at the soil-pile interface:

$$\ln\left(\frac{t_f}{t_0}\right) = \frac{\tau_0}{\tau} \qquad [2.4]$$

Where t_0 and τ_0: constant relating to the characteristics of the material; t_f: time of the failure of pile; τ: shear stress at the interface of pile and soil.

Furthermore, Vialov (1962) has presented stress-strain relationship based on the test results from undisturbed sandy silt and clay. The formula is as follows:

$$\varepsilon = \left[\frac{\sigma \cdot t^{\lambda}}{\omega(\theta+1)^{k}}\right]^{\frac{1}{m}} + \varepsilon_0 \qquad [2.5]$$

Where σ: applied stress; t: time; θ: temperature (°C) below the freezing point; ε_0: instantaneous strain; λ, m, ω and k: constant parameters which represent the property of materials.

Sayles (1968) proved the Vialov's strength formula by studying the creep stress-strain relationship of frozen Ottawa sand and Manchester fine sand for various temperatures. The strength of frozen soil increased with the decrease in temperature because the amount of unfrozen water decreased while the amount of pore ice increased. Yet, the content of unfrozen water in frozen sand was very small so that the effect of unfrozen water on the strength of frozen sand could be neglected, and this assumption was proved by Butkovich's (1954) tests on lake ice and commercial frozen soil. Moreover, he also found out that when the stress was lower than the long-term strength, the strain is less than 14% of elastic strain and so reversible strain was dominant.

Johnston and Ladanyi (1972) conducted both constant and step load tests of grouted piles in two permafrost field sites near Manitoba. The observation indicated that the slip all occurred between the interface of soil and pile. Plus, they also provided a method to predict the long-term adfreeze strength of frozen soil based on the engineering creep theory. The estimated value of long-term adfreeze strength fitted well with the field test results. The normalized creep rate provided by Johnston and Ladanyi was as follows:

$$\frac{\dot{U}_a}{a} = \frac{3^{(n_1+1)/2}\, B_1 \tau_a{}^{n_1}}{n_1 - 1} \qquad [2.6]$$

Where $\dot{U}_a$: steady-state creep rate at radius of a; a: distance from the axis of anchor; n_1 and B: creep parameters related to the property of pile and temperature; τ_a: shear stress at a distance of a.

However, this test was conducted only for one type of anchor and rather special soil conditions. The tested soils were frozen varved clay and silt. Moreover, the relatively high testing temperature was not appropriate to fully demonstrate the effect of temperature on the long-term adfreeze strength of grouted piles or anchors.

A number of researchers, such as Nixon and McRoberts (1976), Weaver (1979) and Morgenstern et al. (1980), conducted both laboratory and field tests to predict the creep of piles in different frozen soils. The redistribution of stress along the pile was found to occur prior to the onset of the secondary creep state. Plus, the time for reaching a uniformly distribution of stress was significantly affected by ground temperature and varied from 1 day to 1 year. Moreover, it was assumed by all the researchers that the deformation of the soil was continuous which indicated a homogeneous soil, and that the shear strain rate remained constant as long as the applied stress did not surpass the pile's adfreeze strength.

Parameswaran (1986) performed a series of tests on small-scale model piles in different frozen soils by using a constant displacement rate test and a constant load test. The test results indicated that Vialov's method of using failure time under short term, displacement rate controlled tests to predict the pile bearing capacity gave much higher value of the allowable strength when compared with results Parameswaran obtained from constant load tests. Therefore, he concluded that Vialov's method provided the lowest value of the allowable stress because he introduced the variable of total time prior to the tertiary creep. However, he also admitted that Vialov's method did give a safe and convenient way of estimating the long term pile bearing capacity in permafrost.

Nixon and Neukirchner (1984) reported significantly reduced pile capacity due to the increase of salinity in frozen ice-rich soil. Their study indicated that the temperature dependent exponent n, would decrease with increasing salinity. Biggar (1991) pointed out that saline fluid in contact with the surface of pile would result in the reduction of the adfreeze bond strength during the freezing process. Biggar and Sego (1993a) performed studies on the creep models for piles in frozen saline soil. They concluded that the creep law for piles in ice-poor frozen saline silt sand could be described adequately by a simple power law to predict the short-term pile displacement. While for the long-term displacement of piles, a flow law would be a better way of predicting the displacement.

2.3 Grouted Anchor Design in Permafrost

Grouted anchors and grouted piles share similar failure and creep mechanisms, so that studying the theory of grouted piles can provide useful technical background toward the design of grouted anchors. This section of the literature review first introduces general assumptions regarding the

design of grouted anchors. The literature review then turns to anchor design concepts applicable to ice-rich permafrost—soil anchors in ice-rich permafrost being the main focus of research (and sole focus of testing) conducted for this project.

General assumptions:

1. weight of the anchor is negligible;
2. shear stress along the anchor is uniformly distributed;
3. the soil is homogeneous, isotropic, and the temperature remains constant;
4. no slip occurs between the pile and soil before the onset of tertiary state.

1. Grouted Anchor Design Considerations

Temperature

The creep behavior of frozen soil shows is significantly time and temperature dependent. In general, the creep displacement rate decreases dramatically with the decrease in temperature. Morgenstern et al. (1980) reported that the displacement rate at 14°F (-10°C) was 10-100 times less than that at 30.2°F (-1°C) when given the same shear stress and pile dimensions. When the temperature is near the freezing point (32°F), the displacement rate will increase greatly. Biggar and Sego (1993a) also reported significant displacement rate increases with a temperature increase of only 1.8°F (1°C).

In general, it is thought that the existence of soil particles will impede the dislocation of ice crystals and thereby minimize the creep rate. A contrasting general assumption held by some researchers is that the presence of soil particles, at low concentration, will reduce friction between ice crystals and therefore accelerate the creep rate. However, results of long–term creep tests, conducted at temperatures near the freezing point by Thompson and Sayles (1972), Roggensack (1977) and McRoberts et al. (1978), suggested that the creep behavior of frozen soil (especially near the freezing point) is a more complicated process. Thompson and Sayles's results with Fairbanks silt indicated that the creep rate of silt is comparable to that of polycrystalline ice. Yet, McRoberts et al. (1978) reported the Norman Wells Silt exhibited a lower creep rate than polycrystalline ice while Roggensack (1977) observed a creep rate for clay higher than that of ice.

The thermal gradient is another temperature consideration in permafrost areas. In general, the thermal gradient of greater than 30m/°C can be expected in many permafrost areas. So it is reasonable to assume that the temperature along the anchor shaft is uniformly distributed.

Soil Type

It is recognized that fine grained frozen soils often exhibit a rheological and viscous character. Such material can be categorized into two types: ice-poor and ice-rich frozen soil. The long-term deformation of fine grained ice-rich soil is dominated by secondary creep while the deformation of ice-poor fine grained soil is controlled by primary creep. In the previous, standard designs of anchors or piles in such soils, adfreeze bond strength is the major concern. Yet it is prudent that the creep behavior of ice-rich fine grained soils be accounted for by a design approach such as that based on limiting deformation. Nixon and McRoberts (1976) and Morgenstern et al. (1980) did such design-related predictions based on the flow law of ice.

Cement

Cement used for applications where it is in contact with permafrost soils is quite different from that used for unfrozen soil applications. Cement used in frozen soil applications should be kept from freezing until the hydration process is complete. Mixtures of cement-based materials used in a permafrost soil environment must have sufficient bond strength for the intended application. The material must possess handling properties that allow for simple and easy placement assuming adverse environmental conditions at the time of construction. Additionally, it is necessary that the cement-based material generate minimal heat during the hydration process, as such heat will degrade the permafrost.

Five types of cement systems were tested by Biggar and Sego (1993a). The first one was neat Ciment Fondu. Test results indicated that temperatures remained above the freezing point until the hydration reaction subsided. The ice-cement interface experience a temperature increase of only 3.6°F (2°C). The final compression strength was 3,160 psi (21,787 KPa). The second type was Fondu: Fly Ash (50:50). Test results showed a curing temperature lower than for the first type but high enough for the system to set and achieve the final compression strength of 1,796 psi (12,383 KPa). The third cement type was Gypsum: Portland Cement (50:50) with 20% of the mixing water replaced by alcohol in order to lower the freezing point during hydration. Test results indicated that no bond developed between ice and pile even though the cement mixture cured. The fourth type was Gypsum: Portland Cement (50:50) with 18% sodium chloride by weight of mix water to depress the freezing point. This type of cement system exhibited a higher increment in temperature during hydration which lasted for only a short time, but the final bond was not strong. The fifth

and last type was API Class C Cement with 2% calcium chloride. This cement performed worst with 50% of cement frozen, but with no temperature increase.

Backfill Properties

Properties of backfill material around the pile or anchor affect the load capacity of anchors and piles greatly. The adfreeze bond strength governs load capacity of anchors and piles by controlling the level of shear strength that can develop between these structures and the frozen backfill material. Also, piles and anchors with rough surfaces provide the additional contact area that of course increases total area of the adfreeze bond. The additional adfreeze bond developed over the additional (rough) area means that total shear strength and therefore total load capacity increases.

Sego and Smith (1989) performed laboratory tests at 23°F (-5°C) with various backfill materials. The backfill materials used in the research were clean sand slurry, silty sand slurry, silty saline sand slurry and ice. Comparison with the test results for nonsaline backfill materials found that similar short-term pile adfreeze strengths were achieved regardless of silt content. Comparisons between ice and nonsaline sand backfill found that the ice generated 40% less adfreeze strength. This strongly indicated that variations in ice content would significantly influence afreeze strength.

Another test looked at pile surface treatment, and showed that it also played an important role in the short-term capacity of piles. Three types of pile surface were used in the test: an uncoated pile, a pile coated with a black lacquer, and pile with a sandblasted surface. The maximum short-term strength was achieved by the pile with sandblasted surface due to the increased roughness of the pile surface.

Salinity

Anchor or pile capacity will dramatically decrease with the increase of salinity in frozen soil. Nixon and Neukirchner (1984) reported this phenomenon in their study of ice-rich frozen soil. And the same test result was shown in the test of ice-poor frozen soil conducted by Biggar and Sego (1993a). The reason for this significant decrease in anchor or pile capacity is that unfrozen saline pore fluid is in direct contact with the pile surface, thereby diminishing the quality of the adfreeze bond (Nixon 1988; Hutchinson 1989). This indicates that solute diffused from the native soil (or contained in the backfill material) and redistributed along the pile or anchor surface would limit

adfreeze bond strength. Sego and Smith (1989) also compared test results for non-saline backfill and saline backfill, and reported a 47% decrease in pile capacity due to salinity. Their research tends to confirm that salinity would be one of the major factors controlling pile bearing capacity.

2. Grouted Anchor Design in Ice-rich Soil

Anchors and piles are some of the simplest and most commonly used methods used to support structures in permafrost areas. This paper focuses on the creep behavior of grouted anchors in ice-rich soil. Therefore the creep behavior of grouted anchors in ice-poor soil is not presented here.

As discussed before, long term pile capacity is governed by the secondary creep rate (see secondary creep state indicated in Figure 2.1) of the ice-rich soil. The creep law is introduced as a mathematical model to predict the pile capacity. Two methods of predicting the movement of anchors or piles are presented in this section.

Weaver and Morgenstern (1981) pointed out the relationship between the adfreeze shear strength and long-term shear strength in the following formula:

$$\tau_a = m\tau_{ult} \quad [2.7]$$

Where τ_a: adfreeze bond shear stress; τ_{ult}: long-term shear stress; m: parameter related to the roughness of pile surface.

And according to Mohr-Coulomb theory, the long-term shear stress can be expressed as follows:

$$\tau_{ult} = C_{ult} + \sigma tan\phi_{ult} \quad [2.8]$$

Where, τ_{ult}: long-term shear stress; C_{ult}: cohesion of frozen soil; ϕ_{ult}: friction angle of frozen soil; σ: normal stress on the shear plane.

In general, the normal stress (σ) is less than 100KPa which is very small compared with cohesion, C_{ult}. Also, the friction angle for fine grained soil is about 20º-30º, which can be ignored. Therefore, the adfreeze stress, τ_a, can be restated, by analogy, as:

$$\tau_{ult} = mC_{ult} \quad [2.9]$$

;McRoberts (1975) recommended that the flow law of ice be expressed as:

$$\dot{\varepsilon}_z = B_1\sigma_z^{n_1} + B_2\sigma_z^{n_2} \quad [2.10]$$

Where B_1 and n_1: creep parameters attained from instantaneous strain; B_1 and n_1: creep parameters attained from steady state strain; σ: normal stress; $\dot{\varepsilon}_z$: normal strain rate.

Both B and n are temperature dependent parameters. Nixon and McRoberts (1976) provided values of B and n for a range of ice temperature as shown in Table 2.1.

Table 2.1 Creep Parameters for Ice at Different Temperatures

Temperature (°C)	B_1 (Year^{-1}, psi)	n_1	B_2 (Year^{-1}, psi)	n_2
0	1.0×10^{-2}	1.34	83×10^{-8}	4
-2	5.0×10^{-4}	1.72	12.4×10^{-8}	4
-5	1.2×10^{-4}	1.92	3.5×10^{-8}	4
-11	2.0×10^{-5}	2.12	0.4×10^{-8}	4

The creep behavior for a cylindrical pile or anchor in frozen soil is similar to that in ice. It is assumed that the pile is incompressible and is under a plane strain condition in which condition the longitude normal strain and the latitude shear strain are equal to zero. For this case, Johnston and Ladanyi (1972) derived the flow law equation:

$$\dot{\gamma} = 3^{\frac{n+1}{2}} B\tau^n \qquad [2.11]$$

Where $\dot{\gamma}$: pile shear strain rate; τ: shear stress; B and n: temperature dependent parameters.

Also, the vertical shear distortion rate can be expressed as:

$$\dot{\gamma} = -\frac{d\dot{u}}{dr} \qquad [2.12]$$

Where $\dot{\gamma}$: pile shear strain rate; $\dot{u}$: pile displacement rate; r: pile radius.

Combine equation [2.11] and [2.12], one can get:

$$-\frac{\dot{d}\dot{u}}{dr} = 3^{\frac{n+1}{2}} B\tau^n$$

Nidai (1963) gave equation [2.13] to relate the shear stress at any radial distance r with the shear stress at the pile-soil interface in a weightless condition.

$$\tau = \tau_a \frac{a}{r} \qquad [2.13]$$

Where τ: shear stress at a distance of r from pile axis; τ_a: shear stress at a distance of a (which is the shear stress at pile-soil interface).

Then integrate both sides by introducing the boundary conditions that at r = a, $\dot{u} = \dot{u}_a$; at r = ∞, $\dot{u} = 0$.

$$\dot{u}_a = \frac{3^{\frac{n+1}{2}} B\tau^n}{n-1} \qquad [2.14]$$

Where $\dot{u}_a$, n, B and τ have the same meaning as in equation [2.11-13].

Compared with equation [2.10], the final relationship between displacement rate and shear stress should have a similar form as:

$$\dot{u}_a = \frac{3^{\frac{n_1+1}{2}} B_1(\tau_a\frac{a}{r})^{n_1}}{n_1-1} + \frac{3^{\frac{n_2+1}{2}} B_2(\tau_a\frac{a}{r})^{n_2}}{n_2-1} \qquad [2.15]$$

Therefore, using equation [2.15], it is possible to relate the steady state displacement rate to the shear stress at the interface of soil and pile.

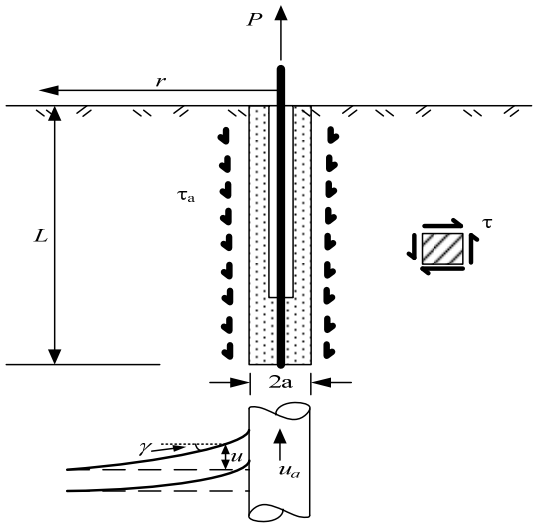

Figure 2.2 Schematic Plot of Shear Stress and Strain in Frozen Soil

Another approach is the isochronous method. This method converts a non-linear visco-elastic-plastic problem into a non-linear elastic-plastic problem. Landayi (1972) introduced this method. A set of Mohr circles at failure could be derived from a repetitive uniaxial tension and triaxial compression tests. Each circle represents a single failure and Fairhurst (1964) expressed the resulting parabolic failure line connecting across the circles by:

$$\tau = \frac{s-1}{r}\sigma_{fu}[1 + r(\frac{\sigma}{\sigma_{fu}})]^{\frac{1}{2}} \quad [2.16]$$

Where r: the ratio of uniaxial compression creep strength to uniaxial tensile strength; s: $s = (r+1)^{\frac{1}{2}}$; σ_{fu}: ultimate normal stress under uniaxial compression strength; σ: applied normal stress.

Vialov (1962) pointed out that the shape of the parabolic line remained the same even though the position would change with temperature and time. And, the values of r and s did not change substantially. In this situation, normal stress was considered as a function of time and temperature. Therefore, the shear stress in equation [2.16] could be rewritten as:

$$\tau = \frac{s-1}{r}\sigma_{fu}(t,\theta)[1 + r(\frac{\sigma}{\sigma_{fu(t,\theta)}})]^{\frac{1}{2}} \quad [2.17]$$

The parabolic failure line was often replaced by a straight line for the practical purposes and could be written as:

$$\tau = c(t,\theta) + \sigma tan\phi = [H(t,\theta) + \sigma]tan\phi \quad [2.18]$$

Where H (t,θ) =c(t,θ) •cotϕ; $c(t,\theta) = \frac{\sigma_{fu}(t,\theta)}{2\sqrt{f}}$; f: flow value, defined as: $f = \frac{1+sin\phi}{1-sin\phi}$; σ: normal stress; τ: shear stress.

In terms of principle stress, the stress difference at failure is:

$$(\sigma_1 - \sigma_3)_f = \sigma_{fu}(t,\theta) + \sigma_3(f-1) \quad [2.19]$$

Where σ_1, σ_3: normal stress; subscription f indicates the normal stress is at failure state.

If we assume the Mohr-Coulomb failure criteria is also valid for the pre-failure stage, the time and temperature dependent uniaxial stress is:

$$\sigma_f(t,\theta) = \sigma_{cu0}(\frac{\dot{\varepsilon}_f}{\dot{\varepsilon}_c})^{\frac{1}{n}} f(\theta) \quad [2.20]$$

Where σ_f: time and temperature dependent normal stress at failure, a function of time and temperature; σ_{co}: normal stress at 32°F (0°C); θ: absolute value of temperature below freezing point; $\dot{\varepsilon}_f$: shear strain rate at failure; $\dot{\varepsilon}_c$: constant number relating to the applied load; f (θ): temperature function.

Equation [2.24] can be rewritten as:

$$(\sigma_1 - \sigma_3) = \sigma_{cu0}\left(\frac{\dot{\varepsilon}^{(c)}}{\dot{\varepsilon}_c}\right)^{\frac{1}{n}} f(\theta) + \sigma_3(f-1) \quad [2.21]$$

Then the creep strain can be derived from equation [2.24] by integration of the steady state creep rate:

$$\varepsilon^{(c)} = \dot{\varepsilon}_c t[\frac{\sigma_1 - f\sigma_3}{\sigma_{cu0} f(\theta)}]^n \quad [2.22]$$

Where $\varepsilon^{(c)}$: creep strain; $\dot{\varepsilon}_c$: constant related to minimum steady state strain rate.

However, equation [2.22] could not fully demonstrate the whole pre-failure stage. One assumption is that only strength is dependent of normal pressure rather than the whole stress-strain behavior. Therefore, the creep behavior before failure can be described by the power law which is dominated by the steady state creep rate as shown by Odquist and Hult (1962):

$$\dot{\varepsilon}^{(c)} = \dot{\varepsilon}_c (\frac{\sigma_1 - \sigma_3}{\sigma_{cu}})^n \quad [2.23]$$

Thus, the whole creep behavior including the pre-failure stage and failure stage could be described by combining use of equations [2.22] and [2.23].

Chapter 3 Laboratory Test

This chapter focuses on the laboratory load tests for grouted anchors. Section 3.1 mainly discusses frozen soil preparation (anchors were installed in artificial "permafrost" material for testing), test equipment preparation, and preparation of the anchors themselves for testing. Section 3.2 describes the test procedure in detail. Section 3.3 presents the results of nineteen anchor load tests covering various conditions of load, soil temperature, and soil moisture content.

3.1 Laboratory Pullout Test Preparation

1. Soil Preparation

The ice silt slurry, needed to simulate anchor embedment soil in this test, was made by mixing dry silt with water and fine ice particles or snow in a 19 liter (5 gallon) bucket. The weight of ice or snow was 20%-40% of the total moisture by weight. After mixing the three components, the slurry was poured into a 190 liter (50 gallon) barrel and frozen in a cold room at a temperature of 14°F (-10°C). Adding ice to the soil slurry mixture prevented non-homogeneity of the mix caused by particle settling. The addition of ice also reduced the time needed to freeze the soil slurry. The testing slurry was prepared with three different moisture contents (50%, 80% and 120% by total weight) in order to evaluate the effects of moisture content on anchor behavior.

Figure 3.1 and Figure 3.2 show the material used to mix the soil slurry and the mixing process. The dry silt was collected from the permafrost tunnel floor in the Cold Regions Research and Engineering Laboratory (CRREL). The silt contained a 5%-10% organic component and also a medium to fine sand component (mostly between sieves #100 and #40) of less than 5%. Other physical properties of the silt are listed in Table 3.1 as follows:

Table 3.1 Physical Properties of Mixing Silt

Physical Property	Plastic Limit	Liquid Limit	Specific Gravity
Measured Value	34%	38%	2.68

Figure 3.1 Materials for Remolding Ice-rich Silt

Figure 3.2 Soil Mixing Process

2. Grouted Anchor Preparation

The grouted anchor used in this test had two lengths which were 24 in (610 mm) and 21 in (533 mm). And the diameter for both two types of anchors was 4 inch (101.6mm). DSI (DYWIDAG System International) threaded bars were used as the anchor tendons. The detailed configuration is shown in Figure 3.3.The threaded bar was 1.38 in (35.05 mm) in diameter with an effective cross section area of 1.495 in^2 (964.5 mm^2) and a unit weight of 5.56 lb/ft (8.27 kg/m). The yield load and ultimate load for the threaded bar was 189 kips (840 KN) and 237 kips (1,054 KN), respectively.

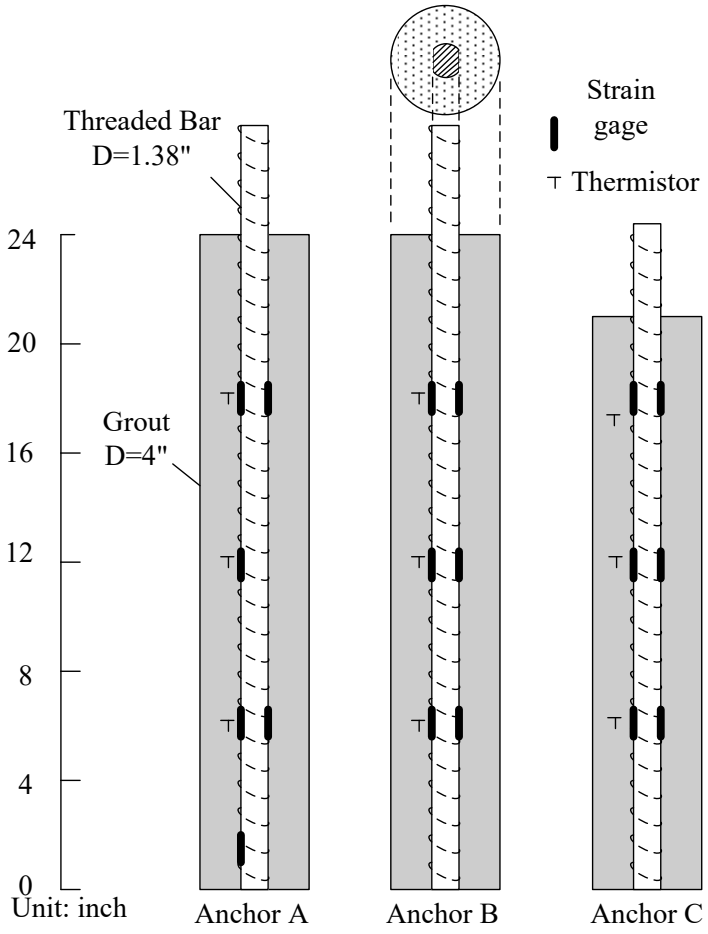

Figure 3.3 Schematic Plot of Tested Anchors

Portions of the threaded bars were ground flat to provide areas suitable for mounting strain gages. Thermistors were also installed in order to measure temperatures along the anchors. All the thermistors were calibrated in ice-water mixture before conducting pullout tests. Some of the strain gages performed poorly during the laboratory testing process because of damage caused by handling the anchors.

Figure 3.4 shows the anchor fabrication process. The grout slurry was made by adding 5.28 gallon (20 liter) of water to 50 lb (22.7 kg) of grout cement in order to make a flowable mixture. First, the thread tendon was placed into the plastic mold and fixed at the center of the mold. Then the non-shrink grout was hand-mixed with water and poured into the plastic mold to form the anchor. During this process, a rubber mallet was used to tap the mold so that the grout filled all of the available volume.

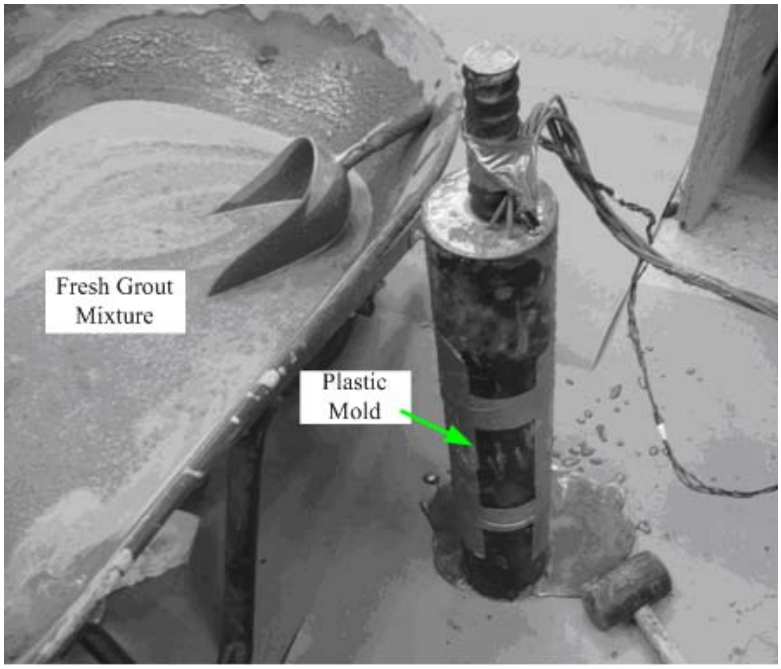

Figure 3.4 Fabrication of Test Anchor

Figure 3.5 shows three anchors after backfilling with cement. In general, the anchors were smooth surfaced except for rough areas reflecting mold imperfections. The anchors were first cured in a damp and warm place for three days. After the initial curing period, the molds were stripped from the anchors. The anchors were then cured for another four days in a water bath. Meanwhile, other grout samples were made in order to determine grout tensile strength. Results indicated that grout tensile strength ranged from 480 psi (3,309 KPa) to 626 psi (4,316 KPa).

Figure 3.5 Configuration of Tested Anchors

3. Load Frame Preparation

The load frame used in the test is shown in Figure 3.8. General load frame largest dimensions are 50 in (1,270 mm) high by 50 in (1,270 mm) deep. The major components of the load frame in testing configuration include: 1. Weights, 2. Lever arm, 3. Steel chain, 4. Main beam, 5. Reaction beams, 6. LVDT stand, 7. Flat steel bar, 8. Frozen silt, 9. Barrel and 10. Columns. Table 3.2 gives detailed information about the load frame elements. The main beam of the frame is supported by four columns and the lever consists of two channel beams. The lever arm ratio is 10:1 and is bolted to the main beam by a flat plate. The steel chain connects the end of the lever arm with a hex nut on top of the anchor. Two sets of perpendicular beams (labeled 5 in Figure 3.6) keep the barrel/soil/anchor assembly in place during testing. The design pullout capacity of the test frame is 7 kips (31 KN), corresponding to a 26.5 psi (183 KPa) shear stress for 21 in (533 mm) anchor and 23.2 psi (160 KPa) shear stress for 24 in (610 mm) anchor .

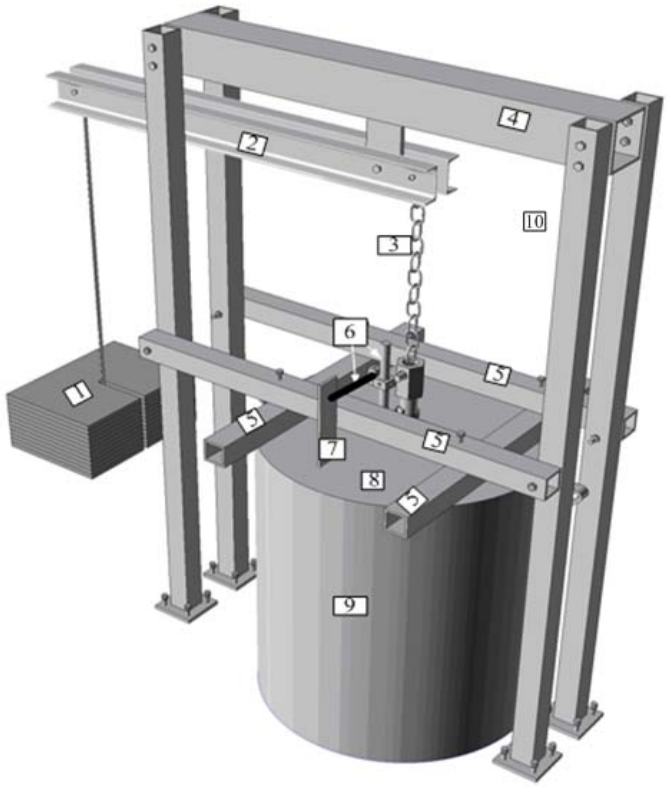

Figure 3.6 Schematic Plot of the Loading Frame

Figure 3.7 illustrates the sections of the principle elements in the load frame.

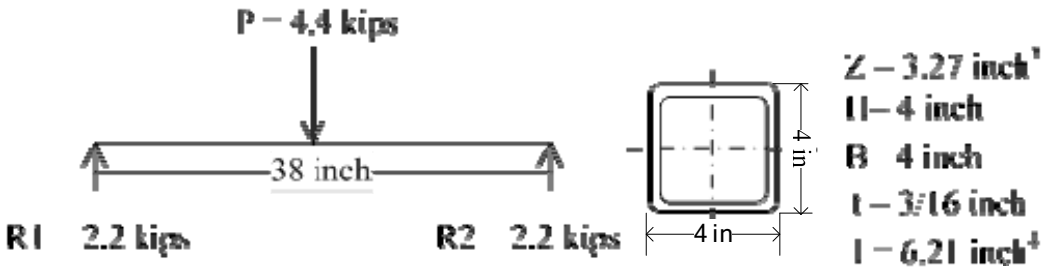

(a) Section of the Main Beam (4)

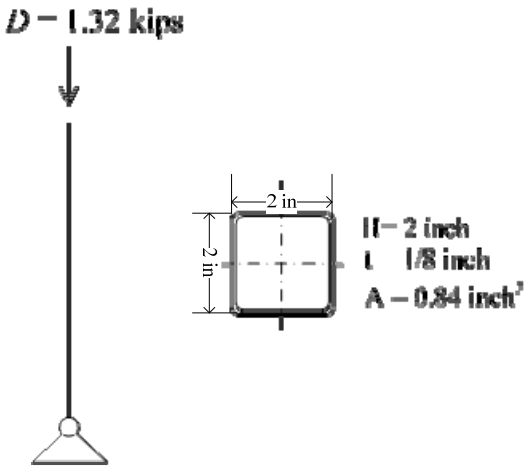

(b) Section of the Column

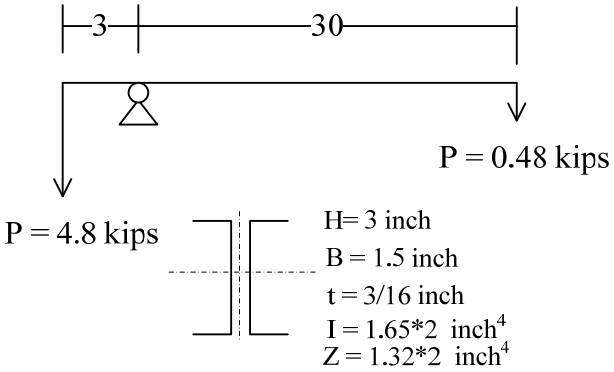

(c) Section of the Column of the Lever (2)

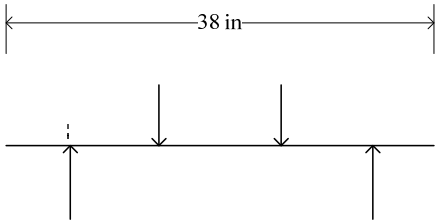

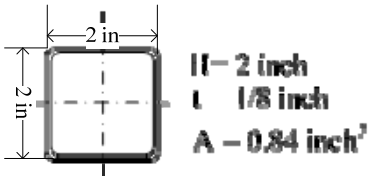

(d) Section of the Reaction Beam (2)

Figure 3.7 Schematic Plot of the Main Components of Loading Frame

Table 3.2 Summary of Load Frame Elements

Parts	Beam Type	Section (in)	Weight (lb/ft)	Length/Piece (in)
Main Beam	Box Beam	$4\times4\times\frac{3}{16}$	8.80	38
Columns	Box Beam	$2\times2\times\frac{1}{8}$	3.04	50
Lever	Channel	$4\times4\times\frac{1}{8}$	4.75	36
Reaction Beam	Box Beam	$2\times2\times\frac{1}{8}$	3.04	38

4. Calibration of the Testing Equipment

In order to minimize the effect of temperature on the test results and improve the measurement accuracy, calibration tests were performed prior to testing of anchors. These included load frame calibration, LVDT calibration, and thermistor calibration. All the calibration tests were conducted at two temperatures: at a cold room temperature of 30.2°F (-1°C) and at a 73.4°F (23°C) room temperature. In general, the effects of the temperature (for this range of temperatures) were found to be so small that variations in the temperature of the testing equipment could be ignored during the anchor tests.

Figure 3.8 shows the calibration curves for the lever arms in three test frames.

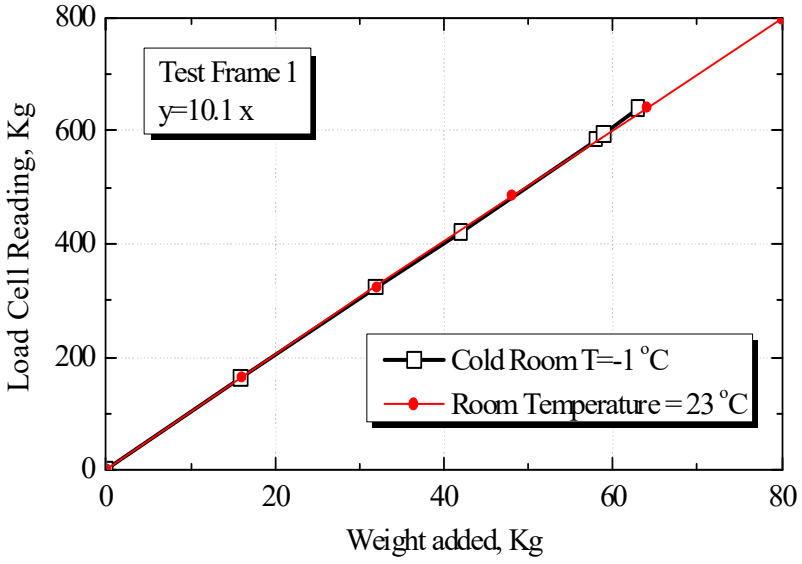

(a) Calibration Curves for Test Frame 1

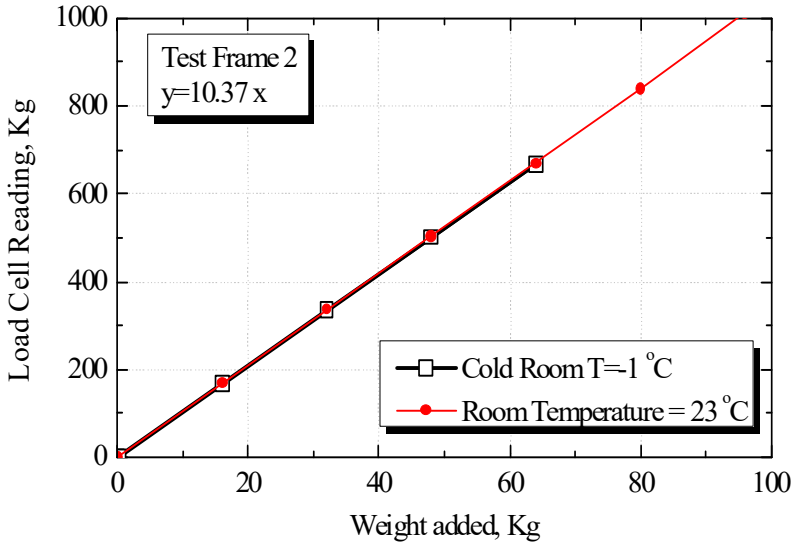

(b) Calibration Curves for Test Frame 2

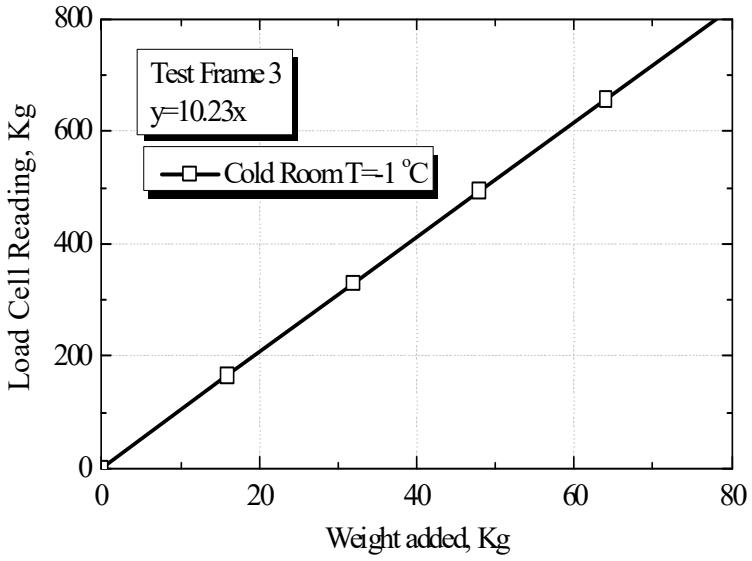

(c) Calibration Curves for Test Frame 3

Figure 3.8 Calibration Curves for Test Frames

The displacements during these tests were measured by LVDTs which were certified as having thermally induced variations, over the manufacturer's stated temperature range, smaller than 0.003%, and a resolution of ±0.001 inch (±0.025mm) after calibration. The working temperature range was -4°F (-20°C) to 176°F (80°C).

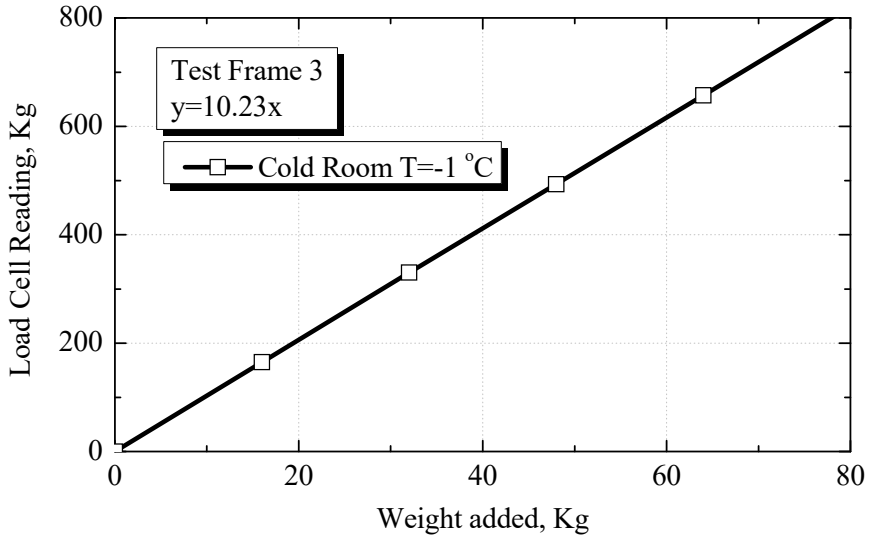

Figure 3.9 Calibration Curve for LVDT in Cold Room

3.2 Laboratory Pullout Test Procedures

1. Preparing Anchor Test Specimens

Two methods were evaluated for installing the pre-made test anchors in the laboratory-mixed frozen slurry that represented permafrost foundation soil, i.e., preparing the anchors for testing. The first method is indicated in Figure 3.10. In this case, the anchor was held in place in the middle of the barrel, and then the laboratory-made, simulated "permafrost" mix was poured into the barrel layer by layer. Sufficient time was required for each layer to freeze thoroughly before adding the next layer. Each layer was about 4 inches thick and compacted by a hand during placement. Finally, the anchor with the completed layerings of simulated permafrost was placed in the cold room for about 2 days at the temperature of 14°F (-10°C). This method of making test anchors quickly proved unsatisfactory. Preliminary tests to evaluate this preparation method found that it produced very little shear strength between the anchor and the surrounding simulated permafrost. The reason for the poor result using the layered-fill technique remains unknown, but the method was abandoned for making additional anchor test samples. Using this test sample preparation method, preliminary tests measured only 2.3 psi (159.9 KPa) in shear stress at 30.8°F (-1°C).

Figure 3.10 Layered Installation Method for Grouted Anchor

The second method of preparing test anchor specimens required two steps: 1) drilling an 8 in (203 mm) diameter hole in the center of a barrel filled with previously frozen simulated permafrost, then 2) placing the anchor in the center of the hole, and backfilling the annular space with ice-rich silt slurry. Details of making such a hole and backfilling with slurry is discussed below.

The barrel full of frozen material is placed horizontally and a stream of hot water is used to thaw material from the center of barrel and form approximately an 8 inch (203 mm) diameter hole as shown in Figure 3.11. This was done for previously made anchor test specimens, where the anchor was removed using the hot water and the hole further expanded (to a full 8 inch diameter) with hot water. Had the anchor test specimens not already been prepared the first (unacceptable way) it would have been even easier to create the 8 inch (203 mm) diameter hole by filling a barrel, containing at its center a hollow 8 inch (203 mm) diameter plastic or metal cylinder, with the simulated permafrost. After the material had frozen, the cylinder could be filled with hot water and then easily removed from the barrel, thus creating the required 8 inch (203 mm) diameter hole.

Figure 3.11 Oversize Hole before Installation of Grouted Anchor

After the hole was made, the anchor was placed in the center of the hole and the annulus backfilled with ice-rich silt slurry (at same moisture content as surrounding frozen material). While the annulus was being filled, a steel bar was used to stir the backfill slurry. Figure 3.12 shows the process of placing the ice-rich silt slurry into the annulus. Then the nearly-ready test specimen was placed into a cold chamber for 2 to 3 days at the temperature of 14°F (-10°C).

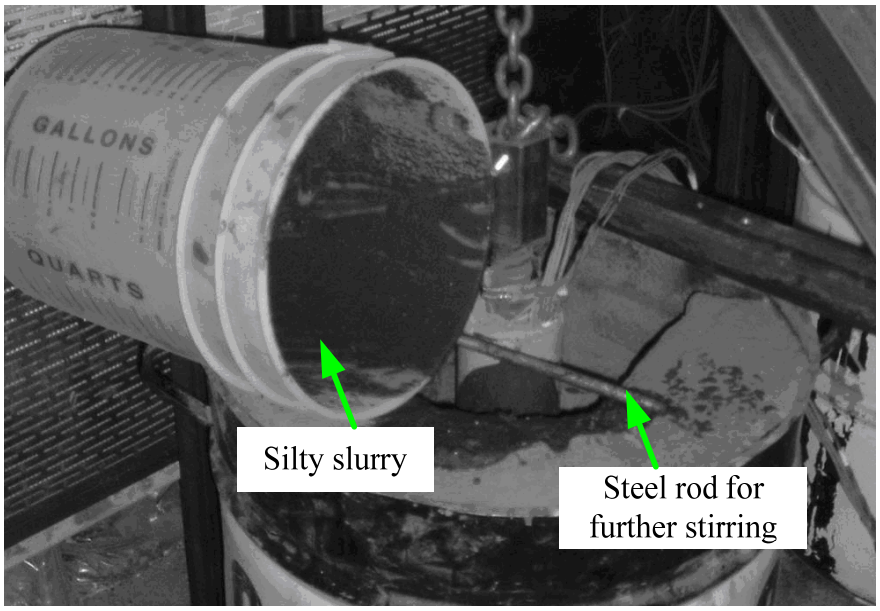

Figure 3.12 Process of Backfilling the Hole with Slurry

2. Load Frame Setup

The load frame system is shown in Figure 3.13. The system includes load frame system and data acquisition system. Three load frame systems were built. The dimension for the tested anchor is 4 inches (101.6 mm) in diameter and 24 inches (610 mm) in length so that the length-diameter ratio is 6.

The anchor was first fixed in the center of the 50 gallon (189 liter) barrel using the second anchor specimen preparation method described in anchor preparation process. The load added to the weight plate was transferred, 10 fold, through the lever to the anchor. The load capacity of the frame was around 6.5 kips.

The data acquisition system included a Linear Variable Differential Transducer (LVDT) with an accuracy of 0.001inch, a dial gage to measure the load added to the steel bar and data logger to record the strain along the bar. For the LVDT, it was connected to a base which was fixed on the anchor tendon and the other side was fastened by a magnetic holder which embedded into the frozen soil at a depth of 4 inches through a flat steel bar. The distance between the anchor tendon and the flat steel bar was 5 inches in order to ensure that there was no relative displacement between the LVDT and the anchor.

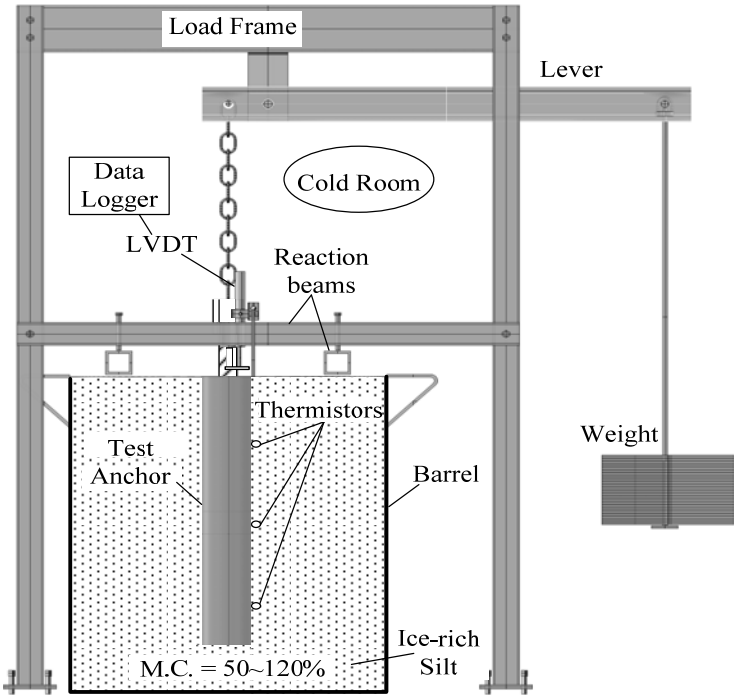

Figure 3.13 Schematic Plot of Loading Frame System

All the anchor load tests were conducted in the cold room laboratory of the Department of Civil and Environmental Engineering at the University of Alaska Fairbanks. Figure 3.14 shows the layout of the test equipment in the cold room. Three testing systems performed simultaneously with three different moisture contents. The temperature for those three testing systems was the same so that the test results were more comparative.

3. Testing Procedure Outline

The testing procedure is generalized as follows:

1. Prepare grouted anchor test specimen;
2. Backfill soil slurry with different moisture content preparation;
3. Load frame system setup and installation;
4. Equipment calibration test;
5. Anchor load test;
6. Collect test data.

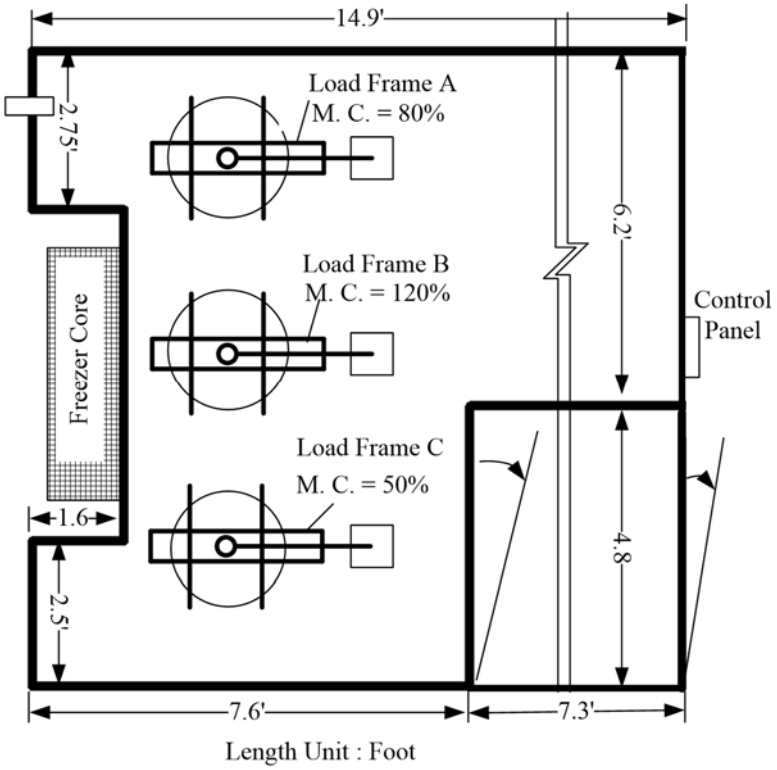

Figure 3.14 Layout of Testing Equipment in Cold Room Laboratory

Chapter 4 Field Tests of Anchor in CRREL Permafrost Tunnel

This chapter:

- Describes the field test site—the CRREL permafrost "tunnel" near Fox, Alaska
- Introduce the HPI Full Bridge sensors and Geokon vibrating sensors
- Describes the drilling process and sensor installation methods
- Describes the loading system setup process
- describes the data acquisition system

4.1 Test Site Overview

1. Introduction to Testing Site

Field testing was conducted in the CRREL (Cold Region Research and Engineering Laboratory) permafrost tunnel, located near Goldstream Creek, 16 miles north of Fairbanks near Fox, Alaska. Figure 4.1 provides an aerial view showing the specific location of CRREL tunnel. The tunnel is located in an area of discontinuous permafrost, near the confluence of Goldstream and Glenn Creeks. Material exposed in the permafrost tunnel has been frozen for tens of thousands of years. The tunnel entrance is located on the eastern side of Goldstream Creek Valley. The long axis of the tunnel lies at an elevation just below the original (pre-dredge mining) floor of Goldstream Valley.

The popularly-named permafrost "tunnel" is actually an adit because it is open at just one end. It is composed of two parts, both excavated by the U.S. Army Corps of Engineers in the early 1960s. One is the nearly horizontal main passage extending from the surface into the hill side, and the other is the inclined winze that extends downward from the right side of the main passage. The main passage is approximately 330 ft (110 m) in length, 6 ft (2 m) to 27.5 ft (2.5 m) in height, 12 ft (4 m) to 15 ft (5 m) in width. Much of the main passage lies roughly 45 ft (15 m) below the surface. The winze is about 135 ft (45 m) in length, beginning about 90 ft (30 m) from the tunnel entrance. The winze extends downward at an incline of 14% through silts, a gravel layer and then into weathered bedrock. Figure 4.2 is the cross section diagram of the tunnel. Extending down the middle of the floor of the main passage is a 4.25ft (1.42 m) wide steel-grate walkway. There is approximately 5 ft (1.67 m) between the edges of the walkway and the tunnel sides. Figure 4.3 shows the layout of the passage.

Figure 4.1 CRREL Tunnel Location

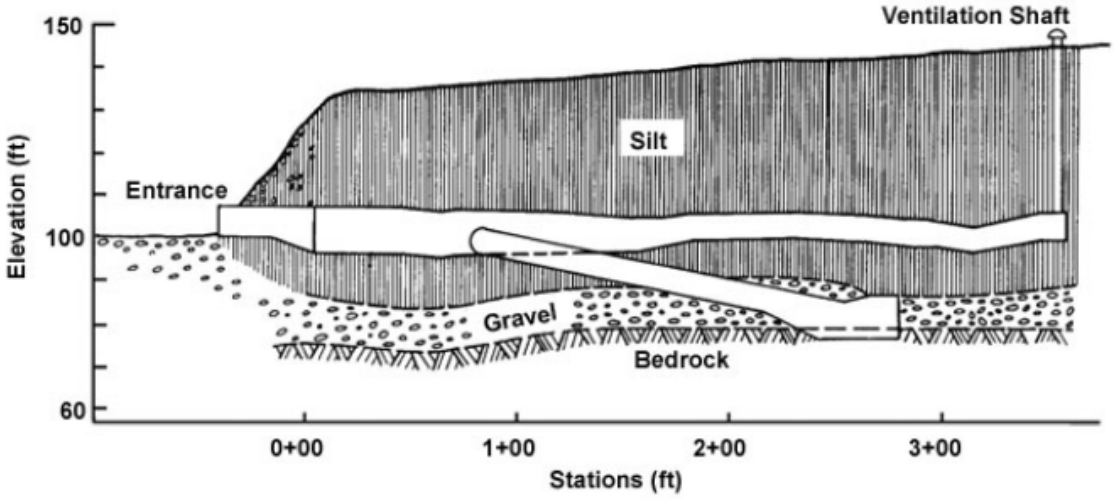

Figure 4.2 Schematic Plot of Cross Section Diagram of the CRREL Tunnel

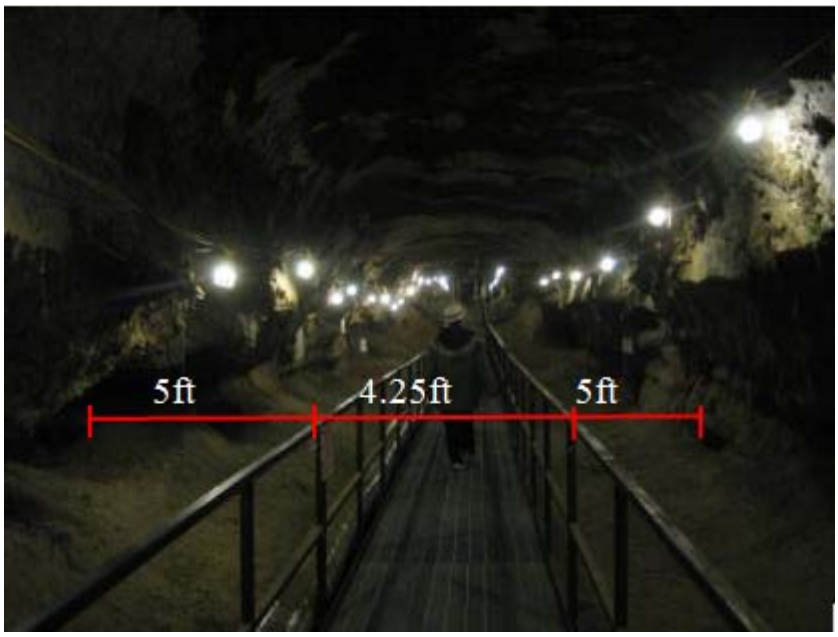

Figure 4.3 Layout of Adit in CRREL Tunnel

2. CRREL Permafrost Tunnel Geology

The soil and rock types exposed in the tunnel are typical of many locations in the Yukon-Tanana Upland region. Bedrock is the estimated 550 year old Precambrian Birch Creek Schist. Overlying the schist bedrock is a 6 ~ 8 ft (2 ~ 2.67 m) layer of Fox gravel. The Fox gravel consists of sub-angular to round aggregate material up to 6 in (152 mm) size (actually cobble size) and wood fragments. The gravel layer is overlain by a thick layer of silt belonging to the Goldstream Formation and a thin silt layer attributed to the Ready Bullion Formation. Both layers of silt are the result of wind and stream deposition. Retransported silt materials found in the permafrost tunnel contain a high volume of ice and also organic material that emits a strong musty odor of decomposition. During ice age times, the cold Fairbanks area was surrounded by glaciers that provided silt and the windy interior Alaska conditions that allowed syngenetic permafrost to develop. The Tanana River floodplain which contains the washout from glaciered areas in the Alaska Range is the main source of windblown silt found in the tunnel. A variety of ground ice types, such as ice wedges, thermokarst cave ice and ice lenses are exposed in the walls of the tunnel. Also exposed at many locations in the tunnel walls are animal fossils and plant remains.

The frozen moisture contents of materials found in the permafrost tunnel vary widely. The gravimetric moisture content of weathered schist (found in a portion of the winze called the Gravel Room) ranges from 6.5% to 19.9%, averaging 11.7%. Sediments with an organic content of 9-

12% may have gravimetric moisture contents in the range of 70-80% while the frozen silt containing cryostructures (visible icy structures, at centimeter scale, within the soil) may commonly exhibit moisture contents of 110-140%. Recent study indicates that cryostructure plays an important role in silt ice content. For sediments with micro-lenticular cryostructure, which are mostly found in the main passage, the gravimetric ice content varies from 80% to 180%. For modified sediments with structureless cryostructure, the gravimetric moisture content varies from 50% to 95%.

3. Anchor Test Location within Permafrost Tunnel

The area selected for anchor tests in the permafrost tunnel is on the right hand side of the tunnel's main passage at a location extending between 99 ft (33 m) and 165 ft (55 m) from the entrance. Vertical section, plan view diagrams and test anchor configuration are shown in Figure 4.4, 4.5 and 4.6, respectively. A total of seventeen anchors were installed. Three types of anchors were tested including: solid steel bar anchors, hollow-core steel anchors and duckbill anchors. In general, the duckbill anchors were installed farthest from the entrance, the solid steel anchors closest to the entrance, and the hollow steel anchors in between.

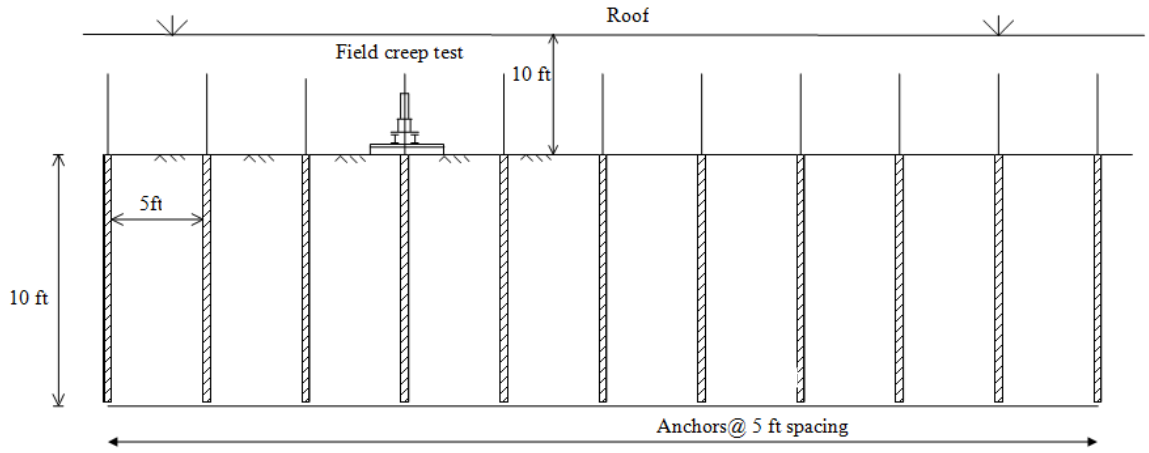

Figure 4.4 Cross Section Portion of Test Area

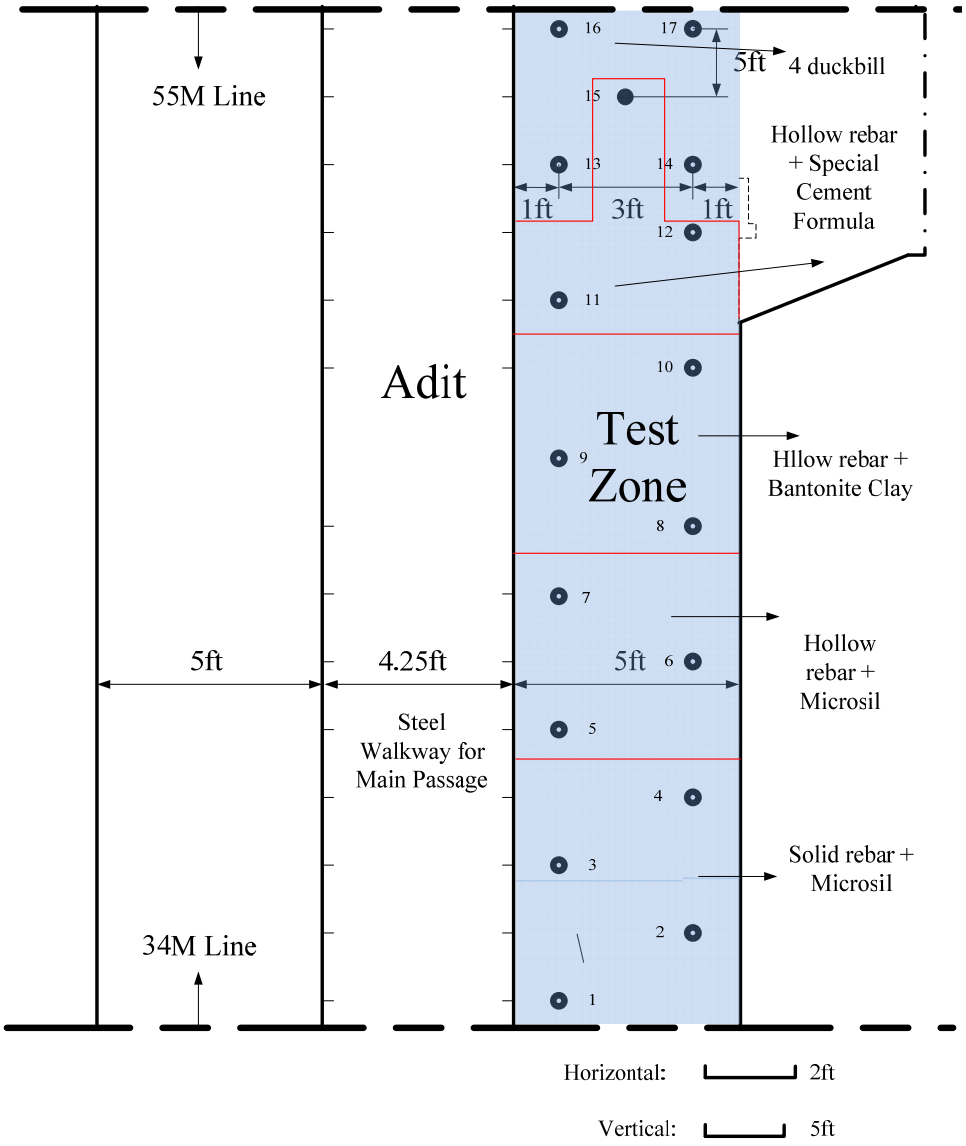

Figure 4.5 Test Anchor Layout Plane View

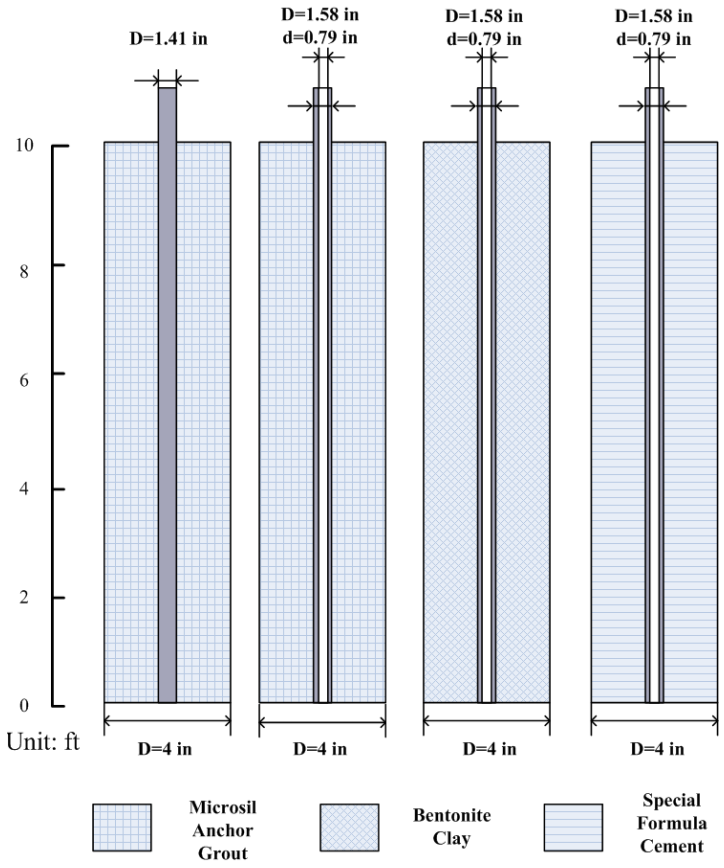

Figure 4.6 Test Anchor Configuration

4.2 Testing Equipment

Figure 4.7 is a diagram of the anchor with sensor locations shown. The Geokon Model 4200 Vibrating Strain Gage was used to measure strain in the grout. The HPI Full Bridge Weldable Strain Gage was used to measure the strain in the anchor rods and temperature at the periphery of the rod. An Omega LVDT was used to measure anchor displacements. The pull-out load was controlled by a constant-pressure hydraulic jack. Figure 4.7 indicates locations of the various sensors with respect to a typical test anchor.

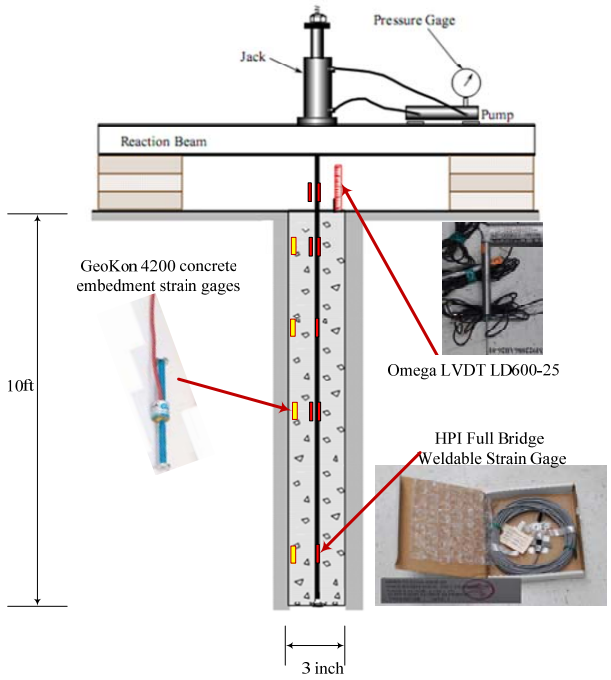

Figure 4.7 Schematic Plot of the Testing System

1. Strain Sensors

The HPI strain gage, shown in Figure 4.8, was used to measure the strain in the steel anchor bars. This weldable strain gage was easy to install and use. This strain gage has four arm bridges which ensure outstanding stability and temperature compensation. The HPI strain gage also eliminates lead wire errors and gives a high sensitivity by providing double the output of a standard gage. Moreover, HPI strain gage is completely pre-wired and waterproof.

The Geokon Model 4200 Vibrating Wire Strain Gage is designed primarily for long-term strain measurements in a concrete mass, as in structures such as foundations, piles, bridges and dams. The Geokon gage is shown in Figure 4.9. These vibrating wire strain gages are known to have excellent long-term stability, maximum resistance to the effects of water, and a frequency output suitable for transmission over very long cables.

Figure 4.8 HPI Strain Gage

Figure 4.10 provides a detailed schematic of the Geokon Vibrating Wire Strain Gage. A length of steel wire is tensioned between two end blocks to measure the strain. The end blocks are firmly in contact with the concrete mass (being actually incased within the concrete mass itself). The distance between the end blocks will change if the concrete mass is deformed which will produce a change in tension of the steel wire. This change in tension is measured as a change in the resonant frequency of the vibrating wire. Electromagnetic coils located close to the gage wire excite the wire and the wire's response frequency is measured. A formula is then used to calculate deformation based on the measured frequency.

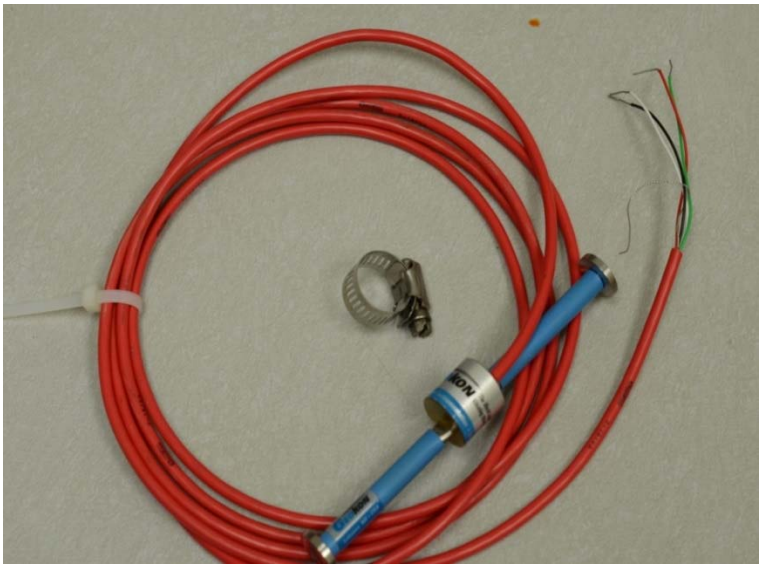

Figure 4.9 Geokon Vibrating Strain Gage

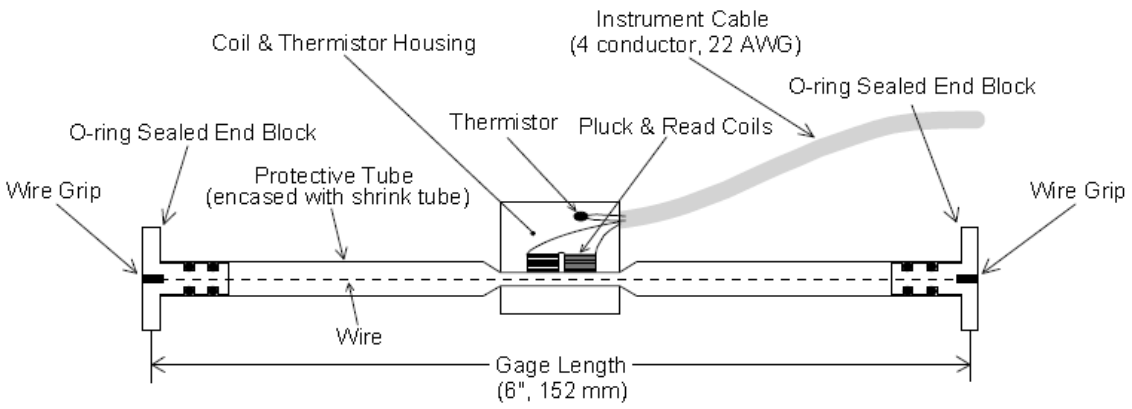

Figure 4.10 Schematic Plot of Components of Geokon Strain Gage

The major advantage of using this type of vibrating strain gage is that it exhibits long term stability. This sensor also contains a thermistor which can be used to measure the temperature at the gage location. Other advantages of using a vibrating strain gage are that wire resistance does not affect the measurements and the returning signal is in the form of frequency rather than voltage level. However, a vibrating strain gage cannot be used to measure dynamic strains in a system where dimensional changes are relatively rapid. On the negative side, these gages are more bulky and expensive than other strain gage types.

2. LVDT

Omega Model LD600-25 LVDT was used during testing to measure the displacement of anchor in response to load. An LVDT is a device that produces an output voltage proportional to mechanical displacement. The LVDT described here contains three coils, i.e., one primary coil and two secondary coils. The primary coil is where the converted DC voltage is applied. One of the secondary coils generates a voltage that corresponds to the change of position of magnetic core. The remaining coil generates zero voltages for the output. A conceptual schematic of LVDT components is shown in Figure 4.11.

Figure 4.11 Omega Model LD600-25 LVDT

4.3 Borehole Drilling Process

1. Drilling Borehole and Drilling System Layout

Seventeen boreholes were drilled in the permafrost tunnel for placement of test anchors. The borehole layout has been shown previously in Figure 4.5. As shown in that figure, 13 of the boreholes received steel bar anchors for the creep testing. The other four are used for duckbill anchor tests. Four inch diameter boreholes were used for the steel bar anchors (all holes 10 feet deep) and 2 inch boreholes for the duckbill anchors (all holes 6 feet deep). For 13 steel bar anchors, there were 3 different types of backfill materials. These included Microsil Anchor Grout, Bentonite Clay and a Special Cement Formula as shown in Figure 4.12.

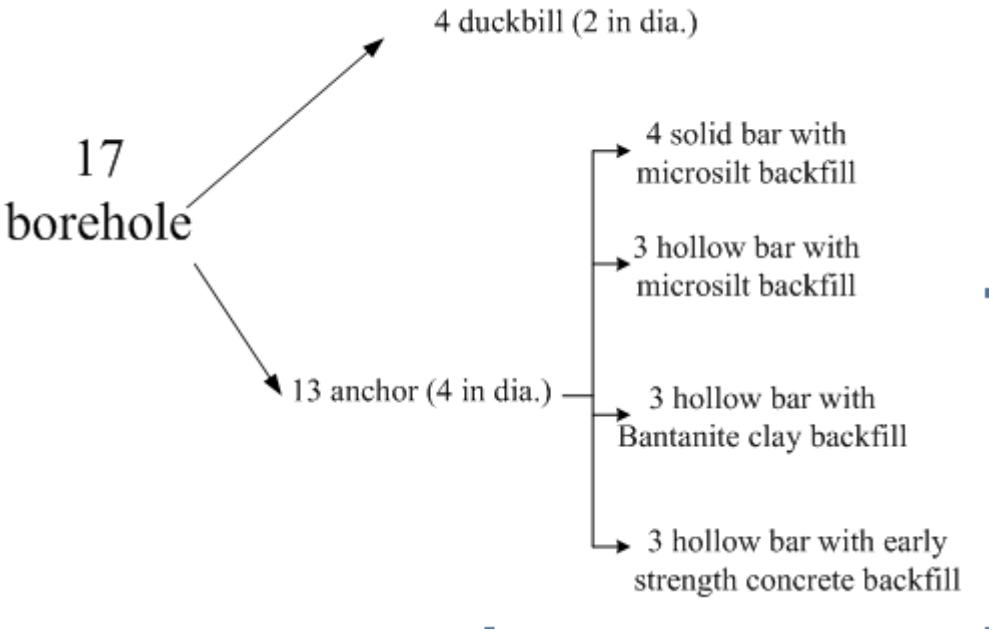

Figure 4.12 Rebar and Backfill Material Design

The main items of drilling equipment consisted of the drill itself, hydraulic pumps and lines, and the power supply.

The drilling machine used in the permafrost tunnel was a Model MP260 manufactured by the TEI Rock Drill Company. The MP260 is a man-portable, 2-wheeled, hydraulically powered drill weighing about 450 lbs (205 kg). Information concerning the size of the drill, including working dimensions, is provided in Figure 4.13. The base of the drill is equipped with leveling screws to maintain plumb alignment while drilling verticaly. The drill was powered by a diesel power unit located outside the tunnel, to the right side of the entrance. The power unit is shown in Figure 4.14 (a). Hydraulic lines transferred power from the power unit to the drill. An air compressor was located outside and to the left of the entrance. The compressor provided compressed air to the vicinity of the drill bit that kept the hole blown free of loose chunks of material. Figure 4.14 (b) shows the portable air compressor unit.

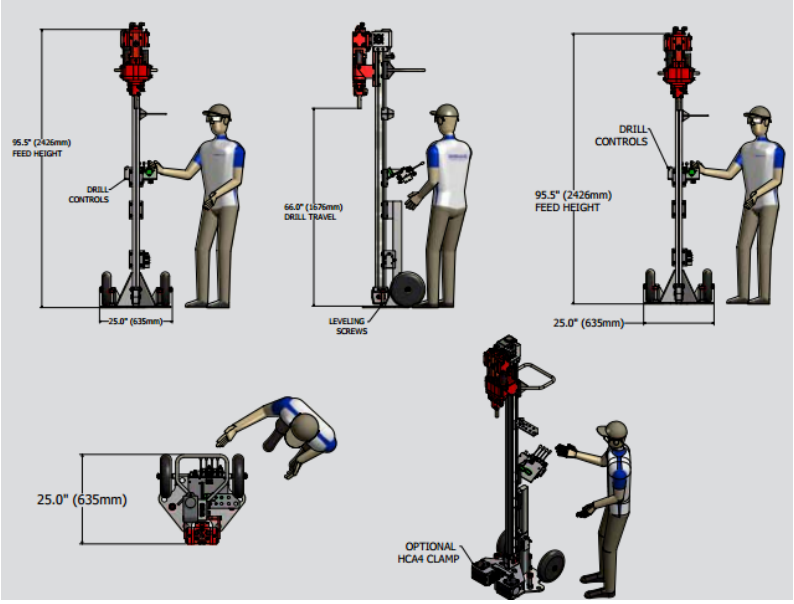

Figure 4.13 Schematic Plot of MP260 TEI Drilling Machine

(a) Diesel Power Supply Unit **(b) Air Compressor**

Figure 4.14 Power Supply and Air Compressor for Drilling Machine

The hydraulic and pneumatic lines entered the tunnel through a hole on the right side of the tunnel entrance. The line access hole is shown in Figure 4.15 and a schematic of the drilling system layout is shown in Figure 4.16. It was necessary to keep all of the aforementioned lines unobtrusive and in tidy alignment within the tunnel to minimize tripping hazards and to maintain a neat appearence.

Figure 4.15 Open Hole for Hydraulic and Compressed Air Lines

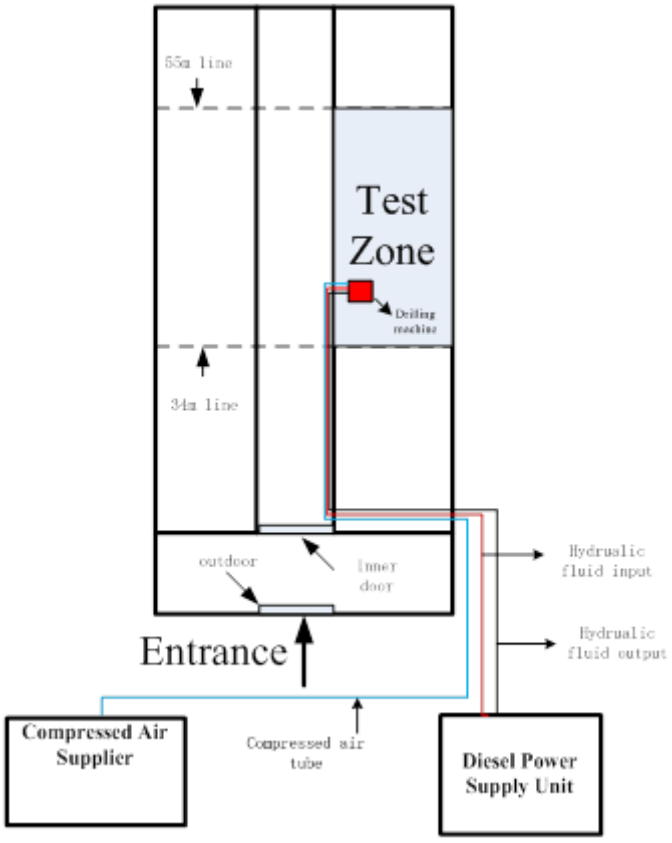

Figure 4.16 Layout of Drilling System

2. Drilling machine setup

Drilling began with boreholes nearest the steel walkway as shown in Figure 4.17. When the drill was in place for each hole, a rod (which had been welded to the top of the drill) was wedged against

the tunnel ceiling to prevent the drilling machine from shaking back and forth or moving vertically. And at the bottom of the drill, the two leveling screw used to plumb the drill. Three lines were connected to the drill head. Two were hydraulic lines that provided drilling power, and the other was a compressed air line for keeping the hole clear. Figure 4.17 shows various aspects of the drill set up.

At the ground surface, there was about a 3~4 in (76~101 mm) dust layer. Before setting up the drill, loose dust within the working area was cleared away. Some of the ground surface, especially at the right side of the test zone, is not flat and the surface was icy. Pieces of board were used as dunnage to fill spaces under the drill and help level it.

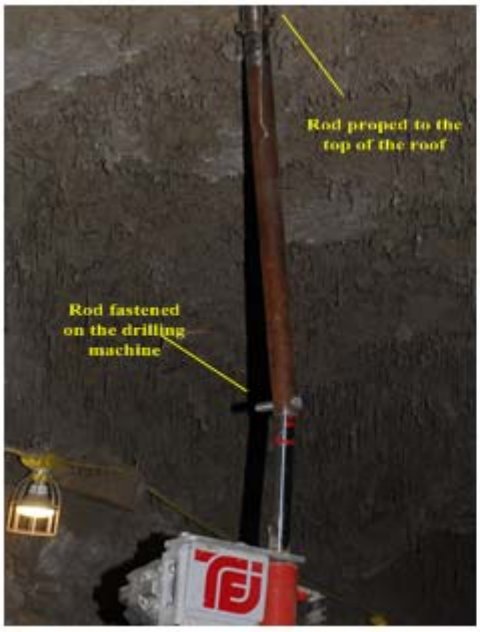

(a)

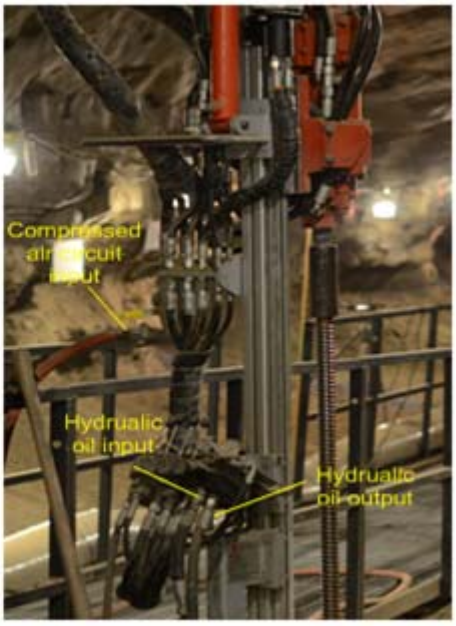

(b)

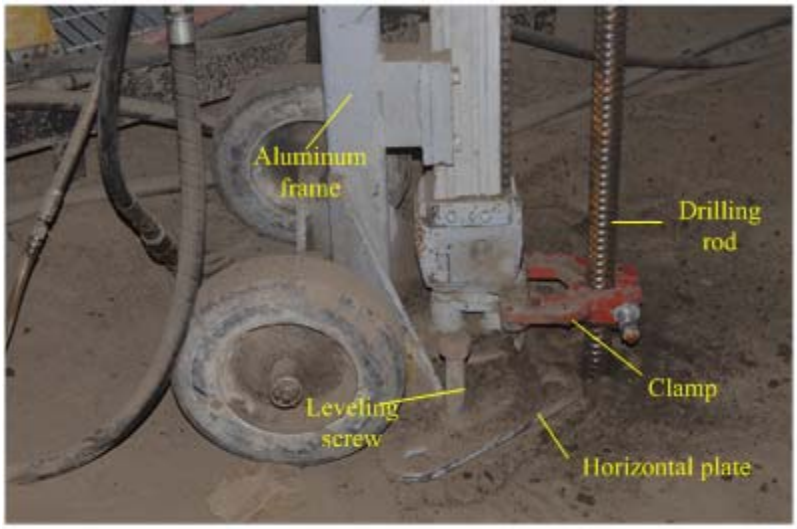

(c)

Figure 4.17 Drill Setup

3. Drilling procedure

After set up, the drilling process began. One end of a 5 ft (1.67 m) hollow bar (drill rod) is connected to the drill head with a coupling device and the drill bit was attached other end of the drill rod. At the start of the drilling process, driller's assistant gripped the drill rod and placed the drill bit at the exact spot to begin drilling. The driller then advanced the drill bit into the soil about 2~4 in (51~101 mm), and stopped to hook the stabilizing clamp, located near the bottom of the drill, around the drill rod as shown in Figure 4.17(c). Compressed air is kept blowing the down the borehole through the hollow drill rod during the drilling process to prevent loose material from blocking the hole. After every 1-2 ft (0.33~0.66 m) of drill bit advance, the drill head was moved up and down several times to refine the shape of the borehole and bring soil cuttings to the ground surface, as shown in Figure 4.19(b). After the bit reached a depth of about 4.5 ft (1.5 m), the top of the drill rod was detached from the drill head and another 5 ft (1.67 m) length of drill rod was coupled to the first drill rod. The top of the second bar was then connected to the drill head, and the drilling process continued to a final depth of 10 ft (3.33 m). After reaching the target depth, the drill rod needs to be removed from the borehole. As Figure 4.19 (d) shows, how the 5-foot (1.67 m) lengths of drill rod are unscrewed for decoupling. During the decoupling process it is necessary to attach a collar device to the top of the lower rod to keep it from dropping back into the borehole (such devices are often referred to as a "crow's foot")

The drilling was done as a two-step process. Three inch diameter pilot holes were drilled using a 3 in (76 mm) diameter drill bit. Then the 3 in (76 mm) drill bit was modified to a 4 in (101 mm) diameter bit by welding large cutting teeth to the outside of the bit. At the time, the drilling contractor simply did not have a 4 in (101 mm) diameter drill bit. Figure 4.18 shows the drill bit after the additional teeth had been added.

Figure 4.18 Drilling Bit with Welded Bit Teeth

(a)

(b)

(c)

(d)

Figure 4.19 Detailed Procedure of Borehole Drilling

4. Drilling sequence

All boreholes except those drilled for the duckbill anchors were of 4 in (101 mm) diameter. Holes for the duckbill anchors were of 2 in (51 mm) diameter. The time required for drilling one borehole varied from 30 to 90 minutes depending on the nature of the frozen soil. Ice-rich silt was relatively easy to drill (represented by boreholes 1 – 4). When the drill bit had to penetrate a gravel layer, the time per borehole could increase significantly (represented by boreholes 4, 10, and 14). Boreholes for all required locations were successfully drilled.

Using to information provided by all 17 boreholes, it was possible to interpret the subsurface character of the of the permafrost soils in the test area. Figure 4.20 illustrates this interpretation to a depth of 10 ft (3.3 m).

For boreholes 13, 14, 16 and 17, which were used to test the duckbills, a 2 in (51 mm) diameter drill bit was used. One anchor is sharpened prior to installation while the other three were not. It was thought that the sharp tip might help with the installation process. Each duckbill anchor was modified by attaching to it a 1/8 inch (3.2 mm) steel cable in addition to the one supplied with the duckbill. The extra cable was added in such a way that it was intended to aid with extracting the duckbill anchors from the ground when testing was completed. All duckbill anchors were installed to a depth of 6 ft (2 m).

The sharpened duckbill anchor was the first one installed. The anchor head was pushed to the required 6 ft (2 m) depth, and the main duckbill-supplied cable was gently pulled until the anchor "set". The cable is then tensioned to 1448 lbs (6,600 KN) by a hollow core Enerpac jack.

An attempt was made to install the second duckbill anchor but it could not be set. Then all three remaining duckbills were sharpened and repetitive attempts were made to install them. None of the remaining three could be set. Then a duckbill anchor was heated to the point that it was almost red hot, and attempts were made to set it. That approach also failed. In a final attempt to install the remaining duckbill anchors, a quart of boiling water was poured down the hole followed by the duckbill anchors. After a wait of 20 minutes, another unsuccessful attempt was made to set the anchors.

As a last resort, the duckbill anchors were placed into the holes, and the holes were filled with fine gravel and water. This method of installation finally succeeded in creating a strong cable-type anchor, but not one that functioned according to the duckbill anchor's intended design.

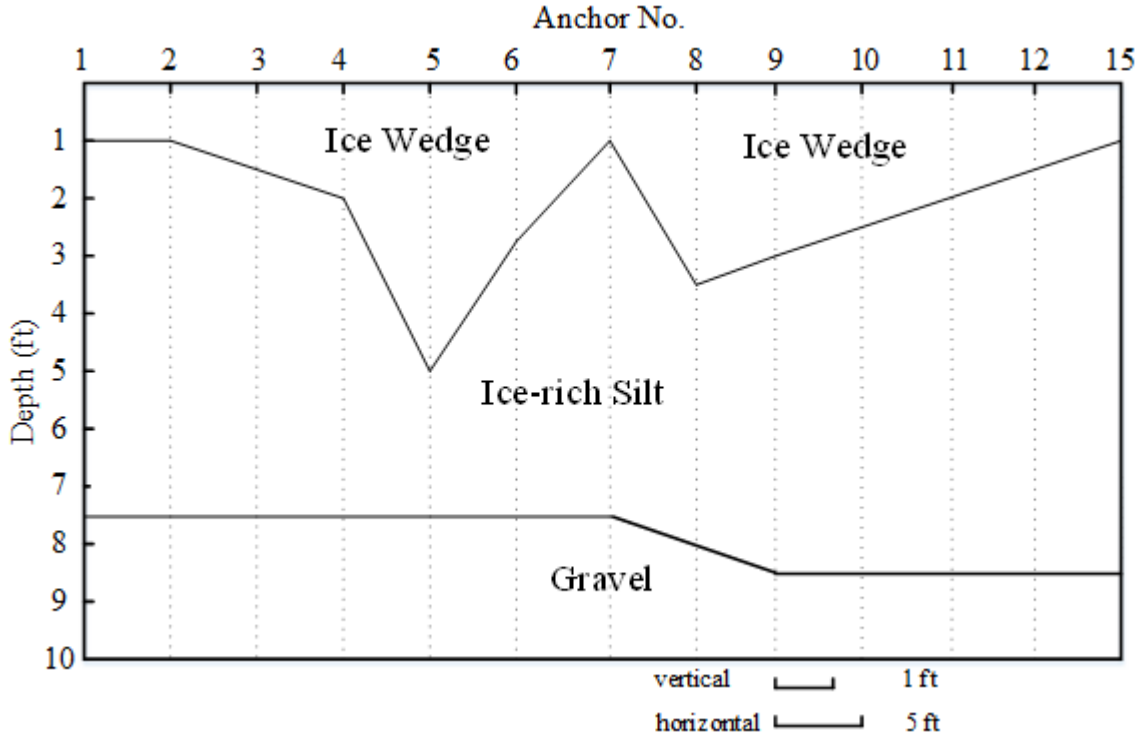

Figure 4.20 Schematic Plot of Soil Profile in Testing Area

4.4 Anchor Preparation and Installation

The general layout of the sensors along the 13 bar-type anchors is shown in Figure 4.7. These anchors were 10 ft long with Geokon strain gages uniformly distributed along the length of the anchor except for the top and bottom 1.5ft. HPI strain gages were placed at the same vertical locations along the anchor but were welded to the steel tendon rather than in the grout. Two of the location in Figure 4.7 show HPI strain gage on both sides to prevent eccentricity. All strain gages

were labeled with numbers such as 1G-1 or 1H-1. The first number is the anchor number. The latter indicates strain gage type (G and H for Geokon and HPI). The last number indicates the vertical location of the sensor along the anchor rod with the numbering sequence beginning at the bottom of the rod.

1. HPI Strain Gage Installation

The HPI strain gage is full bridge weldable strain gage. The head of the strain gage consists of a precision foil gage unit bonded to stainless steel shim, an amplifier and voltage regulator. Two metal tabs extend from part of the gage head which are used to attach the gage to the steel bar. The strain gage resistance for each one is 350 Ohms while the gage factor is different which needs to be recorded ahead of time.

Two types of steel anchor tendons (bars) were used in the field test. One was a hollow-core threaded steel rebar type with inside diameter of 0.78 in (20 mm) and outside diameter of 1.58 in (40 mm). The other was a solid, threaded steel rebar with diameter of 1.41 in (32 mm). The hollow bar was supplied in 5 ft (1.67 m) lengths. The solid threaded anchor bars were supplied 10 ft (3.33 m) long. In order to obtain comparable test results from the two bar types, the solid bars were cut to 5 ft (1.67 m) lengths, and the 5 ft (1.67 m) lengths were coupled together to match the physical configuration of the hollow anchor bars. Figure 4.21 shows a pair of solid and hollow steel bars assembled with couplings.

Sections of the steel bars needed to be polished and milled with flat areas so that the strain gages could be welded in place. Each of the cleaned and polished areas had to be large enough to accommodate the gage itself plus the gage's attachment wings. It was necessary to take great care in preparing the gage attachment areas so that the gage could be oriented properly and securely welded in place. On the other hand it was necessary to minimize the depth of the flattened areas so as to not significantly decrease the cross section of the bar at that location. Figure 4.22 shows a section of rebar with a small milled area.

Figure 4.21 Coupled Hollow and Solid Rebar

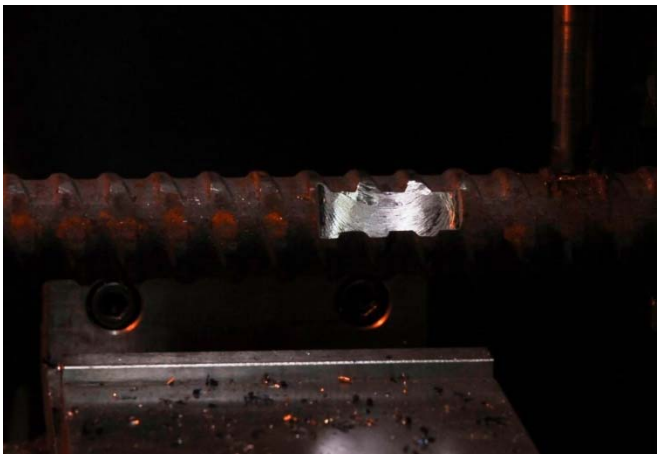

Figure 4.22 Rebar after Milling

After the anchor bars were properly prepared, the next step was to attach the HPI sensors by welding them in place on the anchor bars. The gages were welded in place using a Sunstone D-CD320 spot welder. The welder, shown in Figure 4.23, provided a dual pulse 320 watt-second capacitive discharge. The welding process required first welding the wings (attached to part of the sensor head) to the bar. It was necessary to make sure that the sensor heads were positioned exactly at the center of the prepared areas on the bars. One spot weld at the center of each wing initially affixed the wing to the bar. Following initial attachment of the wing, additional spot welds were added to insure sufficient attachment to survive the anchor testing process. Great care was needed so that the spot welding was done properly. Then the rectangular gaging unit itself was carefully attached to the bar with several spot welds. All spot welding was done using specific patterns of weld placement in order to prevent damage to the gage components while achieving a high strength attachment. During the spot welding process, welds at certain locations along the margin of the gage could not be too close to the gage's critical components. The critical strain sensing components were incased in stiff plastic and could be easily damaged by excessive heating caused

by improper welding technique. Figure 4.24 shows the rebar with welded HPI strain gage. Note the numerous tiny spot welds that hold the gage securely in place.

Figure 4.23 Sunstone Spot Welder

Figure 4.24 Rebar with Welded HPI Strain Gage

After the six HPI strain gages were welded to each anchor bar, silicone caulk was applied over and around the mounting locations to prevent corrosion in the immediate vicinity of the sensors. Figure 4.25 shows the final appearance of sensor components after attachment to the anchor bar.

Figure 4.25 HPI Strain Gage with Silicone Caulk Protection

2. Geokon Strain Gage Installation

The Geokon strain gages and cables were loosely attached along the outside of the anchor bars using polyethylene zip-ties. Figure 4.26 shows the typical pre-installation configuration of the anchor bar/strain gage assembly. Care was needed to avoid applying large forces to the end blocks of the sensors. The zip-ties were adjusted loosely to facilitate relative movement between the anchor bars, the Geokon gages, and the cables during placement of the grout. Such movements were necessary to prevent damage to the sensor components. Care was taken not to damage the sensor assemblies with the vibration needed to densify the grout during placement.

As shown in Figure 4.26, a strip of foam was wrapped between the sensor and rebar (see beneath the zip-ties). This foam layer provided a cushion between the zip-ties and anchor bar so that the vibration characteristics of the wire in the strain gage would not be affected by the ties. It was thought that, without the foam cushion, overly-tight zip-ties might influence the resonant frequency of the vibrating gage wire. Such an effect might have resulted in unstable readings or no readings at all. After the zip-ties were in cinched in place the vibration actuator coil was affixed to the gage body with a hose clamp as shown in Figure 4.26.

Finally, after all of the HPI and Geokon sensors were installed, the last step in preparing the anchor rod was to attach a “centralizer” to the rebar. One centralizer device was wired to each anchor 5in (127mm) from the bottom to ensure that the steel bar remained in the center of the hole during the grouting. Centralizers were simple devices made from short sections of PVC pipe as shown in Figure 4.27. Some of the centralizers used on the solid anchor bars had to be modified to allow for

passage of the grout tube to the bottom of the anchor. Of course grout was delivered to the bottom of the hollow-core bars through the center passage of the those bars, so no centralizer modifications were required.

Figure 4.26 Geokon Vibrating Wire Strain Gage Installation

Figure 4.27 Centralizer

After the centralizer was attached, zip-ties were used to fasten sensor wires together as necessary, and the labeling of all sensors was checked a final time. Figure 4.28 shows the completed anchor assembly before installation.

Figure 4.28 Anchor Bar with All Sensors

3. Anchor Installation Process

The instrumented anchor bar assemblies were prepared at a location away from the dusty, cold permafrost tunnel. Final installation of the anchor bars was a simple matter. The bar assemblies were transported to the permafrost tunnel and each was placed into its respective borehole. Anchor rod assemblies were handled very carefully at all times prior to being inserted into the floor of the permafrost tunnel.

Insertion of the anchor bar assembly into the borehole was accomplished by two men as shown in Figure 4.29. While lowering the anchor into the hole, much care was taken to prevent the sensors from contacting the wall of the borehole. While one person lowered the anchor into the borehole, the other handled/fed instrumentation wires to assist the insertion. After insertion of each bar, a piece of cloth was put at the top of the hole to prevent debris from entering the hole. Figure 4.30 shows the anchor bar after installation.

Figure 4.29 Anchor Installation Process

Figure 4.30 Anchor after Installation

4. Backfill Material Preparation and Grouting

Three types of backfill materials were used including Microsil Anchor Grout, Bentonite (Montmorillonite) Clay and Special Cement Formula.

The Microsil Anchor Grout was manufactured by a Canadian Company. This was an unsanded, Portland cement-based, expanding grout containing silica fume, fly ash, and other additives. This type of backfill material gains strength quickly and resists water washout which is ideal for anchors in a soil media. Moreover, this backfill material can achieve excellent physical properties during curing at temperature down to 41°F (5°C) and it also exhibits freeze/thaw durability. The recommended water to cement ratio was 0.27 for a pumpable consistency and 0.31 for a flowable consistency.

The volume of the backfill material for one borehole is calculated by the following equation:

$$V = R * \frac{\pi}{4} * D^2 * H * 12 \qquad [4.1]$$

V: Volume (in^3);

R: Redundancy factor, R= 1.3;

D: Diameter of the borehole, D= 4.0 in;

H: depth of the borehole, H= 10ft.

The volume of backfill material for each borehole was 1,508 in^3 (24.71 liter). The redundancy factor is to take the shrinkage volume of the backfill material into account.

5. Backfill Material Mixing

The equipment used for mixing the grout backfill is shown in Figure 4.31. Inside the container were three sets of impeller blades (at bottom, middle and top of container) that stirred and blended the grout mixture. After sufficient mixing, the grout mixture was released from the grout mixing tank through a valve at the bottom of the tank.

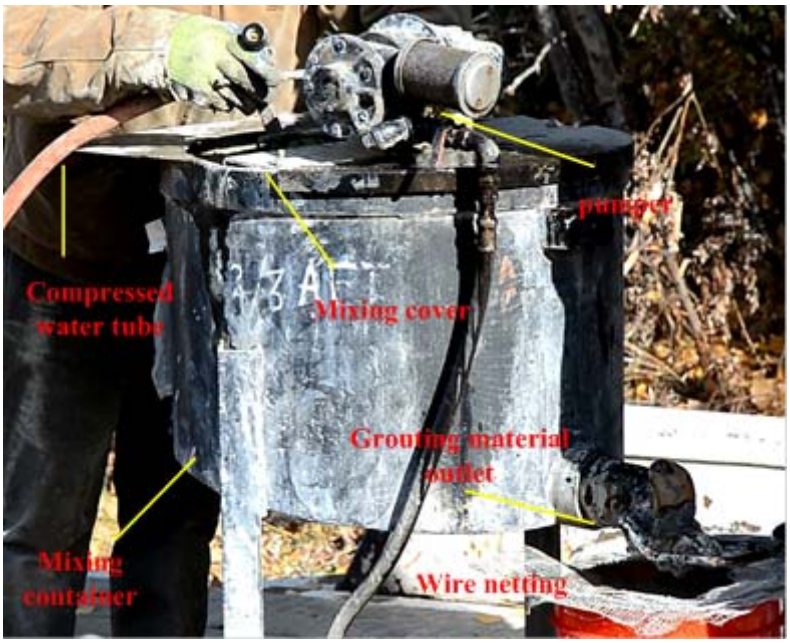

Figure 4.31 Backfill Material Mixing Equipment 1

This equipment shown in Figure 4.31 was used to mix the Microsil Anchor grout and Bentonite clay grout. The mixing procedures for those two materials were essentially the same. First, a certain amount of water was added to the tank and the motor driving the mixing impellers was started. Then the prescribed amount of powdered grout material was slowly added to the tank and the mixture was blended for about 1 minute until the mixture reached a flowable paste-like consistency. It was necessary to pre-heat the mixing water used for the bentonite clay grout to 90°F.

The early strength cement could not be mixed in the regular grout mixing tank. The grout tank's mixing impellers were not powerful enough or otherwise suitable for handling the high viscosity of this grout mix. It became necessary to use other mixing equipment, i.e., the standard, small-batch concrete mixer shown in Figure 4.32.

Figure 4.32 Backfill Material Mixing Equipment 2

A batch of cement grout was produced by first adding about half of the components (water, sand and cement) and mixing for several minutes. After those materials appeared to be well mixed, the remaining half of the components were added to the batch and mixing was allowed to continue for a total of about 10 minutes.

High pressure grout pumping equipment is required to completely fill the annulus between the borehole walls and the anchor bar. The grouting equipment used in the permafrost tunnel is shown in Figure 4.33. After mixing the grout was carried into the tunnel by workers and poured into the grout pump's hopper. From the hopper the grout was gravity-fed into the pump unit itself from where it was pressurized, then delivered through a grout tube to the base of the solid anchor bar, thereby filling the borehole annulus from the bottom up. The grout tube was a fairly substantial metal tube that could come into direct contact with the sensors while the grout was being pumped into the annulus. Therefore, careful handling of the tube was necessary to prevent damaging the sensors.

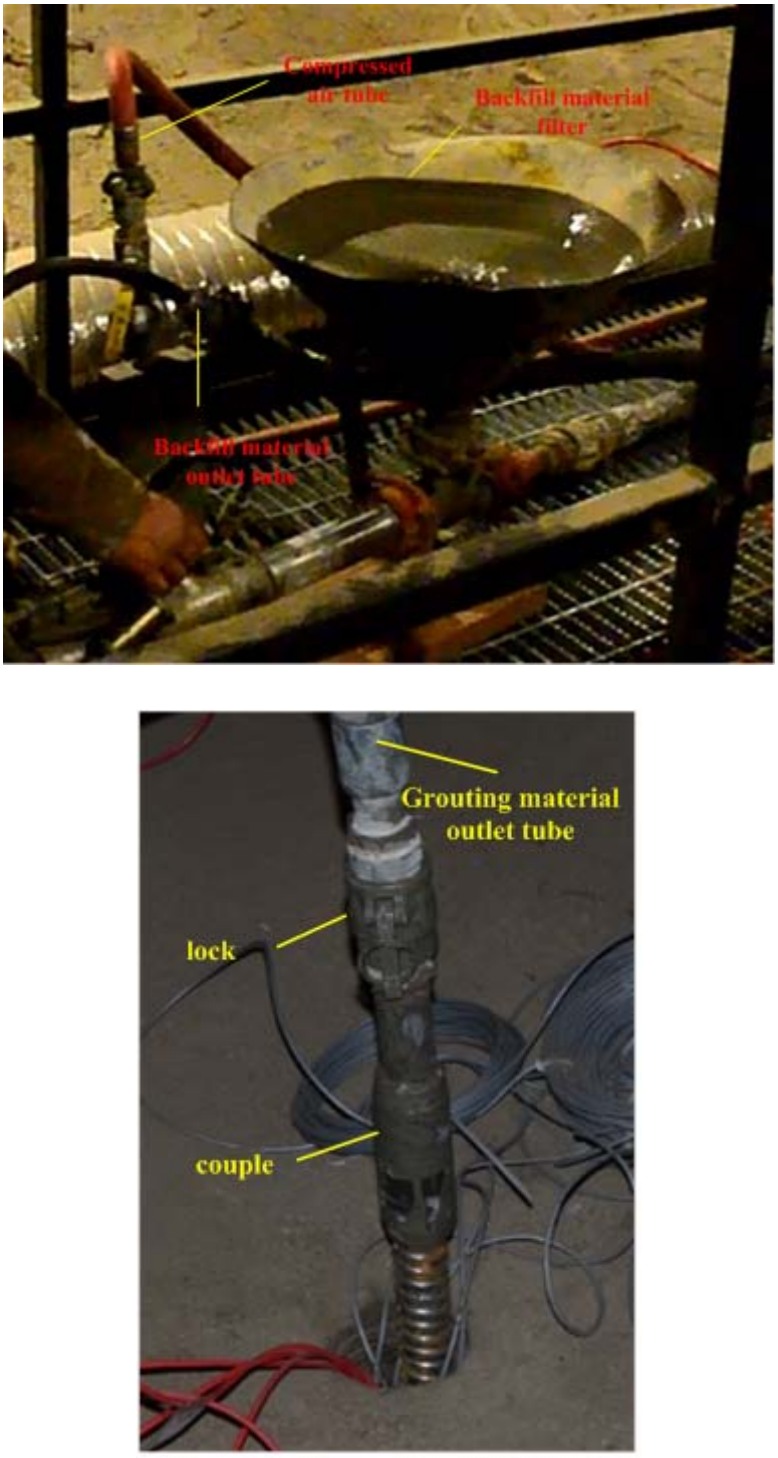

Figure 4.33 Grouting Equipment and Connection

After the borehole had been fully grouted, it is necessary to hold the top of the anchor for several minutes. It was necessary for the grout to set enough so that the steel bar would remain stable in the center of the borehole. A successfully grouted anchor is shown in Figure 4.34.

As previously shown in Figure 4.5, anchor bar numbers 1 through 5 were solid type grouted with Microsil Anchor Grout. Bar numbers 6 and 7 were hollow core type grouted with Microsil Anchor Grout. Bar numbers 8 through 10 were grouted with bentonite clay. Bar numbers 11, 12 and 15 were grouted with a special early strength formula cement.

Figure 4.34 Fully Grouted Anchor

4.5 Loading System Setup

The field test system is composed of two parts: loading system and data acquisition system. In the following section, each system is systematically introduced and the set up process is discussed.

1. Loading system for shallow anchor

The loading system is composed of a hydraulic pump and two hydraulic jacks as shown in Figure 4.35. The hydraulic pump is capable of 10,000 psi (68,900 KPa) maximum pressure with the accuracy of ± 200 psi (1,378 KPa). The hollow core hydraulic jacks used in the permafrost tunnel each had a capacity of 30 tons (266.9 KN) with a maximum stroke of 6.13 in (155.70 mm). Each had an effective "piston" area of 7.22 in^2 (4,658 mm^2). The outside and inside diameters of the jack units were 2 in (51 mm) and 1.31 in (33 mm) respectively.

Figure 4.36 is an overhead view of the hydraulic pump system. The hydraulic pump provided hydraulic pressure, through a main pressure control switch, to a manifold that offered two hydraulic line attachment points, each with the capability of independent pressure control. Therefore, it was possible for the single pump to simultaneously supply two jacks with the correct hydraulic pressures needed for maintaining two different loads.

There were three steps in adjusting the pump to provide the required jack load. If the target load was, say, 5 tons (44.5 KN), the first step was to adjust the main valve. The effective area of the jack was 7.22 in^2 (4,658 mm^2), so a 5-ton load would require 1385 psi (10,000 pounds / 7.22 in^2 = 1385 psi). Because of the accuracy of the pump, the main pressure adjustment had to be set 200 psi (1,378 KPa) above the target pressure, which meant that the reading on the main piezometer should be about 1,600 psi (11,024 KPa).

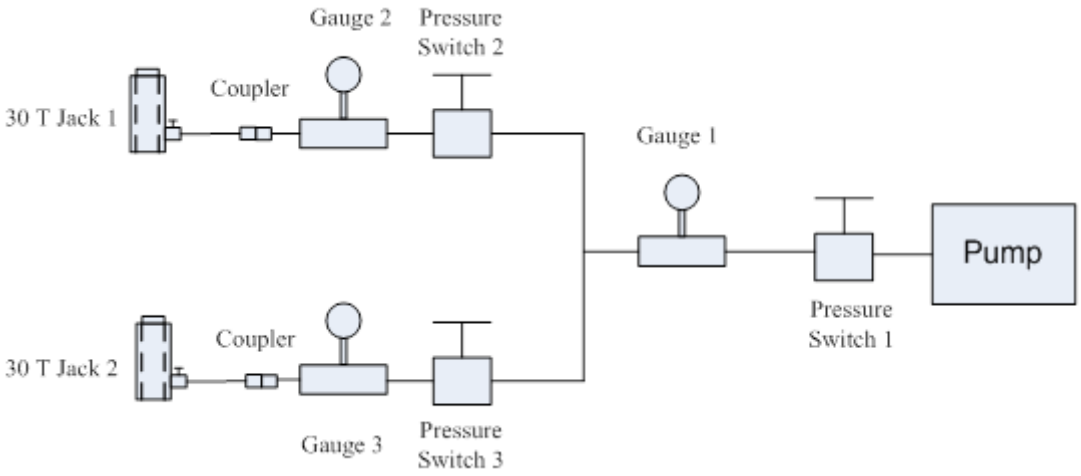

Figure 4.35 Schematic Plot of the Loading System

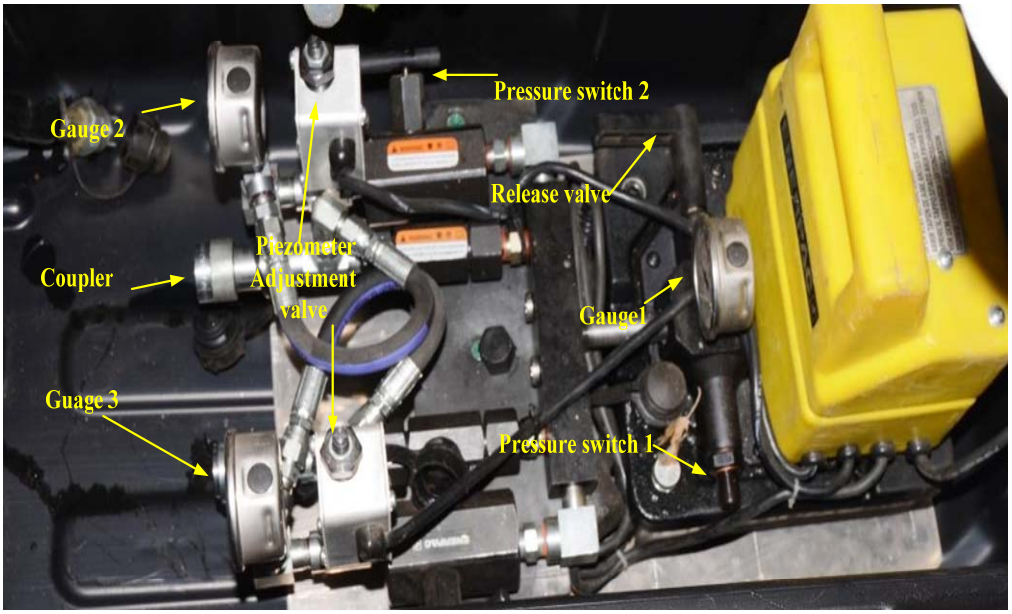

Figure 4.36 Hydraulic Pump

After adjusting the main valve to 1,600 psi (11,024 KPa), the next step is to adjust separate piezometers shown in Figure 4.36. This required series of specific, somewhat complicated

adjustment that is unnecessary to explain in this report. Suffice to say that an experienced operator, using the one pump, could easily set up two hydraulic lines to provide two jacks with two different pressures.

The hydraulic jack is shown in Figure 4.37. To prepare for use, the hydraulic jack was placed on a specially designed, load bearing base, and the jack's pressure coupling was connected to the hydraulic line. The hydraulic coupling contained a one-way valve that allowed the jack to maintain pressure even if hydraulic line pressure dropped to zero.

As Figure 4.38 suggests, the ground surface in the permafrost tunnel was not ideally flat. Before the testing system could be set up over a particular anchor, the ground surface at that location needed to be cleaned of loose silt and leveled. Leveling of the surface prior to jack placement was necessary so that the jacking force would be directly in line with the axis of the anchor. Any significant misalignment of jack and anchor axes would introduce a moment into the jacking force that would negatively affect the test results.

Figure 4.37 Hydraulic Jack

Figure 4.38 Cleaning Ground Surface

After the surface was made reasonably flat, a specially designed coupling adaptor was threaded onto the top of the steel bar, as shown in Figure 4.39. The diameter of the upper part of the coupling was 1.18 in (30 mm) in order to fit through the opening in the center of the jack. The diameter of the lower part of the coupling was 1.58 in (40 mm) to fit the threads on the anchor bar.

Next, with the jack base placed on its side as shown in Figure 4.40, the bundle of sensor cables (wires) from the test anchor were fed through the bottom of the jack base and out through the hole in the side of the base. All wires were passed through the hole in the side of the base and then connected to the data acquisition system. As shown in Figure 4.40, all the wires were labeled. Wires exiting the jack base were grouped according to labeling and fastened together with zip-ties to preserve order and prevent tangling. Then lift the base up and leave the couple within the base.

Then, being careful of the wires, the jack base was lifted up and placed over the anchor, allowing the small-diameter end of the coupling adaptor to extend up through the top of the base. With the bottom of the jack base now firmly in contact with the ground surface, the position of the jack base was slid around (adjusted slightly) until the small-diameter end of the threaded adaptor coupling passed through the center of the hole in the top of the base.

Then the following steps were required in order to attach the jack to the test anchor. The jack was lifted and placed on top of its base such that the small-diameter end of the threaded adaptor protruded through the body of the hollow core jack and exited at the center of the top of the jack. After placing and centering the jack, a steel load bearing plate (load plate) was placed over the top

of the threaded adaptor and onto the top of the jack. Finally, a load bearing nut connected the threaded adaptor to the load plate, thus completing the physical connection between jack and anchor as indicated in Figures 4.41, 4.42, and 4.43. As also shown in these three figures, the LVDT was attached to a steel bar that had been firmly driven into the ground. Care was taken to make sure that the LVDT was installed perpendicular to the surface of the load plate.

Figure 4.39 Anchor with Connecting Couple

Figure 4.40 Testing Base Setup

Figure 4.41 Steel Plate and Nut Setup

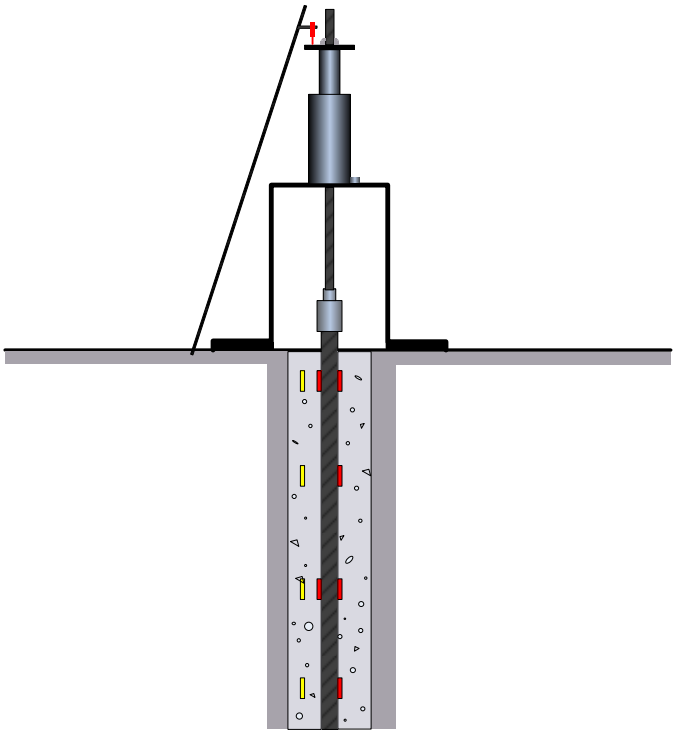

Figure 4.42 Schematic Plot of Testing System

Figure 4.43 Actual Setup of Testing System

2. Loading system for duckbill

The four duckbill anchors were tested using two of the load frames previously used to test anchors in the UAF laboratory—covered in Chapter 3. Detailed information about the load frame system is presented in load frame preparation of Section 3.1 of this report. Figure 4.44 (a) shows one of the load frames actually being used for duckbill anchor testing in the permafrost tunnel. Two sets of loading systems are built up simultaneously. Figure 4.44 (b) provides a close-up view of the LVDT setup.

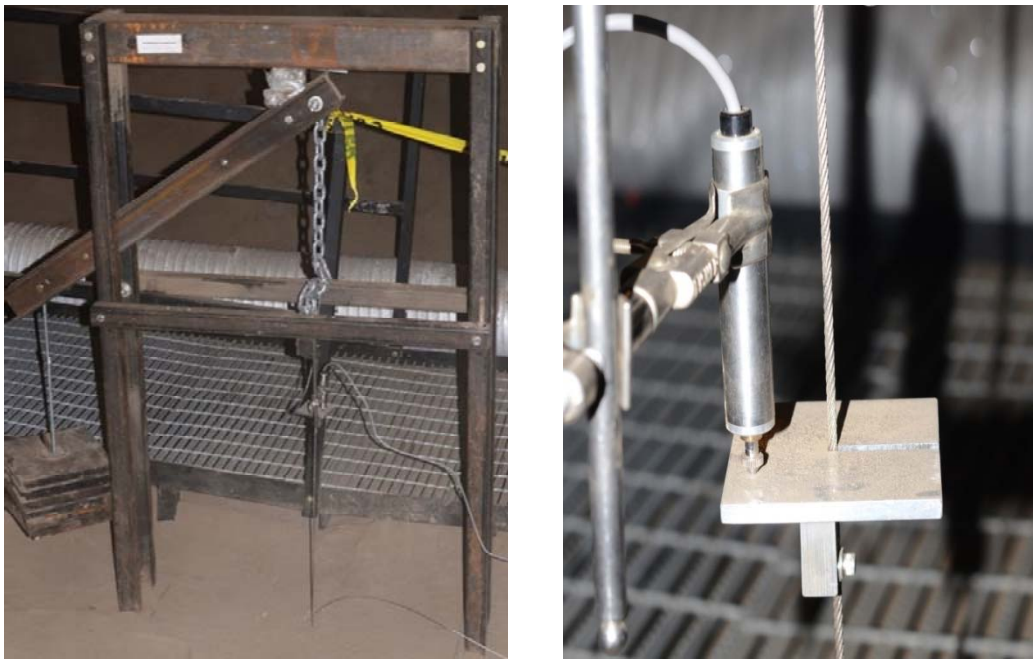

(a) (b)

Figure 4.44 Duckbill Anchor Testing System

4.6 Data Acquisition System Setup

All test data was automatically recorded by the CR1000 data logger shown in Figure 4.45. The data acquisition system consisted of 1 CR1000 Control Panel, 2 AM16/32 Relay Multiplexers and 1 AVW200 Vibrating-Wire Interface. The function of each instrument is described as follows. The CR1000 provided a 12V output power to the Multiplexers and AVW200 and 5V output power to the 2 LVDTs. The CR1000 recorded all data from the multiplexers and also analyzed that data according to a program contained in the CR1000. Multiplexers provided the many data channels needed for a single data logger to simultaneously record data from many sensors. Without multiplexing capability, only 4 HPI or Geokon strain gages could be connected to one CR1000 data logger. With the two AM16/32 multiplexers it was possible to obtain data from as many as 32 HPI or Geokon sensors. The AVW200 Vibrating-Wire Interface was needed to allow the data logger to read the data signal from the Geokon vibrating wire sensors.

The DC power unit, shown in Figure 4.46, converted available AC power into direct current to supply power to the data acquisition system. With this high quality power unit the DC output voltage could be adjusted exactly as needed. The required output voltage was 12V and the fluctuation was held within ±0.1V.

The wiring diagram of data acquisition system is shown in Figure 6. A detailed explanation of data logger set up and operation is beyond the scope of this report section.

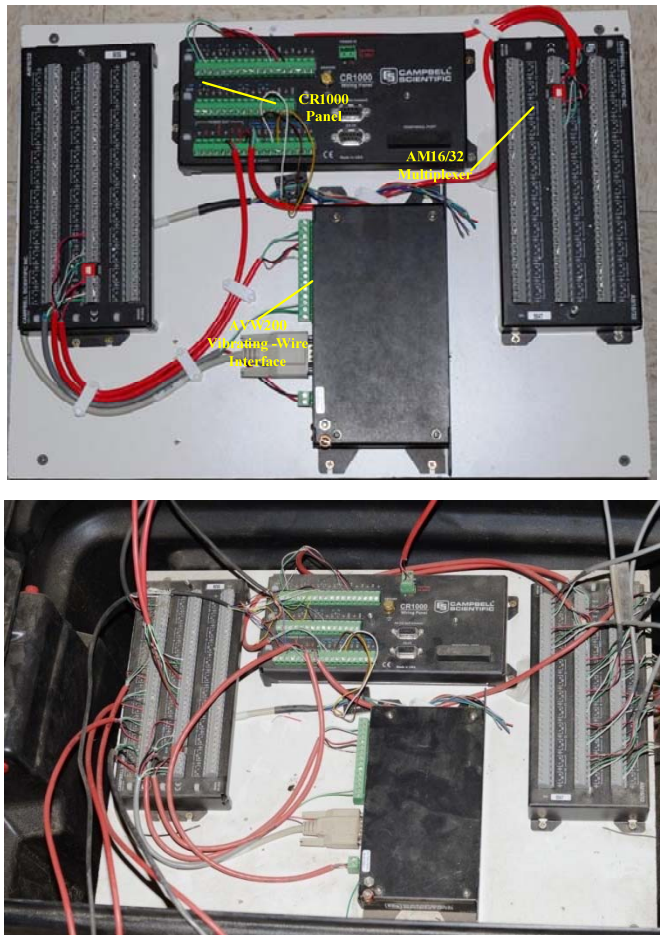

Figure 4.45 Data Acquisition Panel

The data acquisition system was housed in a protective plastic box with cover as shown in Figure 4.45. A protective box was a vital component of the data logging system. The surface of the permafrost tunnel, being generally covered with 3~4 in (76~101 mm) dry silt, provided a very dirty environment for electronic equipment. The box not only kept the data logging equipment clean, but provided protection against impact and other miscellaneous sources of damage.

Figure 4.46 DC Power Supply Unit

4.7 Duckbill Removal and Anchor Pullout Test

The pullout test was conducted on August 28, 2013. The removal of duckbills took longer time than expected because 3 out of 4 of the duckbills were backfilled with gravel and water. And among all the other 13 anchors, only three which grouted with Bentonite clay were pulled out at 35 ton (348 KN) load level. All of the three pulled out anchors failed at the interface between rod and clay. All the others were loaded to a maximum load of 55 ton (548 KN) but still could not be pulled out. The ultimate capacity of the rebar was 121. 2 kip (604 KN), corresponding to 60.6 ton so that no load level above 55 ton (548 KN) was applied to the anchors just for safety concerns.

Firstly, the duckbill removal procedures were introduced and two different methods were demonstrated. Secondly, a brief introduction of the pullout test system setup and loading schedule were presented. Finally, the test results and data analysis process were illustrated.

2. Duckbill Removal

There were two removal methods used in this process. The first method was to use a 6 in diameter (152.4 mm) soil sample corer to drill down to 6 ft (2 m) as shown in Figure 4.47. At the beginning, this machine worked very well and the surrounding soil melted as the drilling bit went down. Yet when drilling bit reached a depth of about 3 ft (1 m), the electric motor could not provide enough power to drilling down and the surrounding soil froze back at a relatively fast speed which also impeded the drilling process. This method failed to remove any duckbill.

The second method was to first drill a lead hole beside the duckbill by using a diesel spire auger as shown in Figure 4.48. The aim of the lead hole is to allow the drilling fragments falling into the lead hole rather than blocking the drilling bit and freezing back quickly. Then repeat method one and the melting soil directly felt down into the lead hole which facilitated the drilling process. Extra care should be paid to ensure that the soil sample corer did not cut the duckbill cable.

Figure 4.47 Soil Sample Corer

(a) **(b)**

Figure 4.48 Spire Auger

2. Pullout Test System Setup

The testing system was the same as for creep test except for the capacity of the jack. The jack used for the pullout test was 60 ton (598 KN) and for the creep test was 30 ton (299 KN). And the effective area of the jack cylinder was 12.73 in^2 (8212.89 mm^2) for pullout test and 7.22 in^2

(4658.06 mm^2) for creep test. As shown in Figure 4.49 (a), the upper rod was welded with 2 HPI strain gages and was connected with the anchor rod with a couple. Four iron plates were placed near the anchor to spread the applied load to the ground. All the wires of the sensors went through the gap between two plates. Figure 4.49 (b) gives the final setup appearance of the loading system. The jack was sat on a base and on top of it was an iron plate. A nut was threaded in and LVDT was placed perpendicular to the iron plate by a magnetic holder.

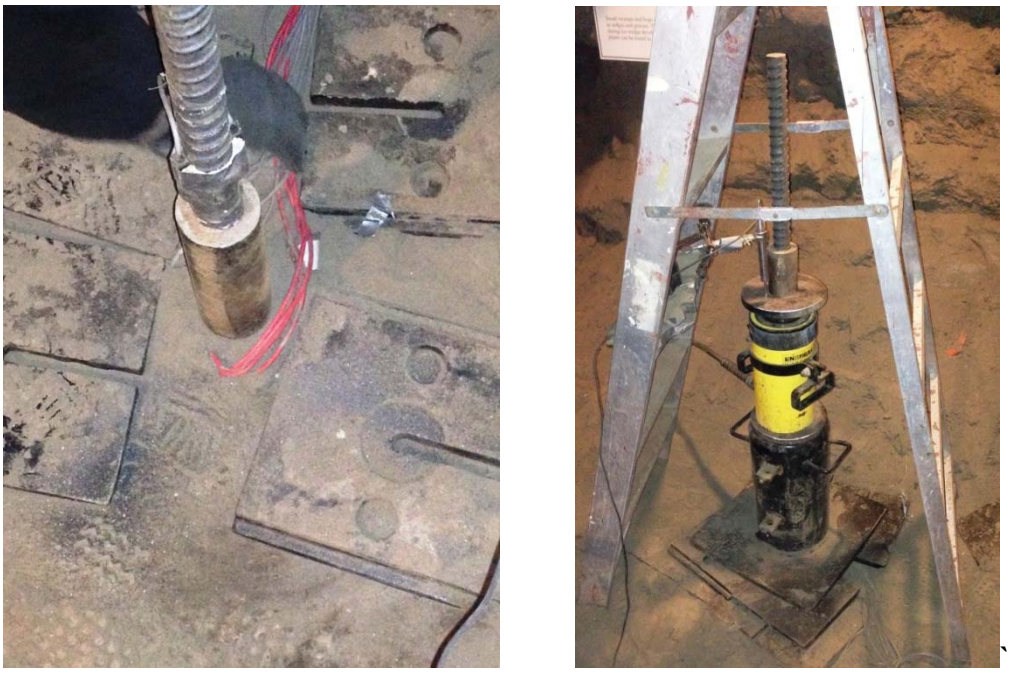

(a) **(b)**

Figure 4.49 Pullout Test System Setup

For each grouting materials (Microsil Anchor Grout, Bentonite clay and Special Formula Cement), one anchor was chosen as a representative of this type of grouting material and was tested with a load interval of 5 ton (50 KN) up to 55 ton (548 KN) in order to determine the ultimate uplift capacity. Then the rest of the anchors were tested with a loading schedule of 15 ton (149 KN), 30 ton (299 KN), 45 ton (448 KN) and 55 ton (548 KN). Before conducting pullout test, an alignment pressure of 200 psi (1378 KPa), corresponding to 2,546 lb (12.7 KN) load was applied to fasten the loading system. Table 4.1 gives detailed information of grouting material and loading schedule for each anchor.

Table 4.1 Anchor Loading Schedule

Anchor	Grouting Material	Loading Schedule (ton)
1	Microsil (with Solid Rebar)	15, 30, 45, 55
2		15, 30, 45, 55
3		15, 30, 45, 55
4		15, 30, 45, 55
5	Microsil (with Hollow Rebar)	15, 30, 45, 55
6		5, 10, 15, 20, 25, 30, 35, 40, 45, 50, 55
7		15, 30, 45, 55
8	Bentonite clay (with Hollow Rebar)	5, 10, 15, 20, 25, 30, 35, 40, 45, 50, 55
9		15, 30, 45, 55
10		15, 30, 45, 55
11	Special Formula Cement (with Hollow Rebar)	15, 30, 45, 55
12		5, 10, 15, 20, 25, 30, 35, 40, 45, 50, 55
15		15, 30, 45, 55

Chapter 5 Test Results and Data Analysis

In this chapter, both the laboratory and field test results are presented. For the laboratory test results, the creep curve of remolded Fairbanks silt with different moisture contents is discussed in detail. For the field test results, the grouting temperature, duckbill tests and bar anchor tests are presented. The comparison of grouting temperature change is aimed at analyzing the effect of grout type on the surrounding soil. The duckbill test results indicate that creep of the duckbill anchor can be ignored; most of the strain is apparently due to cable stretch. The anchor test results are divided into two parts: one is analyzing load distributions along the anchor shafts. The other is analyzing the displacement vs. time curves for the anchors so that bearing capacities can be determined.

5.1 Laboratory Pullout Test Results and Analysis (UAF Laboratory)

In total, nineteen anchor tests were conducted by using the methods described in Chapter 3. Detailed information of the pullout test results is included in Appendix A. Table 5.1 lists only the test results for the 19 anchors.

The upper limit of predicted displacement rate is based on temperature of 30.2ºF (-1ºC) and lower limit 28.4ºF (-2ºC). Based on the test results, equation [5.1] is used to express the test results:

$$\tau_f = \tau_m \theta^b \left(\frac{\dot{u}_a}{a} \right)^{1/n} \qquad [5.1]$$

Where n: stress exponent; τ_f: measured failure shear stress; τ_m: general creep modulus; b: temperature exponent; θ: absolute value of temperature below freezing point.

Table 5.1 Pullout Test Results for 19 Anchors (Cold Room)

Temperature °F (°C)	Water Content (%)	Average shear stress (psi)
29.8 (-1.2)	50	16.4
29.5 (-1.4)	50	15.8
29.8 (-1.2)	80	5.5
29.8 (-1.2)	80	10.3
29.7 (-1.3)	80	11.8
29.7 (-1.3)	80	8.0
30.2 (-1.0)	120	6.8
(-1.0)	120	10.1
(-1.4)	120	5.0
(-1.4)	120	7.0
(-1.4)	120	9.2
(-1.4)	120	11.2
(-1.6)	120	11.3
(-1.6)	120	13.3
(-1.2)	120	3.0

Table 5.2 gives the regression parameters for equation [5.1] based on the pullout test. The stress exponent n was greater than 3 which back calculated from regression results and varied with water content. The temperature exponent only changed slightly with temperature.

Table 5.2 Summary of Regression Analysis (27.5~32°F)

Moisture Content	τ_m(psi)	b	n	R^2	S_E (psi)
120%	4.0	0.86	6.07	0.78	1.7
80%	3.7	1.27	3.90	0.67	2.0
50%	5.5	1.07	3.91	0.98	1.2

1. Effect of Temperature and Water Content

As shown in Figure 5.1, the creep rates increase with the increase of soil water content. For the same ultimate shear stress, the creep rate of soil with water content of 120% is almost 10 times of that for soil with 50% water content.

Figure 5.2 gives the effect of soil temperature on the creep behavior of grouted anchors. For the same water content (120%) and same ultimate shear stress, the creep rate for a temperature of 30.2 ºF is about 2 to 3 orders of magnitude greater compared with that of 27.5 ºF. Therefore, the effect of temperature on the creep rate is much larger than the effect of water content.

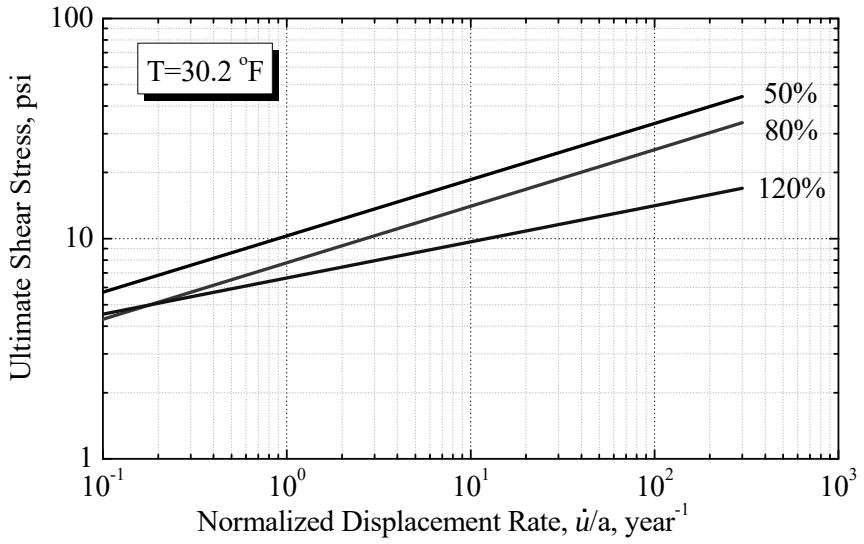

Figure 5.1 Effect of Soil Water Content on Anchor Creep Behavior

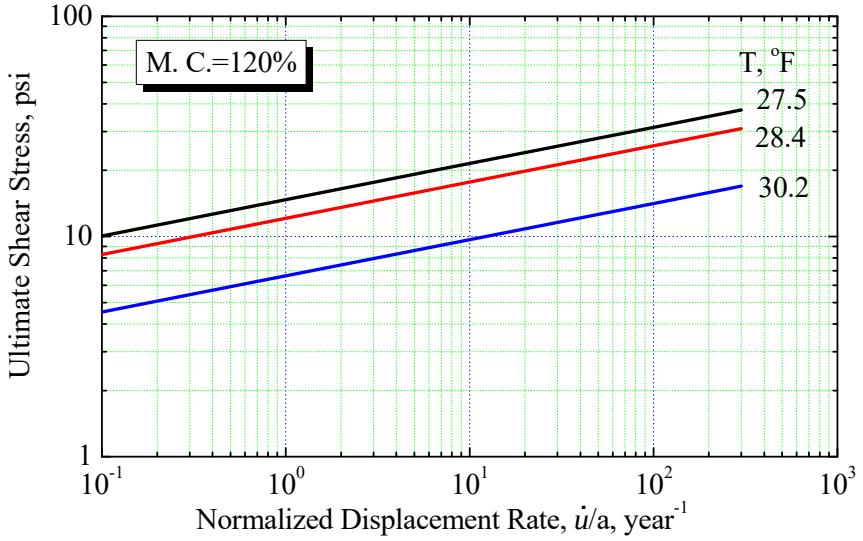

Figure 5.2 Effects of Soil Temperature on Anchor Creep behavior

2. Design Chats for Creep Rate at Different Temperature and Water Content

Based on the test results and regression analyses, design charts for the allowable shear stress at different temperatures and water contents could be developed based on equation [5.1]. Figure 5.3, 5.4 and 5.5 shows the allowable shear stress for soils with water content of 120%, 80% and 50% respectively.

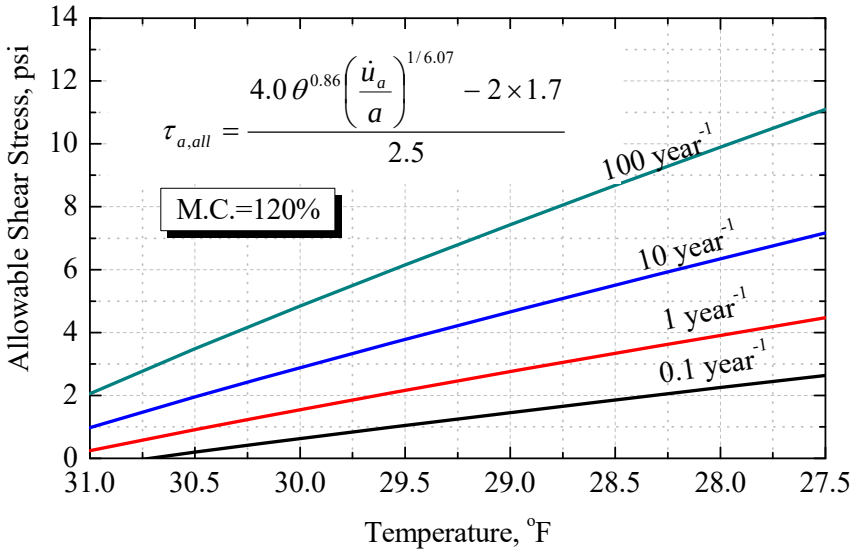

Figure 5.3 Design Chart for Ice-rich Soil with 120% Water Content

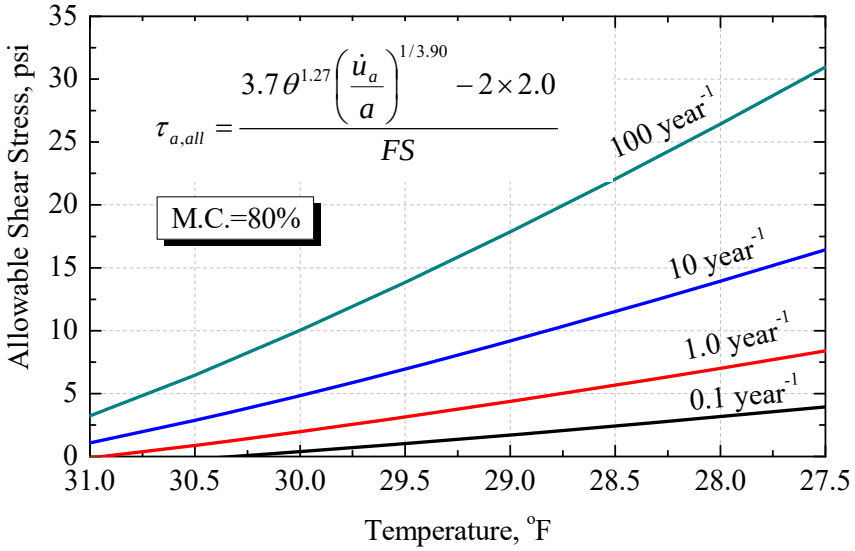

Figure 5.4 Design Chart for Ice-rich Soil with 80% Water Content

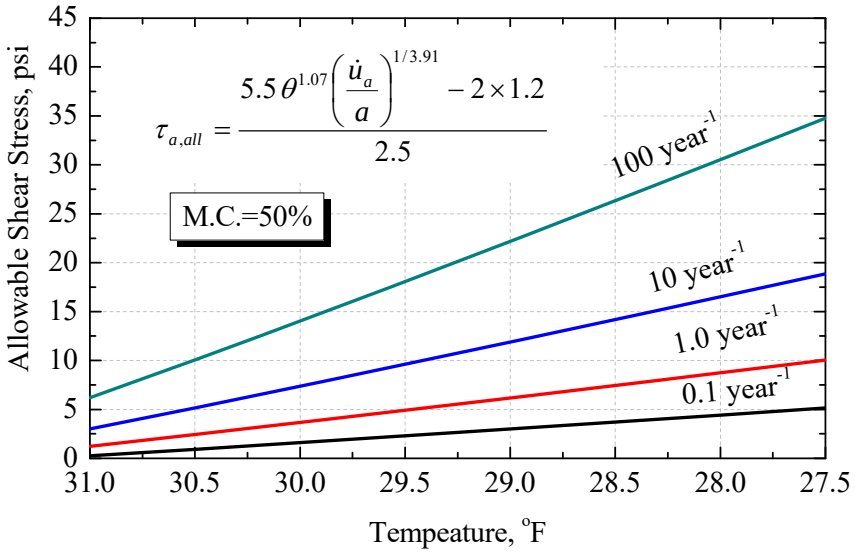

Figure 5.5 Design Chart for Ice-rich Soil with 50% Water Content

5.2 Grouting Temperature Test Results and Analysis (Permafrost Tunnel)

All the backfill materials were poured into the borehole on September 11, 2012. The grouting time for each anchor was about 3-5 minutes. After that, temperature was monitored for each anchor with Geokon sensor for 8 days in order to know the freeze back process of the anchor. The location of the Geokon sensors are 1.5 ft (0.5 m), 3.83 ft ft (1.28 m), 6.16 ft ft (2.05 m), 8.5 ft ft (2.83 m) from the bottom to the top. And the test results are comprehensively illustrated as follows.

In general, the average maximum temperature for three different backfill materials are 50.32^{0}F (10.18^{0}C) for Microsil, 83.61^{0}F (28.67^{0}C) for Bentonite Clay and 47.12^{0}F (8.40^{0}C) for special formula cement. The reason for Bentonite clay having the highest temperature is because it was mixed with warm water (32.2 ^{0}C or 90^{0}F) with a water to cement ratio of 1:1. The maximum temperature increase is 23.4^{0}F (13^{0}C), 57.1^{0}F (31.7^{0}C) and 21.4^{0}F (11.9^{0}C) for Microsil, bentonite clay and special formula cement respectively. Moreover, the special formula cement took the least time to freeze back to original temperature and bentonite clay took the longest time to freeze back.

Figure 5.6 give the temperature vs. time curves for anchor 2 which was a solid anchor bar and was grouted with Microsil. From the figure, one can tell that the initial temperature from bottom to top is about 25.3^{0}F (-3.7^{0}C), 25.9^{0}F (-3.4^{0}C), 26.4^{0}F (-3.1^{0}C) and 26.6^{0}F (-3.0^{0}C). The temperature gradient can be calculated by using the temperature difference divided by depth between the bottom and top sensor, which is 0.18^{0}F/ft (0.3^{0}C/m). And this result confirms the assumption that the temperature along the shallow anchor can be considered as a constant. The figures indicate that the temperature for the sensors at top were almost back to the initial temperature (temperature surrounding soil before grouting materials poured into borehole) after 10,000 minutes (6.9 days) while the temperature for the sensor at the bottom took somewhat longer to freeze back. One can determine the period time of grouting process from the figures by looking at the difference of the starting point of temperature change for different sensors. The grouting time for the anchor is about 5 minutes. The inset figure in the right upper corner of Figure 5.6 shows the maximum temperature rise due to the hydration process is about 0.54^{0}F (0.3^{0}C). Figure 5.7 shows the temperature vs. time curves for anchor 8 which had a hollow core anchor bar and was grouted with bentonite clay. The maximum temperature for bentonite clay was (50.8^{0}F) 28.2 ^{0}C which was much greater than that of Microsil. Figure 5.7 indicates that the temperature dropped back to initial temperature after 6,000 min (4.2 day). The freeze back time for anchor 8 was shorter than that of anchor 2.

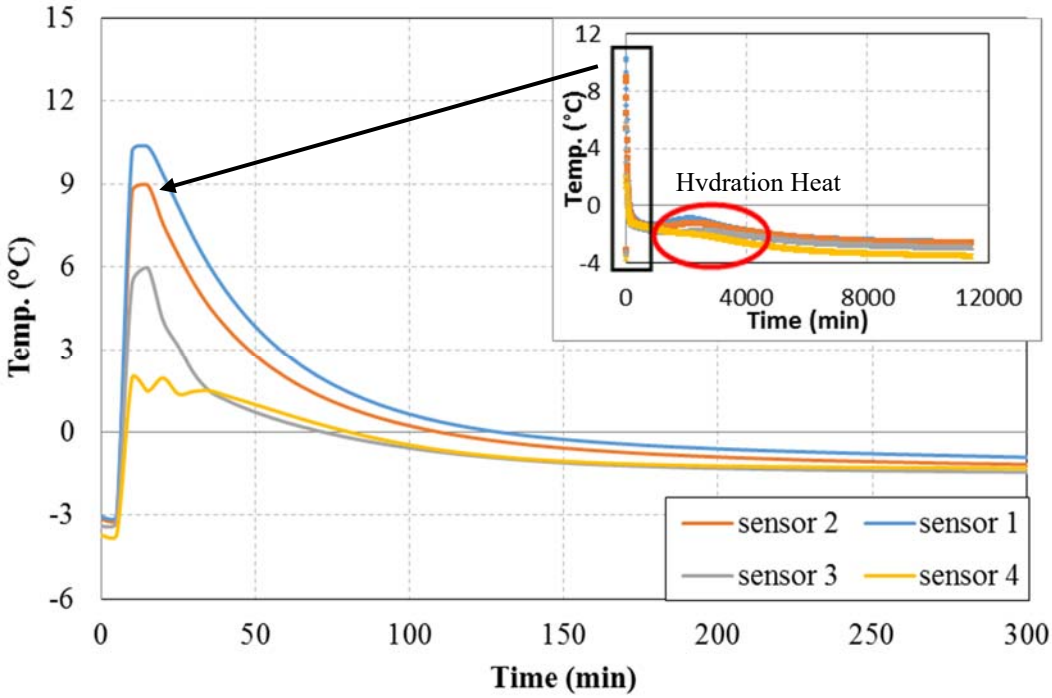

Figure 5.6 Grouting Temperature vs. Time for Anchor 2 (Solid Rebar with Microsil Anchor Grout)

In Figure 5.7, one sees that the initial temperatures for anchor 8 at different depths were almost the same (27.3^{0}F). And the time for grouting process for anchor 8 was less than 5 minutes. Moreover, the duration of temperature above 32^{0}F for bentonite clay were much longer compared with other grout types. This phenomenon might be caused by the high temperature of the mixing water which was 90°F (32.2°C). The high temperature will cause more thawing of the surrounding frozen soils which should take longer time to freeze back. Yet, the total time to freeze back for anchors with bentonite clay were shorter compared with anchors with Microsil. Part of the reason might be that the hydration process, and therefore the output of hydration heat, for Microsil lasted for a long time. On the other hand, use of the bentonite clay grout involved no hydration process and therefore no heat of hydration.

Figure 5.8 is the grouting temperature vs. time curve for anchor 11 which has hollow bar with special formula cement. The highest temperature anchor 11 experienced was 47.1°F (8.4°C). The initial temperature for anchor 11 from the bottom sensor to the top sensor were 25.7°F (-3.5°C), 26.2°F (-3.2°C), 26.6°F (-3.0°C) and 26.6°F (-3.0°C) respectively and the temperature gradient from bottom to top was about 0.13°F/ft (0.24°C/m). During the whole process, the heat generated from the hydration process was less than anchor 2 and the time to freeze back was also shorter. At

4,000 minutes (2.8 days), the temperature had already dropped back to the initial condition and no more hydration heat was generated after that. Figure 5.8 shows that a small amount of hydration heat was generated right after the temperature dropped to about 28.4°F (-2°C) which increased the temperature by approximately 0.9°F (0.5°C). The special cement formula produced less total hydration heat and required much less reacting time compared to Microsil grout. The reaction time for anchor 11 was only 300 minutes (5 hours). This relatively short time of reaction time will decrease the thermal disturbance of the surrounding soil and also reduce the time to freeze back dramatically.

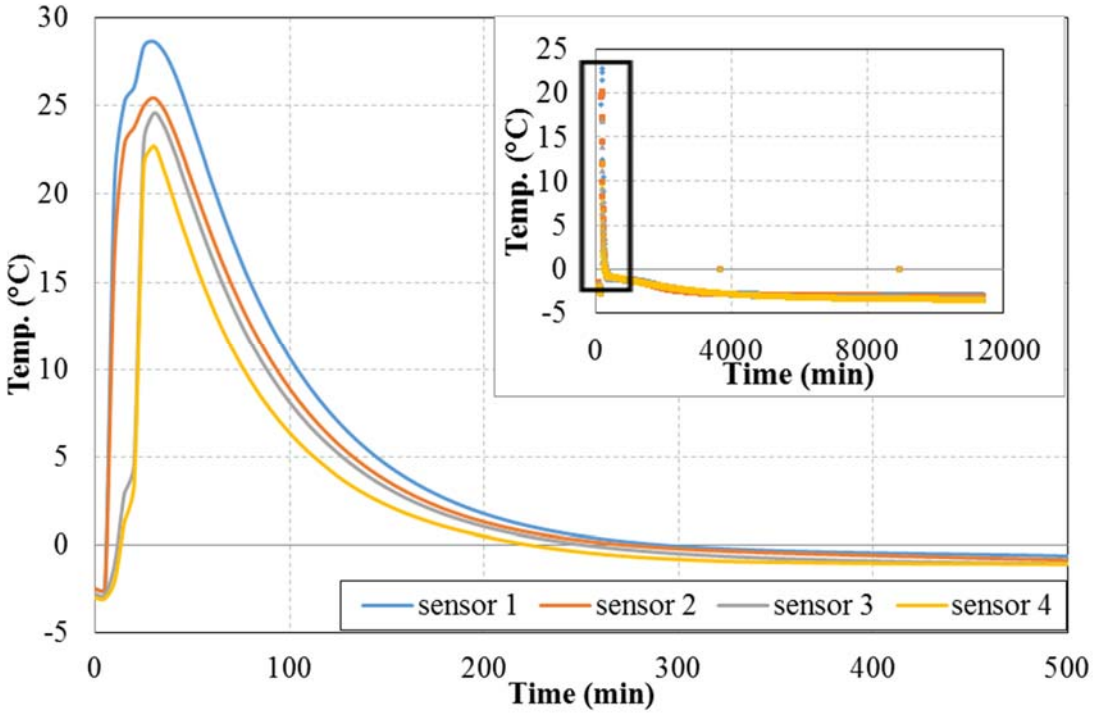

Figure 5.7 Grouting Temperature vs. Time for Anchor 8 (Hollow Rebar with Bentonite Clay)

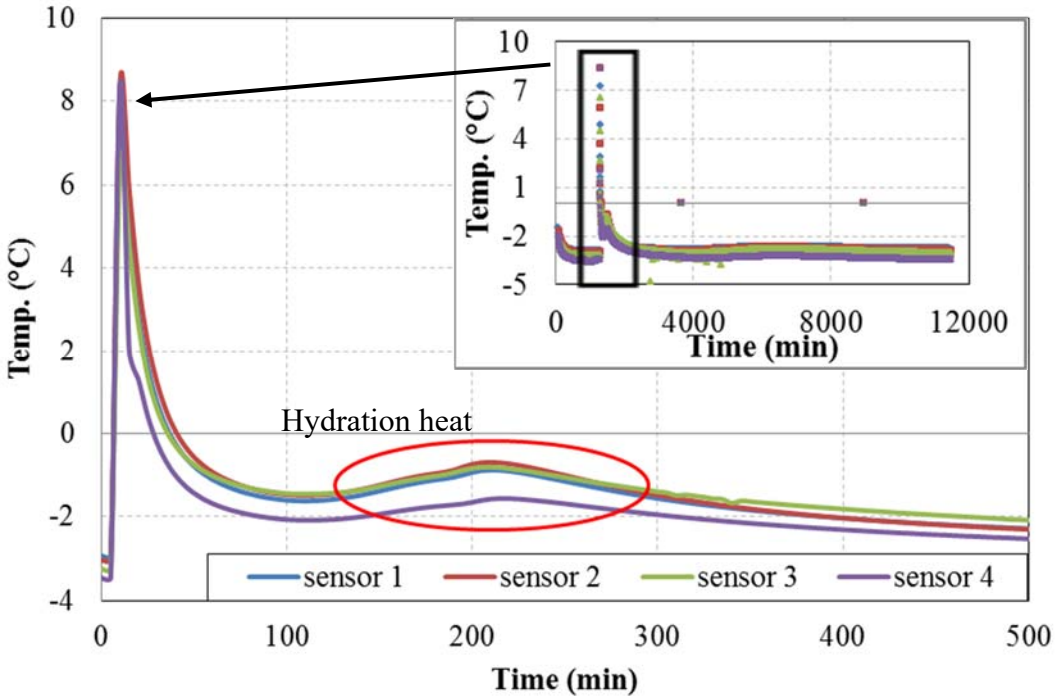

Figure 5.8 Grouting Temperature vs. Time for Anchor 11 (Hollow Rebar with Special Cement Formula)

Figure 5.9 gives the temperature curves with three different backfill material within 300 minutes (5 hours) at the location 3.83 ft (1.28 m) above the bottom of the anchor. The anchor grouted with bentonite clay had the longest time period with the temperature above 32°F (0°C), which was 240 minutes (4 hours). While the anchor with Microsil or special cement formula experienced a temperature above 32°F (0°C) of 60 minutes (1 hour) and 30 miutes (0.5 hour), respectively. The highest temperature for bentonite clay is 76.3°F (24.6°C), which is the largest among them.

Figure 5.10 is the temperature curves with different backfill material for the whole freeze back process. Although bentonite clay was mixed at a high temperature, that material generated no heat of hydration heat generated during the entire freeze back process. Microsil generated the largest amount of hydration heat while special cement formula generated very limited heat and for only a short period of time. Both bentonite clay and Microsil took about 8,000 minutes (133 hours) to freeze back to the initial temperature. Special cement formula took only 4,000 minutes (66 hours) to freeze back.

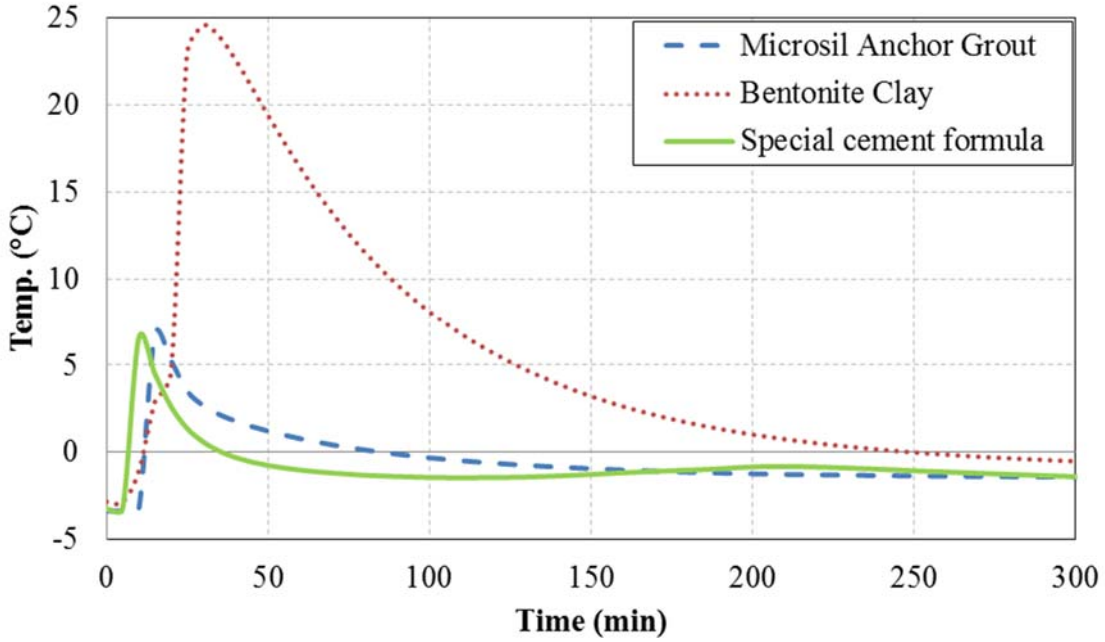

Figure 5.9 Temperature vs. Time with Different Backfill Materials within 5 Hours

In summary, of the three types of grout material, Bentonite clay provides the highest maximum temperature which will cause severe thermal disturbance of the in situ soil. Yet, the time to freeze back is shorter than Microsil because no extra heat (heat of hydration) is generated after backfill. For Microsil backfill material, even though the maximum temperature is not as high as Bentonite clay, the heat generated by hydration after backfill will increase the time for soil to freeze back to its original temperature. The special cement formula has a lower maximum temperature than Bentonite clay grout and also requires freeze back time than Microsil because of the special cement's lower hydration heat. Therefore, special cement formula is recommended, as the best of the three materials tested, for use as anchor grout in a permafrost area.

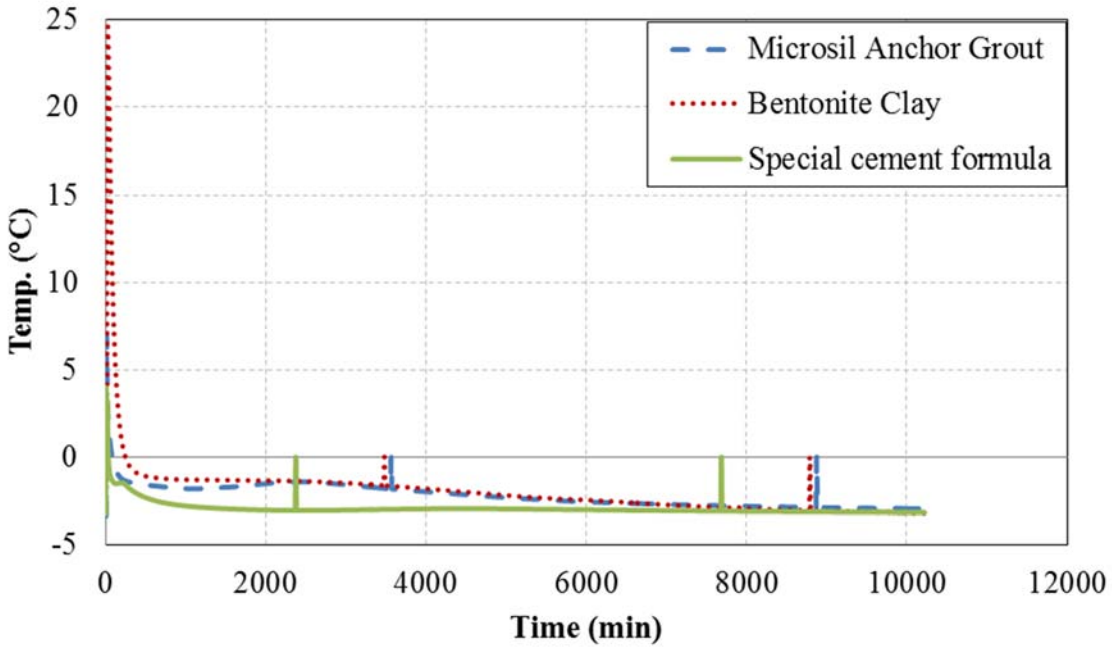

Figure 5.10 Temperature vs. Time for Different Backfill Materials

5.3 Duckbill Test Results and Analysis (Permafrost Tunnel)

Four duckbill anchors were tested in the permafrost tunnel. These were tested at anchor locations designated 13, 14, 16 and 17 in Figure 4.5.

For the in situ tests, only one of the duckbill anchors (Duckbill 13) was successfully installed in the normal way (set with a jack load). After numerous attempts at normal installation, the three remaining duckbill anchors were inserted into their respective boreholes and then a gravel backfill material was placed into fill the hole, followed by enough water to fill the voids in the gravel. This installation method created a six foot long, frozen gravel "plug" above the head of the duckbill anchor The freeze back time for the saturated gravel was relatively short, less than 2 days. All duckbill anchor tests were conducted using load increments of 220 lb (1 KN) starting with 440lb (2 KN) and continuing to 1,320 lb (6 KN). Duckbill anchors 13 and 17 were subjected to long-term creep tests. Loads of 1,320 lb (6 KN) were held for almost one month. Both short term and long term test results indicated that the apparent creep behavior of the anchors was mainly generated by stretching of the duckbill cable. Total displacements measured at the ground surface for all of the duckbill anchors was acceptable.

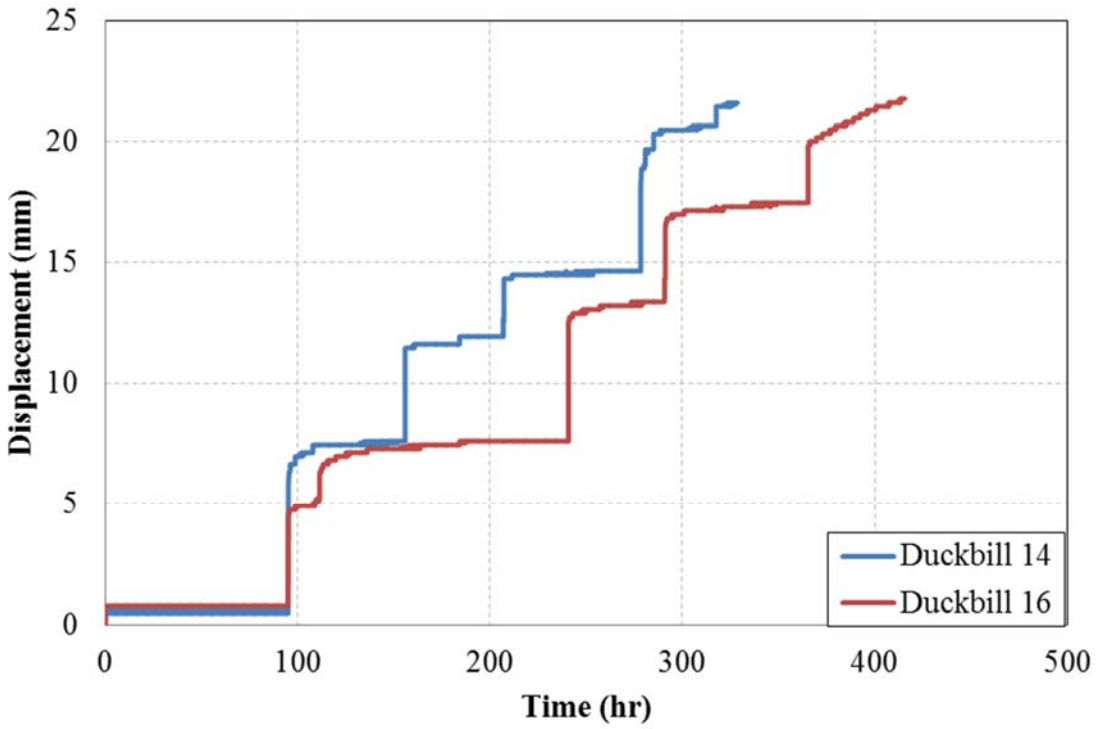

Figure 5.11 Displacement vs. Time for Duckbill 14 and 16 (Short-term Tests)

Figure 5.11 shows the test results for two of the duckbill anchors. As shown in Figure 5.11, both of the anchors experienced very limited displacement at each load level after the relatively instantaneous cable stretch caused by applying each load increment. The slopes of the displacement vs. time curves were nearly horizontal. The displacement slowly increased after load application by 0.11 in (2.70 mm) and 0.16 in (4.13 mm) for Duckbill 14 and 16 respectively at the 1320 lb (6 KN) load level. The cause of this relatively large displacement significantly after placing the final load increment is unknown. However, it is thought that it might have been due to breaking of cable strands as the total test load approached the ultimate strength of the cable. The total displacements for duckbill anchors 14 and 16 were 0.84 in (21.44 mm) and 0.85 in (21.60) mm respectively.

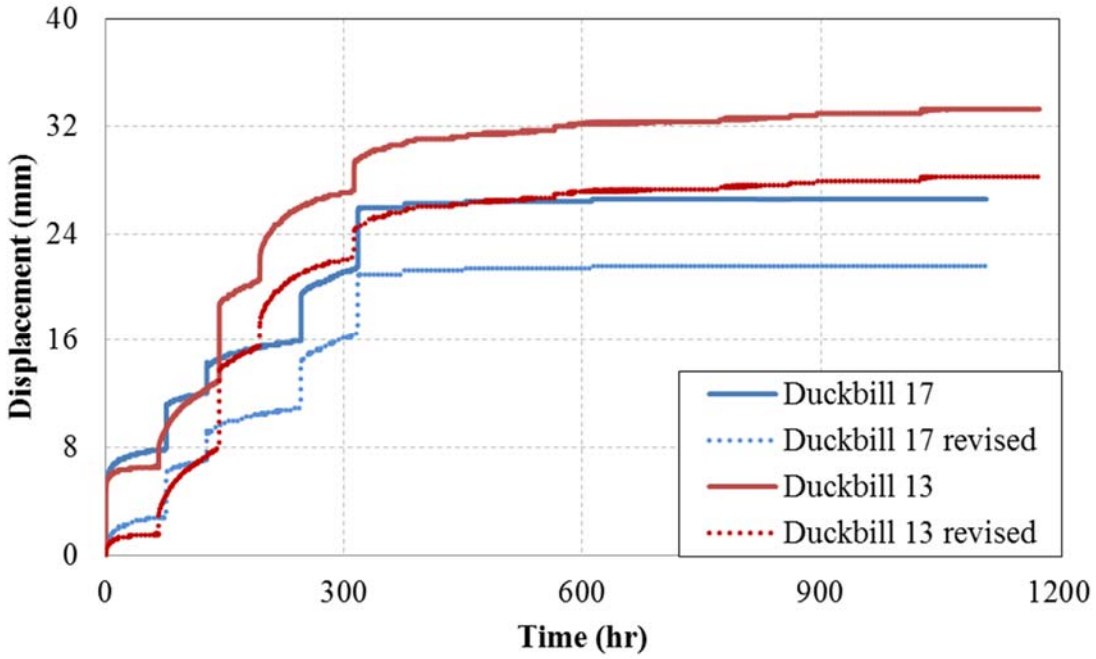

Figure 5.12 Displacement vs. Time for duckbill 13 and 17 (Long-term Tests)

Figure 5.12 shows the final testing results for Duckbill 13 and 17. At the starting load level, both of the anchors seemed to experience large, rapid displacements compared with Duckbill anchors 14 and 16. The load frames themselves moved due to their unintentional placement, for these two tests, on soft silt material covering the floor of the tunnel. The large initial movement occurred only during the first 20 minutes. After the first 20 minutes the displacements were much more similar to those seen for duckbill anchors 14 and 16. Figure 5.12 contains two sets of lines for anchors 13 and 17 as indicated in the figure's key. One set of lines plots the original data. The second (revised) set of lines is for corrected data from which the initial effect of load frame movement has been subtracted. After revision, the total displacements for Duckbill anchors 13 and 17 were 0.85 in (21.59 mm) and 1.11 in (28.28 mm) respectively. As mentioned previously, Duckbill 13 was the only duckbill anchor that was installed without gravel backfill. Therefore, a larger displacement for Duckbill 13 is reasonable due to the longer (completely unbounded) length of the cable.

Long term creep testing of Duckbill anchors 13 and 17 at 1,320 lb (6 KN) load level was conducted from December 23, 2012 to January 23, 2013. The test result for Duckbill 17 was consistent with those of Duckbill 14 and 16. The total displacement at the 1320 pound (6 KN) load level was 0.027 in (0.69 mm) for the long term test, which was very limited and can be considered as essentially

no creep. Even for Duckbill 13, with its effectively longer anchor cable, the total displacement at this load level was only 0.138 in (3.50 mm), an amount considered tolerable.

In sum, both the short term and long term creep test results indicated that the total displacement of duckbill anchors with a load of 1,320 lb (6 KN) or less was limited to acceptable range. Due to the difficulties encountered in installing three of the four duckbill anchors in permafrost, and the longer total displacement noted for the properly installed duckbill anchor, a modified installation method is recommended. It is suggested that difficult installations in permafrost soils might benefit from our experience of placing the duckbill anchor in a predrilled hole (of minimal diameter to allow anchor insertion), and backfilling the hole with saturated fine gravel or other locally available, similarly workable material. An incidental benefit of such installation should minimize cable stretch—especially for short term loads as long as the cable retains its original "bond length" within the frozen backfill material.

5.4 Load Distribution along Anchor Shaft for Bar-Type Anchors (Permafrost Tunnel)

In this section load redistribution along the length of the bar-type anchors is comprehensively analyzed. Figure 5.13 shows the location of the sensors. Two types of sensors were used to measure the strain in the rebar and in the backfill materials. The HPI full bridge sensors were welded-attached along the steel anchor bars at 1.5 ft (0.5 m), 3.83 ft (1.23 m), 6.16 ft (2.05 m) and 8.5 ft (2.83 m) from bottom to the top respectively, as shown in Figure 5.15. At 1.5 ft (0.5 m)and 6.16 ft (2.05 m), HPI sensors were welded to both sides of the bars in order to eliminate the effect of eccentricity. The upper part of the anchor which extends above the ground surface was also fitted with two HPI sensors to measure the load applied to the sensor (actually attached to the anchor bar adaptor). Four Geokon 4200 sensors which could be used to measure the strain in the concrete were installed within the anchor grout at the lower four locations.

Figure 5.14 gives the strain vs. depth curves for the steel rod of anchor 1. Anchor 1 contained a solid steel tendon and was backfilled with Microsil Anchor Grout. The negative value of the strain means that the sensor is in tension. At a relatively low load level, say 5 tons, the lower part of the anchor barely experienced any strain change which indicates that the load has not been transferred to the lower part due to the adfreeze bond strength between the anchor shaft and the surrounding soil. At all load levels, the strain distribution is non-linear. This phenomenon has also been

discussed in Biggar and Sego (1993b) who mentioned the non-uniformity of stress distribution at various load levels for Dywidag bar anchors with grout backfill. In general, the strain distribution along the anchor shaft becomes increasingly nonlinear at higher load levels (20 ton), where the strain in the upper part of the anchor becomes very much higher than that at the bottom.

Yet, Biggar and Sego (1993b) could not describe the stress change with time for a given load because the readings of the strain gages were only recorded at the end of each load increment. In our test, the readings were recorded at time intervals of 1 minute. So a much better understanding of the load redistribution process could be attained. At each load level, the strain change was largest during the first 20 hours after loading and became very small after that. This indicates that the strain redistribution could be finished in 20 hours.

Take anchor 1 as an example to illustrate the process of load redistribution. At load level of 5 ton (44.5 KN), just after the moment of loading, the load was transferred to a depth of 4 ft (1.33 m) and the bottom part did not experience any load increment. Twenty hours later, the load had transferred to a depth of 6 ft (2 m) but the strain change at 4 ft (1.33 ft) was the larger at 55 microstrains. After 20 hours the load distribution changed only slightly which indicates that the redistribution process had almost finished. At the next load level, 10 ton (89.0 KN), the load has been transferred to the bottom of the anchor and the adfreeze bond has broken all along the anchor shaft. The largest strain change due to redistribution occurred at 8.5 ft (2.83 m) which was 58 microstrains. A similar process could be observed at other load levels. Moreover, at higher load level of 20 ton (178 KN), the strain between 1.5 ft (0.5 m) to 4 ft (1.33 m) increased dramatically. At this load a crack between the bar and the grout had appeared at the top of the anchor.

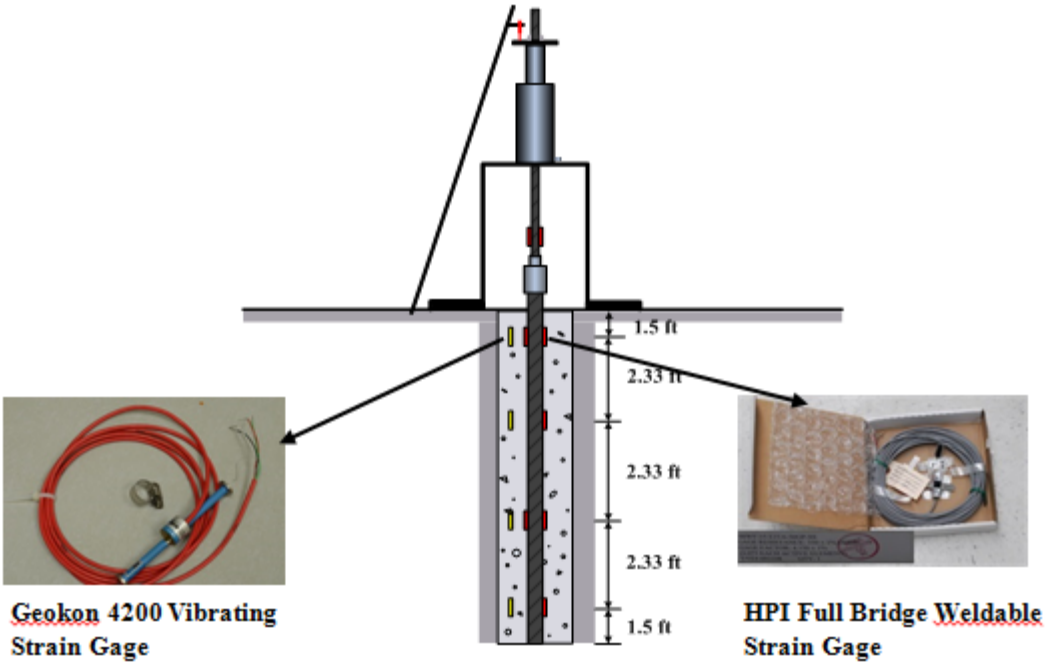

Figure 5.13 Schematic Plot of Strain Gage Location

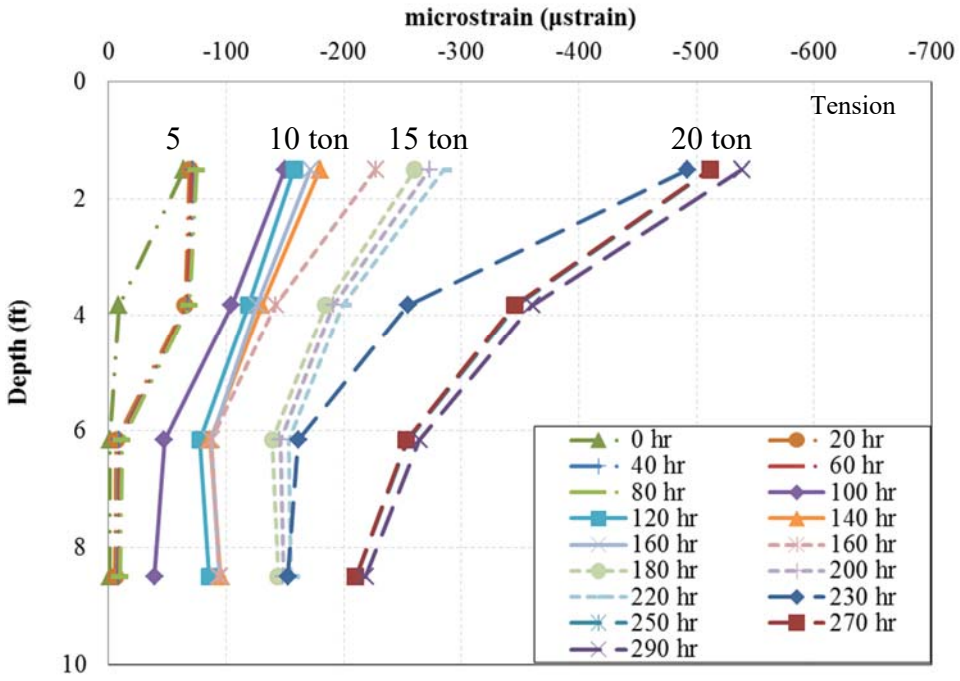

Figure 5.14 Strain vs. Depth for Anchor 1 at Different Time in Rebar

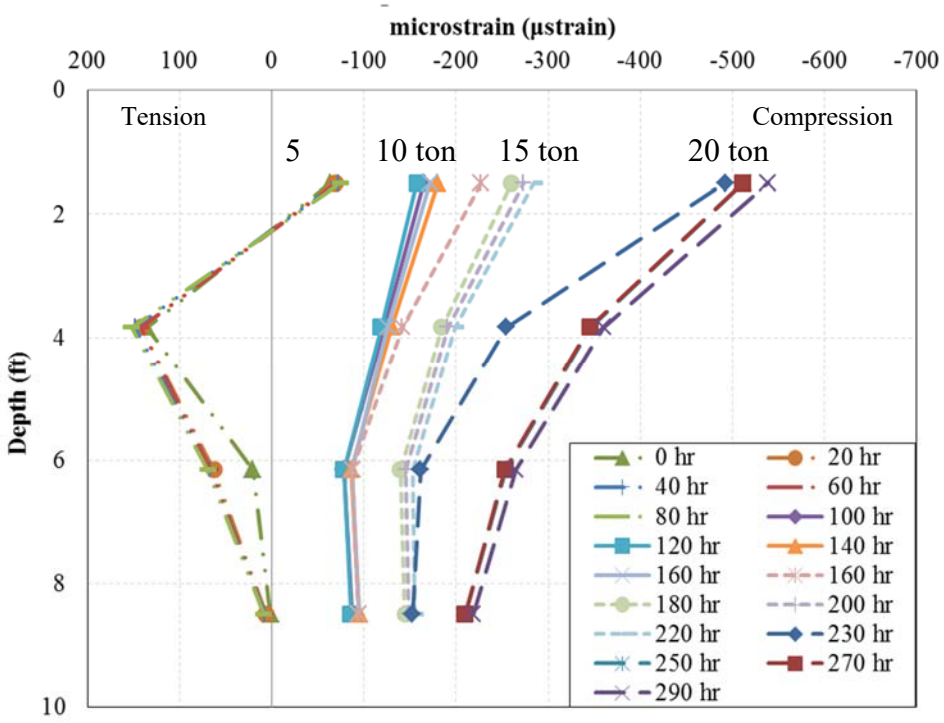

Figure 5.15 Strain vs. Depth for Anchor 1 at Different Time in Grout

Figure 5.15 gives the strain vs. depth curves for the grout of anchor 1. Microsil cement grout was used for anchor 1. The bottom Geokon sensor did not work so there were data points only at three elvations in Figure 5.17. At a low load level, the strain levels within the Microsil grout were similar to those in the steel bar. At 15 ton (133.4 KN) load level, the strain within the top 1.5 ft (0.5 m) of grout had started to decrease, meaning that a crack had occurred at a high location in the grout.

Figure 5.16 gives the strain vs. depth curves for the anchor bar of anchor 5. Anchor 5 contains the hollow steel bar and is backfilled with Microsil Anchor Grout. The load level for anchor 5 starts at 7 ton (62.3 KN) and ends at 12 ton (106.8 KN). The reason for raising the starting load level is that the displacement vs. time curve for anchors 1 and 3 did not show the creep behavior at the lowest level.

A relatively long-term creep test was also performed on anchor 5, at the 12 ton (106.8 KN) load level, to determine the trend of load redistribution. The long-term creep test lasted for 800 hours, starting from December 23, 2012 to January 24, 2013. From the figure, the strain appears to become more linear with time and increased load. Soon after the moment of loading, the curve

was highly non-linear. The strain distribution between 4ft (1.33 m) and 8.5 ft (2.83 m) becomes fairly linear later in the testing (the curves at right). The tentative general conclusion is that the strain distribution tends toward linear with time is supported by the long term test data (farthest curve to right).

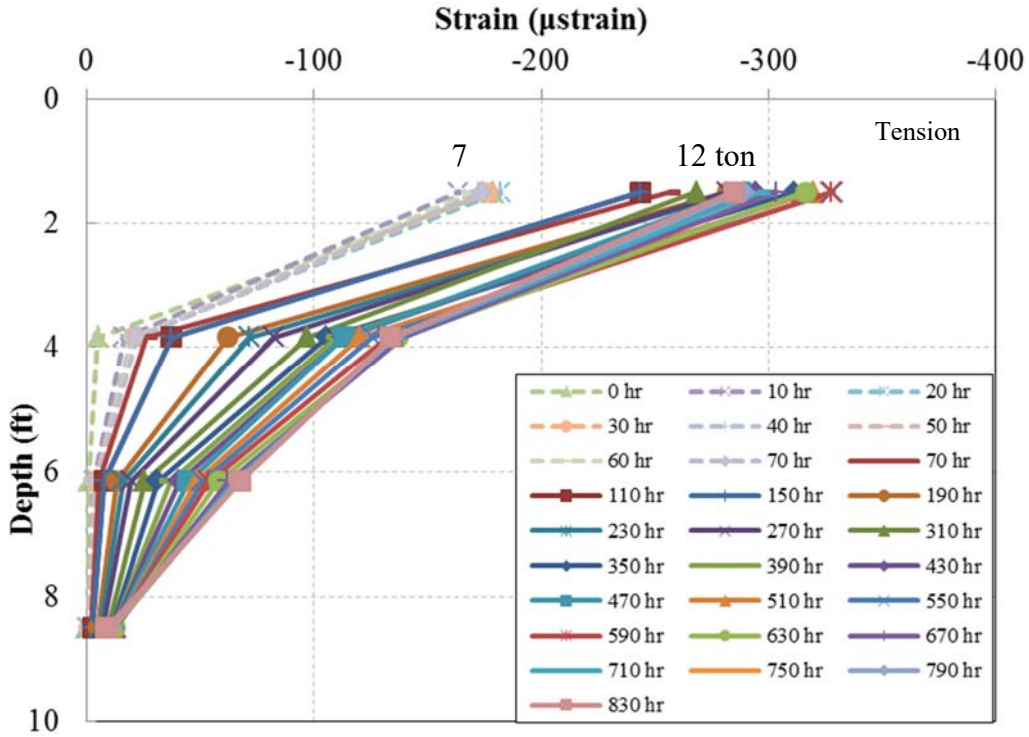

Figure 5.16 Strain vs. Depth for Anchor 5 at Different Time in Rebar

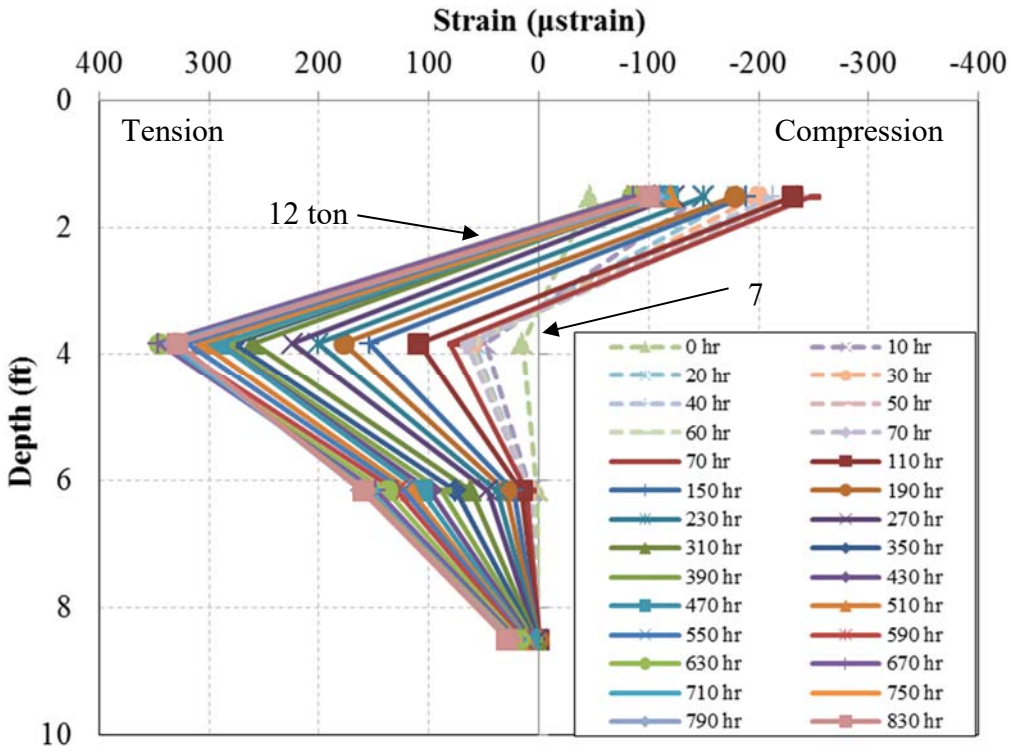

Figure 5.17 Strain vs. Depth for Anchor 5 at Different Time in Grout

Figure 5.17 shows the strain vs. depth curve within the Microsil cement grout used for anchor 5. Positive values shown in the figure indicate that the grout was in compression while negative values indicate tension. Negative values indicate that cracks had developed in the grout. From the figure, one might be able to estimate the location of the crack. In this case, the crack was perhaps between 2 ft (0.67 m) to 4ft (1.33 m) from the top of the anchor. The strain in the anchor 5 bar at 7 tons (62.3 KN) is larger than that for the anchor 5 grout at 10 tons (89.0 KN) by over 100 microstrain. This is because that the load in the grout transferred to rebar after the grout cracked. Moreover, the load distribution in the grout also tended to be linearized at the end of the test which also proves the assumption discussed previously. So the assumption that the load distribution along the anchor shaft is linear is reasonable and valid for long term creep analysis.

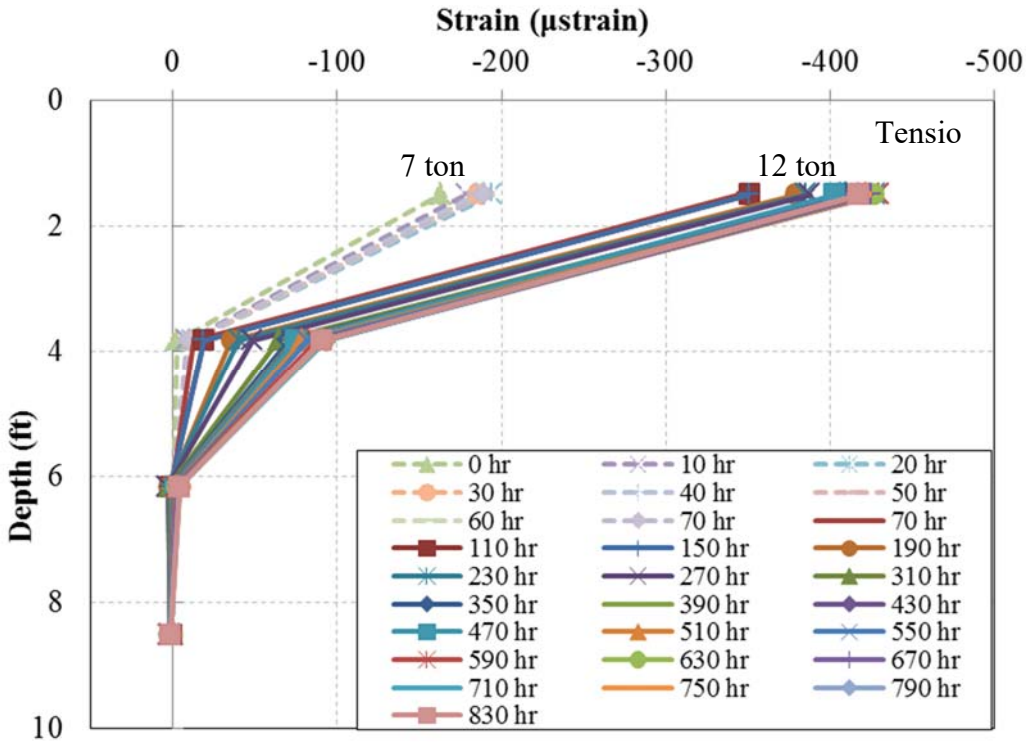

Figure 5.18 Strain vs. Depth for Anchor 6 at Different Time in Rebar

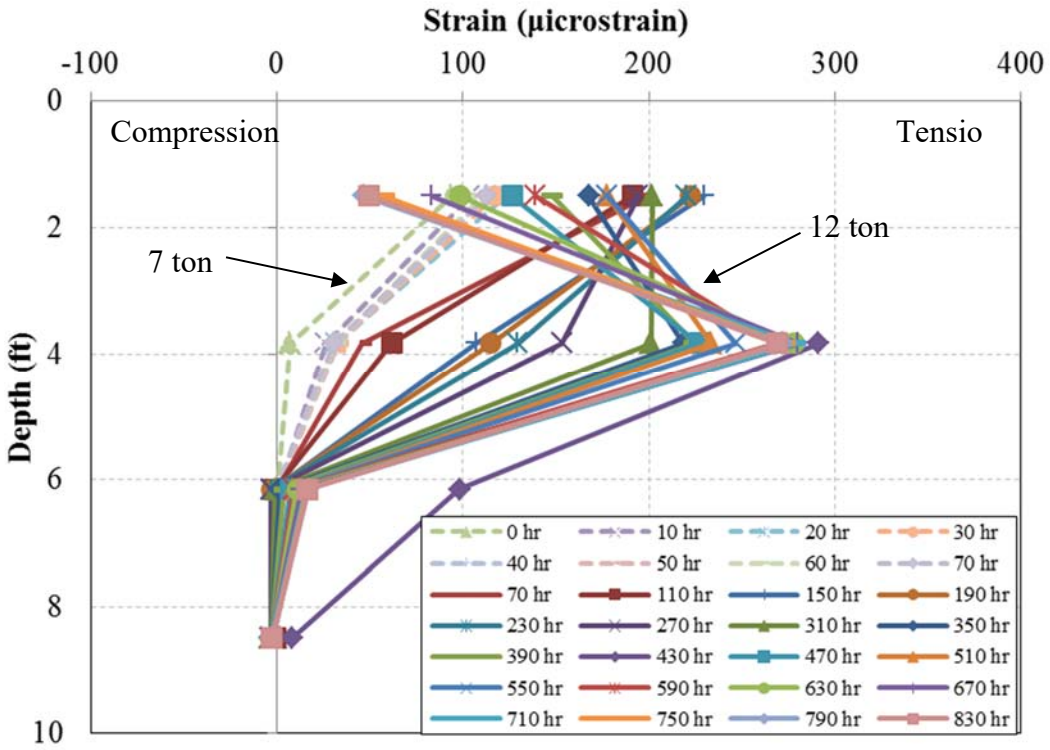

Figure 5.19 Strain vs. Depth for Anchor 6 at Different Time in Grout

Anchors 6 and 5 had the same types of rebar and grout (hollow steel bar and Microsil cement grout). Figure 5.18 and 5.19 are the test results for anchor 6. The test results were very consistent with that of anchor 5. From Figure 5.18, one can tell that the crack in the grout occurred at 430 hour and the location was at the top between 0 ft (0 m) and 2 ft (0.67 m). The final load distribution of anchor 6 had a trend of linearization even though the curve after 830 hour was not linear along the anchor shaft. Briaud (1998) mentioned that the grout would crack with the strain magnitude of 10^{-4}. Figure 5.19 also proved this conclusion. At 7 ton (62.3 KN), the average strain at 1.5 ft (0.5 m) was about 100 microstrain and the load distribution curve was reasonable. Yet at 12 ton (106.8 KN) , the strain at 1.5 ft (0.5 m) started to decrease gradually and the strain at 4 ft (1.33 m) increased on a large scale due to the reason that the load bearing by the upper part of the anchor has been transformed to the lower part due to the crack of the grout. Moreover, the bottom of the grout in anchor 6 did not experience large load through the whole process until the end of the test and the curve became relatively linear.

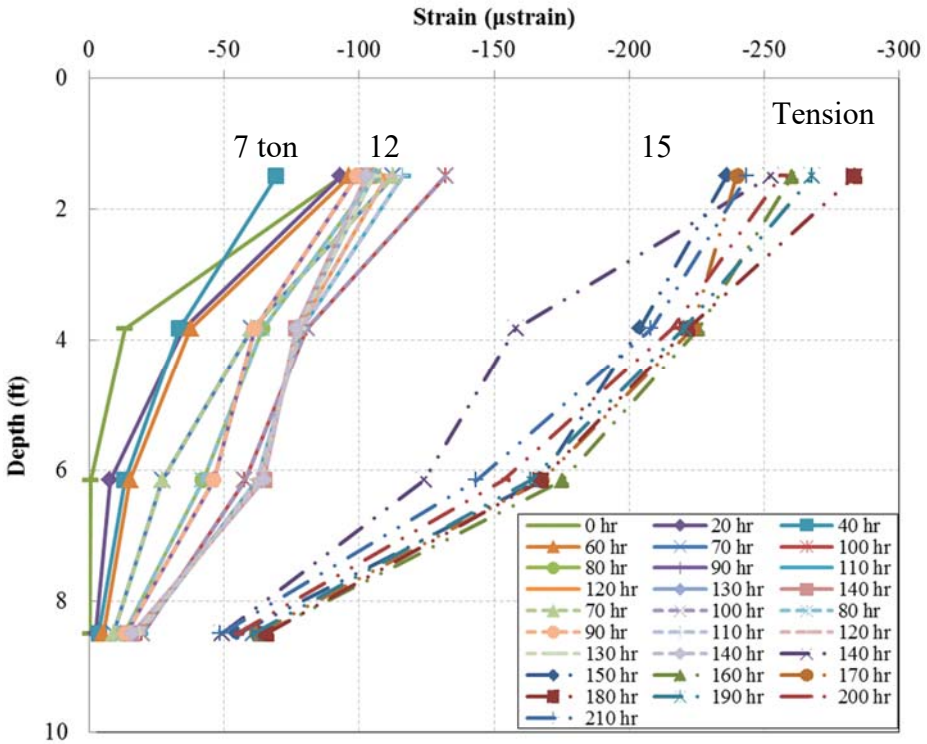

Figure 5.20 Strain vs. Depth for Anchor 8 at Different Time in Rebar

Figure 5.20 and 5.21 are the strain vs. depth curves for anchor 8 which used hollow steel bar and bentonite clay. Compared with other anchors, the load distribution in clay was very different. For Figure 5.20, at 7 ton (62.3 KN) load level, the strain transferred into the end of the anchor right

after the load is applied and the load distribution was highly non-linear for all load levels. From Figure 5.21, at the same load level, only the strain from 3ft (1 m) to 6 ft (2 m) was positive which meant that the clay has already cracked at the beginning of loading. After the clay cracks, all the load was transferred to rebar. Moreover, the positive strain in clay might largely result from the remaining adfreeze bond between the anchor shaft and the soil. This is reasonable due to the high backfill material temperature at the initial condition. The high temperature would lead to more ice-rich soil melting which in turn provided much larger adfreeze bond for anchor 6.

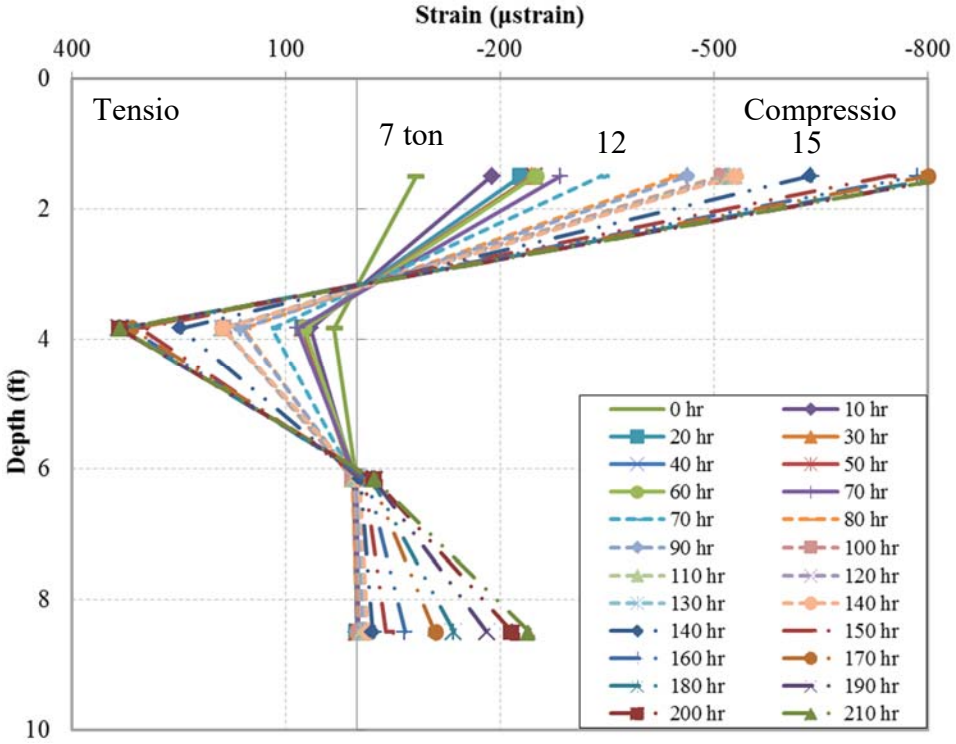

Figure 5.21 Strain vs. Depth for Anchor 8 at Different Time in Clay

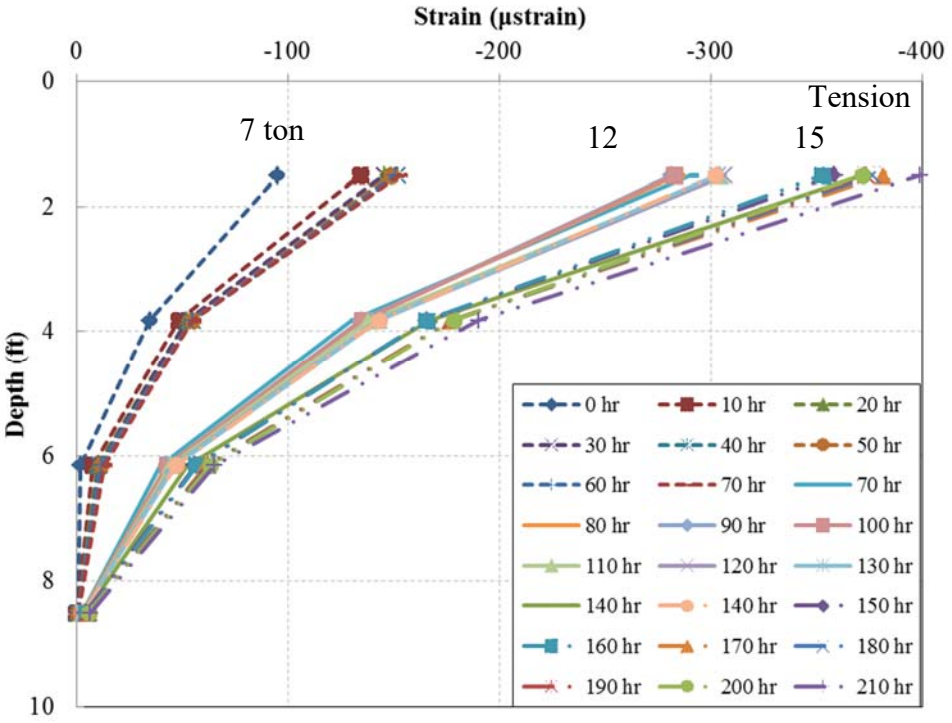

Figure 5.22 Strain vs. Depth for Anchor 12 at Different Time in Rebar

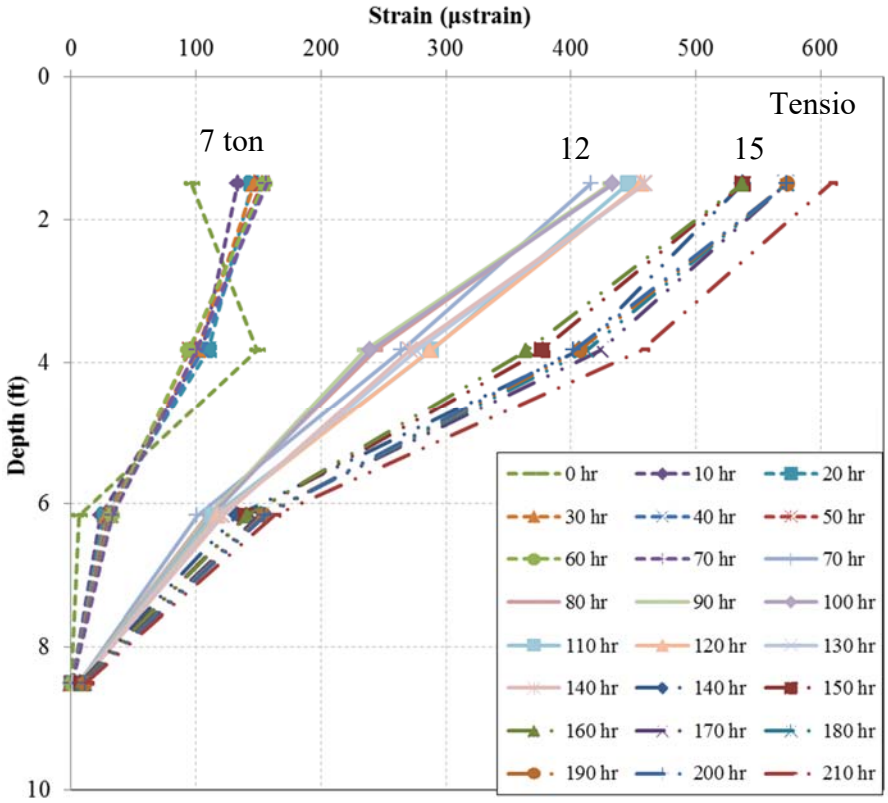

Figure 5.23 Strain vs. Depth for Anchor 12 at Different Time in Grout

Figure 5.22 and 5.23 shows the strain vs. depth both in grout and rebar for anchor 12 which used hollow steel bar and special cement formula grout. The strains in rebar at three load levels were smaller than that of other anchors. Part of the reason is that the grout did not crack during the whole loading process which could bear the applied load. The maximum strain changes in rebar were 23 microstrain at 7 ton (62.3 KN) , 8 microstrain at 12 ton (106.8 KN) and 47 microstrain at 15 ton (133.4 KN). Plus, this special designed cement formula could bear larger strength compared with Microsil Anchor Grout. It did not show any crack within the loading range. Both of the load distribution at the end of the test tended to be linearized.

In sum, the load distribution curve for the anchor is non-linear within the testing time and tends to become linearized with time goes by. Plus, during the load redistribution process, the maximum change of strain occurs within 20 hours after the load applied to the anchor and after that, the strain change is very limited. And the curve tends to be linearized at last.

Microsil Anchor Grout will crack under a strain of 100 microstrain or over. Bentonite clay backfill materials could not bear any strain, and it cracks immediately after the load applied. And the cement grout with special designed formula exhibits the best, will not show any crack within 15 ton (133.4 KN).

5.5 Displacement vs. Time Curves (Permafrost Tunnel)

As part of the testing program it was of course necessary to collect accurate data regarding the vertical movement of the anchor with respect to time. However, an equipment problem occurred that made acquisition of these data a two-step process. It was: 1) necessary to collect the raw displacement data during load testing, and then 2) process all displacement data to compensate for the equipment problem as explained in Appendix and this section only provides the revised displacement vs. time curves. Discusses on (corrected) displacement results for a selection of anchors is included at the end.

The hydraulic pump used throughout the permafrost tunnel testing process was found to be incapable of maintaining a constant pressure. Pump pressure variations made the raw displacement data unusable. After some thought, it was possible to develop a mathematical procedure for transforming raw displacements into useable data. All of the raw displacement data was revised according to the procedure explained in the following pages.

Figure 5.24 shows the typical displacement vs. time curve (creep curve) for one of the anchors tested. The jagged upper line in the figure shows that the difference between maximum and minimum load could be larger than 3 tons (26.69 KN)) at each load level. This much variation was not acceptable. The lower two lines are the displacement vs. time curves before and after adjustment.

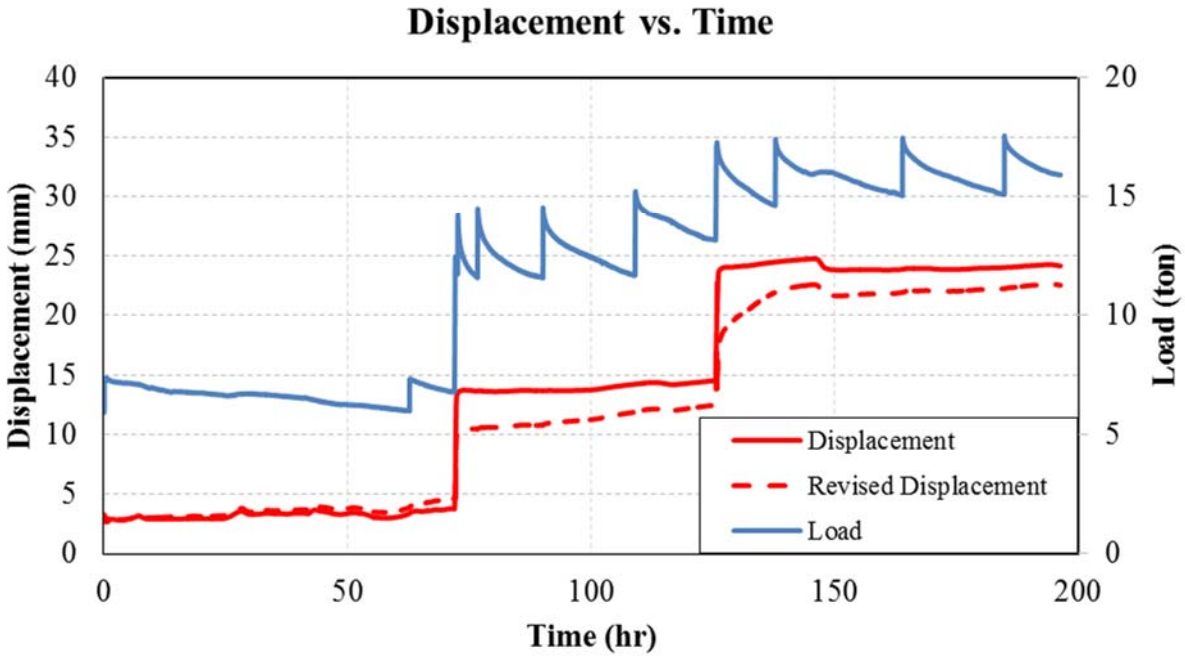

Figure 5.24 Typical Displacement vs. Time Curve

The displacement vs. time curves for different anchors vary dramatically even if the grout materials are the same. Reasons for this could include:

Inconsistency of the soil profiles at different anchor locations As discussed at the beginning of Chapter 4, the soil profiles contain various combinations of wedge ice, silt and gravel.

Gravel influence For some anchor locations, gravel layers of varying thickness were noted.

Variable diameters of anchor boreholes During the drilling process, the majority of the holes were expanded from a smaller (3 inch) predrilled hole. The diameter of holes could vary from hole to hole as well as vary somewhat within individual holes. Variations in borehole diameter could have significantly influenced the data.

Adfreeze bond strength variations due to grout hydration heat Adfreeze bonds between the grouted-filled anchor shafts and the native permafrost soils may have varied significantly due to the different amounts of hydration heat generated by the different grout types.

Figure 5.25 is the displacement vs. time curve for anchor 4 which had a solid steel anchor bar and Microsil Anchor Grout backfill material. The average strain rates at 7 ton (62.3 KN), 12 ton (106.8 KN) and 15 ton (133.5 KN) were 7.066×10^{-5} hr^{-1}, 6.001×10^{-5} hr^{-1} and 5.660×10^{-5} hr^{-1}. The strain rate decreased with the increment of normal stress which indicates one of the interesting properties of ice-rich soil. Pekarskaya (1965) mentioned before that ice was known to creep at low stresses. For ice-rich soil at higher stress conditions, ice itself could heal or restore the broken bonds during the strain process which would in turn slow down the speed of creep. This test result confirms the 1965 findings.

Another interesting finding is that the primary creep of undisturbed Fairbanks Silt is very short. At higher load levels, say 12 tons (106.8 KN) and 15 tons (133.5 KN), the primary creep can be neglected. Thompson and Sayles (1972) also pointed out that this phenomenon was maintained for strains exceeding 20%. And a stress exponent of 4 that was determined for higher stress levels that agreed with other researchers' results.

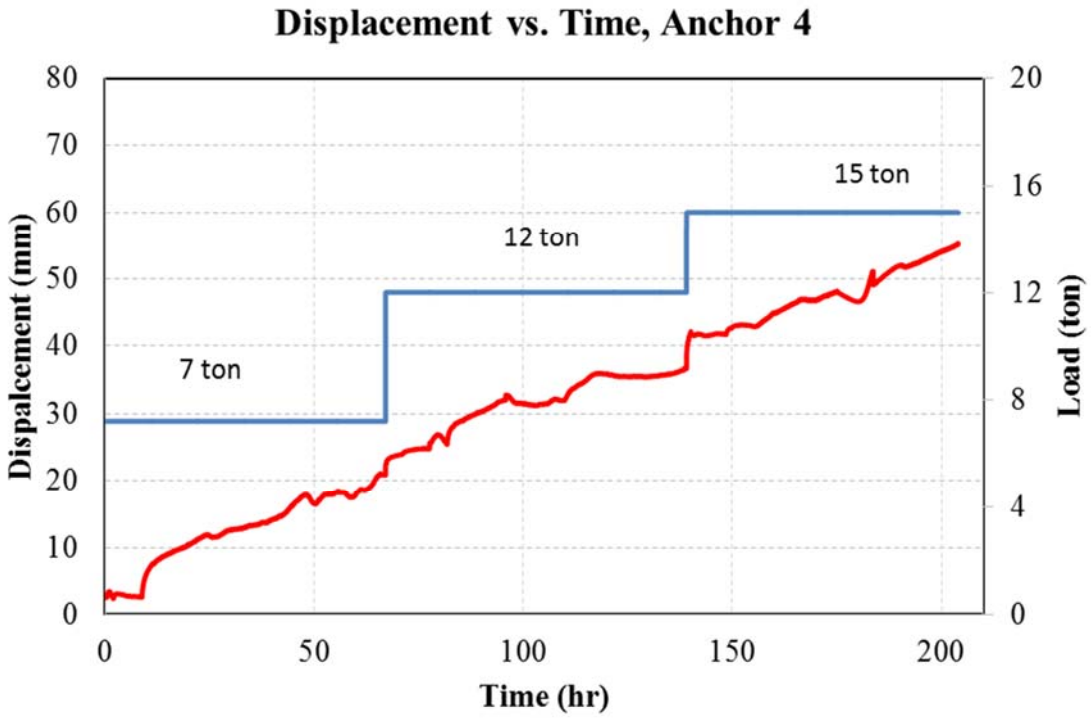

Figure 5.25 Displacement vs. Time Curve for Anchor 4

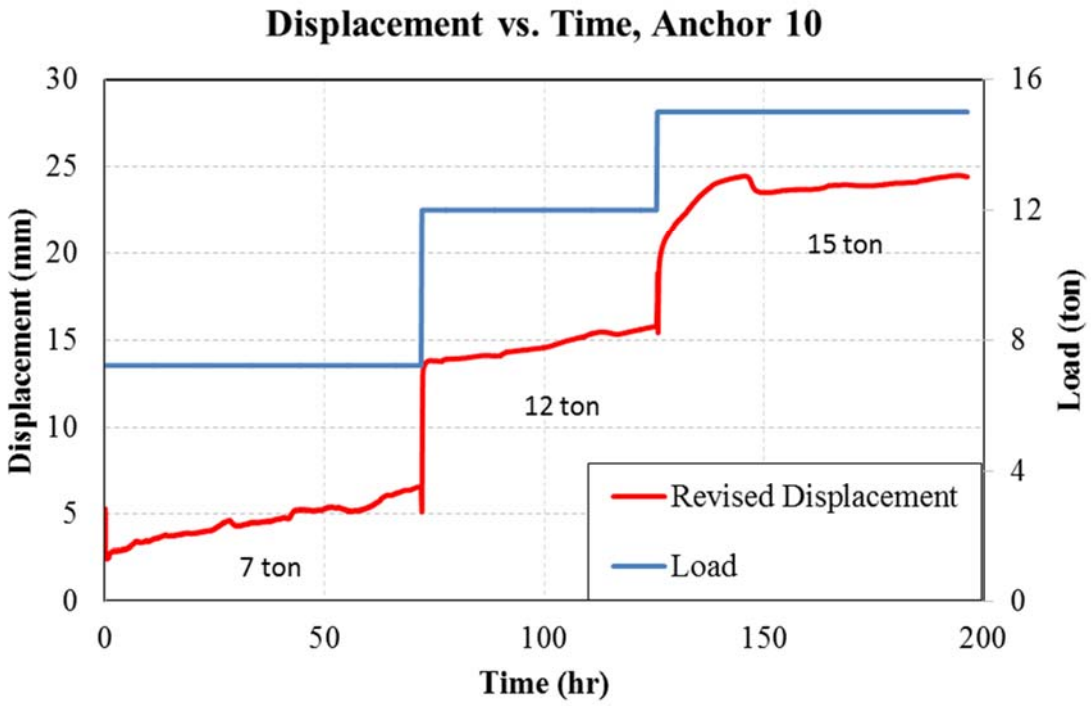

Figure 5.26 Displacement vs. Time Curve for Anchor 10

Figure 5.26 presents the displacement vs. time curve for anchor 10 which had a hollow anchor bar and was backfilled with Bentonite Clay. The average strain rates at 7 ton (62.3 KN), 12 ton (106.8 KN) and 15 ton (133.5 KN) were 1.552×10^{-5} hr^{-1}, 1.291×10^{-5} hr^{-1} and 5.956×10^{-6} hr^{-1} respectively. In general, the strain rate for anchor 10 is much smaller than that of anchor 4. The anchor experienced a large strain as load increments were added, but rapidly went into a low rate of secondary creep. No tertiary creep stage was observed during the test.

Figure 5.27 shows the displacement vs. time curve for anchor 11 which had a hollow steel anchor bar and was backfilled with special cement formula. The average strain rates at 7 ton, 12 ton and 15 ton were 5.261×10^{-6} hr^{-1}, 1.991×10^{-6} hr^{-1} and 7.326×10^{-7} hr^{-1}. The strain rates for anchor 11 were much smaller than anchors 8 and 10. The anchor failed at 15 tons and the time at failure was about 153.7 hrs.

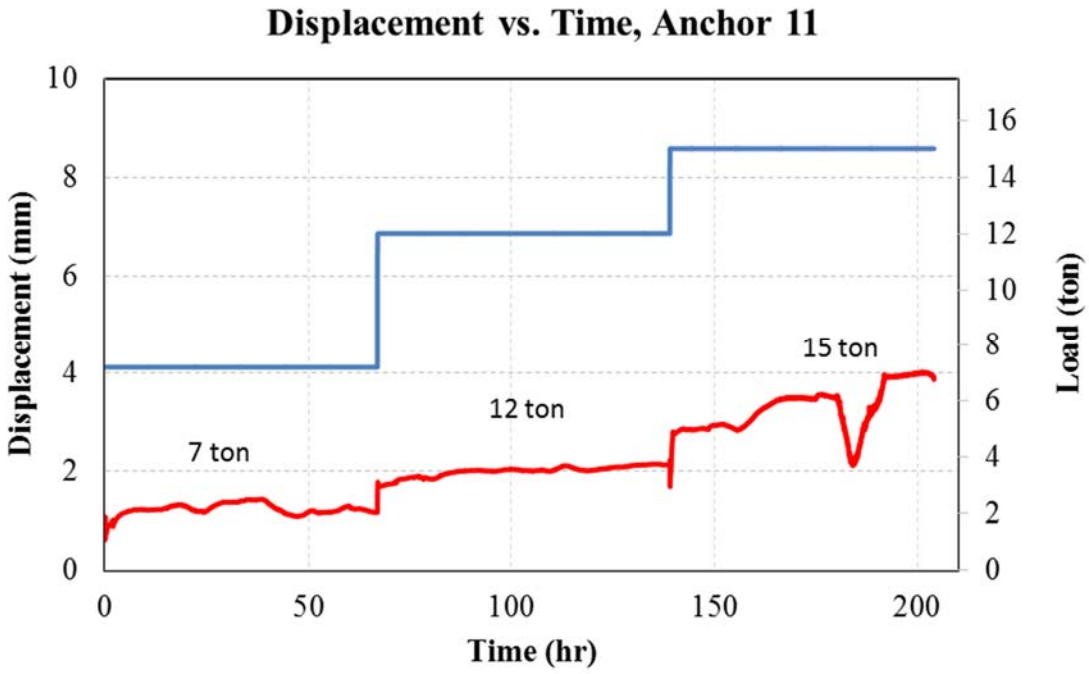

Figure 5.27 Displacement vs. Time Curve for Anchor 11

The displacement vs. time curves for the other anchors are included in Appendix C. In sum, the total displacements varied from 0.157 in (4 mm) to 2.362 in (60 mm). The strain rates varied across a range between 10^{-5} min^{-1} and 10^{-6} min^{-1}. Hydraulic pump problems

notwithstanding, the average strain rate at different load level can be considered fairly linear.

5.6 Pullout Test Results and Analysis

Among all the 13 anchors, only the anchors grouted with Bentonite clay were pulled out and the ultimate pullout capacity was 35 ton (349 KN). At 35 ton load level, two phenomena indicated the anchor failure: displacement records kept continuously increasing and the hydraulic pump lost pressure in a rapid speed. Figure 5.28 shows the appearance for anchor 4 after failure. The failure occurred at the interface between rebar and Bentonite clay and the surrounding frozen soil was not been pulled upward at all.

Figure 5.29 shows the appearance of anchor 6 and 12 after pullout test. Both of them did not fail at 55 ton (548 KN) load level. Also, the bond between grouting material and rebar were quite strong and no crack was observed. Several iron plates were broken after the pullout test due to extremely high pressure (about 9,000 psi or 62 MPa). For anchor 12 in Figure 5.29 (b), it seemed that it was uplifted by about 1 in (25.4 mm). In fact, before the creep test, the ground was not flat and some of the frozen soil had been removed. So it gives an illusion that the anchor had been pulled out.

Figure 5.28 Anchor 4 After Failure

(a) Anchor 6 **(b) Anchor 12**

Figure 5.29 Anchor 6 and Anchor 12 After Test

Figure 5.30-32 give the displacement vs. time curves for anchor 6, 8 and 12. The maximum displacement was 0.30 in (7.52 mm) for anchor 6 and 0.44 in (11.15 mm) for anchor 12. Anchor 8 failed immediately after 35 ton (349 KN) was applied to the anchor. For each load level, ten data points were recorded and the time interval for each load level was 5 min. all of the anchors experience a 0.04 in (1 mm) displacement right after 5 ton (50 KN) load level. After the pullout test, one more displacement data was recorded so that the total settlement of the system could be determined. For example, the first and last recorded data for anchor 6 was 8.66×10^{-4} in (-0.022 mm) and 0.097 in (2.463 mm). So the total settlement of the loading system was the difference between those two readings which was 0.098 in (2.490 mm). Moreover, after unloading process, the displacement was very limited compared with the peak value. This indicates that most of the displacement was caused by the extension of rod rather than the movement of the entire anchor.

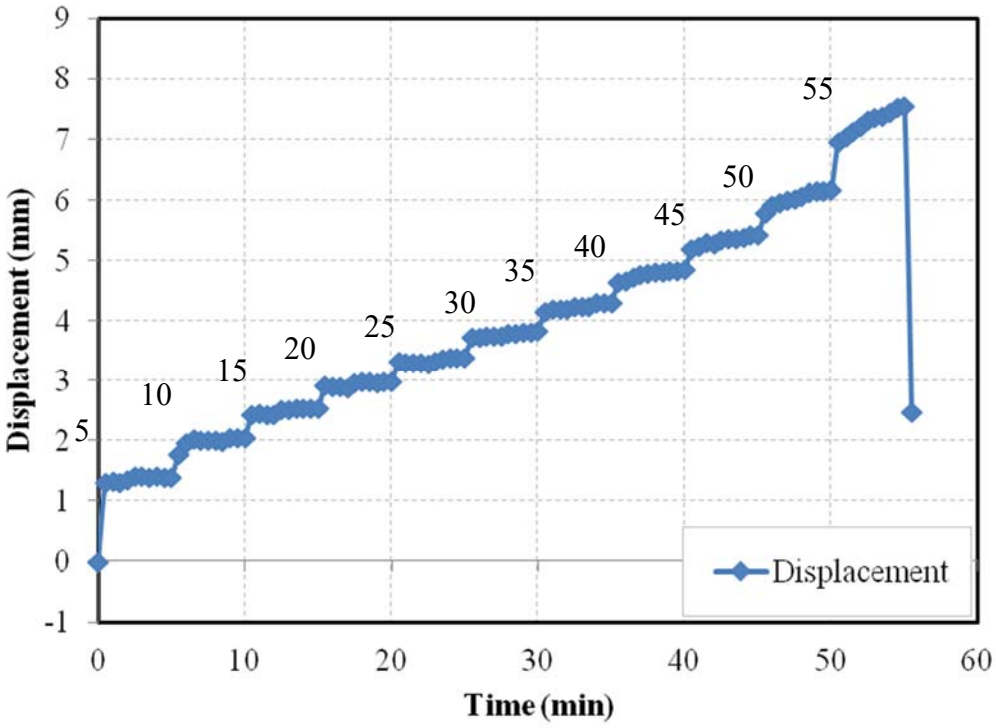

Figure 5.30 Displacement vs. Time for Anchor 6 (Pullout Test)

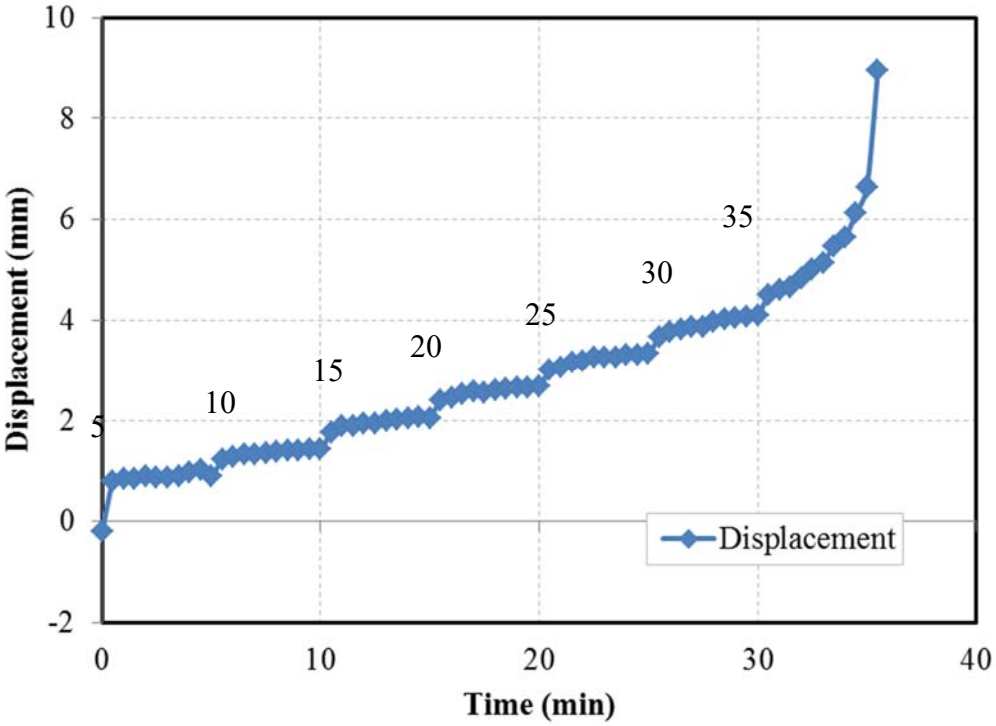

Figure 5.31 Displacement vs. Time for Anchor 8 (Pullout Test)

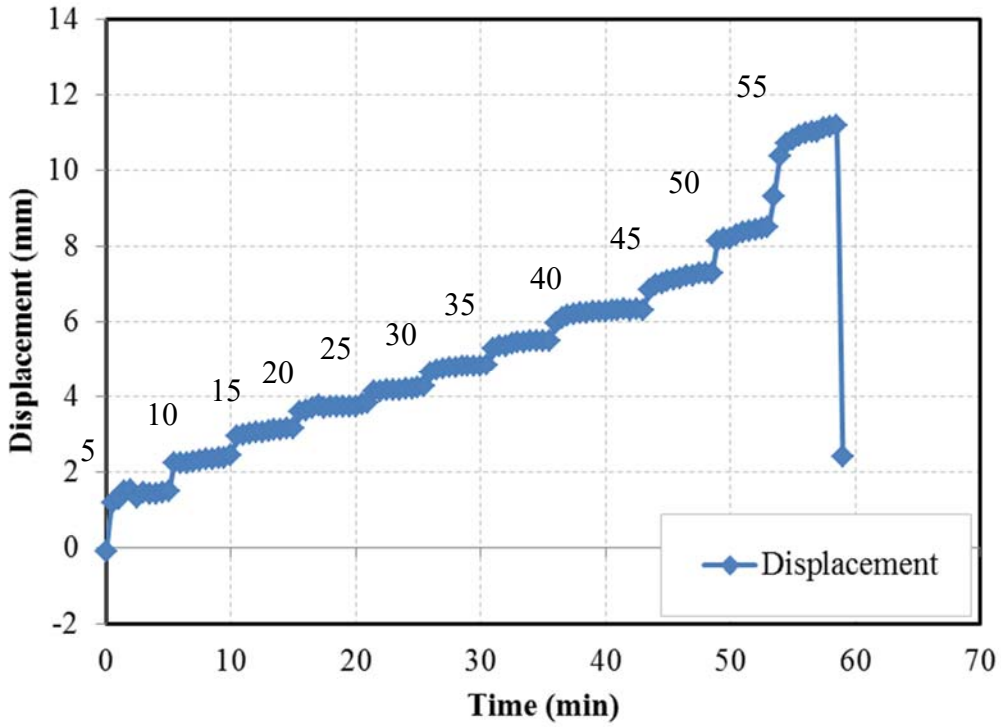

Figure 5.32 Displacement vs. Time for Anchor 12 (Pullout Test)

Figure 5.33 and 5.34 illustrate the load distribution curve within the rebar and grout respectively. The load distribution curve in the rebar increased consistently with the increment of the applied load. The load distribution curve in rebar was highly nonlinear compared with creep test result. One explanation of this phenomenon is that it takes a time period for the load to transfer to the bottom of the anchor. Yet the loading interval for pullout test is only five minutes which is too short compared with creep test (each load level lasts for 3 days). So this highly nonlinear short-tern load distribution curves not in contrast with the conclusion that the load tends to be uniformly distributed along the anchor shaft.

While the load distribution curve in grout followed different pattern. Within 20 ton (199 KN) load level, only the upper 6 ft (2 m) of the anchor bare the applied load and the load distribution decreased with increase in depth. When the applied load exceeded 20 ton, crack occurred in the upper part and only rebar bare the applied load. Also, the peak load transferred from the top to a depth of 4 ft (1.33 m) and the load from 0~4 ft decreased on a large scale. At 55 ton (548 KN) load level, the strain in the grout broke down due to such high pressure.

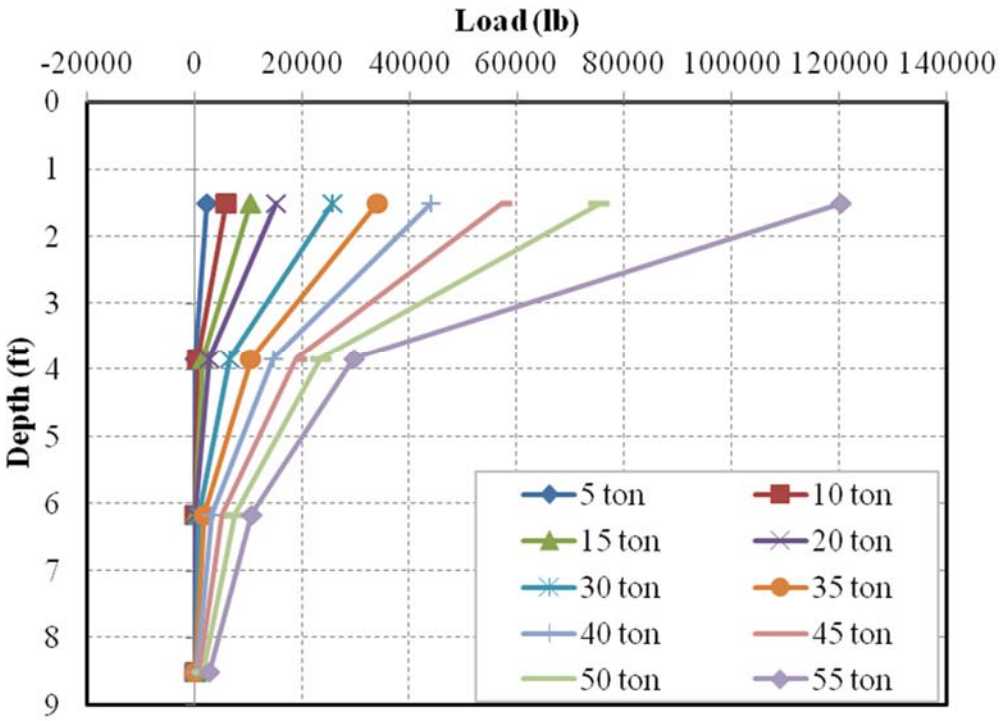

Figure 5.33 Load vs. Depth in Rebar for Anchor 6

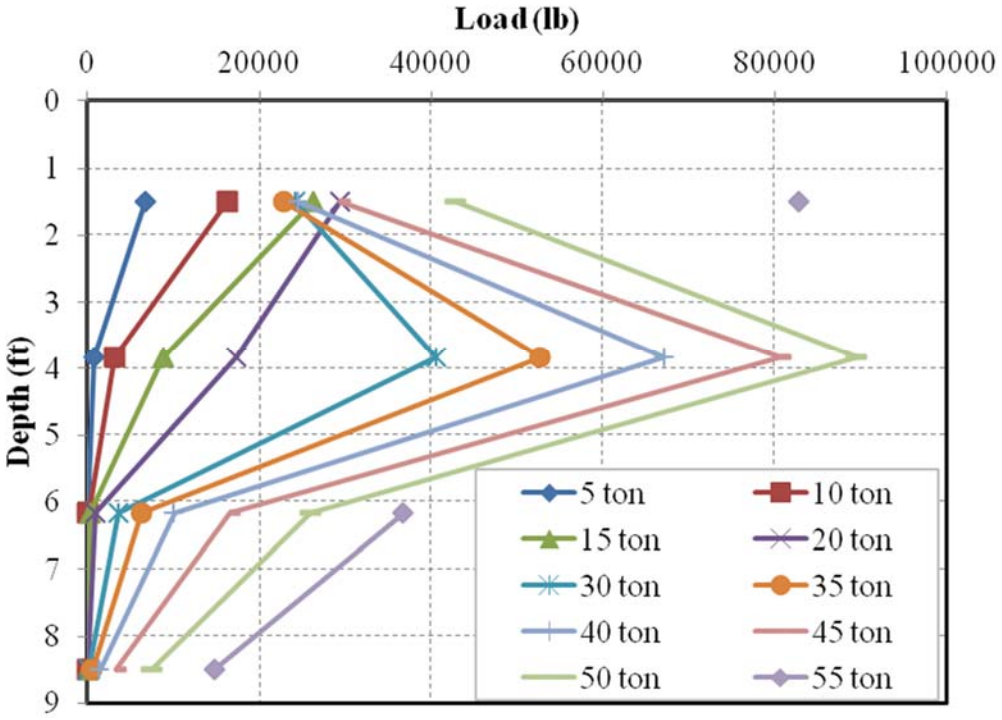

Figure 5.34 Load vs. Depth in Grout for Anchor 6

Figure 5.35 and 5.36 gives the load distribution curve for anchor 8 which is hollow rebar backfilled with Bentonite clay. The load distribution in the rebar is quite consistent with that in anchor 6. The load transferred to the bottom of the anchor at 15 ton (149 KN) and after that the whole anchor bare the applied load. From Figure 5.36 one can tell that load in the grout at 3.5 ft (1.17 m) was approximately equals to zero which indicates that the crack occurred at this place. Moreover, this crack occurred at first load level (5 ton) also indicates that Bentonite clay could not bear even a little tension. Since the failure was occurred at the interface between clay and rod, the upper part of clay could be considered as part of the frozen soil and did not move with the anchor rod. When the applied load transferred to the lower part of the anchor, the clay at the top served as a block which impeded the upward movement of the rest anchor. And this could explain why the grouting material beneath 3.5 ft experience tension and top 3.5 ft experience a load level larger than the applied load.

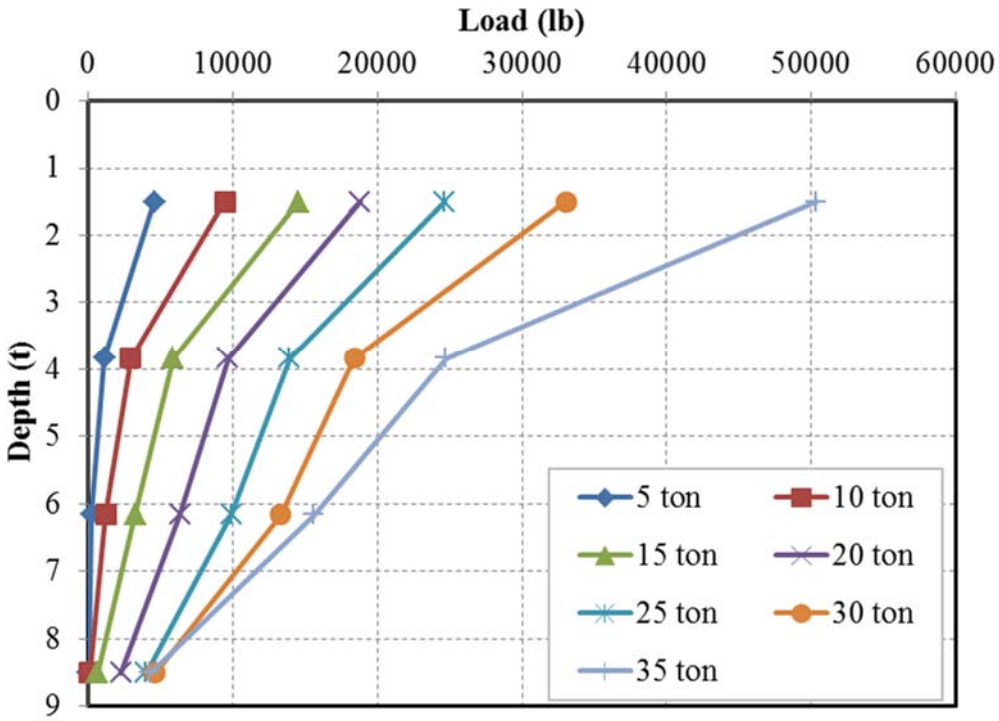

Figure 5.35 Load vs. Depth in Rebar for Anchor 8

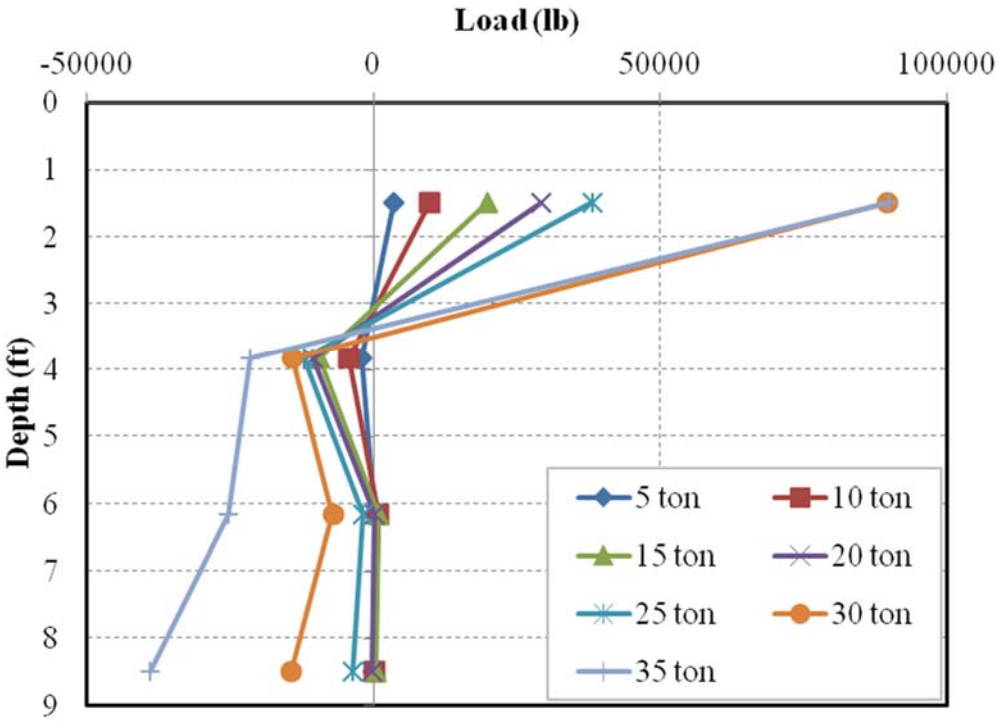

Figure 5.36 Load vs. Depth in Grout for Anchor 8

Figure 5.37 and 5.38 show the load distribution curve for anchor 12. Load distribution in the rebar was linearly distributed at lower load level and showed nonlinear behavior at higher load level. For the load distribution in grout, due to the malfunction of sensors, it could not be completely plotted. Yet, one can still tell from the graph that the applied load did not transfer to the bottom until 30 ton load level.

All the other test results for pullout test could be found in Appendix F.

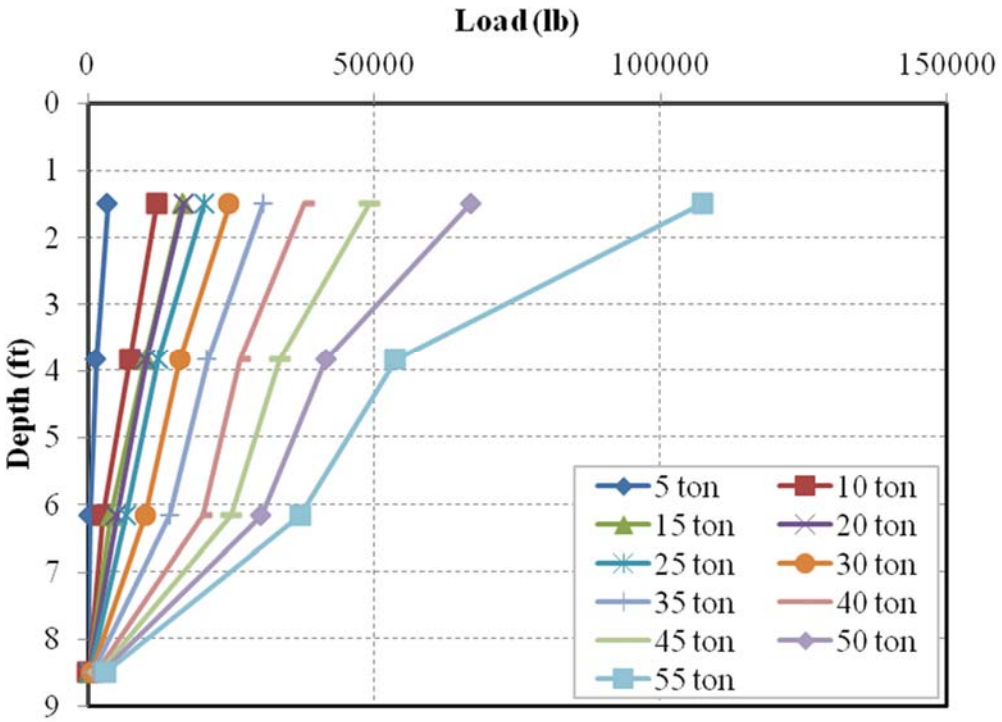

Figure 5.37 Load vs. Depth in Rebar for Anchor 12

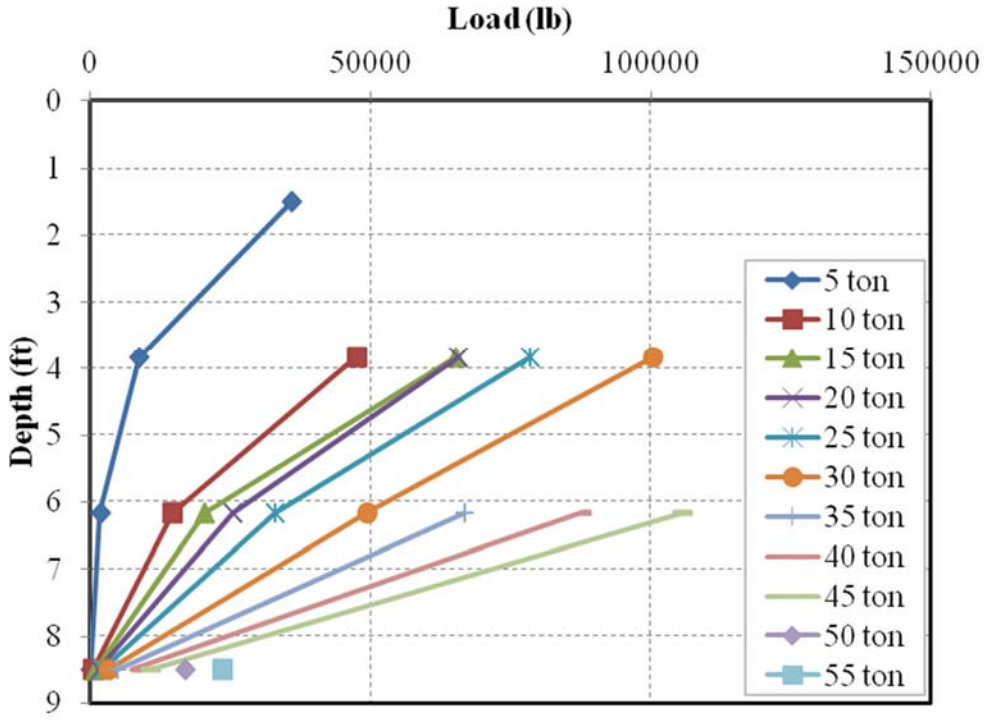

Figure 5.38 Load vs. Depth in Grout for Anchor 12

Chapter 6 Conclusion and Recommendation

This chapter presents a summary of the research based on laboratory and field tests. Recommendations are offered that address future needs and practical aspects of using shallow anchors in ice-rich silt soils.

6.1 Conclusion

The major findings of the study are:

1. The guideline is not applicable for ice-rich soil with temperatures ranging from 32ºF (0ºC) to 27.5ºF (-2.5ºC). The results of laboratory tests based on the regression analysis indicate a displacement rate of 0.2 to 300 $year^{-1}$.
2. Increments of soil temperature and water content will result in an increase in soil creep displacement rate. Special attention is required when the soil is near melting point, where the shear stress is much less than at a lower temperature.
3. The analysis of grouting temperature indicates that the average time period of temperature above 32ºF (0ºC) is about 4-5 hours. And the total time required for the temperature to return to near its to initial temperature appears to be about 3-5 days. For the two cement-based grouts tested, the hydration heat generated a maximum of 0.9ºF (0.5ºC) temperature in close proximity to the anchor.
4. The load distribution both in the rebar and anchor are not linear at the start of loading. The load distribution along the anchor tended toward linearity. If this conclusion regarding load linearity is correct, then the assumption is correct that shear stresses are linearly distributed along anchor shaft.
5. Microsil Anchor Grout cracked when strain attained a magnitude of 10^{-4}. Bentonite clay cracked at the start of 7 ton (62.3 KN) load level. Neither the Microsil grout nor the bentonite clay can bear large tensile loads.
6. Both the short-term and long-term load test results for duckbill indicated very limited creep displacement. Most of the displacement measured during duckbill anchor testing was considered to be the result of cable stretch. The duckbill anchors could not be installed in the factory-recommended way. The duckbill anchors were first placed in pre-drilled holes. Then, after trying several different methods of “setting” the anchors by jacking load, the installation was finally accomplished by simply filling the pre-drilled hole (after the duckbill had been placed at the bottom of the hole) with fine gravel and water, and allowing time for freeze back..

7. The strain rate of the steel tendon type anchors tested decreases with an increase in applied load (at higher load level). Moreover, the primary creep was found to be very limited, and therefore can be ignored for ice-rich Fairbanks silt. This result was quite different from the laboratory test which used remolded Fairbanks silt.
8. The total displacement of all steel tendon type anchors after 9 days of continuous load testing (3 days at 7 tons + 3 days at 12 tons + 3 days at 15 tons) was measured. Variation in the results was found to be high with displacements ranging between a minimum of 4 mm and the maximum of nearly 60 mm. Many factors could have contributed to this large variation such as the inconsistency of borehole diameter, inconsistency of soil profile and different properties of backfill materials (see list of possible factors in Section 5.5).
9. Only anchors backfilled with Bantonite clay were pulled out and the ultimate uplift resistance was 35 ton. The failure occurred at the interface with anchor rod and clay. All other anchors were tested to 55 ton and none were pulled out.

6.2 Recommendations

1. Use care in applying the results of this study. The study specifically focused on the creep behavior of specific anchor and grout types installed in ice-rich silt. Findings of this research do not pertain to all anchor types in all soils. Further investigation is required to determine the creep behavior of different types of soils.
2. Ignore primary creep for the anchor and soil types addressed in this research. Primary strain was found to constitute less than 10 percent of the total strain. Moreover, using the strain rates of high load level to determine the total displacement will results in a non-conservative result.
3. Do not use anchor displacement estimates based only on tests at high load levels for making design estimates. Design assumptions based on load tests only at high loadings may be non-conservative.
4. In order to be conservative, the design approach to using soil anchors in ice-rich silt permafrost must pay attention to the fact that creep increases dramatically near the freezing point. Design measures are required to ensure that soil in the vicinity of the anchors remains hard-frozen (likely -1 °C or lower depending on salinity). More research needs to focus on the behavior of anchors in ice-rich soil near melting point.
5. Loads should not be applied to anchors in ice-rich permafrost within 5 days of grouting. This study indicated that, during the grouting process, the soil in the immediate vicinity of the anchor experiences 4-5 hours of temperature above 0ºC. Project data indicated that 3-5 days were required (conservatively) for the soil temperature get back to its initial condition.

6. The design process must consider the fact that an increase in the soil's ice content will decrease the load capacity of the anchor. For example, anchor designs based on the assumption of silt with a 15 or 20 percent ice volume may fail if the ice volume is, say, 40 or 50 percent. Sufficient test hole data to accurately characterize the ice content of icy silts is needed prior to considering use of anchors—basically, the less ice the better. More research is needed to study details of this mechanism.
7. As long as the soil can keep frozen, the ultimate uplift capacity is much larger than that for unfrozen soil.

References

Adam, J. I. and Hayes, D.C. (1967). "The uplift capacity of shallow foundations." Ontario Hydro Research Quarterly, 9(1), 89-104.

Adams, J. I. and Klym, T. W. (1972). "A study of anchorages for transmission tower foundations." Canadian Geotechnical Journal, 9(1), 89-104.

Barnes, P. et al. (1971). "The friction and creep of polycrystalline ice." Proc. Roy. Soc. London, A (324), 127-155.

Barnes, P. et al. (1971). "The friction and creep of polycrystalline ice." Proc. Roy. Soc. London, A (324), 127-155.

Biggar, K. W. and Kong, V. (2001). "An analysis of long-term pile load tests in permafrost from the Short Range Radar site foundations."

Biggar, K. W. and Sego, D. C. (1993a). "Field pile load tests in saline permafrost.I: Test procedures and results." Can. Geotech. J., 30, 34-45.

Briaud, J. L. et al. (1998). "Long-term behavior of grouted anchors and tieback walls." Texas Transportation Institute, Texas A&M University, Austin, Texas, 3-12.

Budd, W. F. (1969). "The dynamics of ice masses." ANARE Sci. Rep., A(IV) Glaciology, No. 108.

Butkovich, T. R. (1954). “Ultimate strength of ice.” U.S. Army, CRREL, Hanover, Tech. Translation, 11.

---------- (1960). “Creep of ice at low stress.” U.S. Army Snow Ice and Permafrost Research Establishment Wilmette, Illinois, NO.72.

Butkovich, T. R. and Landauer, J. K. (1959). “The flow law for ice.” U.S. Army Snow Ice and Permafrost Research Establishment Wilmette, Illinois, NO.56.

Fairhurst, C. (1964). “On the validity of the Brazilian test for brittle materials.” Int. J. Rock. Mech. Mining Sci., 1, 535-546.

Glen, J. W. (1952). “Experiments on the deformation of ice.” J. Glaciol. , 2, 111-114.

Glen, J. W. (1955). “The creep of polycrystalline ice.” Proc., Roy. Soc. London, A (228), 519-538.

Hanna, T. H and Carr, R. W. (1971). “The loading behavior of plate anchors in normally and over-consolidated sands.” Proc., 4th European conf. on soil mechanics and foundation engineering, Budapest, Hungary, 589-600.

Haynes, F. D. et al. (1975). “Strain rate effect on the strength of frozen silt.” U.S. Army, CRREL, Research Rpt. 350, 27.

Hooke, R. L. et al. (1972). “Creep of ice containing fine grained dispersed sand.” J. Galaciol., 11(63), 327-336.

Horvath, R. G. (1995). “Influence of loading rate on the capacity of a model pile in clay.” Can. Geotech. J., 32, 364-368.

Hult, J. A. H. (1966). “Creep in engineering structures.” Blaisdell Publ. Co., Waltham, Mass., 115.

Hutchinson, D. J. (1989). “Model pile load tests in frozen saline silty sand.” M. S. Thesis, Department of Civil Engineering, the University of Alberta, Edmonton.

Johnston, G. H. and Ladanyi, B. (1972). “Field tests of grouted rod anchors in permafrost.” Canadian Geotechnical Journal, 9, 176-194.

Joshi, R. C., Sharma, H. D. and Sparrow, D. G. (1989). “Comparison of pile load test methods.” Can. Geotech. J., 26, 742-744.

Ladanyi, B. (1972). “An engineering theory of creep of frozen soil.” Can. Geotech. J., 9(1), 63-80.

McRoberts, E. C. (1975). “Some aspects of a simple secondary creep model for deformations in permafrost slopes.” Can. Geotech. J., 12, 98-105.

McRoberts, E. C. et al. (1978). “Creep tests on undisturbed ice-rich silt.” Proc., 3rd Int. Permafrost Conf., Vol. 1, Edmonton, Alta., 539-545.

Meier, M. F. (1960). “Mode of flow of Saskatchewan Glacier.” U.S. Geological Survey Tech. Rep., 315, 70.

Mellor, M. and Testa, R. (1969a). “Effect of temperature on the creep of ice.” J. Glaciol. , 8, 131-145.

Morgenstern, N. R. et al. (1980). “The behavior of friction piles in ice and ice-rich soils.” Can. Geotechnical J., 21, 24-31.

Nadai, A. (1963). “Theory of flow and fracture of soils.” Vol. 2, McGraw-Hill, New York.

Nixon, J. F. (1988). “Pile load tests in saline permafrost at Clyde River, Northwest Territories.” Can. Geotech. J., 17, 405-415.

Nixon, J. F. and McRoberts, E. C. (1976). “A design approach for pile foundations in permafrost.” Can. Geotechnical J., 13, 40-57.

Nixon, R. J. and Neukirchner (1987). “Design of vertical and laterally loaded piles in saline permafrost.” Proc., 3rd Int. Specialty Conf. on Cold Reg. Eng., Edmonton, Vol. 1, 131-144.

Odquist, F. K. G. and Hult, J. (1962). “Creep in metallic Materials (in German), Springer, Berlin.

Parameswaran, V. R. (1986). “Failure time in creep.” Mechanics of Materials, 6 (1), 89-91.

Paterson, W. S. B. and Savage, J. C. (1963b). “Measurements on Athabasca Glacier relating to the flow law of ice.” J. Glaciol., 68 (15), 4537-43.

Reed-Hill, R. E. (1973). “Physical metallurgical principles.” 2nd Edition, Van Nostrand Company, 920.

Roggensack, W. D. (1977). “Geotechnical properties of fine-grained permafrost soils.” Ph. D Thesis, Univ. of Alberta, Edmonton, Alta, 499.

Sabatini, P. J., Pass, D. G. and Bachus, R.C. (1979). “Permafrost grouted anchors.”

Sayles, F. H. (1968). “Creep of frozen sands.” U.S. Army, CREEL, Tech. Rpt, 190, 54.

Sayles, F. H. (1973). “Triaxial and creep tests on frozen Ottawa sand.” Proc., 2nd Int. Conf. on permafrost, Yakutsk, U.S.S.R., North American Contribution, National Academy of Science, Washington D. C., 384-391.

Sayles, F. H. and Haines, D. (1974). “Creep of frozen silt and clay.” U.S. Army Corps of Engineers, CRREL, Tech. Rep., 252, 50.

Sego, D. C. and Smith, L. B. (1989). “The effect of backfill properties and surface treatment on the capacity of adfreeze pipe piles. Can. Geotech. J., 26, 718-725.

Shreve, R. L., and Sharp, R. P. (1970). “Internal deformation and thermal anomalies in lower Blue Glacier, Mount Olympus, Washington, U.S.A.” J. Glaciol., 9 (55), 65-86.

Thomas, P. (1973a). “The creep of ice shelves: theory.” J. Glaciol., 12, 45-53.

Thompson, E. G. and Sayles, F. H. (1972). “In situ creep of room in frozen soil.” Proc. Am. Soc. Civ. Eng. 98 (SM9), 899-915.

Vialov, S. S. (1959). “Rheological properties and bearing capacity of frozen soils.” U.S. Army,, CRREL, Hanover, Tech. Translation 74.

Vialov, S. S. (1962). “Strength and creep behavior of frozen soils and calculation in ice-rich retaining structures. U.S. Army, CRREL, Hanover, Tech. Translation 76.

Vialov, S. S. and Porkhaev, G. V. (1976). “Handbook for the design of bases and foundations of buildings and other structures on permafrost.” National Research Council of Canada, Technical Translation, 1865.

Weaver, J. S. (1979). “Pile foundations in permafrost.” Ph.D. Thesis, Department of Civil Engineering, the Univ. of Alberta, Edmonton.

Weaver, J. S. and Morgenstern, N. R. (1981). “Simple shear creep tests on frozen soils.” Can. Geotech. J., 18, 217-229.

William N. Findley, James S. Lai and Kasif Onaran (1972). “Creep and Relaxation of Nonlinear Vsicoelastic materials.” North Holland Publishing Company.

Appendix A Displacement vs. Time Curves

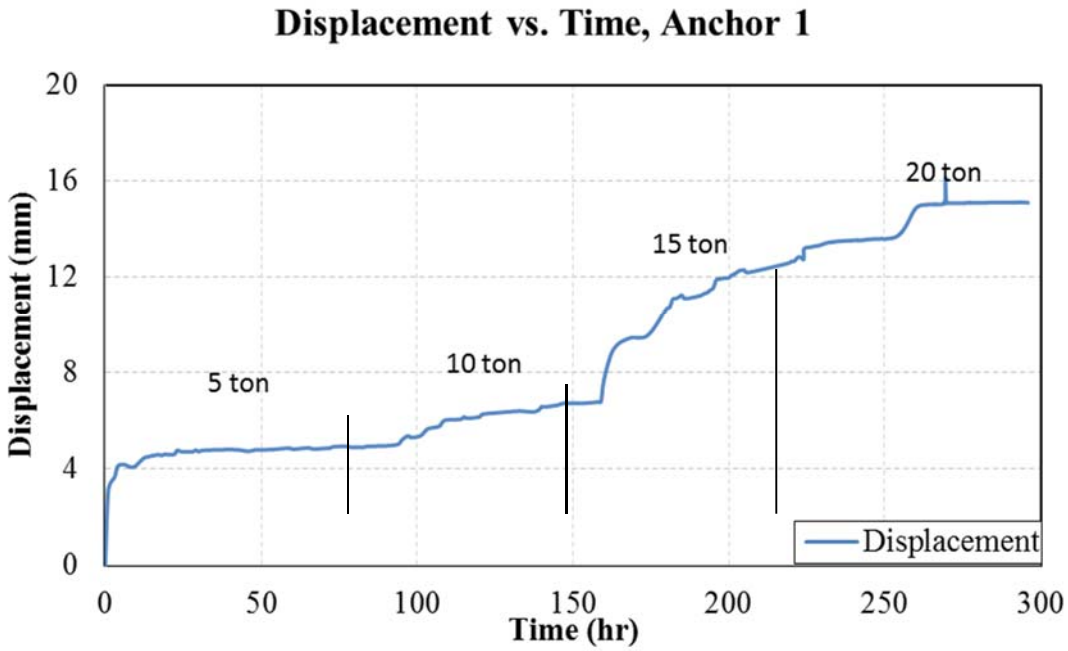

Figure A.1 Displacement vs. Time for Anchor 1

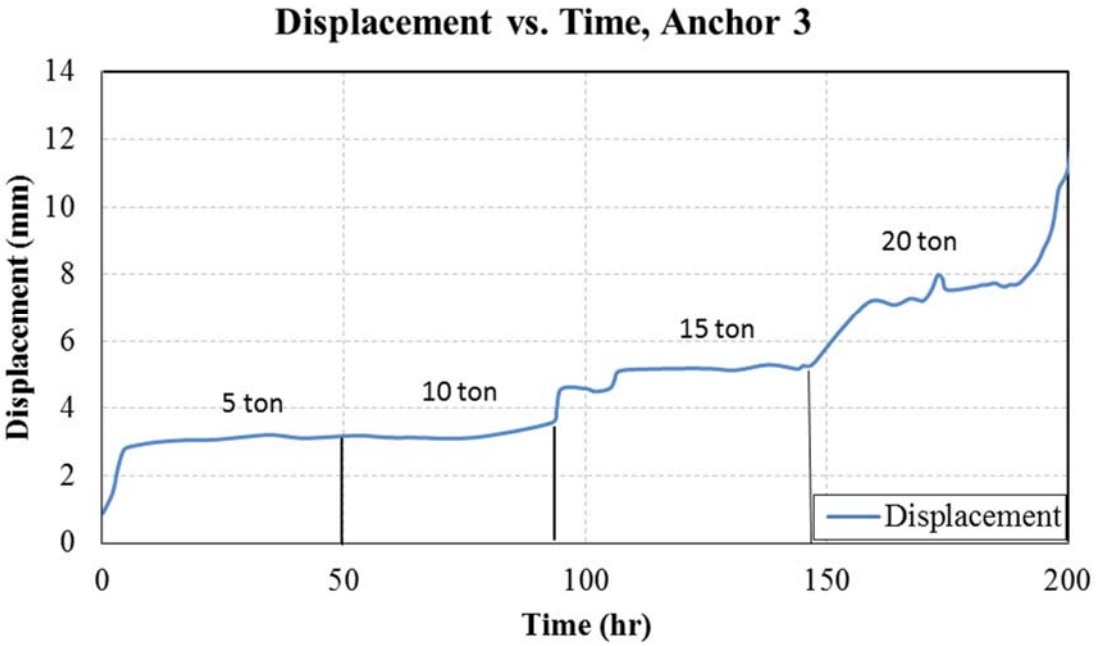

Figure A.2 Displacement vs. Time for Anchor 3

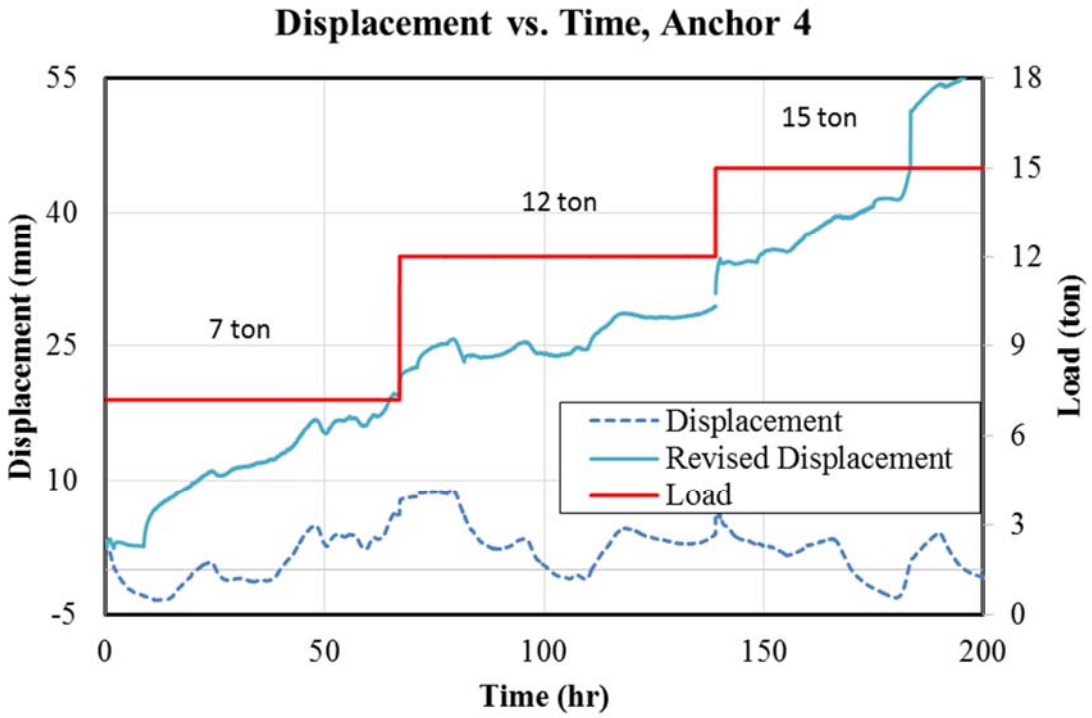

Figure A.3 Displacement vs. Time for Anchor 4

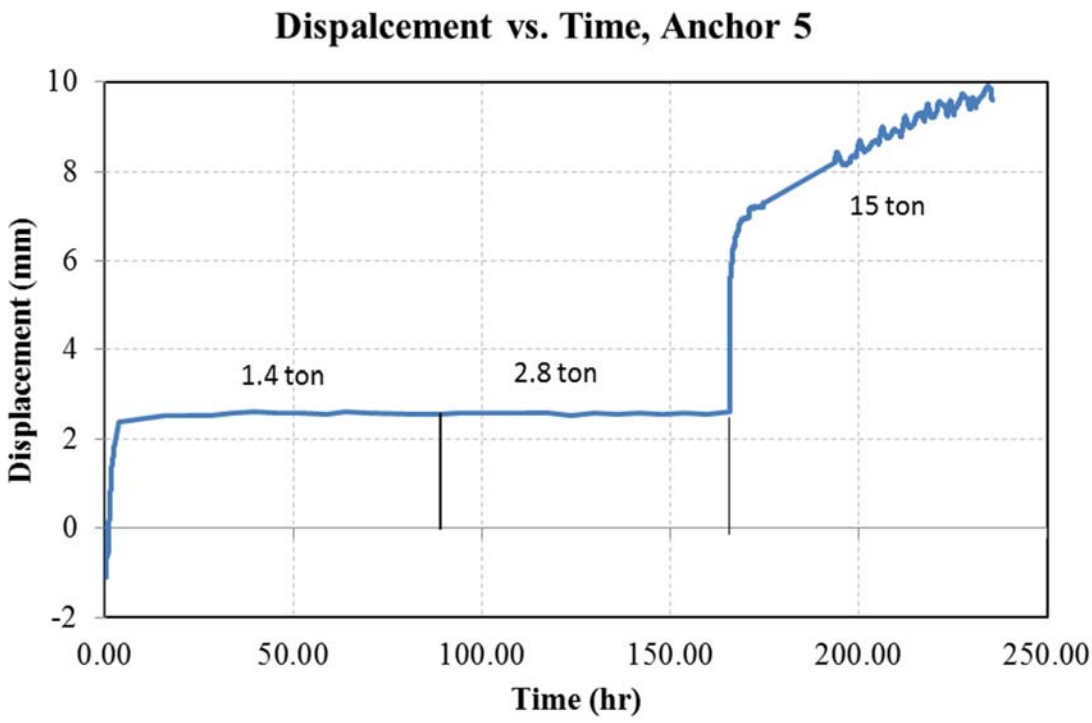

Figure A.4 Displacement vs. Time for Anchor 5

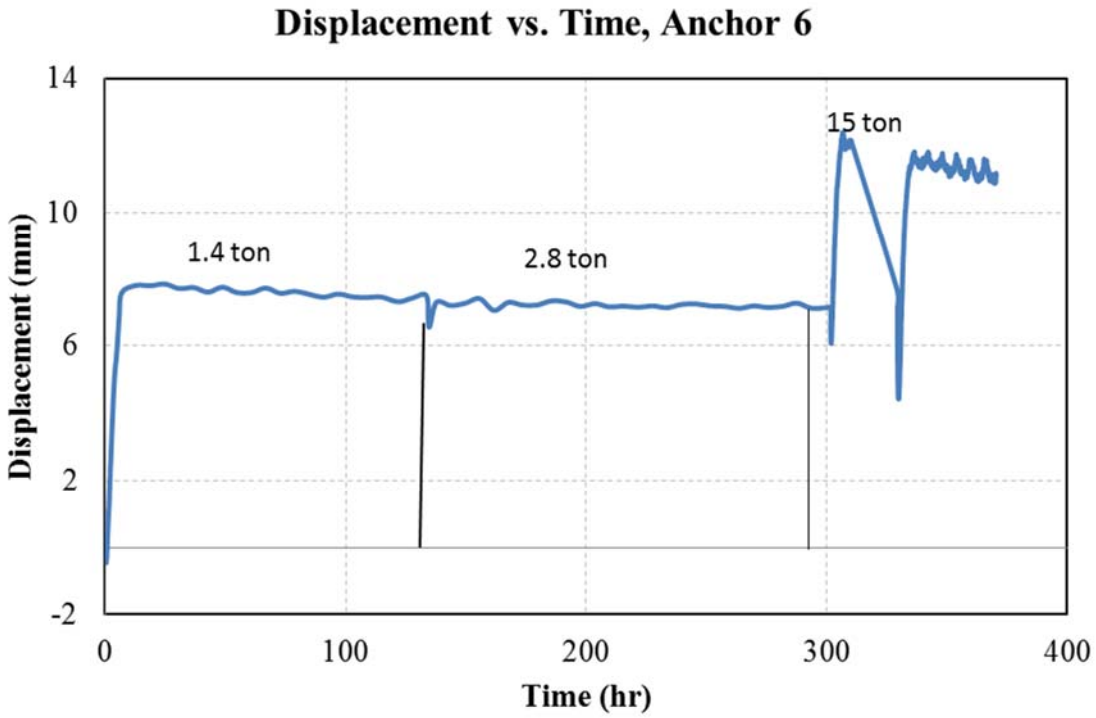

Figure A.5 Displacement vs. Time for Anchor 6

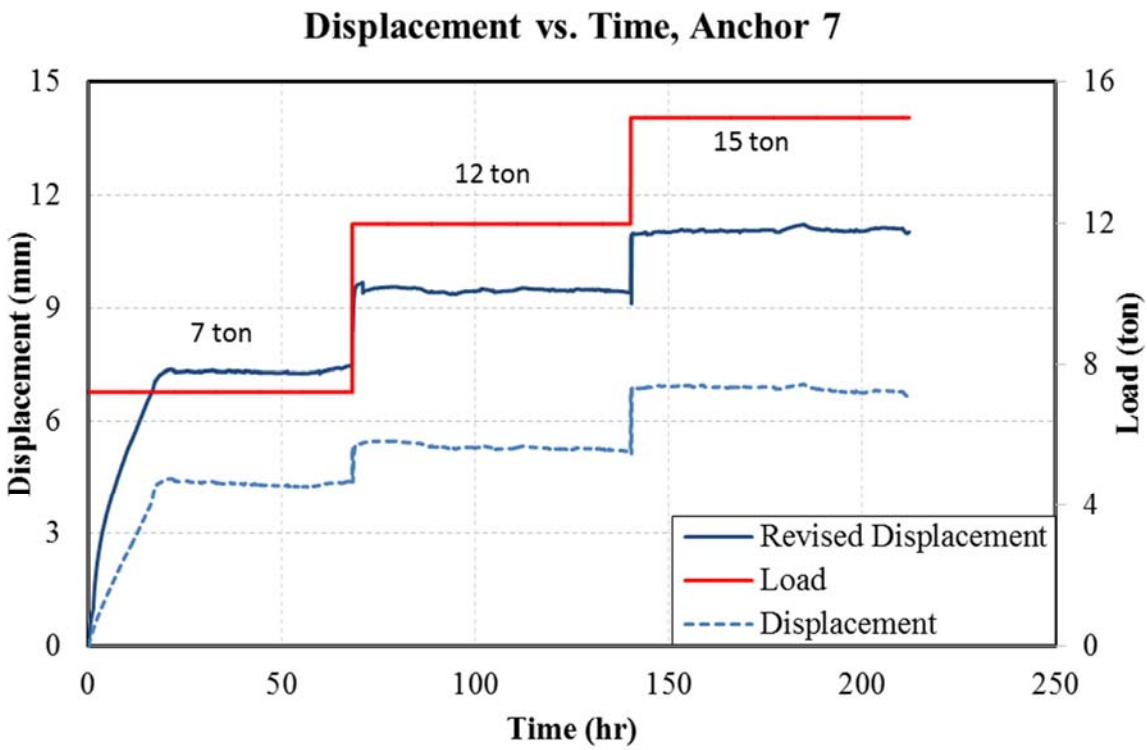

Figure A.6 Displacement vs. Time for Anchor 7

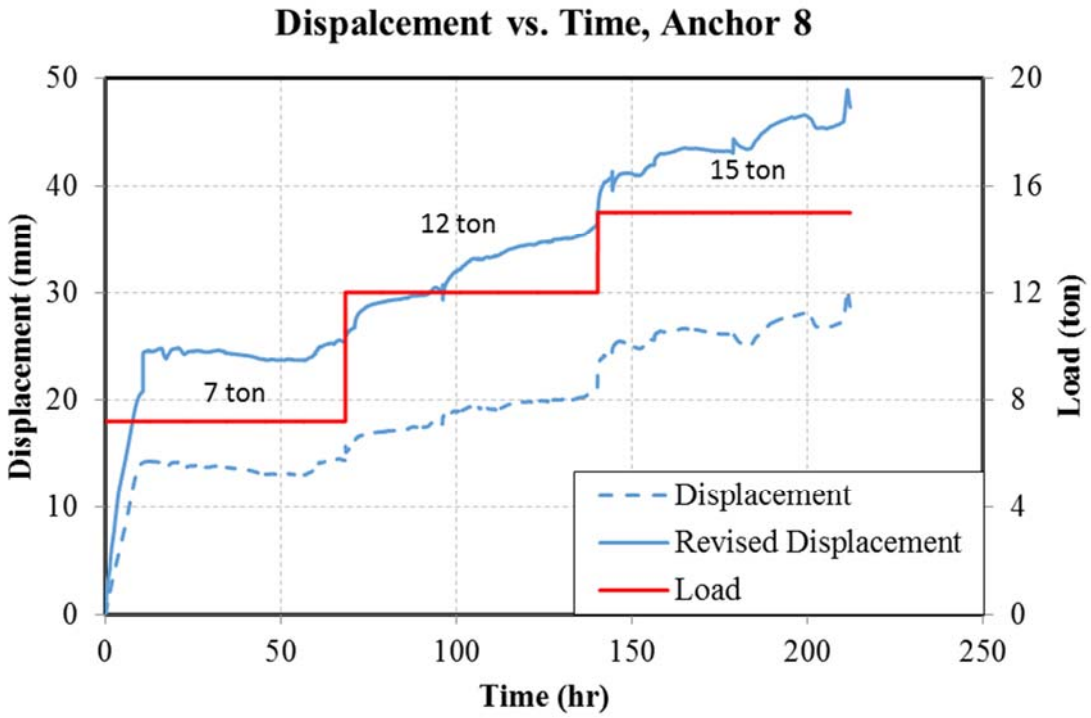

Figure A.7 Displacement vs. Time for Anchor 8

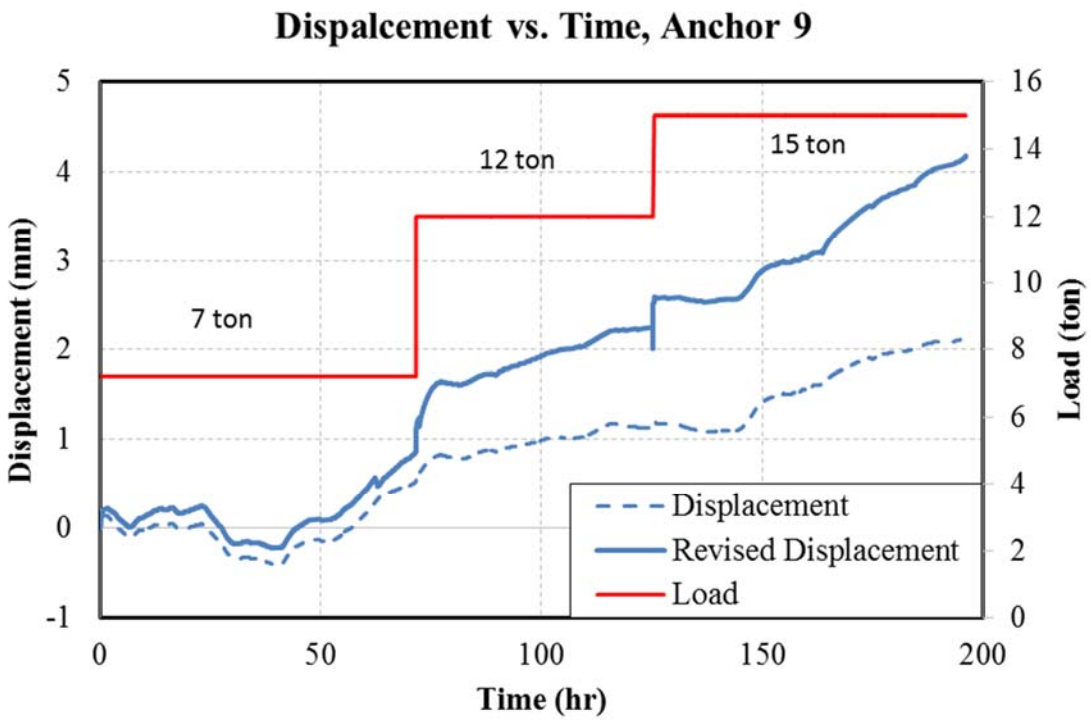

Figure A.8 Displacement vs. Time for Anchor 9

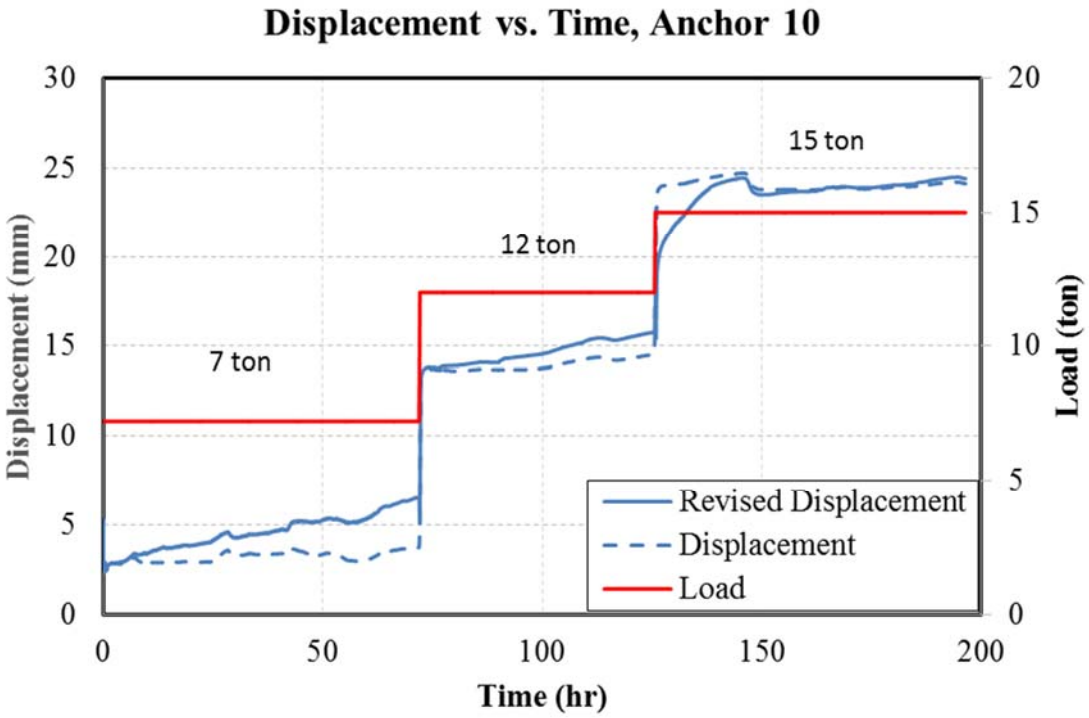

Figure A. 9 Displacement vs. Time for Anchor 10

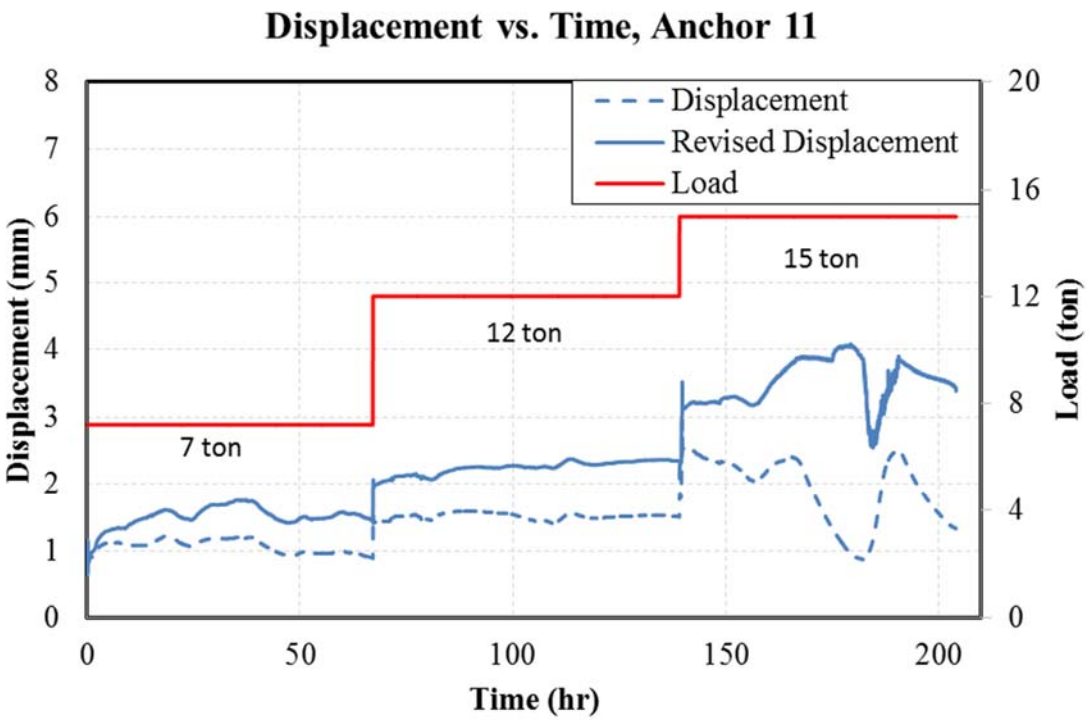

Figure A.10 Displacement vs. Time for Anchor 11

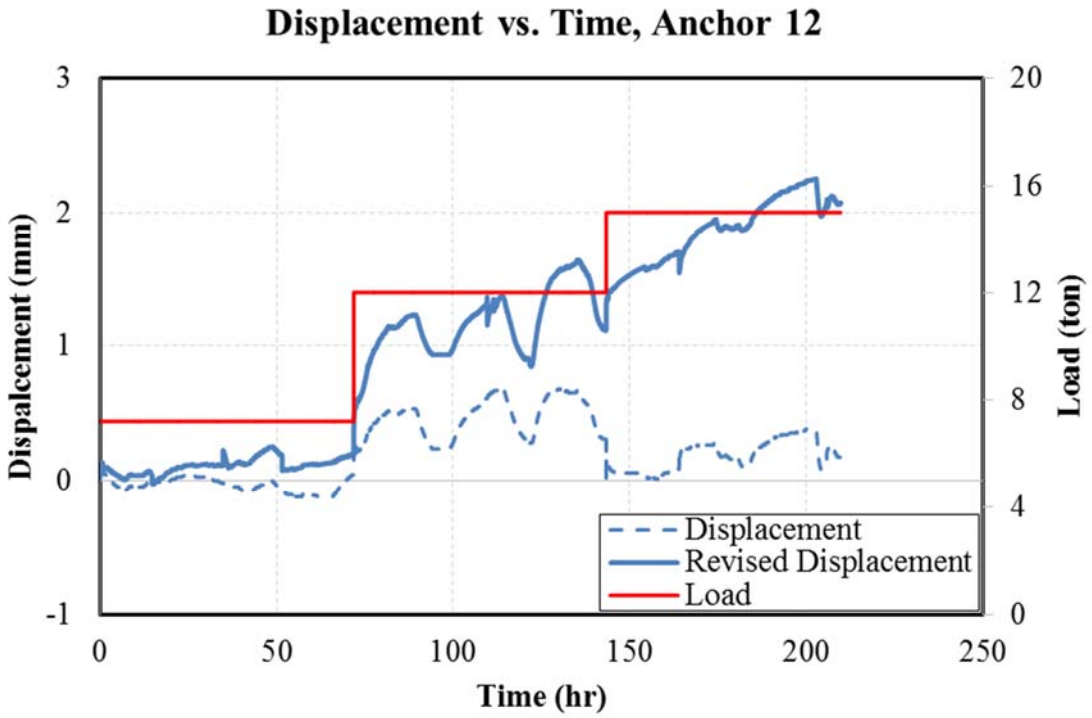

Figure A.11 Displacement vs. Time for Anchor 12

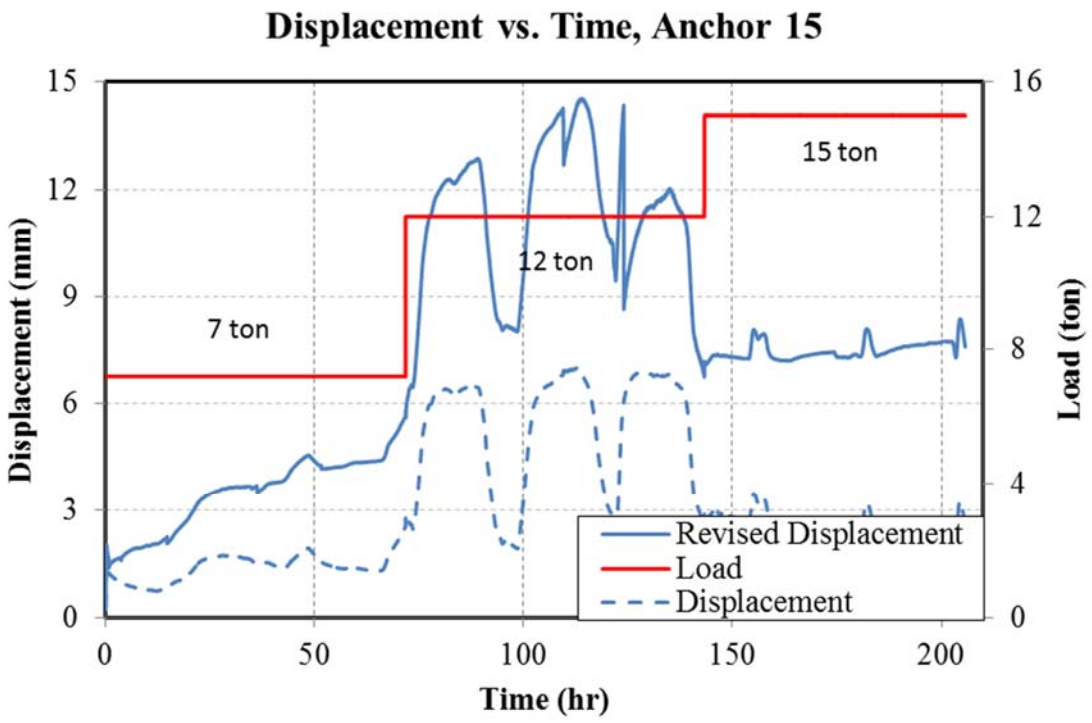

Figure A.12 Displacement vs. Time for Anchor 15

Appendix B Grouting Temperature

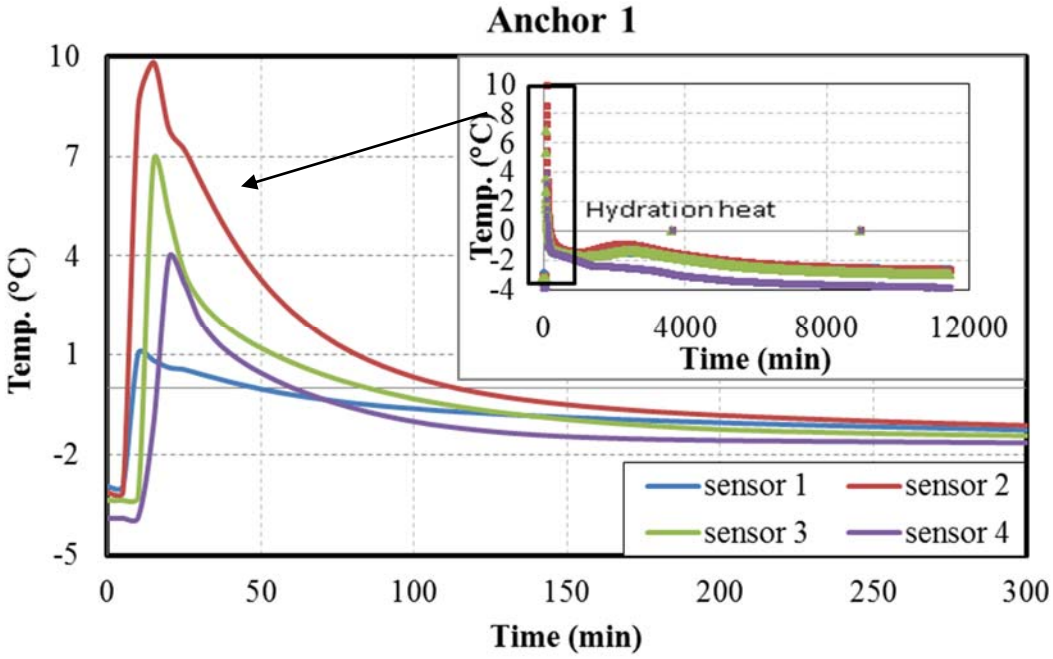

Figure B.1 Grouting temperature vs. time for anchor 1

(solid bar with Microsil Anchor Grout)

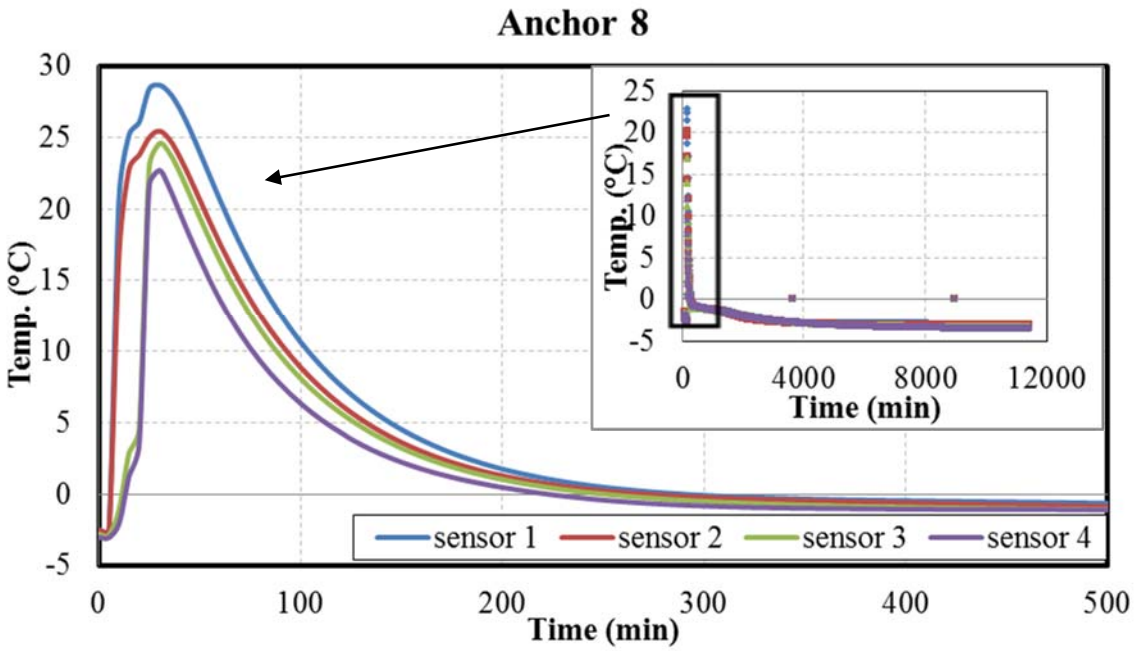

Figure B.2 Grouting Temperature vs. Time for Anchor 8

(Hollow Rebar with Bentonite Clay)

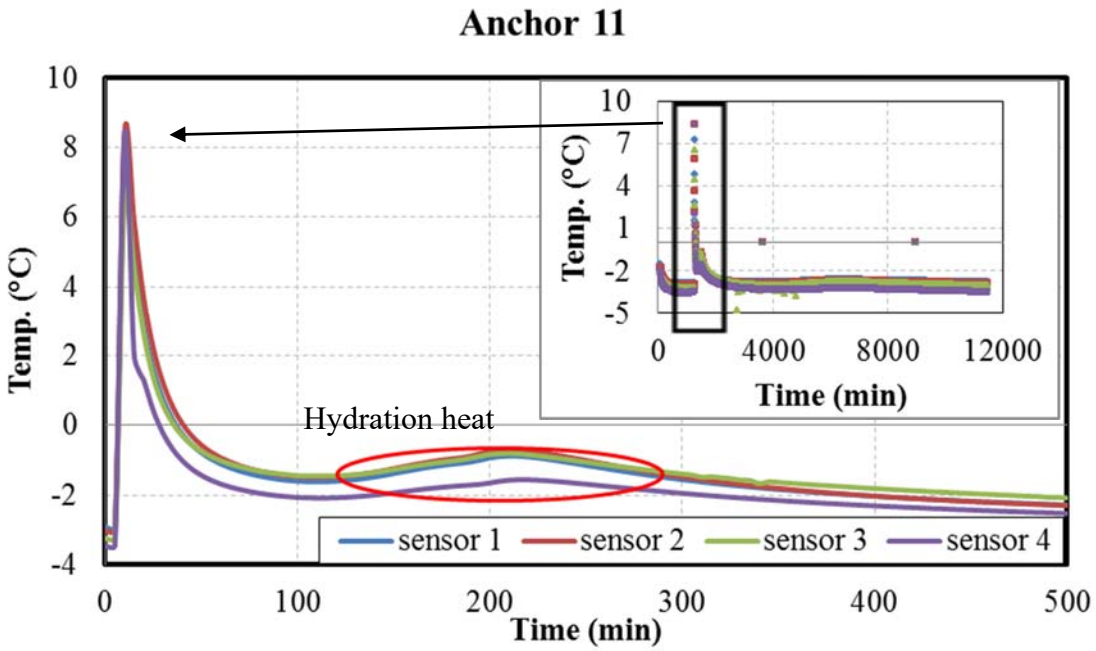

Figure B.3 Grouting Temperature vs. Time for Anchor 11

(Hollow Rebar with Special Cement Formula)

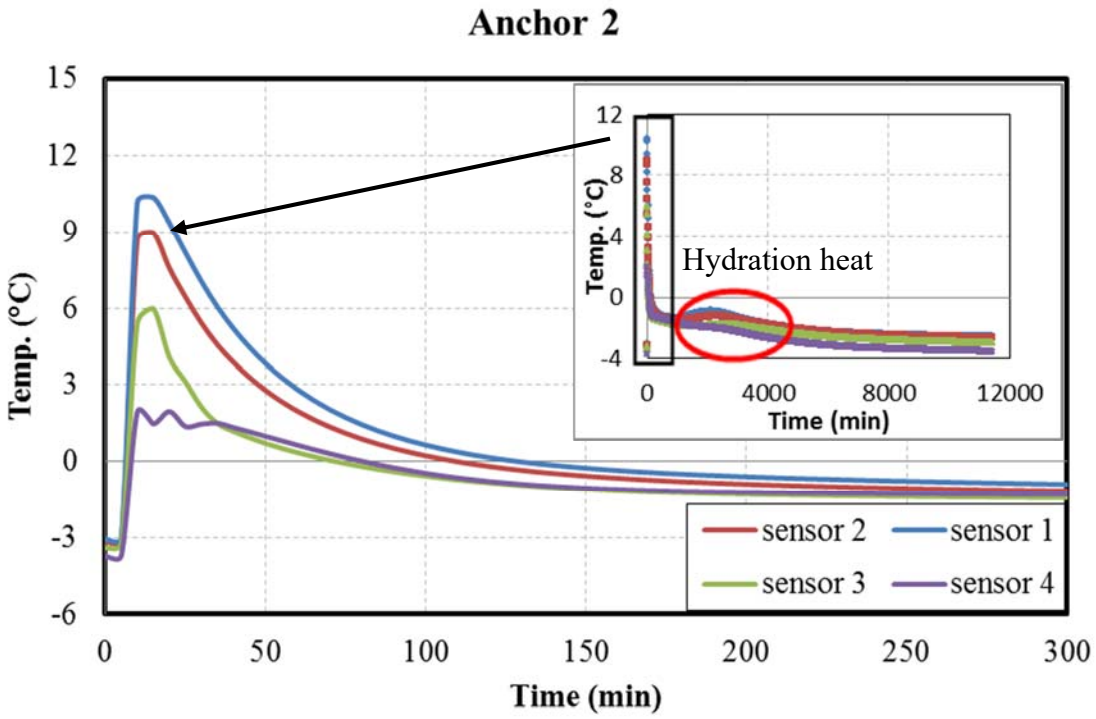

Figure B.4 Grouting Temperature vs. Time for Anchor 2

(Solid Rebar with Microsil)

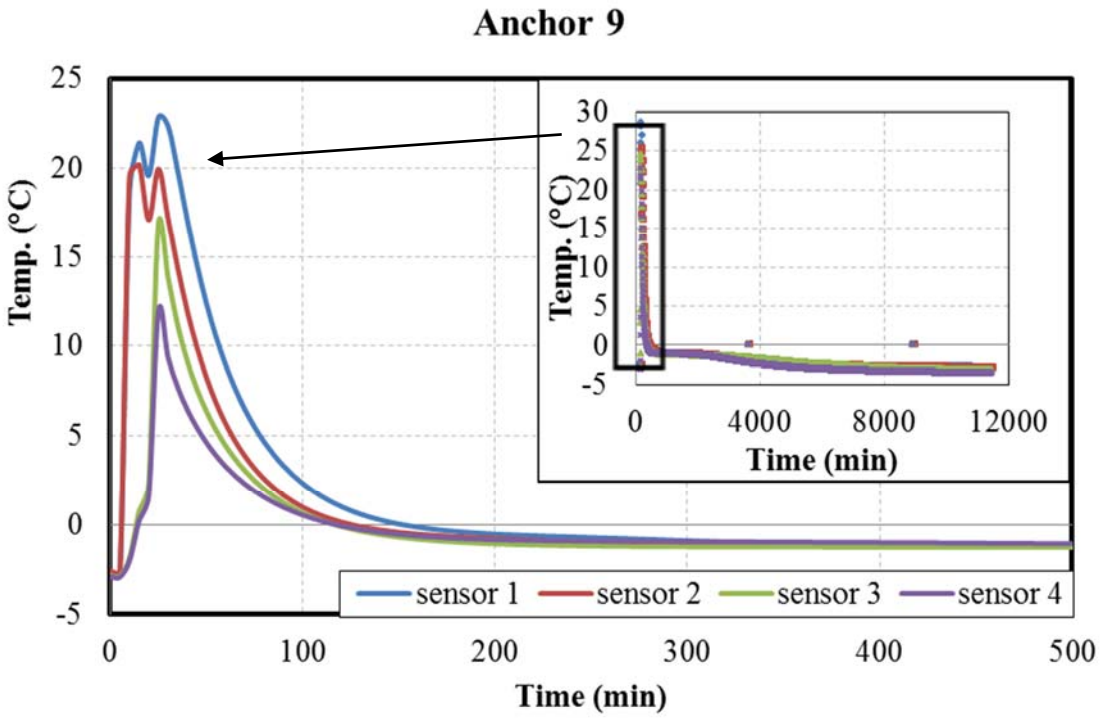

Figure B.5 Grouting Temperature vs. Time for Anchor 9
(Hollow Rebar with Bentonite Clay)

Appendix C Load Distribution

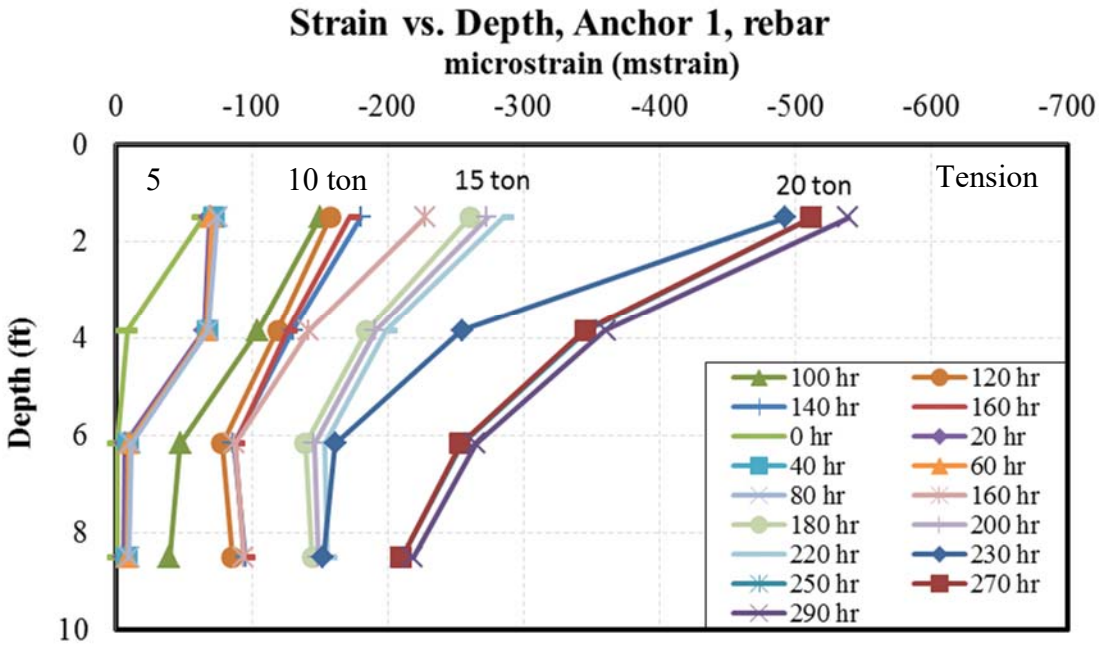

Figure C.1 Strain vs. Depth for Anchor 1 at Different Time in Rebar

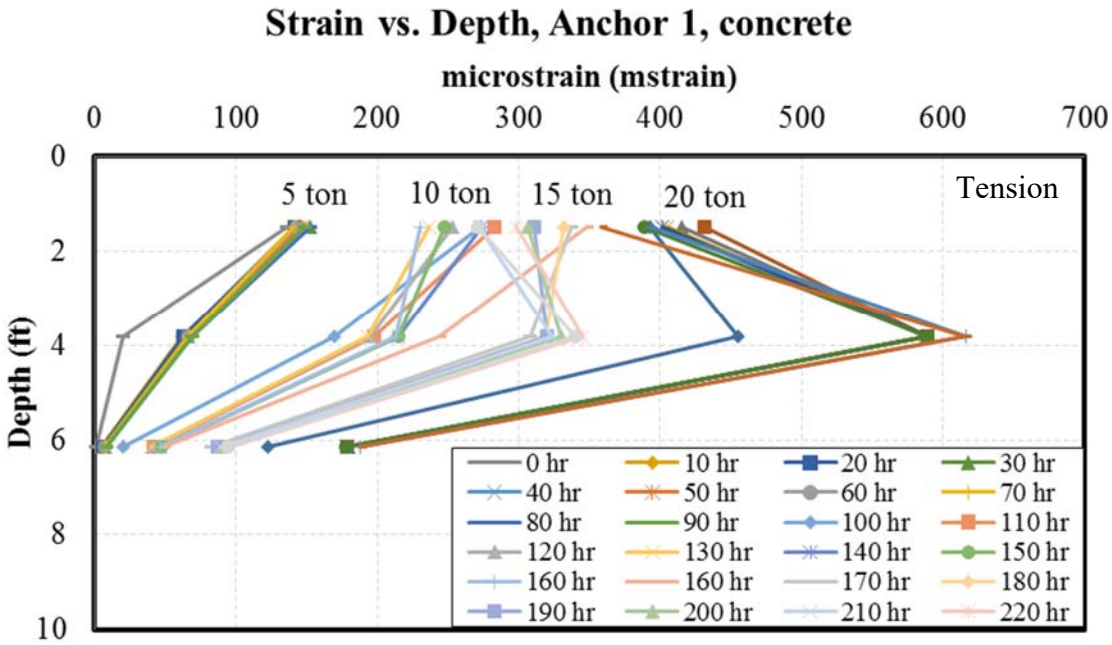

Figure C.2 Strain vs. Depth for Anchor 1 at Different Time in Grout

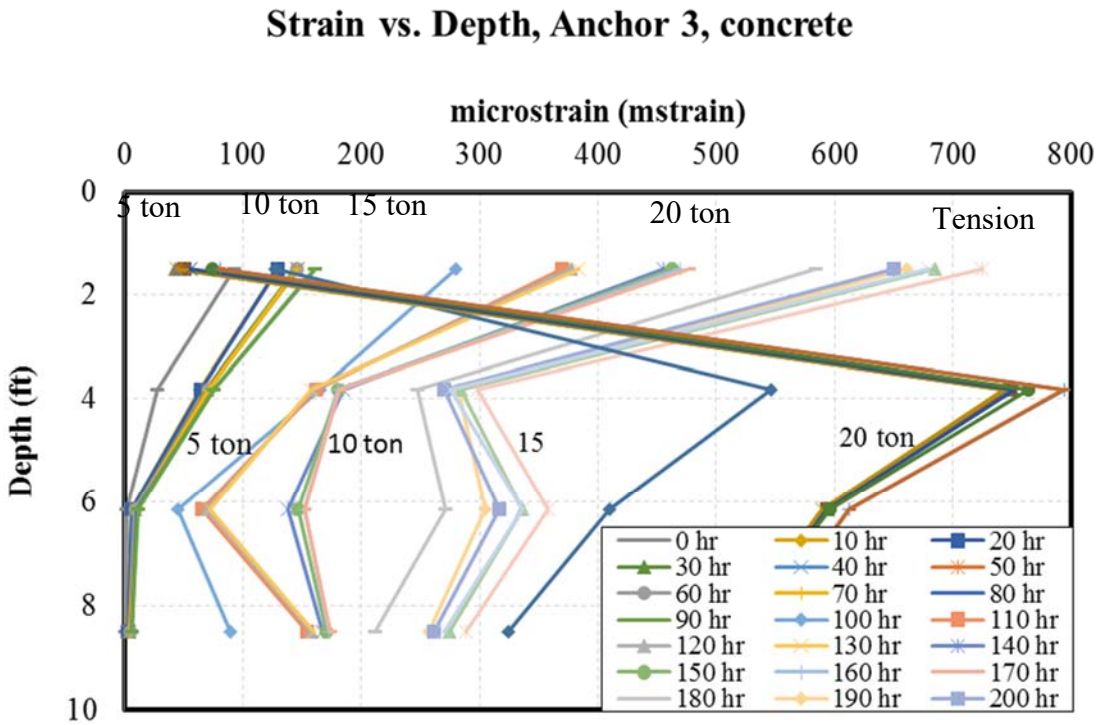

Figure C.3 Strain vs. Depth for Anchor 3 at Different Time in Rebar

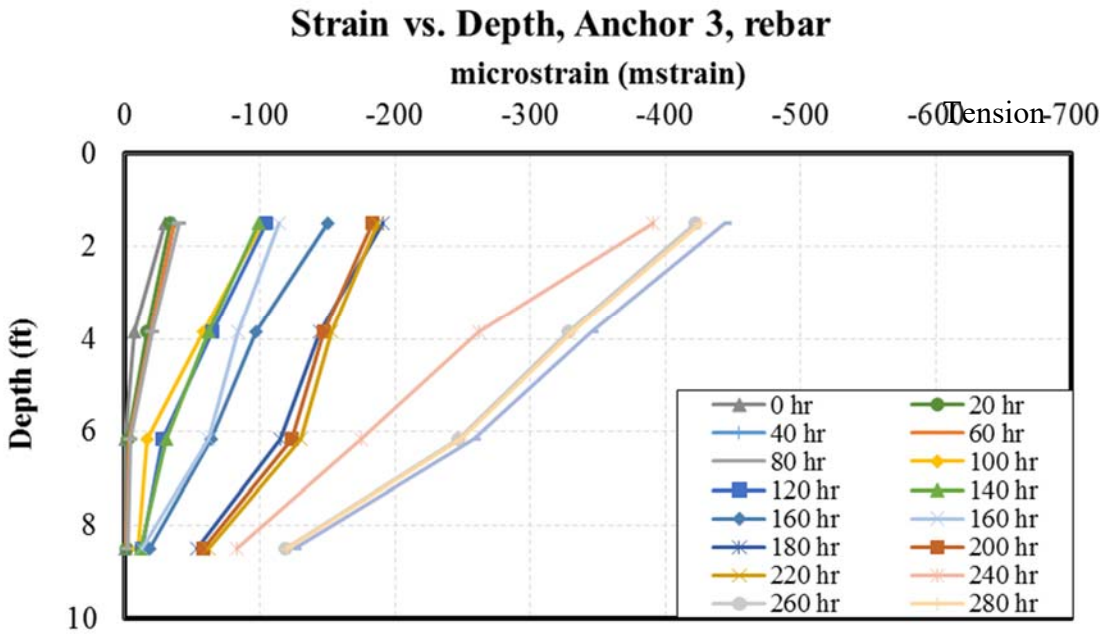

Figure C.4 Strain vs. Depth for Anchor 3 at Different Time in Grout

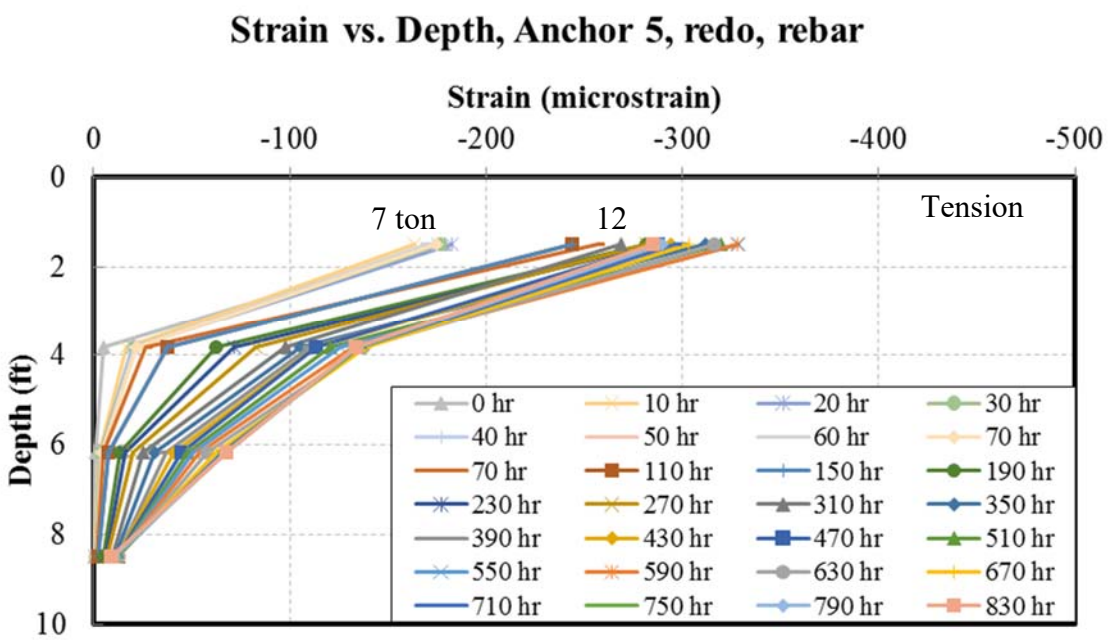

Figure C.5 Strain vs. Depth for Anchor 5 at Different Time in Rebar

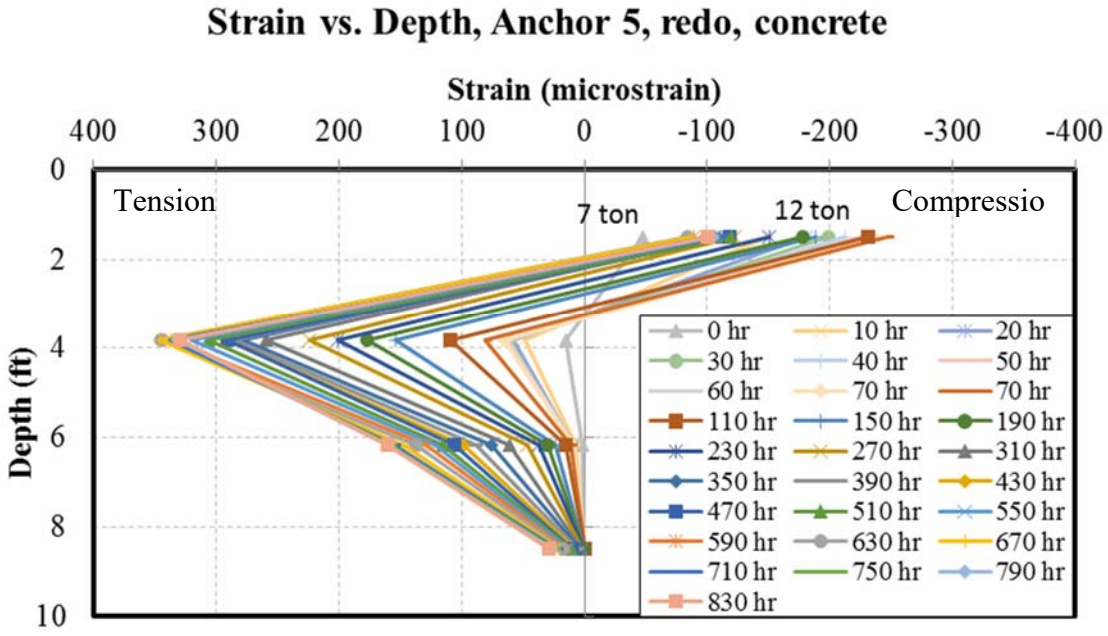

Figure C.6 Strain vs. Depth for Anchor 5 at Different Time in Grout

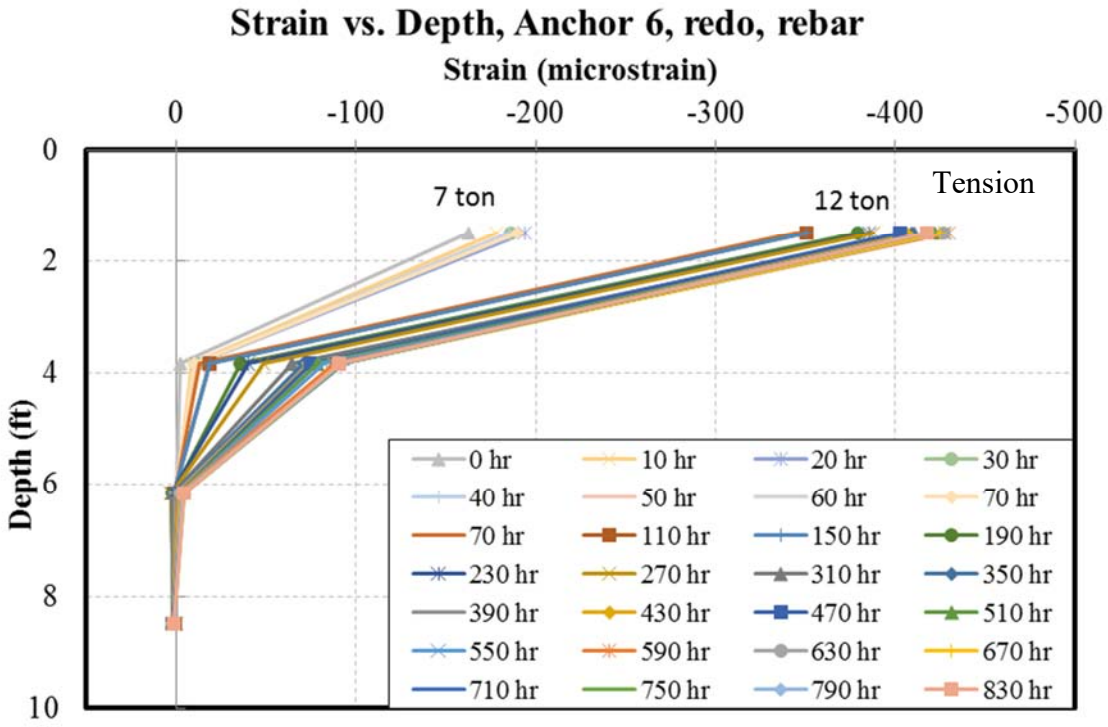

Figure C.7 Strain vs. Depth for Anchor 6 at Different Time in Rebar

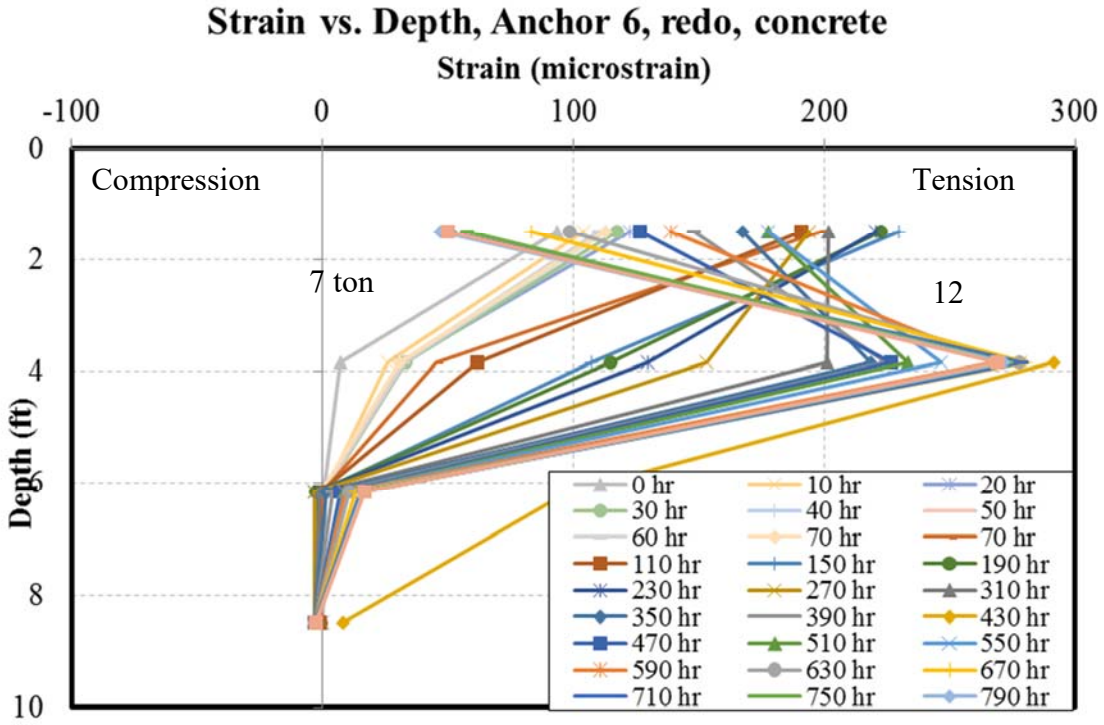

Figure C.8 Strain vs. Depth for Anchor 6 at Different Time in Grout

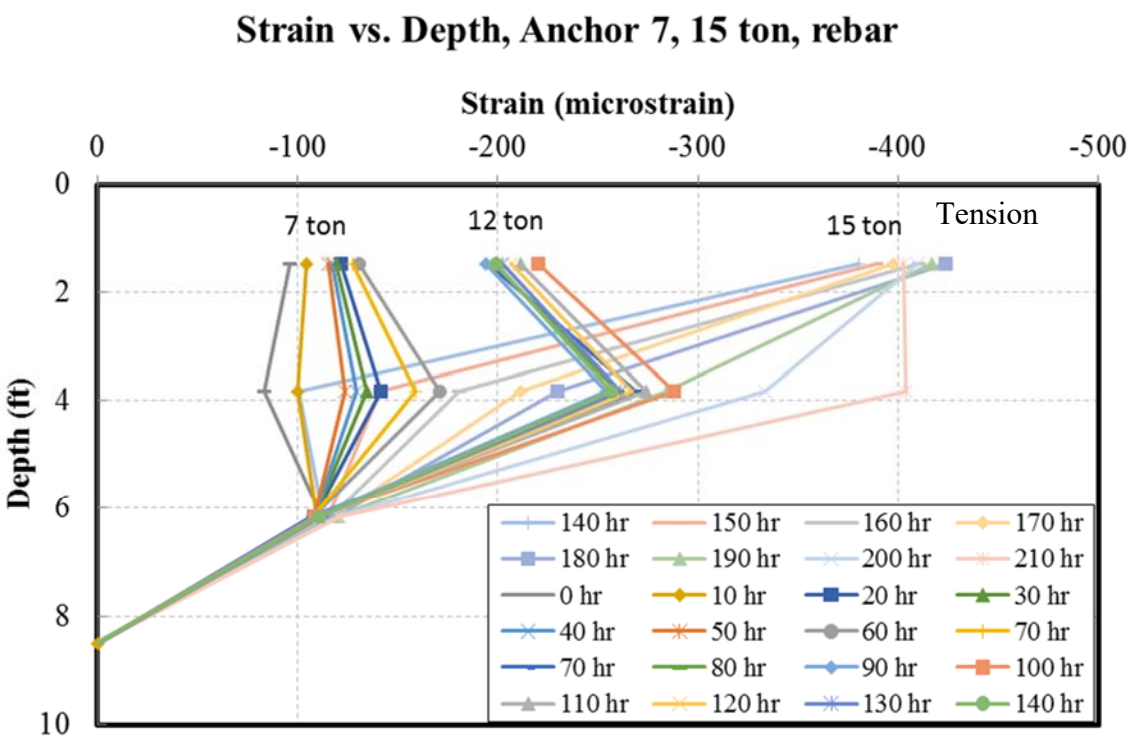

Figure C.9 Strain vs. Depth for Anchor 7 at Different Time in Rebar

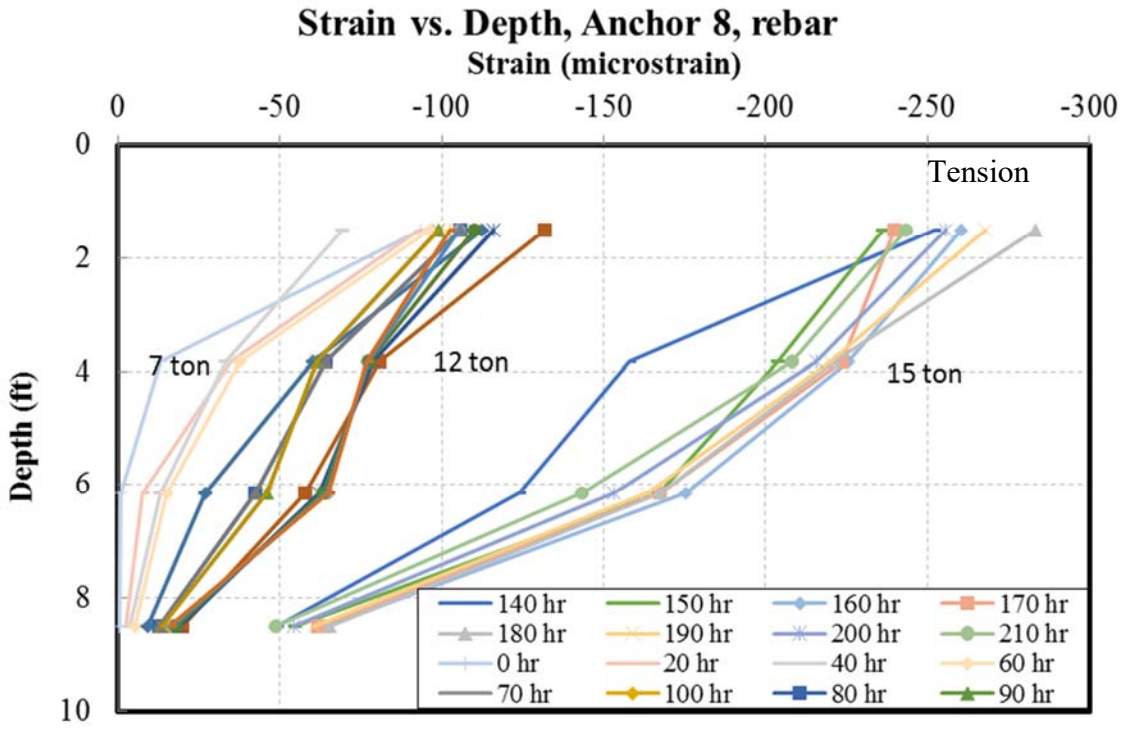

Figure C.10 Strain vs. Depth for Anchor 8 at Different Time in Rebar

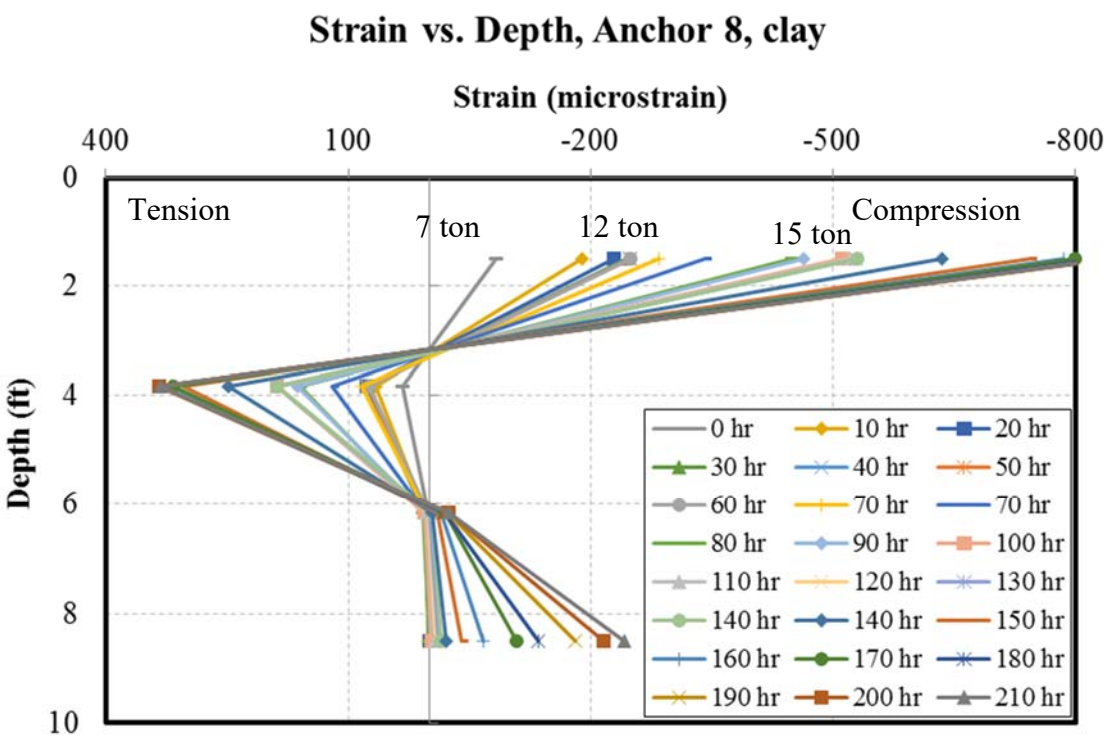

Figure C.11 Strain vs. Depth for Anchor 8 at Different Time in Clay

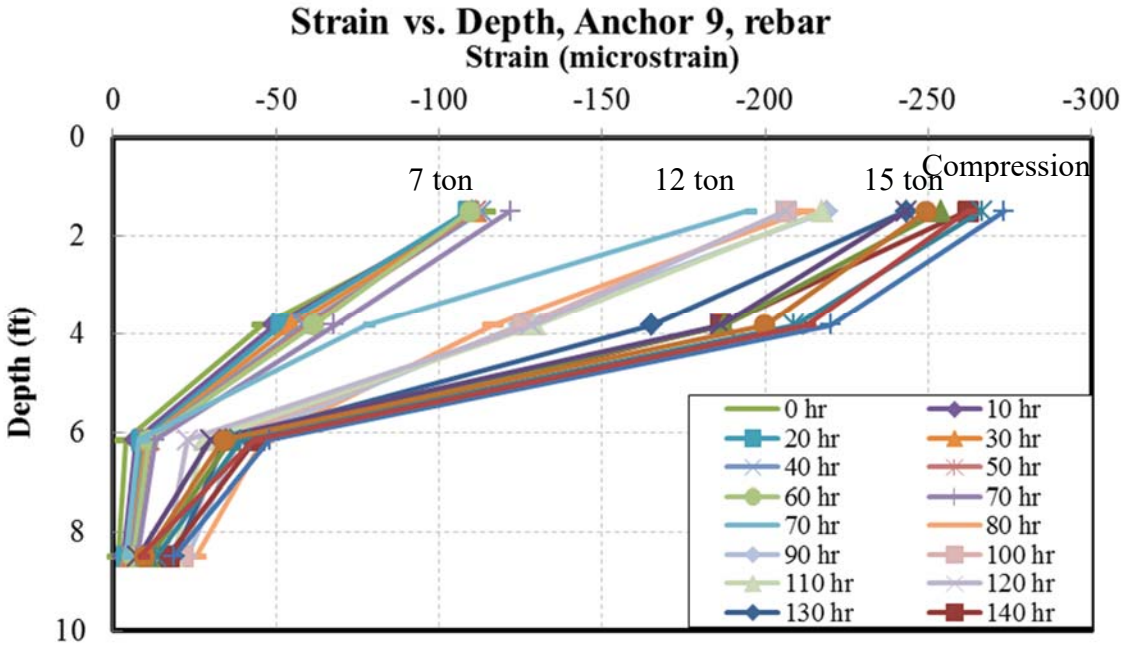

Figure C.12 Strain vs. Depth for Anchor 9 at Different Time in Rebar

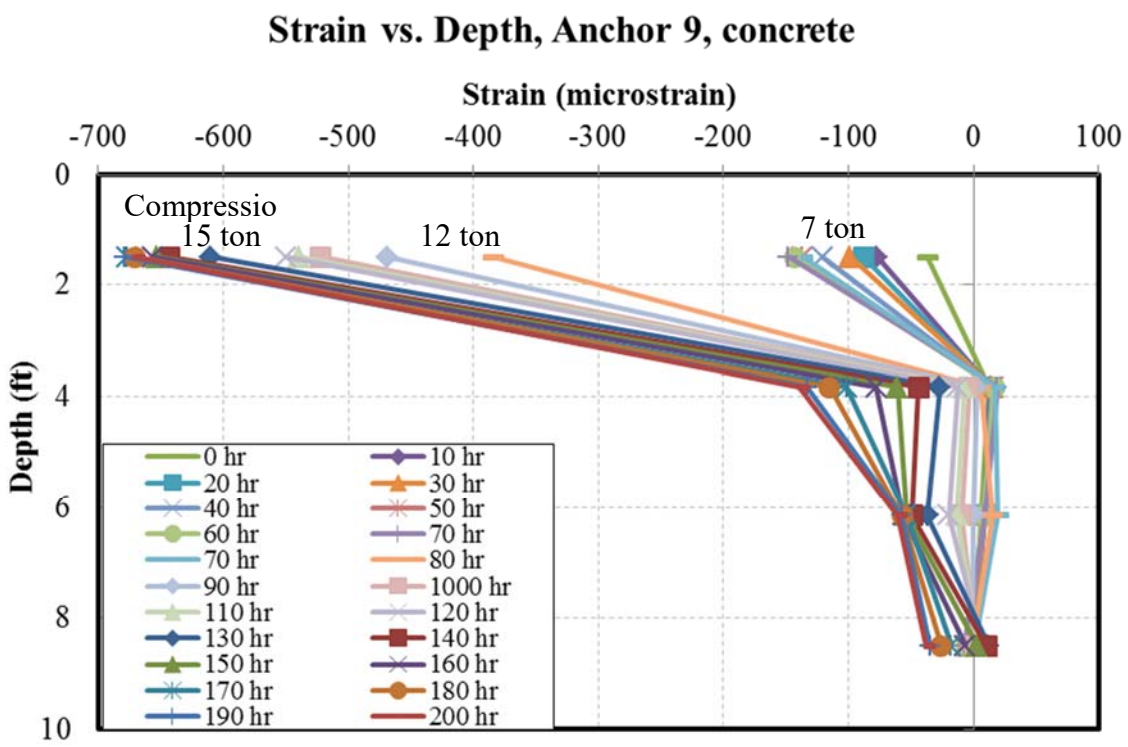

Figure C.13 Strain vs Depth for Anchor 9 at Different Time in Grout

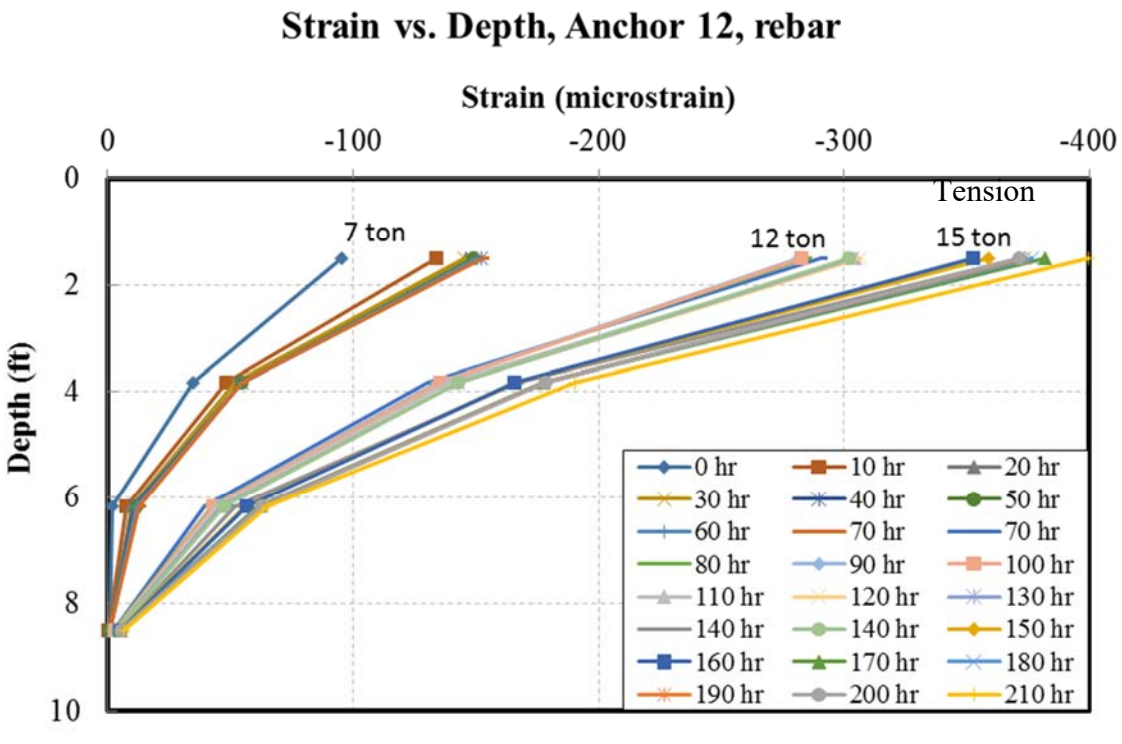

Figure C.14 Strain vs. Depth for Anchor 12 at Different Time in Rebar

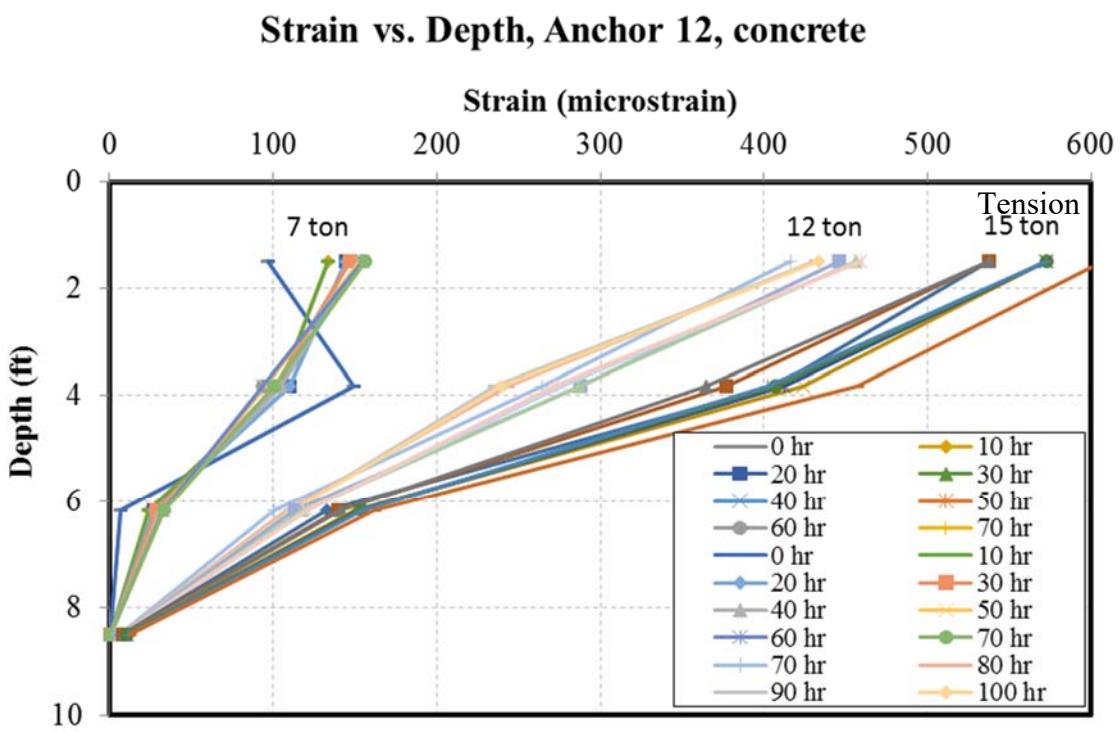

Figure C.15 Strain vs. Depth for Anchor 12 at Different Time in Grout

Appendix D Displacement vs. Time Curve Revision

The displacement revision is based on several assumptions. They are:

Instantaneous strain is negligible for a long-term creep test

The total strain of the anchor is explained as:

$$\varepsilon = \varepsilon_0 + \varepsilon^c \quad [D.1]$$

Where ε: total strain; ε_0: instantaneous strain; ε^c: creep strain.

The instantaneous strain contains both elastic strain, ε^e, and plastic strain, ε^p. The elastic strain constitutive equation is represented by Hooke's law:

$$\varepsilon^e = \frac{\sigma}{E} \quad [D.2]$$

Where ε^e: elastic strain; σ: applied stress; E: Young's modulus.

And the plastic portion is often written as:

$$\varepsilon^p = A \cdot \sigma^k \quad [D.3]$$

Where: ε^p: plastic strain; σ: applied stress; A: constant depending on material property; k: time dependent variable.

The creep strain is often expressed as:

$$\varepsilon^c = \dot{\varepsilon}^c_{min} t \quad [D.4]$$

Where: ε^c: creep strain; $\dot{\varepsilon}^c_{min}$: minimum strain rate of steady state creep; t: time.

Therefore, the total strain could be rewritten as:

$$\varepsilon = \frac{\sigma}{E} + A \cdot \sigma^k + \dot{\varepsilon}^c_{min} t \quad [E.5]$$

One sees above that only the last term of the equation is time dependent. This makes our adjustment reasonable. The elastic strain change due to the change of applied load can be accounted for knowing the load change. The plastic strain change due to the fluctuation of applied load cannot be determined because unloading steps were not included as part of the test. Yet, when the applied load reaches its peak value, the total strain value has already included the plastic strain part. Therefore, the adjustment curve has also included the effect of applied load on the strain curve. Finally, as for the effect of applied load on creep strain, it is reasonable to assume that creep strain can be neglected due to the short period of time.

Andersland and Ladanyi (2004) has pointed out that in practice, for short-term processes, the instantaneous strain is only governed by Hooke's law. While for a long-term process, the instantaneous strain consists of elastic, plastic and primary creep strain, all of which, together, are represented by one variable, called the pseudo-instantaneous strain. This strain value is defined where the extension of the steady-state creep curve intersects with the strain axis. Similarly, Vialov (1959) also mentioned that the pseudo-instantaneous portion is less than 10% of the total strain when the time interval is greater than one day and could be ignored for practical purposes. Therefore, other researchers' analysis results appear to corroborate the validity of our method of only adjusting the time independent strain.

Viscoelastic material assumption

For linear viscoelastic materials, the response output could be calculated from the step input by using Boltzmann's superposition principle. Yet, Ladanyi (1971) summarized the previous research on frozen soil and concluded that non-linearity is one of the properties of frozen soil which made the superposition principle not applicable for creep tests in frozen soil. For non-linear viscoelastic materials, the loading history must be taken into account to determine the total strain. Several methods had been provided by Hoff (1954), Vialov (1959, 1962) and Turner (1966) to solve problems for non-linear viscoelastic materials. One of the more simple ways is to use a modified version of the superposition principle which includes terms accounting for the effect of loading. This results in quite a complicated formulation for use on practical problems.

For practical purposes, most researchers assume that the strain of frozen soil is only a function of stress, temperature and time. The loading history effect is therefore ignored during stress strain analyses. As a result of these considerations, the linear superposition principle was considered a reasonably valid approach with respect to revising the research project's raw creep data.

Linear viscoelastic material is defined such that applied stress is proportional to strain at any given time, and the linear superposition principle is applicable. The following two equations are mathematical expressions of linear requirement:

$$\varepsilon[c\sigma(t)] = c\varepsilon[\sigma(t)] \quad \text{[D.6]}$$

$$\varepsilon[\sigma_1(t)+\sigma_2(t-t`)] = \varepsilon[\sigma_1(t)] + \varepsilon[\sigma_2(t-t`)] \quad \text{[D.7]}$$

Where ε: strain; σ: stress; c: constant value; t: time; t`: time when stress starts to change.

Equation D.6 indicates that the strain output increases c times (c is a constant) when the stress input increases by c times. And equation D.7 indicates that the sum of two strain outputs resulting from two arbitrary stress inputs (at different times) equals the single strain output resulting from the sum of two stress inputs acting separately. Figure D.1(a) further illustrates the superposition principle of equation D.6, and Figure D.1(b) illustrates the superposition principle indicated in Equation D.7.

In our test, the stress input σ(t) is a function of time rather than a constant, so the whole stress input could be approximated by the sum of a series of constant stresses, as shown in Figure D.2:

$$\sigma(t) = \sum_{i=1}^{n} \Delta\sigma_i H(t - t_i) \qquad [E.8]$$

Where σ(t): stress input function; $\Delta\sigma_i$: stress change during the time interval of t_i; $H(t-t_i)$: time dependent function.

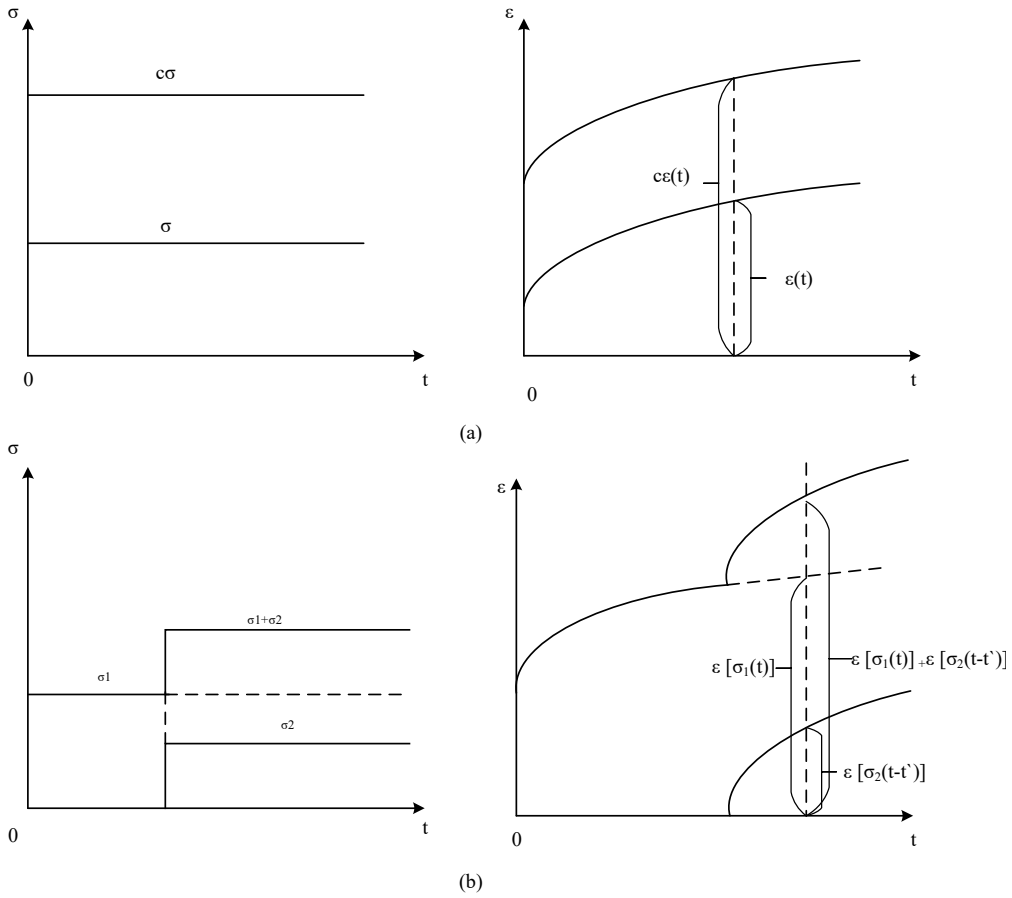

Figure D.1 Boltzmann's Superposition Principle

According to Boltzmann's superposition principle, the strain output resulting from a series of stress inputs should be the same as the sum of strain outputs resulting from each stress input separately. Therefore, the overall strain output under variable stress input is:

$$\varepsilon(t) = \sum_{i=1}^{n} \Delta\sigma_i H(t - t_i) J(t - t_i) \quad [D.9]$$

Here $J(t-t_i)$ is called creep compliance, which describes the slope of the stress vs. strain curve.

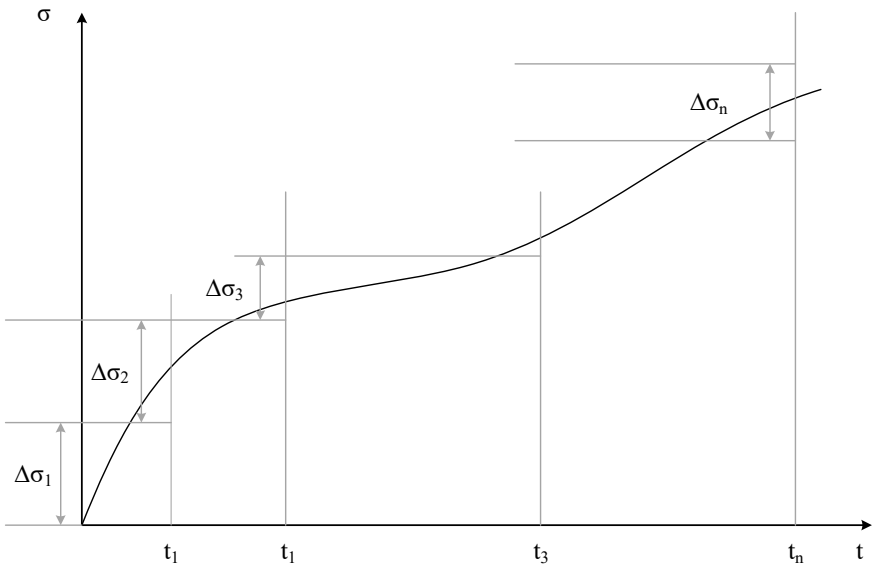

Figure D.2 Schematic Plot of the Input Stress

Figure D.4 gives the displacement vs. time curve before and after adjustment. The intended (designed) load was 12 tons (106.8 KN), while the maximum actual applied load was 14.16 tons (125.97 KN). Also, from the figure one can tell that even though the load kept dropping during the entire loading period, the load vs. time curve is approximately linear.

A conversion factor, k, is defined as the ratio of change in displacement divided by change in load. Using the two HPI strain gages mounted on the exposed anchor rod (actually on the adapter unit at the top of the anchor bar), the real applied load was recorded. And the total displacement was recorded using an LVDT. Both the applied load and displacement data were recorded every minute. As discussed previously, the elastic and plastic strains are time independent, and the creep strain could be ignored due to the short time interval between load variations. So the revised displacement curve was calculated by multiplying the difference between designed load and applied load by a conversion factor. The upper red dash line shown in Figure D.3 is the revised curve. Compared with the real displacement curve, the revised curve, at the beginning of the load

spike, is lower as expected due to the large difference between designed load and applied load. Then, with time, the applied load approaches the designed load and the revised displacement tends to coincide closer with the measured curve.

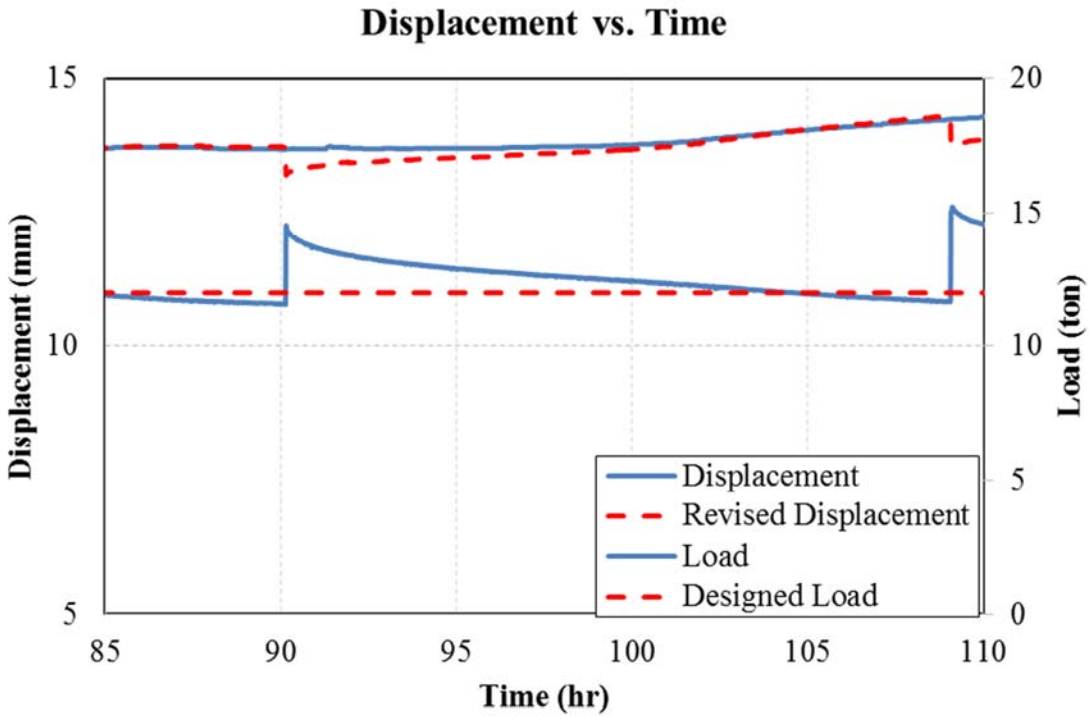

Figure D.3 Comparison of the Original and Revised Displacement Curve

After individual segments of the displacement curve were revised, the segments were assembled end-to-end to form the continuous time displacement curves shown in Figure D.4. At 7 ton (62.3 KN) load level, the applied load was below the designed load, so the revised curve should be above the real displacement curve due to compensation for the applied load. For 12 ton (106.8 KN) load level, the applied load was larger than designed load which resulted in a lower revised curve as shown in Figure D.4.

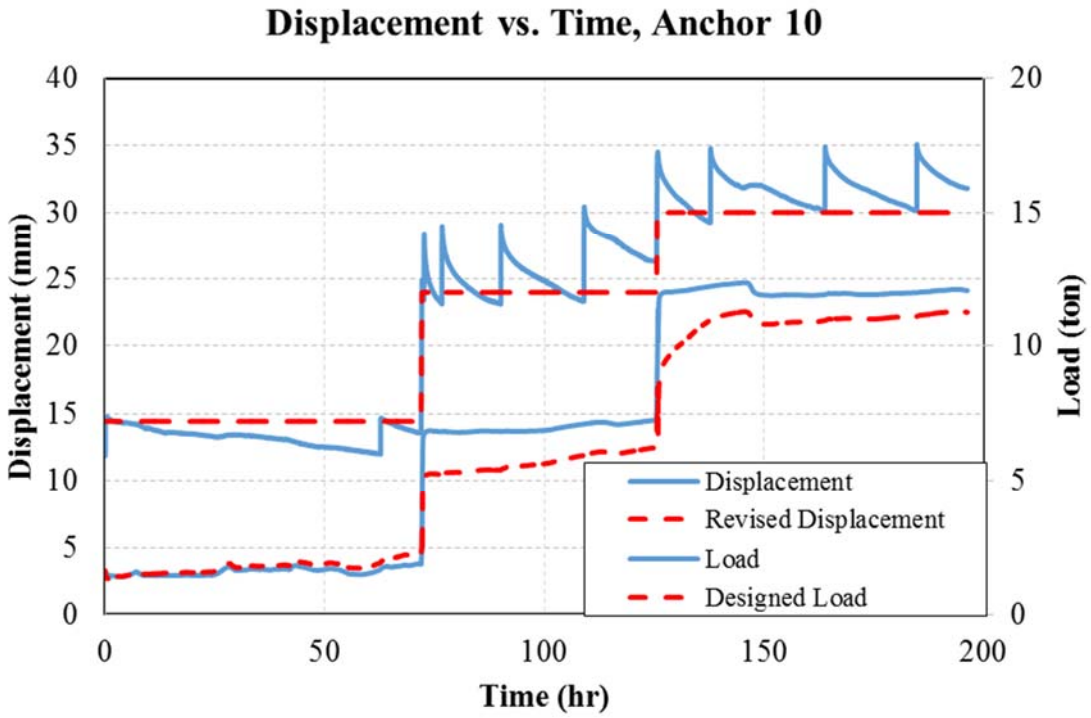

Figure D.4 Comparison of the Original and Revised Displacement (Total)

Appendix E Pullout Test Results

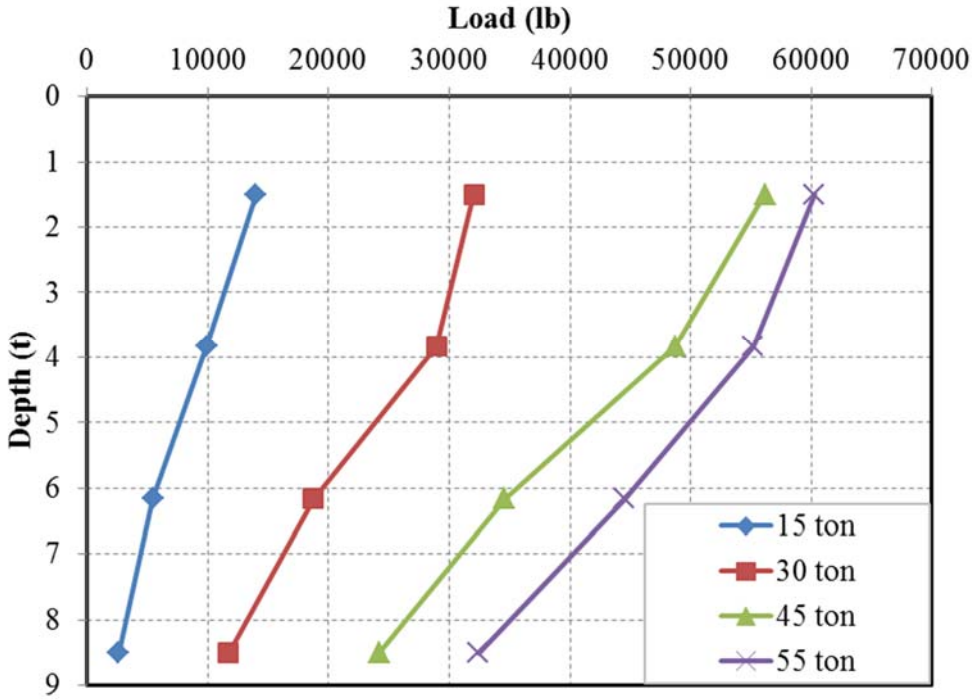

E.1 Load vs. Depth in Rebar for Anchor 1

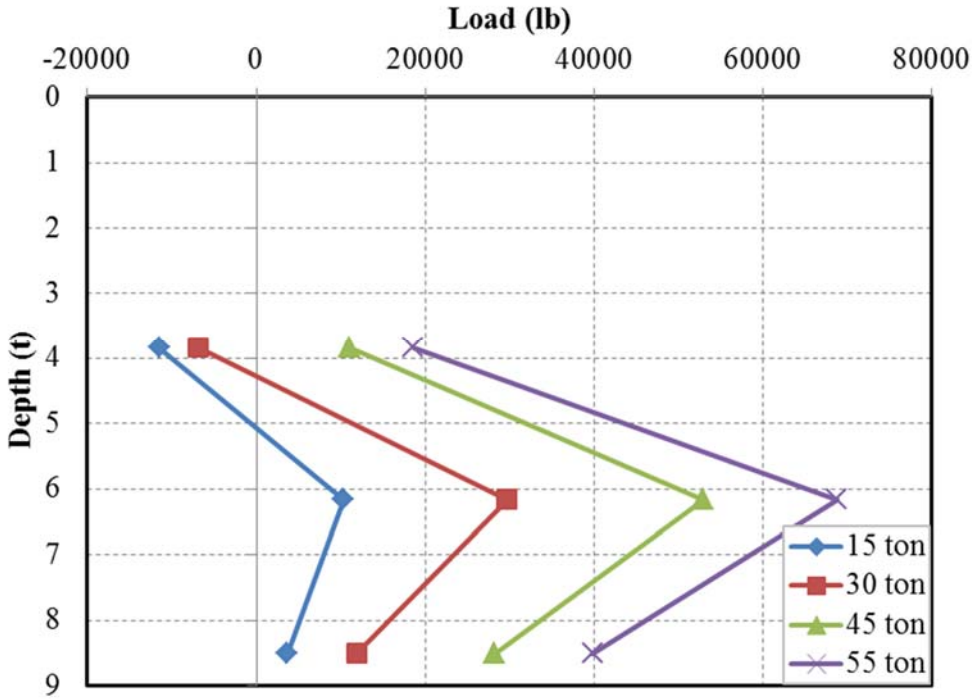

E.2 Load vs. Depth in Grout for Anchor 1

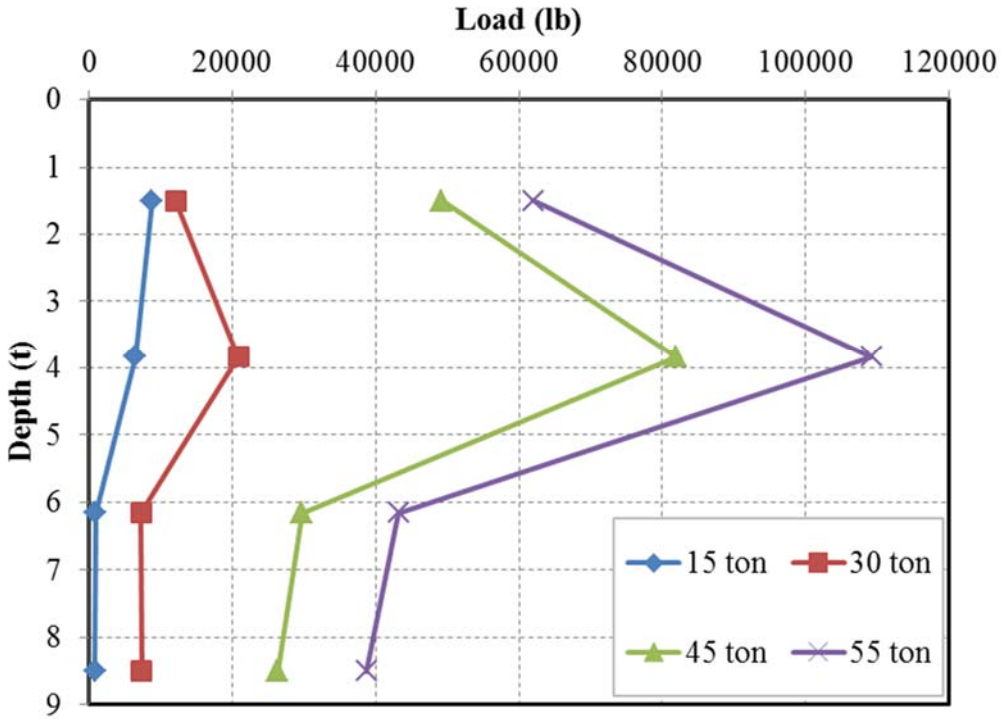

E.3 Load vs. Depth in Rebar for Anchor 2

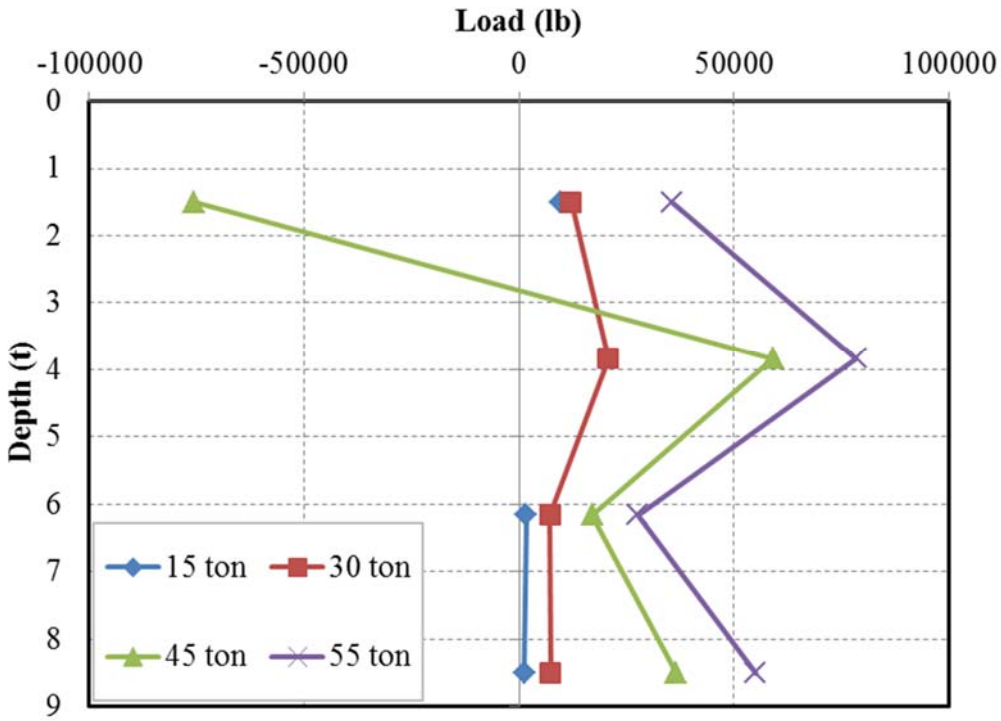

E.4 Load vs. Depth in Grout for Anchor 2

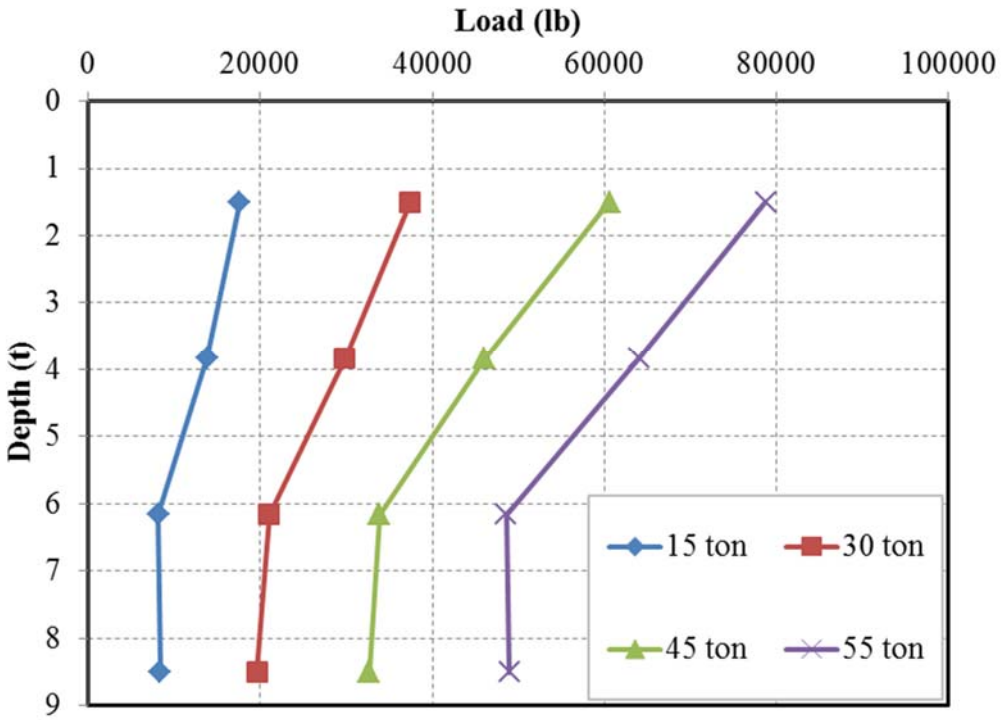

E.5 Load vs. Depth in Rebar for Anchor 3

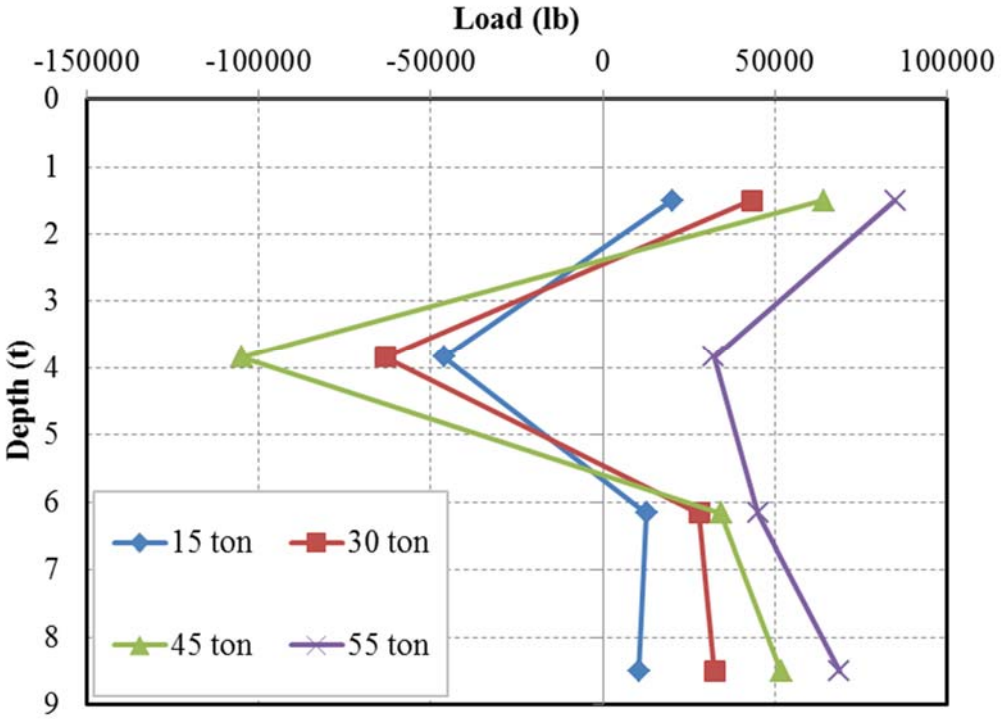

E.6 Load vs. Depth in Grout for Anchor 3

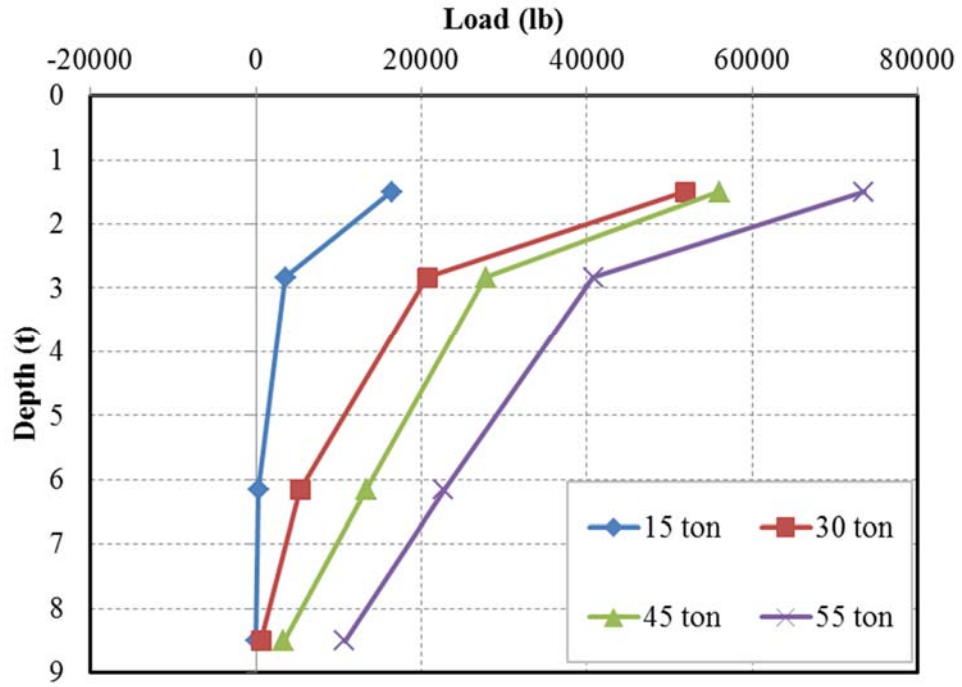

E.7 Load vs. Depth in Rebar for Anchor 4

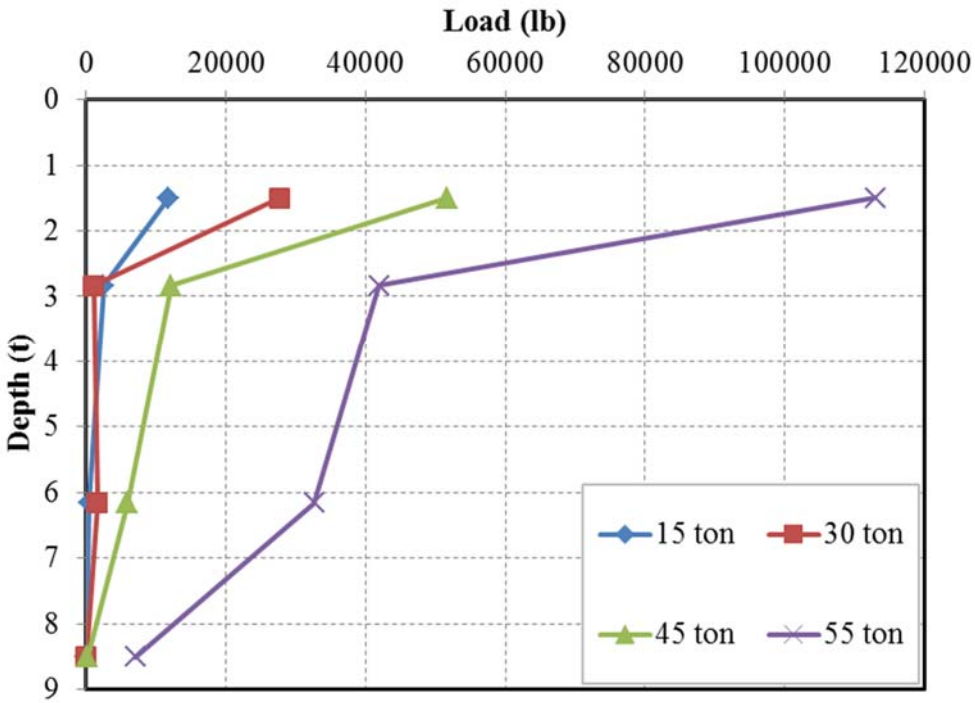

E.8 Load vs. Depth in Rebar for Anchor 5

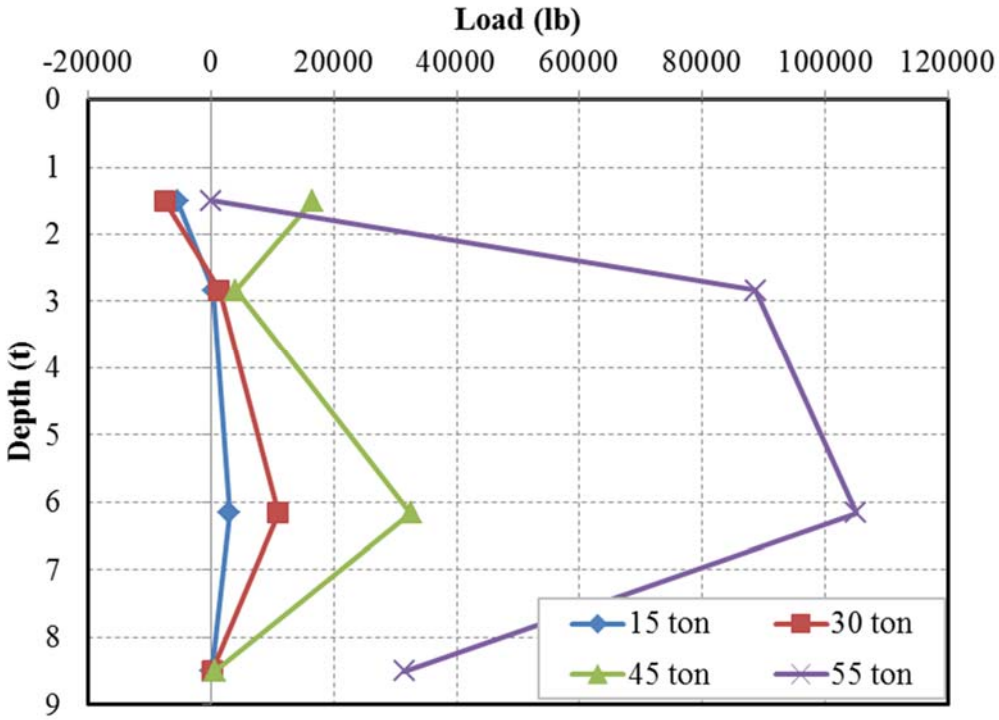

E.9 Load vs. Depth in Grout for Anchor 5

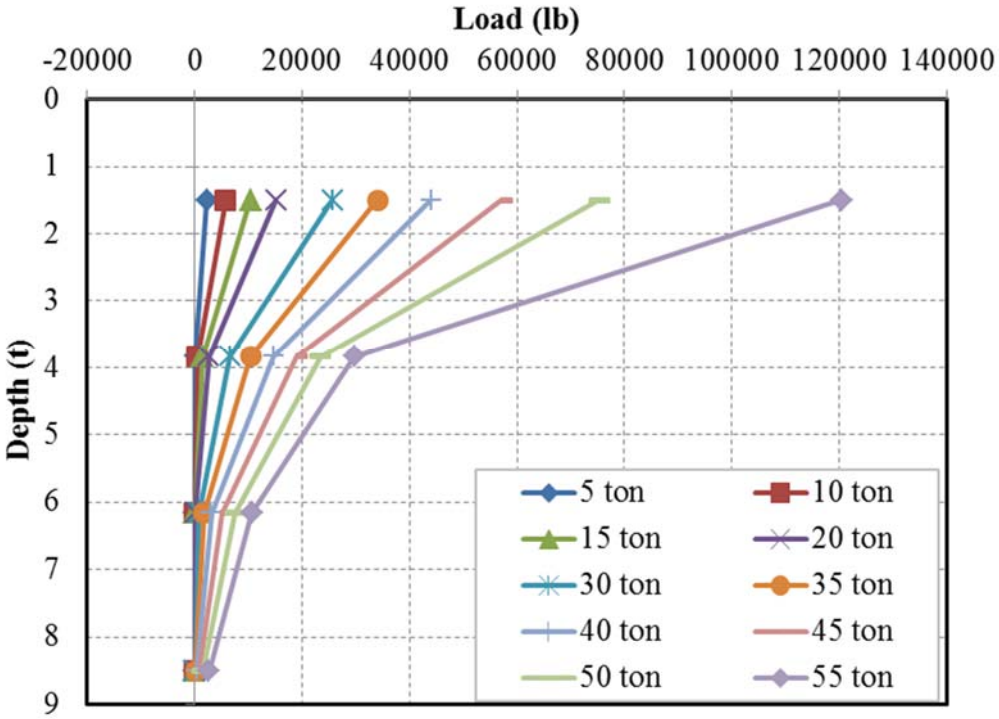

E.10 Load vs. Depth in Rebar for Anchor 6

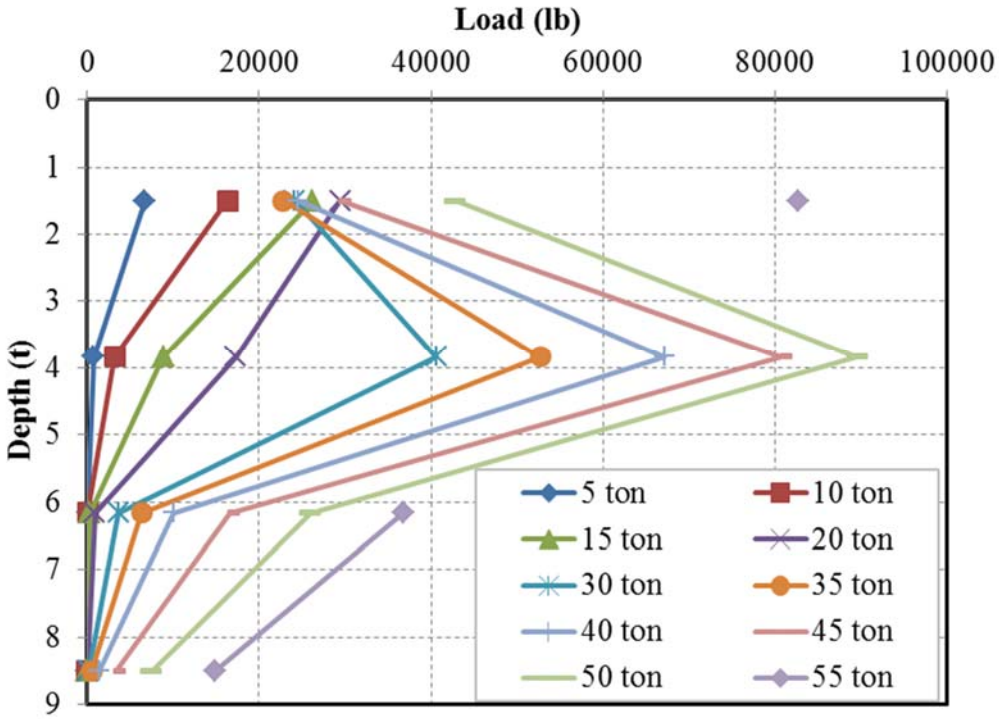

E.11 Load vs. Depth in Grout for Anchor 6

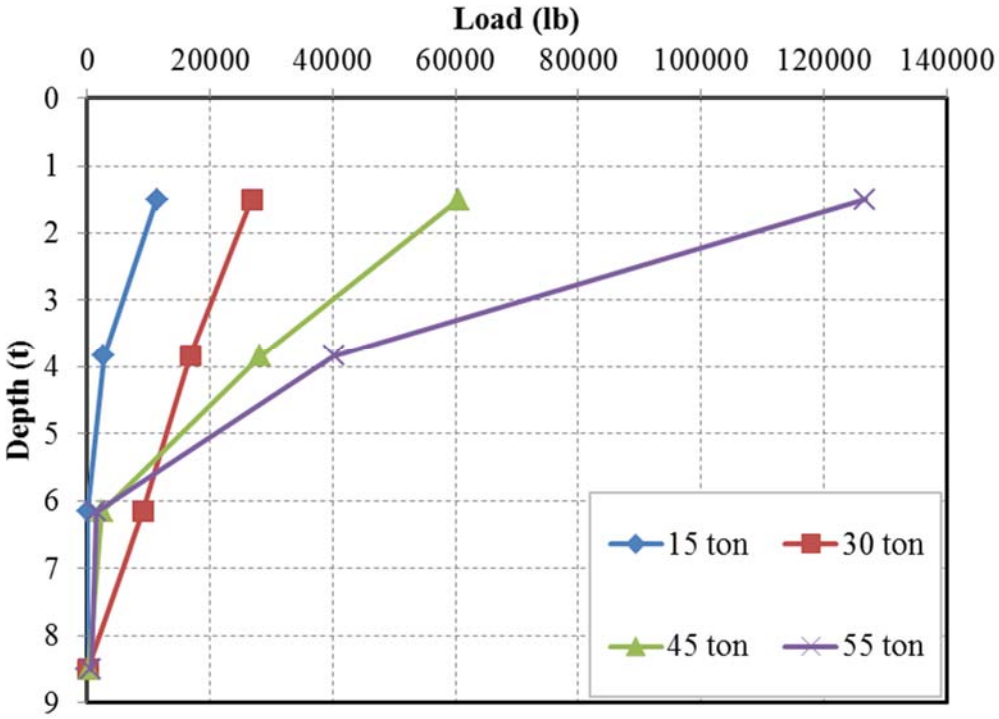

E.12 Load vs. Depth in Rebar for Anchor 7

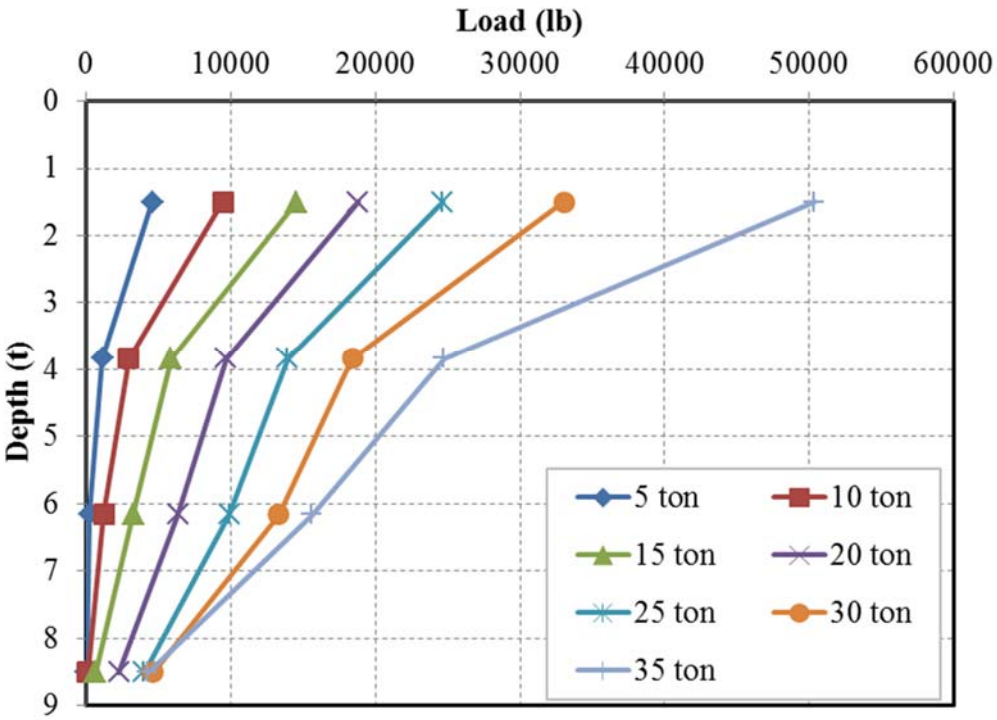

E.13 Load vs. Depth in Rebar for Anchor 8

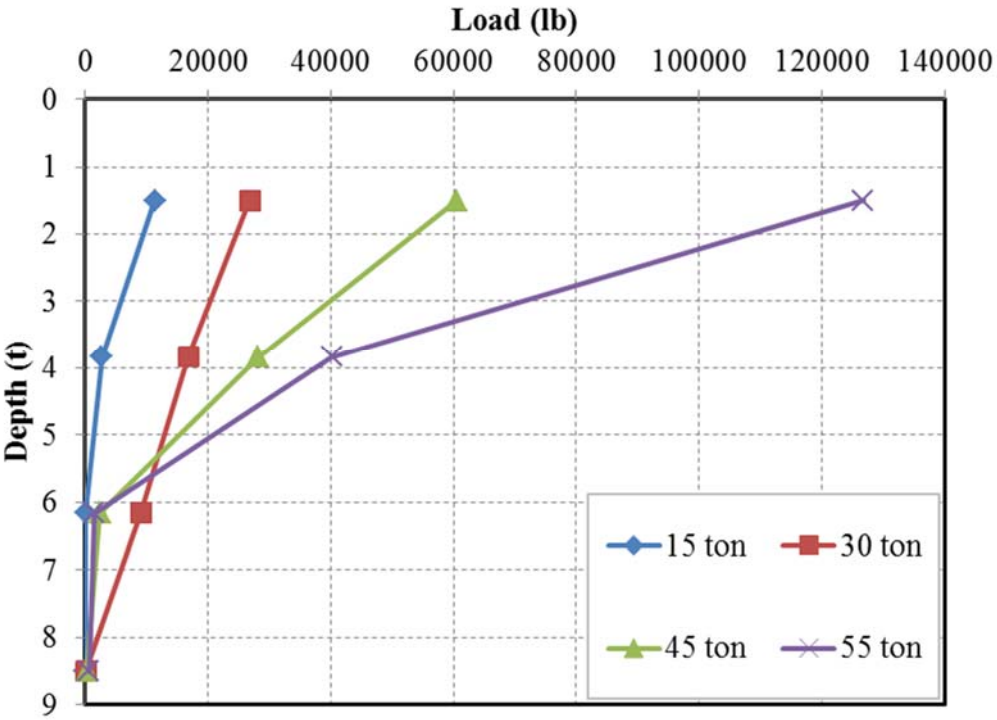

E.14 Load vs. Depth in Grout for Anchor 8

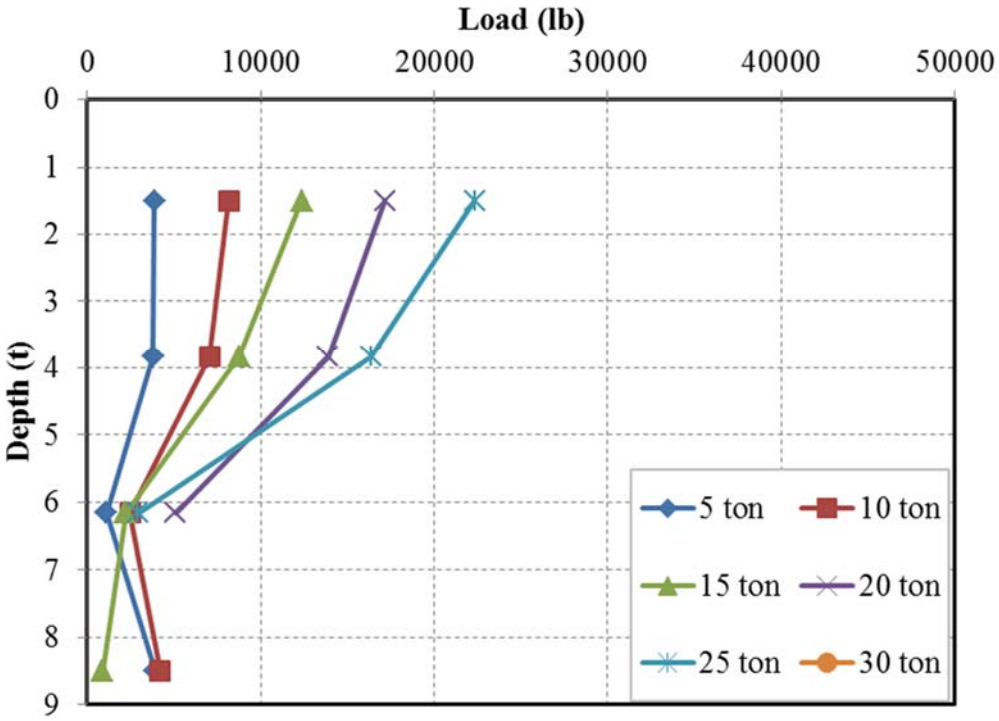

E.15 Load vs. Depth in Rebar for Anchor 9

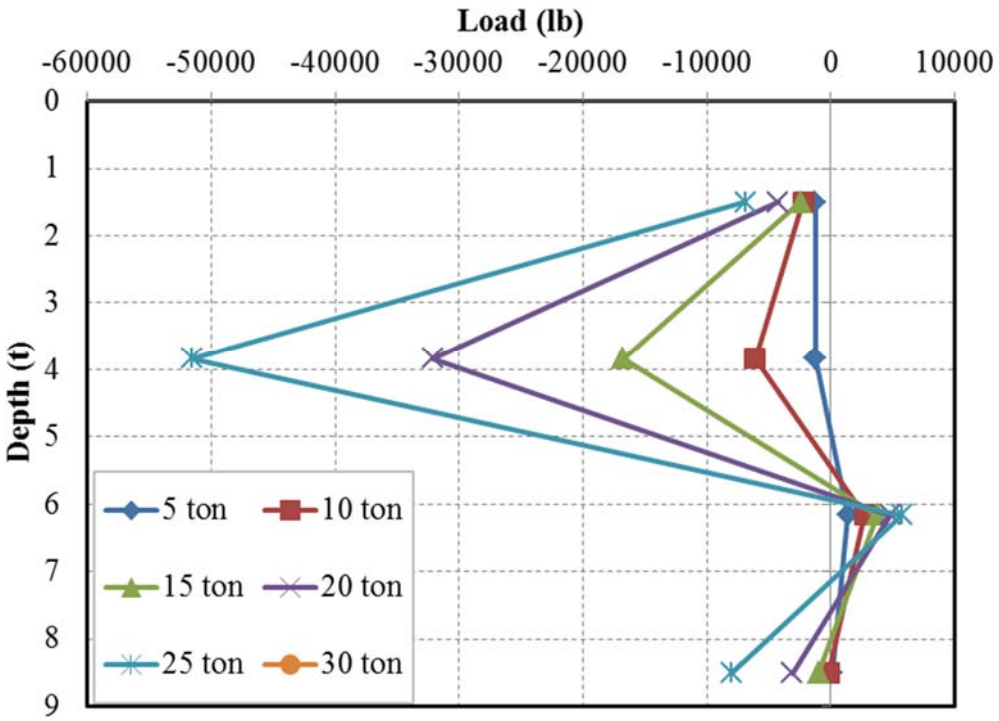

E.16 Load vs. Depth in Grout for Anchor 9

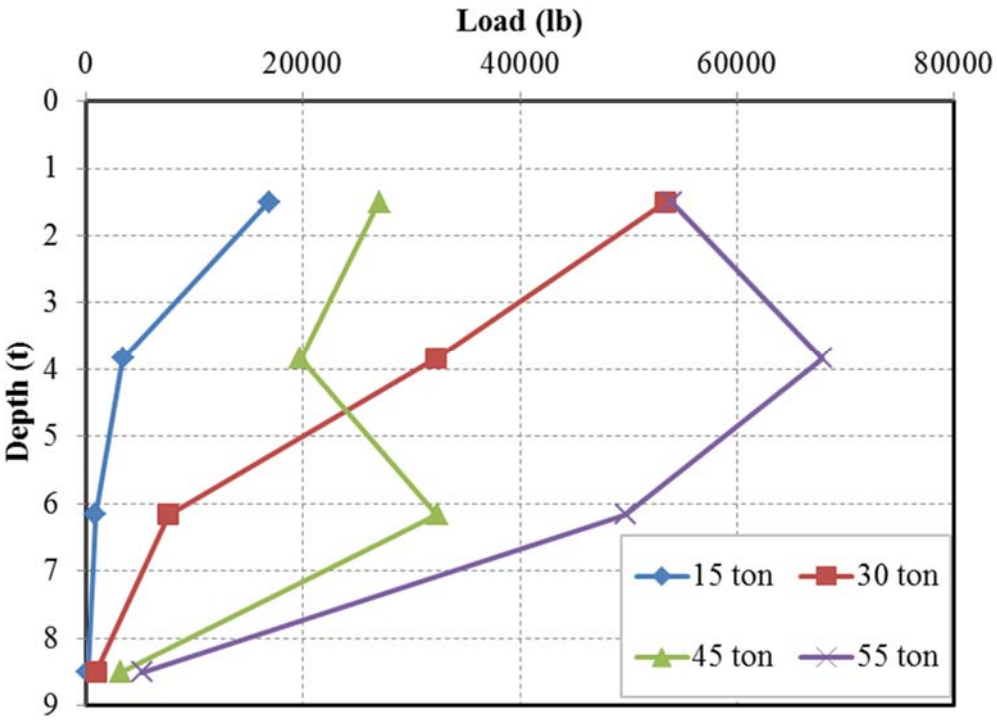

E.17 Load vs. Depth in Rebar for Anchor 11

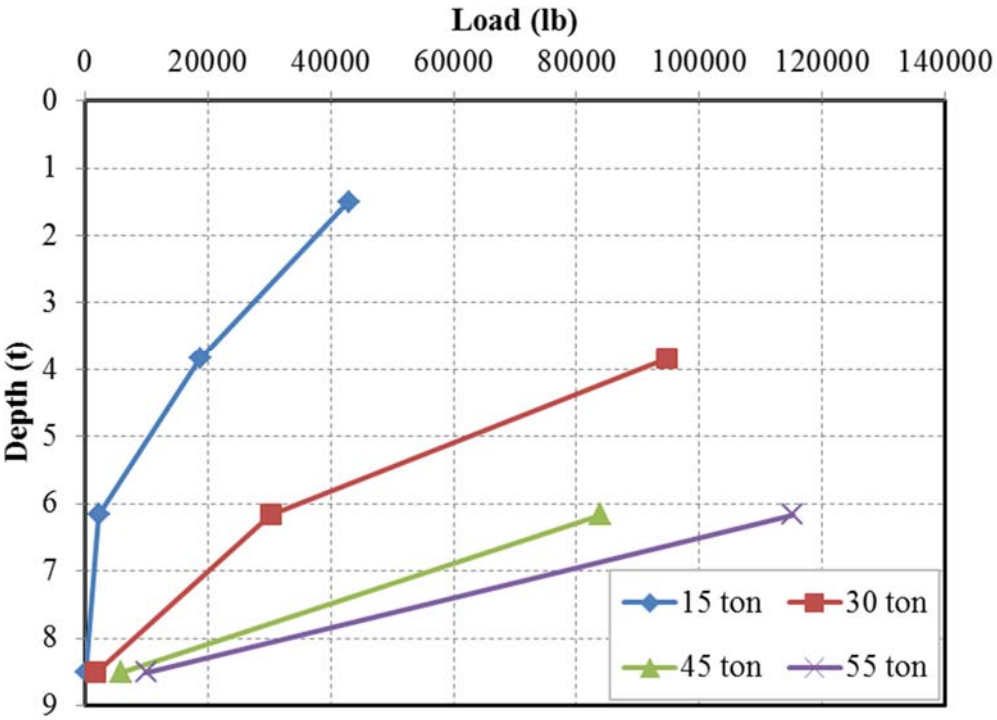

E.18 Load vs. Depth in Grout for Anchor 11

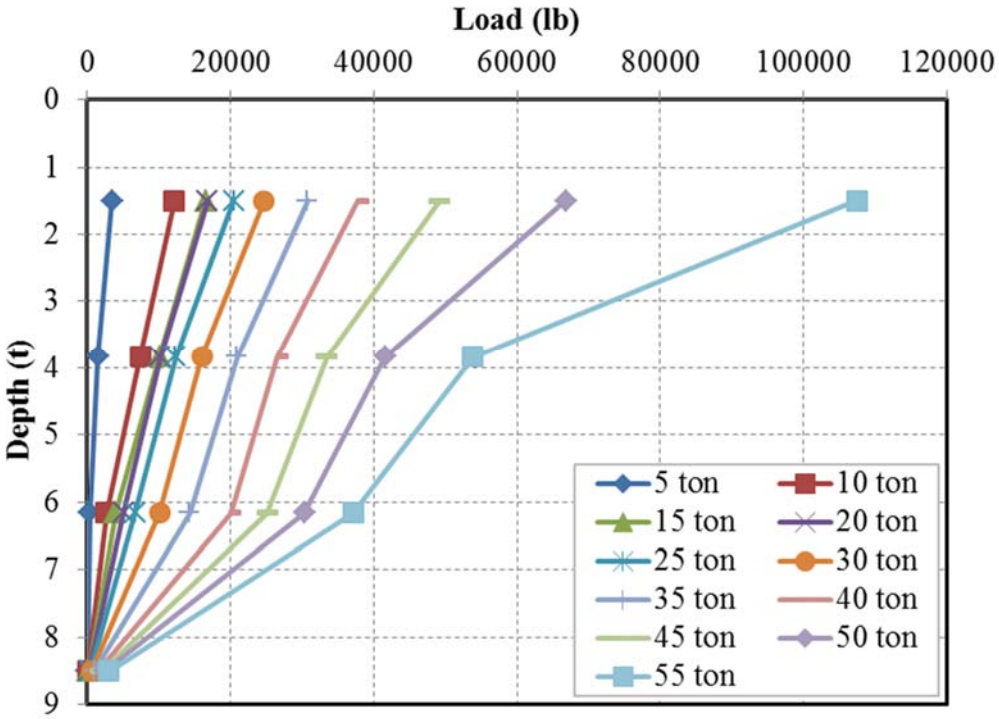

E.19 Load vs. Depth in Rebar for Anchor 12

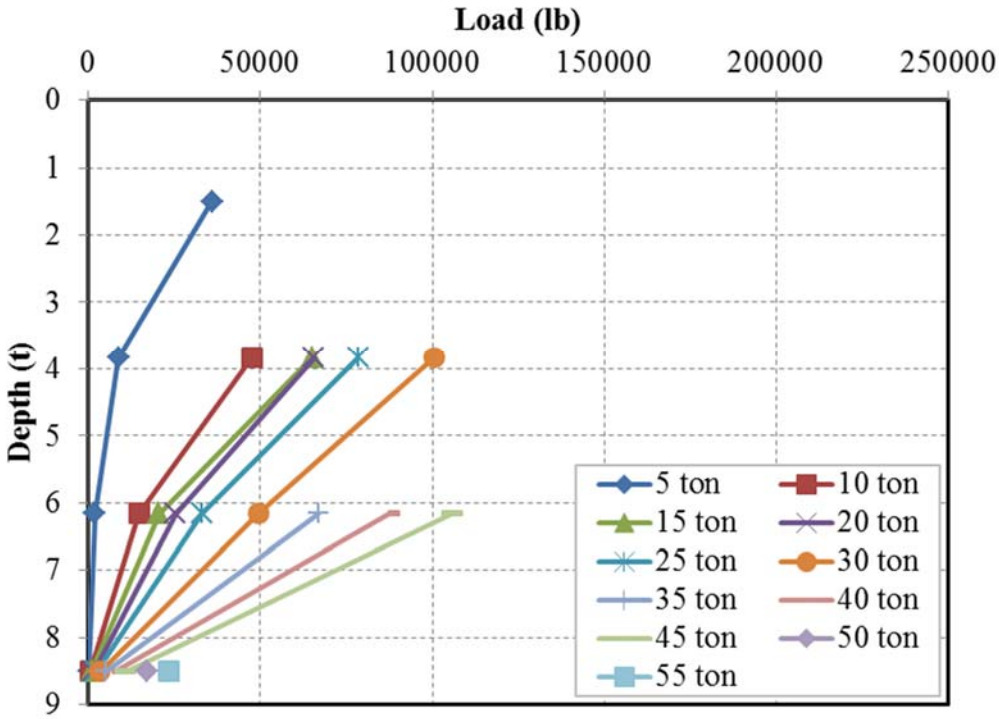

E.20 Load vs. Depth in Grout for Anchor 12

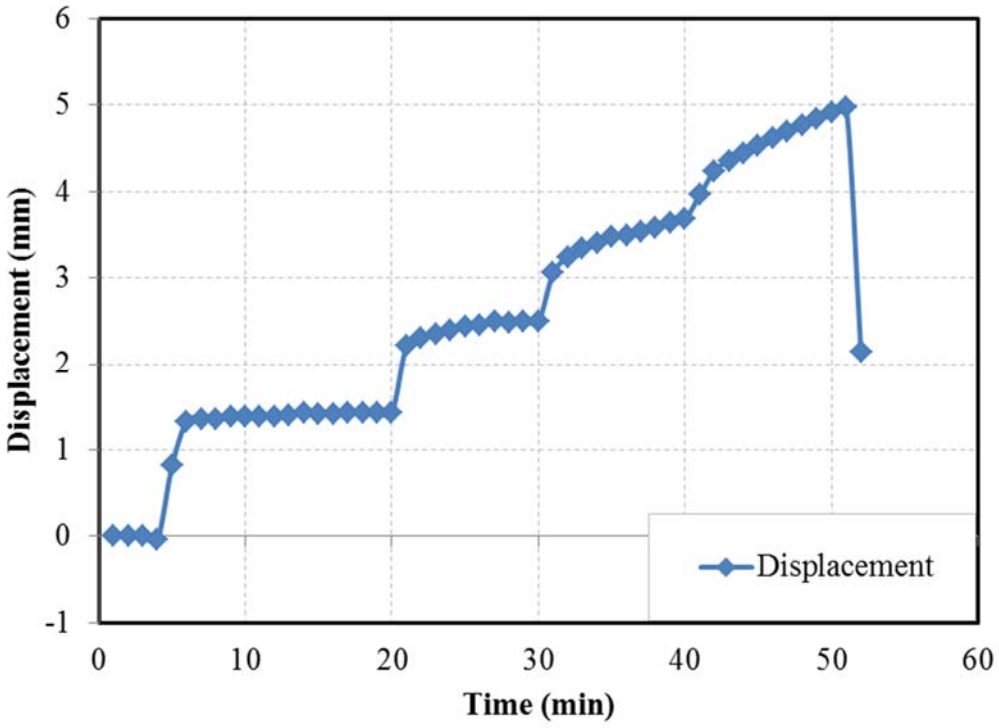

E.21 Dispalcement vs. Time for Anchor 1 (Pullout Test)

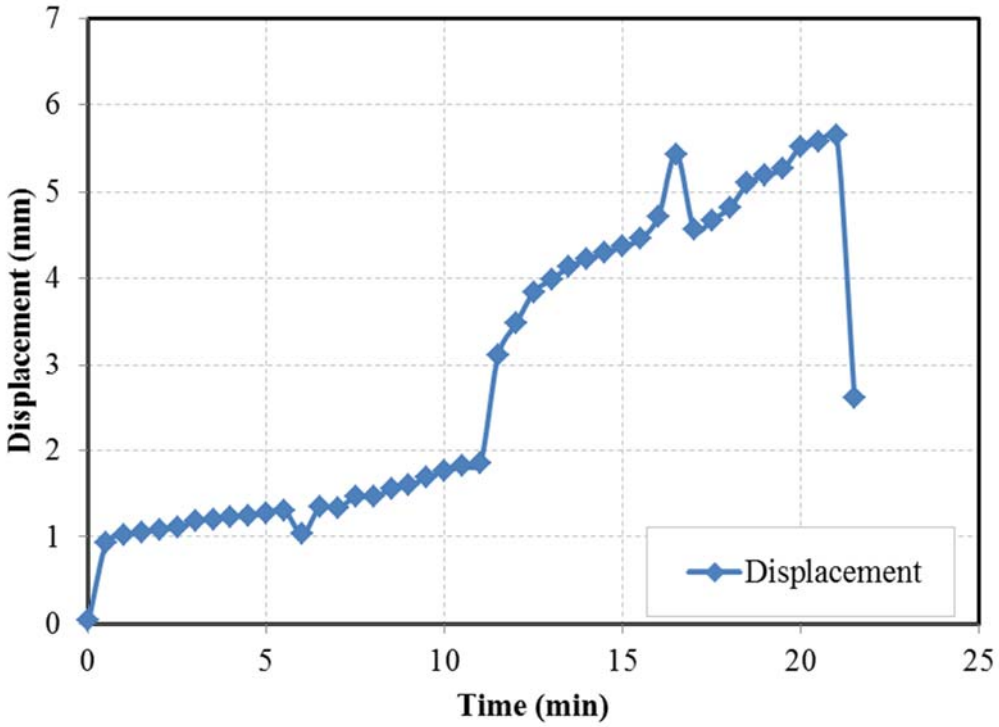

E.22 Displacement vs. Time for Anchor 2 (Pullout Test)

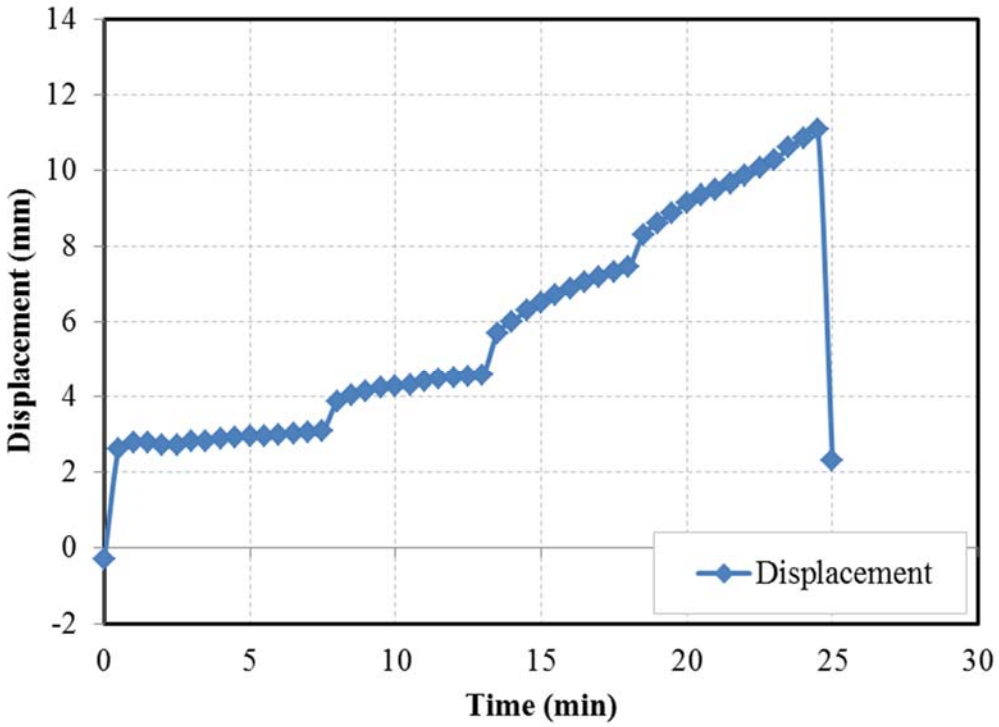

E.23 Displacement vs. Time for Anchor 3 (Pullout Test)

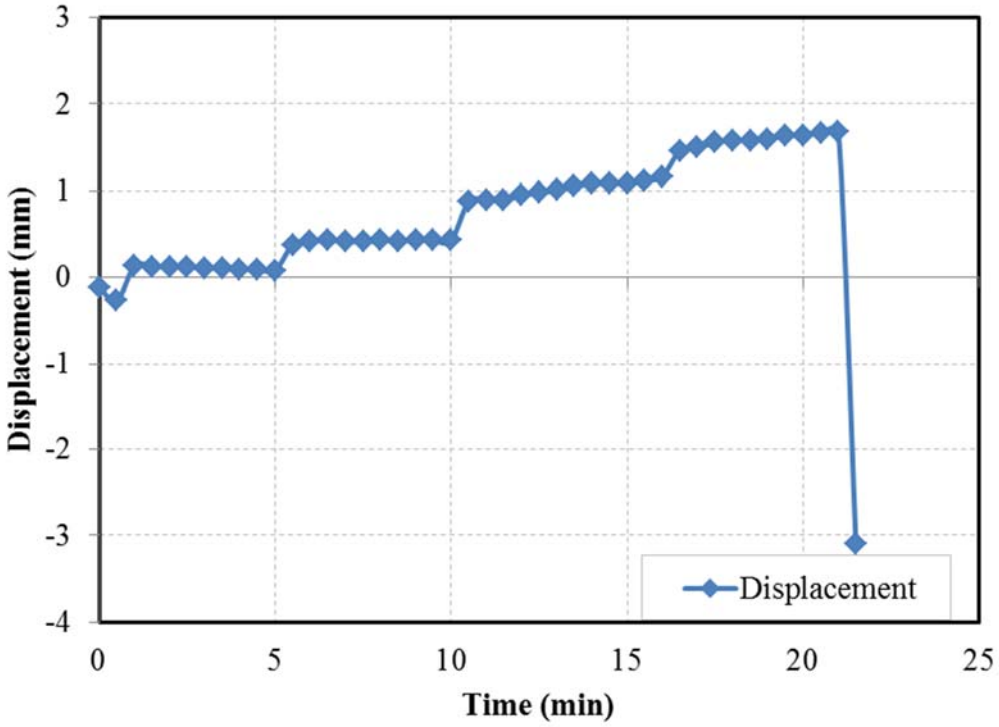

E.24 Displacement vs. Time for Anchor 4 (Pullout Test)

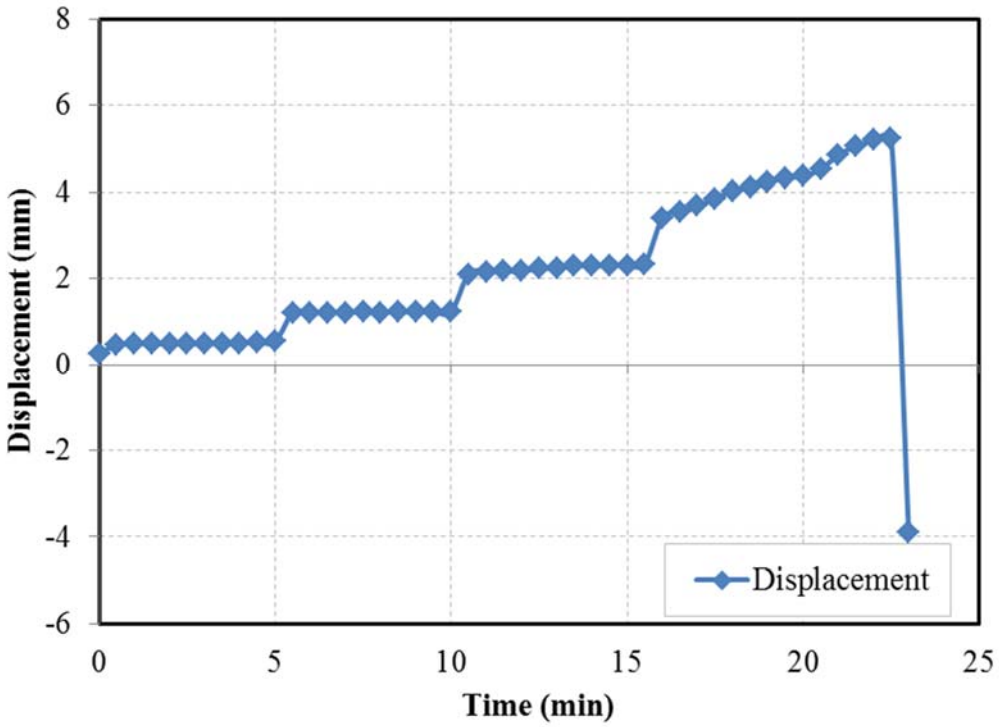

E.25 Displacement vs. Time for Anchor 5 (Pullout Test)

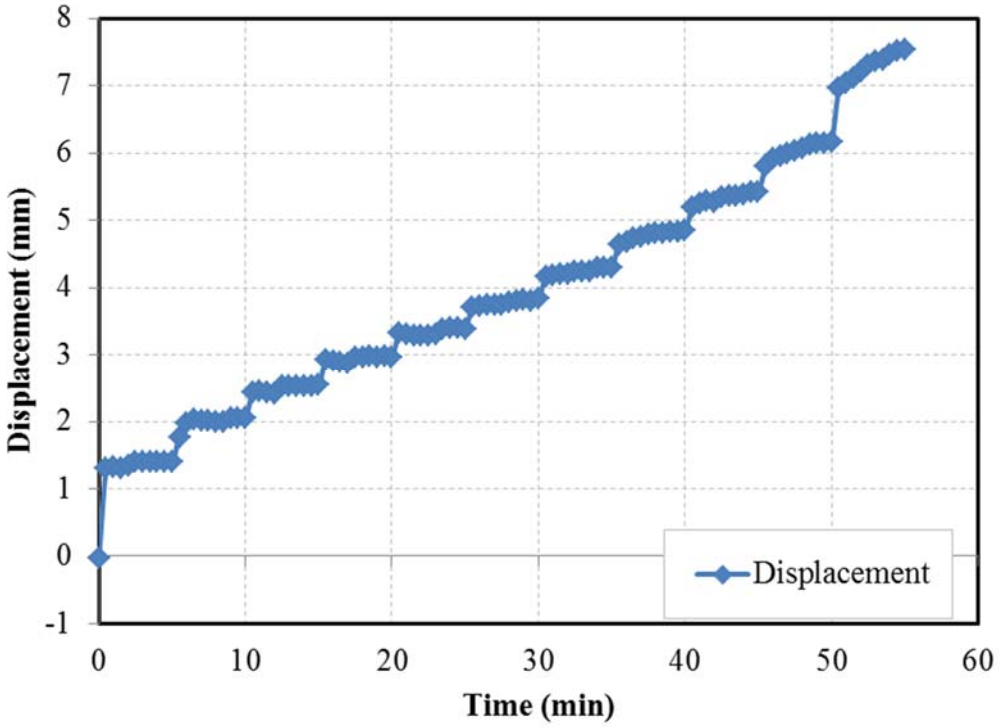

E.26 Displacement vs. Time for Anchor 6 (Pullout Test)

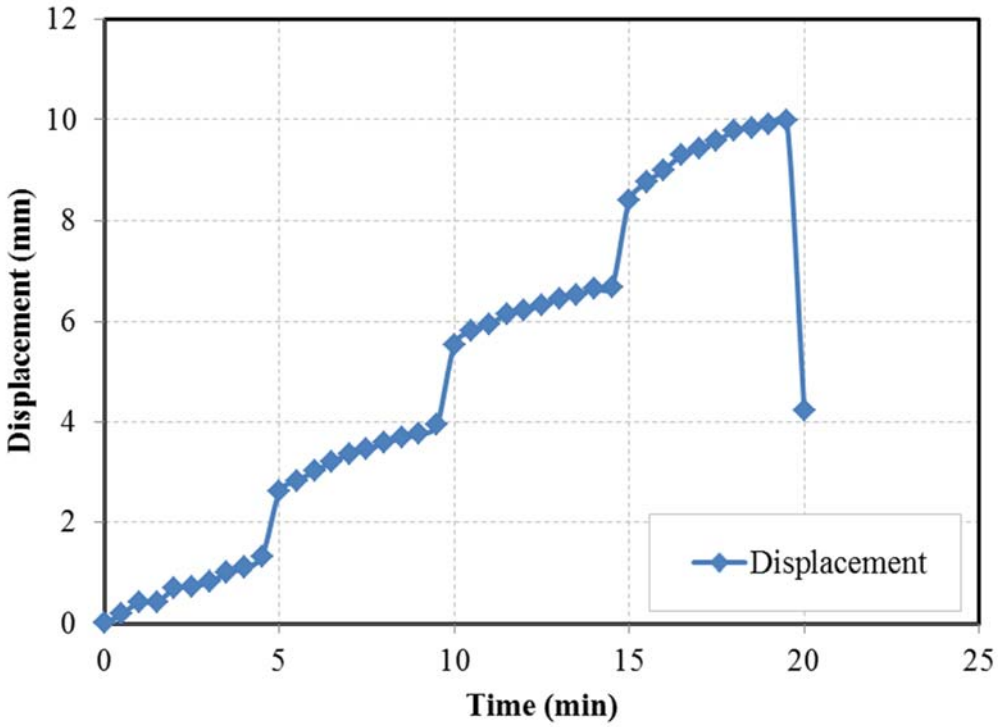

E.27 Displacement vs. Time for Anchor 7 (Pullout Test)

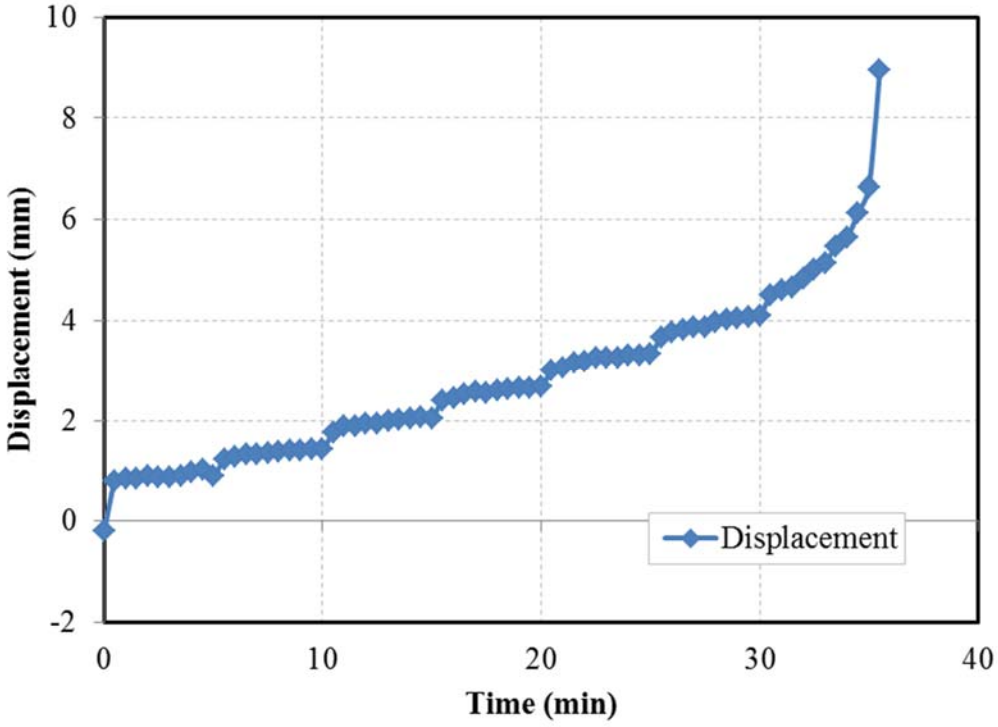

E.28 Displacement vs. Time for Anchor 8 (Pullout Test)

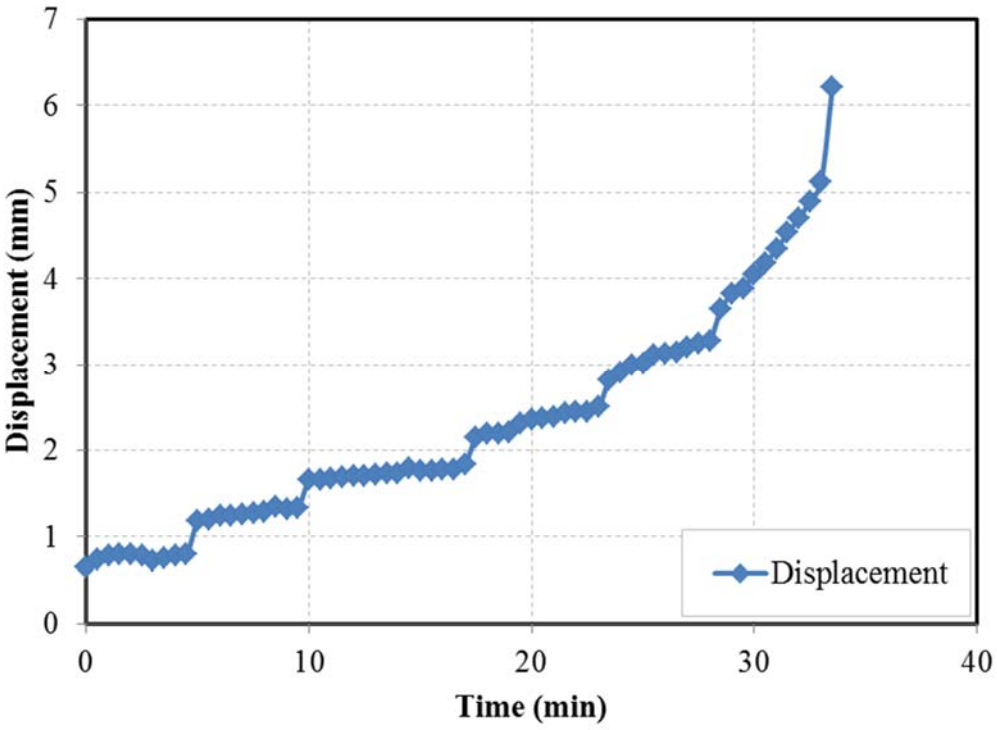

E.29 Displacement vs. Time for Anchor 9 (Pullout Test)

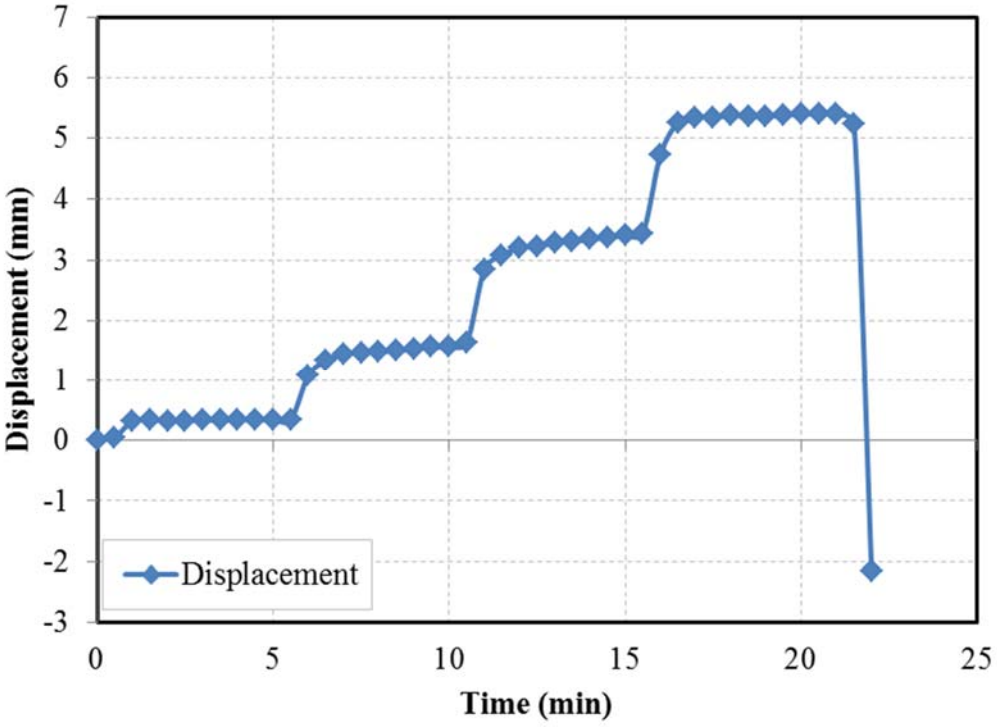

E.30 Displacement vs. Time for Anchor 11 (Pullout Test)

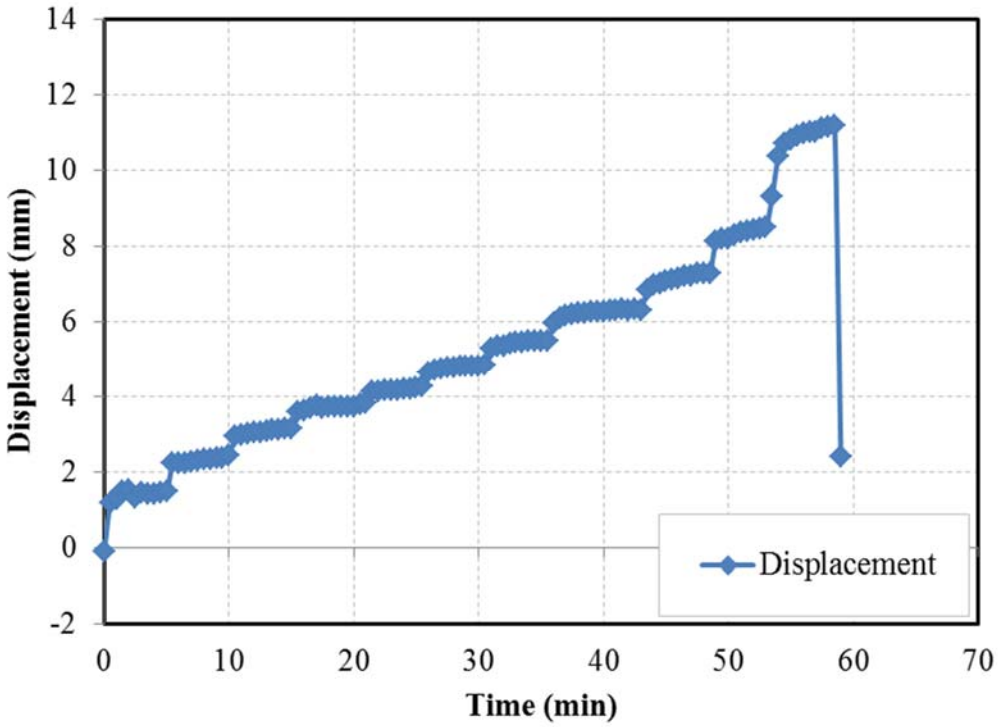

E.31 Displacement vs. Time for Anchor 12 (Pullout Test)

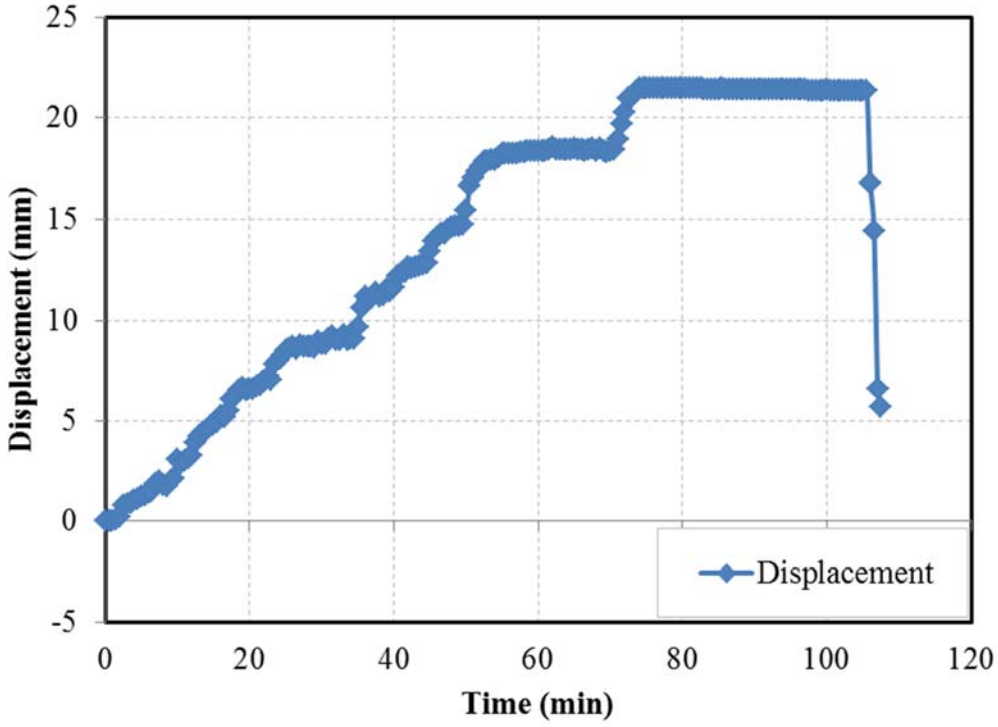

E.32 Displacement vs. Time for Anchor 15 (Pullout Test)